

NASA CR-72415
GESP-35

CAVITY REACTOR CRITICAL EXPERIMENT

Volume II

N68-28612
(ACCESSION NUMBER) (THRU)
146 1
(PAGES) (CODE)
CR-72415 22
(NASA CR OR TMX OR AD NUMBER) (CATEGORY)

GPO PRICE $
CFSTI PRICE(S) $
Hard copy (HC)
Microfiche (MF)
ff 653 July 65

by
G. D. Pincock, J. F. Kunze



Prepared for

NATIONAL AERONAUTICS AND SPACE ADMINISTRATION

Contract C-67747-A

GENERAL ELECTRIC COMPANY

Nuclear Systems Programs

Idaho Falls, Idaho

LEGAL NOTICE

This report was prepared as an account of Government sponsored work. Neither the United States, nor the Commission, nor any person acting on behalf of the Commission:

A. Makes any warranty or representation, expressed or implied, with respect to the accuracy, completeness, or usefulness of the information contained in this report, or that the use of any information, apparatus, material, method, or process disclosed in this report may not infringe privately owned rights; or

B. Assumes any liabilities with respect to the use of, or for damages resulting from the use of any information, apparatus, material, method, or process disclosed in this report.

As used in the above, "person acting on behalf of the Commission" includes any employee or contractor of the Commission, or employee of such contractor, to the extent that such employee or contractor of the Commission, or employee of such contractor prepares, disseminates, or provides access to, any information pursuant to his employment or contract with the Commission or his employment with such contractor.

NASA CR-72415
GESP-35

CAVITY REACTOR CRITICAL EXPERIMENT

VOLUME II

by

G. D. Pincock and J. F. Kunze

Prepared for

NATIONAL AERONAUTICS AND SPACE ADMINISTRATION

May 31, 1968

Contract C-67747-A

Technical Management
NASA-Lewis Research Center
Cleveland, Ohio
Nuclear Systems Division
Robert E. Hyland, Project Manager
Advanced Systems Division
John C. Liwosz

PRECEDING PAGE BLANK NOT FILMED

ABSTRACT

This report is the second volume pertaining to cavity reactor critical experiments performed at the National Reactor Testing Station. This volume describes experiments with a full gaseous core of uranium hexafluoride and the mockup experiments using sheet fuel. All the prior and current cavity reactor experiments were conducted using sheet fuel. The gaseous core experiments described in this report were designed to evaluate the adequacy of the sheet fuel mockups.

ACKNOWLEDGEMENTS

The authors wish to thank those individuals who contributed significantly to the experiment. Among these are the following who deserve specific acknowledgement:

L. S. Masson for the design of equipment for the first gaseous core reactor; the reactor operators, C. G. Cooper, R. R. Jones, and D. H. Suckling; and Mrs. P. L. Chase for assistance in data reduction;

Dr. R. E. Wood of General Electric Company and R. E. Hyland of the National Aeronautics and Space Administration for program coordination and consultation.

PRECEDING PAGE BLANK NOT FILMED.

TABLE OF CONTENTS

		Page
1.0	INTRODUCTION	17
2.0	DESCRIPTION OF TEST SETUP AND PROCEDURES	18
2.1	Reactor Description	18
2.2	Experimental Procedures	18
3.0	SUMMARY OF TEST RESULTS	24
3.1	Fundamental Characteristics	24
3.2	Geometry.	24
3.3	Critical Mass Comparisons	25
3.4	General Flux and Power Distribution Comparisons	27
3.5	Material Worth Comparisons	28
3.6	Temperature and Impurity Effects	29
4.0	MOCKUP NO. 1 EXPERIMENT	44
4.1	Initial Loading	44
4.2	Rod Worths and Reactivity Measurements . .	45
4.3	Power Distribution Measurements	47
4.4	Gold Foil Data	49
4.5	Neutron Flux Distribution	50
5.0	UF_6 EXPERIMENT-BERYLLIUM AND D_2O REFLECTOR	78
5.1	Initial Loading	79
5.2	Rod Worth and Reactivity Measurements . . .	79
5.3	Power Distribution Measurements	82
5.4	Gold Foil Data	83
5.5	Neutron Flux Distribution	84
5.6	Noise Measurements.	85

TABLE OF CONTENTS
(Continued)

		Page
6.0	UF_6 EXPERIMENT - PURE D_2O REFLECTOR	119
	6.1 Rod Worth and Reactivity Measurements . . .	119
	6.2 Power Distribution - Bare Catcher Foils . . .	120
	6.3 Gold Foil Data - Bare Foils	121
7.0	MOCKUP NO. 2 EXPERIMENT - PURE D_2O REFLECTOR	131
	7.1 Initial Loading	132
	7.2 Rod Worth and Reactivity Measurements . . .	132
	7.3 Power Distribution	135
	7.4 Gold Foil Data	136
	7.5 Thermal Neutron Flux Distribution	137
8.0	MOCKUP NO. 2 EXPERIMENT - D_2O AND Be REFLECTOR	174
	8.1 Initial Loading	174
	8.2 Rod Worth and Reactivity Measurements . . .	174
	8.3 Power Distribution	175
	8.4 Gold Foil Data	176
	8.5 Thermal Neutron Flux Distribution	177
9.0	COMPARISON OF MOCKUP AND UF_6 REACTOR. . .	199
	9.1 Critical Mass and Reactivity Worths.	199
	9.2 Power Distribution	203
	9.3 Gold Foil Data	204
	9.4 Thermal Neutron Flux	206
10.0	NUCLEAR CALCULATIONAL MODEL.	232

TABLE OF CONTENTS

(Continued)

		Page
REFERENCES		237
INDEX		238-240

TABLES

2.1	Tabular Rod Worth - Actuator No. 4	20
2.2	Tabular Subcritical Rod Worth Curve, Cavity Reactor	21
2.3	Effective Delayed Neutron Parameters	22
3.1	Characteristics of Cavity Reactor Critical Experiment.	30
3.2	Material Compositions of Cavity Reactor Critical Experiment	31
3.3	Beryllium Radial Reflector Characteristics.	32
3.4	"Critical" Configuration Data	33
3.5	Critical Loading Comparisons	34
3.6	Summary of Fuel Worth	35
4.1	Inverse Multiplication	51
4.2	Material Worth Measurements.	52
4.3	Catcher Foil Data - UF_6 Mockup No. 1	53-4
4.4	Catcher Foil Cadmium Ratios - UF_6 Mockup No. 1.	55
4.5	Gold Foil Data - UF_6 Mockup No. 1	56-7
4.6	Power Normalization Factors - UF_6 Mockup No. 1.	58
4.7	Gold Cadmium Ratios - UF_6 Mockup No. 1	59
4.8	Thermal Neutron Flux Distribution - UF_6 Mockup No. 1	60
5.1	Inverse Multiplication - Initial Loading - UF_6 Reactor with Be and D_2O Reflector	87

TABLE OF CONTENTS

(Continued)

Page

TABLES

(Cont'd)

5.2 Material Worths - UF_6 Experiment 88

5.3 Catcher Foil Data - UF_6 Experiment 89-91

5.4 Catcher Foil Cadmium Ratios - UF_6 Experiment . . . 92

5.5 Gold Foil Data - UF_6 Experiment 93-94

5.6 Power Normalization Factor. 95

5.7 Gold Foil Cadmium Ratios - UF_6 Reactor 96

5.8 Thermal Neutron Flux Distribution - UF_6 Reactor - Be and D_2O Reflector. 97

6.1 Bare Catcher Foil Data Pure D_2O Reflector - UF_6 Reactor. 122

6.2 Bare Gold Foil Data - UF_6 Reactor - Pure D_2O Reflector 123

6.3 Power Normalization Factors - UF_6 Reactor - Pure D_2O Reflector 124

6.4 Comparison of Gold Foil Data in Reflector Regions UF_6 Reactor Assemblies. 125

7.1 Material Weights in Mockup No. 2. 138

7.2 Fuel Loading Increments - Mockup No. 2 with Pure D_2O Reflector 139

7.3 Inverse Multiplication - Initial Loading - Mockup No. 2 with Pure D_2O Reflector 140

7.4 Actuators 3 and 6 Tabular Rod Worth Curve - Mockup No. 2 141

7.5 Fuel Weights Before and After Cleaning in Boiling Water. 142

7.6 Fuel Sheet Weight Percent Uranium from Chemical Analyses 142

TABLE OF CONTENTS

(Continued)

Page

TABLES

(Cont'd)

7.7 Fuel Worth Results - Mockup No. 2 - All D_2O Reflector 143

7.8 Fuel Worth Measurements Radially Across Active Core 144

7.9 Catcher Foil Data - Mockup No. 2 - Pure D_2O Reflector 145

7.10 Gold Foil Data - Mockup No. 2 - Pure D_2O Reflector 146-147

7.11 Power Normalization Factors - UF_6 Mockup No. 2. . 148

7.12 Gold Foil Cadmium Ratios - Mockup No. 2 - Pure D_2O Reflector 149

7.13 Thermal Neutron Flux - Mockup No. 2 - Pure D_2O Reflector 150

8.1 Inverse Multiplication - Initial Loading of Mockup No. 2 After Inserting Beryllium in Radial Reflector. 178

8.2 Fuel Worth Measurements Mockup No. 2 - Be in Radial Reflector 178

8.3 Catcher Foil Data - Mockup No. 2 - Be in Radial Reflector 179

8.4 Catcher Foil Cadmium Ratios Mockup No. 2 - Be in Radial Reflector 180

8.5 Gold Foil Data - Mockup No. 2 - Be in Radial Reflector 181-182

8.6 Gold Foil Cadmium Ratios - Mockup No. 2 - Be and D_2O Reflector 183

8.7 Thermal Neutron Flux Mockup No. 2 - Be and D_2O Reflector 184

9.1 Comparison of Control Rod Worth. 207

TABLE OF CONTENTS

(Continued)

Page

TABLES

(Cont'd)

9.2 Core Average Fuel Worths 208

9.3 Corrections to Critical Mass for Geometric Differences 209-210

9.4 Comparison of Thermal Neutron Flux Mockup and UF_6 Reactors - Be and D_2O Reflector. 211

10.1 Nuclear Model Region Composition. 233

10.2 Spherical Calculational Model of UF_6 Experiment - One Region Core. 234-235

FIGURES

2.1 Location of beryllium in the radial reflector. 23

3.1 Comparison of radial power distribution within the cavity between Mockup No. 2 with beryllium in the radial reflector and UF_6 reactor with pure D_2O reflector 36

3.2 Comparison of axial power distribution within the cavity between Mockup No. 2 with beryllium in the radial reflector and UF_6 reactor with pure D_2O reflector 37

3.3 Average gold foil activity per watt of reactor power in the radial reflector. 38

3.4 Average gold foil activity per watt of reactor power in the end reflector 39

3.5 Average thermal neutron flux per watt of reactor power in the reflector regions 40

3.6 Effect of core loading on fuel worth for all cavity reactor assemblies 41

3.7 Core loading effects on core average aluminum worth with respect to uranium worth 42

3.8 Effects of core loading on core average worth of type 1100 aluminum 43

4.1 Core layout - Mockup No. 1 reactor 61

TABLE OF CONTENTS

(Continued)

Page

FIGURES

(Contd)

4.2	Fuel sheet support screen layout on Mockup No. 1 . .	62
4.3	Fuel tray installation pattern and nomenclature - Mockup No. 1	63
4.4	Inverse multiplication curve, average of three channels - Mockup No. 1	64
4.5	Material locations for aluminum, teflon, carbon reactivity measurements - Mockup No. 1	65
4.6	Radial power distribution from bare catcher foils - Mockup No. 1	66
4.7	Axial power distribution from bare catcher foils at core center - Mockup No. 1	67
4.8	Catcher foil cadmium ratio radial profile - Mockup No. 1	68
4.9	Catcher foil cadmium ratio axial profile - Mockup No. 1	69
4.10	Radial distribution of bare gold foil activity - Mockup No. 1	70
4.11	Axial distribution of bare gold foil activity - Mockup No. 1	71
4.12	Bare gold foil activity distribution in the reflectors - Mockup No. 1	72
4.13	Gold foil cadmium ratio radial profile - Mockup No. 1	73
4.14	Gold foil cadmium ratio axial profile - Mockup No. 1.	74
4.15	Gold foil cadmium ratios in the radial and end reflectors - Mockup No. 1	75
4.16	Thermal neutron flux distribution radially through axial center of core - Mockup No. 1	76
4.17	Thermal neutron flux distribution axially through radial center of core - Mockup No. 1	77
5.1	General arrangement of cavity reactor showing heating equipment and UF_6 transfer system	98
5.2	View of separation plane with UF_6 tank in reactor. . .	99
5.3	UF_6 transfer control panel	100

TABLE OF CONTENTS

(Continued)

Page

FIGURES

(Cont'd)

5.4	Inverse multiplication curve - Channel No. 2 - UF_6 reactor with beryllium in reflector	101
5.5	UF_6 physical characteristics	102
5.6	Reactivity effect of cooling the UF_6 tank - UF_6 reactor with beryllium in reflector	103
5.7	Reactivity effect of cooling the UF_6 tank, second measurement - UF_6 reactor with beryllium in reflector	104
5.8	Effects of core loading on uranium worth - UF_6 reactor with beryllium in reflector	105
5.9	Radial power distribution from bare catcher foils - UF_6 reactor with beryllium in reflector	106
5.10	Axial power distribution from bare catcher foils - UF_6 reactor with beryllium in reflector	107
5.11	Catcher foil cadmium ratio radial profile - UF_6 reactor with beryllium in reflector	108
5.12	Catcher foil cadmium ratio axial profiel - UF_6 reactor with beryllium in reflector	109
5.13	Radial distribution of bare gold foil activity - UF_6 reactor with beryllium in reflector	110
5.14	Axial distribution of bare gold foil activity - UF_6 reactor with beryllium in reflector	111
5.15	Bare gold foil activity distribution in the reflectors - UF_6 reactor with beryllium in reflector	112
5.16	Gold foil cadmium ratio radial profile - UF_6 reactor with beryllium in reflector	113
5.17	Gold foil cadmium ratio axial profile - UF_6 reactor with beryllium in reflector	114
5.18	Gold foil cadmium ratios in the radial and end reflectors - UF_6 reactor with beryllium in reflector	115
5.19	Thermal neutron flux distribution radially through axial center of core UF_6 reactor, Beryllium in the reflector	116
5.20	Thermal neutron flux distribution axially through radial center of core UF_6 reactor, Beryllium in the reflector	117
5.21	Results of noise analysis of UF_6 reactor	118

TABLE OF CONTENTS

(Continued)

Page

FIGURES

(Cont'd)

6.1	Radial power distribution from bare catcher foils - UF_6 reactor with pure D_2O reflector.	126
6.2	Axial power distribution from bare catcher foils - UF_6 reactor with pure D_2O reflector.	127
6.3	Radial distribution of bare gold foil activity - UF_6 reactor with pure D_2O reflector	128
6.4	Axial distribution of bare gold foil activity - UF_6 reactor with pure D_2O reflector	129
6.5	Bare gold foil activity distribution in the reflectors UF_6 reactor with pure D_2O reflector.	130
7.1	Core support structure	151
7.2	Fuel element numbering system within the active core	152
7.3	Fuel tray and fuel sheet orientation	153
7.4	Cavity reactor fuel element loading schedule	154
7.5	Fuel element loading schedule - Mockup No. 2 pure D_2O reflector	155
7.6	Inverse multiplication - Mockup No. 2, pure D_2O reflector - Average of three channels	156
7.7	Control rod worth curves.	157
7.8	Aluminum locations for reactivity measurements . . .	158
7.9	Location of fuel elements which were reduced in loading by 10 sheets of fuel to measure the reactivity worth of fuel	159
7.10	Uranium worth within the active core - Mockup No. 2, pure D_2O reflector	160
7.11	Location of fuel elements involved in fuel worth measurements Mockup No. 2, pure D_2O reflector . .	161
7.12	Radial power distribution from bare catcher foils - Mockup No. 2, pure D_2O reflector.	162
7.13	Axial power distribution from bare catcher foils - Mockup No. 2, pure D_2O reflector	163
7.14	Catcher foil cadmium ratio radial profile - Mockup No. 2, pure D_2O reflector	164

TABLE OF CONTENTS

(Continued)

Page

FIGURES

(Cont'd)

7.15	Catcher foil cadmium ratio axial profile - Mockup No. 2, pure D_2O reflector	165
7.16	Radial distribution of bare gold foil activity - Mockup No. 2, pure D_2O reflector.	166
7.17	Axial distribution of bare gold foil activity - Mockup No. 2, pure D_2O reflector.	167
7.18	Bare gold foil activity distribution in the reflectors Mockup No. 2, pure D_2O reflector	168
7.19	Gold foil cadmium ratio radial profile - Mockup No. 2, pure D_2O reflector.	169
7.20	Gold foil cadmium ratio axial profile - Mockup No. 2, pure D_2O reflector.	170
7.21	Gold foil cadmium ratios in the radial and end reflectors Mockup No. 2, pure D_2O reflector	171
7.22	Thermal neutron flux distribution radially through axial center of core Mockup No. 2, pure D_2O reflector	172
7.23	Thermal neutron flux distribution axially through radial center of core Mockup No. 2, pure D_2O reflector	173
8.1	Inverse multiplication curve - average of three channels Mockup No. 2	185
8.2	Uranium worth within the active core - Mockup No. 2 .	186
8.3	Radial power distribution from bare catcher foils - Mockup No. 2	187
8.4	Axial power distribution from bare catcher foils - Mockup No. 2	188
8.5	Catcher foil cadmium ratio radial profile - Mockup No. 2, Beryllium in D_2O reflector	189
8.6	Catcher foil cadmium ratio axial profile - Mockup No. 2, Beryllium in D_2O reflector	190
8.7	Radial distribution of bare gold foil activity - Mockup No. 2, Beryllium in D_2O reflector.	191
8.8	Axial distribution of bare gold foil activity - Mockup No. 2, Beryllium in D_2O reflector	192

TABLE OF CONTENTS

(Continued)

Page

FIGURES

(Cont'd)

8.9	Bare gold foil activity distribution in the reflectors Mockup No. 2, Beryllium in D_2O reflector	193
8.10	Gold foil cadmium ratio radial profile - Mockup No. 2, Beryllium in D_2O reflector	194
8.11	Gold foil cadmium ratio axial profile - Mockup No. 2, Beryllium in D_2O reflector	195
8.12	Gold foil cadmium ratios in the radial and end reflectors Mockup No. 2, Beryllium in D_2O reflector	196
8.13	Thermal neutron flux distribution radially through axial center of core Mockup No. 2, Beryllium in D_2O reflector	197
8.14	Thermal neutron flux distribution axially through radial center of core Mockup No. 2, Beryllium in D_2O reflector	198
9.1	Core loading effects on fuel and aluminum worth	212
9.2	Comparison of fuel worths on the mockup and UF_6 experiments	213
9.3	Effect of core loading on aluminum worth with respect to uranium	214
9.4	Comparison of relative radial power distributions - beryllium in D_2O reflector	215
9.5	Comparison of relative axial power distributions - beryllium in D_2O reflector	216
9.6	Comparison of relative radial power distributions - pure D_2O reflector	217
9.7	Comparison of relative axial power distributions - pure D_2O reflector	218
9.8	Radial comparison of catcher foil cadmium ratios - beryllium in D_2O reflector	219
9.9	Axial comparison of catcher foil cadmium ratios - beryllium in D_2O reflector	220
9.10	Comparison of relative radial distribution of bare gold foil activity - beryllium in D_2O reflector	221
9.11	Comparison of relative axial distribution of bare gold foil activity - beryllium in D_2O reflector	222

TABLE OF CONTENTS

(Continued)

Page

FIGURES

(Cont'd)

9.12 Comparison of relative radial distribution of bare gold foil activity - pure D_2O reflector 223

9.13 Comparison of relative axial distribution of bare gold foil activity - pure D_2O reflector 224

9.14 Comparison of gold foil activity in the radial reflector beryllium in D_2O reflector. 225

9.15 Comparison of gold foil activity in the end reflector beryllium in D_2O reflector. 226

9.16 Radial comparison of gold foil cadmium ratios - beryllium in D_2O reflector. 227

9.17 Axial comparison of gold foil cadmium ratios - beryllium in D_2O reflector. 228

9.18 Gold foil cadmium ratio distribution in the reflector regions - beryllium in D_2O reflector 229

9.19 Comparison of radial thermal neutron flux distribution - beryllium in D_2O reflector 230

9.20 Comparison of axial thermal neutron flux distribution - beryllium in D_2O reflector 231

10.1 Nuclear model regions (side view of cylinder) 236

1.0 INTRODUCTION

This document contains the data from a series of cavity reactor critical experiments performed by the General Electric Company for the National Aeronautics and Space Administration, Lewis Research Center. The purpose of these experiments was to compare the critical mass, flux distributions, fuel worth, etc. obtained on uranium-foil mockups of a gaseous core with the results from an actual gas-core experiment. A series of experiments [1]* had been completed recently in which various sized gaseous cores of a cavity reactor were simulated by a distribution of sheets of metallic fuel, highly enriched in U^{235}. Previous work had also been performed at another installation on a cavity reactor with fuel lining the wall of the cavity [2] and on a dispersion of uranium-carbon rods within the cavity [3]. For the experiments discussed in this document, the fueled region of the reactor was centered within the cylindrical cavity and was approximately 40% of the full cavity volume. The mockup reactor was first tested in January 1967. The second mockup test was completed in November of the same year. The UF_6 reactor loading began May 11, 1967, was first made critical assembly on May 17, 1967, and was completed in September 1967.

The basic reactor assembly was the same as used for earlier cavity reactor experiments performed by the General Electric Company [1]. The cavity was cylindrical, 121.9 cm (4 ft) long by 182.9 cm (6 ft) in diameter and was completely surrounded by a 88.9 cm (35 in.) thick D_2O reflector-moderator on the ends and 89.5 cm thick on the sides. One set of configurations contained a ring of beryllium, 10.16 cm thick, surrounding the cavity region in the radial D_2O tank. There was a 30.5 cm (12 in.) diameter void through the center of the movable reflector tank. This hole was a mockup of exhaust nozzle.

Measurements were made to determine critical mass, reactor material worths within the cavity, power distribution, neutron flux distribution and rod worths. The beryllium in the radial reflector was removed and its reactivity worth determined with the UF_6 reactor and the second mockup assembly.

The first volume of the cavity reactor critical experiment report (Reference 1) contained the results of a series of experiments of different core diameters and different locations of the beryllium in the radial reflector. Calculations of the critical masses of these configurations did not correlate satisfactorily with the experimental results. A suspected difficulty was the presence of direct streaming paths through the fuel-sheet structure of the core. Therefore, it was felt necessary to perform an experiment with gaseous UF_6 in a uniform geometry. The comparison of the sheet fuel mockup with the UF_6 experiment showed a nominal 15% discrepancy in critical mass. An improved sheet fuel mockup design (herein called Mockup No. 2) was constructed and compared with the UF_6 experiment. A significant improvement was observed with the second mockup, giving a critical mass bias of 1.04 ± 0.02 with respect to the gas experiment.

* See page 237 for references

2.0 DESCRIPTION OF TEST SETUP AND PROCEDURES

2.1 Reactor Description

The overall reactor assembly was the same as previously used for other cavity reactor experiments performed by the General Electric Company. For a detailed description refer to Reference 1. The cavity was 121.9 cm long by 182.9 cm in diameter and was surrounded by 88.9 cm of D_2O. The D_2O contained about 0.22 mole percent H_2O. The total reactor assembly was a right cylinder 365.8 cm (12 ft) long by 304.8 cm (10 ft) in diameter. The D_2O was contained in two separate tanks, a movable tank mounted on a four-wheel dolly and a fixed tank. The two tanks separated at one end of the cavity. Therefore, the movable tank was essentially one of the end reflectors and was moved into position at the end of the cavity by an electric motor, gear driven, lead screw mechanism. The table separation permitted access to the cavity as well as providing definite shutdown of the reactor. The other end of the reactor contained clad boron carbide control rods which were used for normal reactor control and emergency scram. The number of control rods used could be varied, and the selection was such that the control rod worth was always greater than 4%Δk.

A ring of beryllium 10.16 cm thick and 109 cm long, as shown in Figure 2.1, was in the radial reflector region for most of the experiments. The beryllium was not centered axially over the cavity, but was off center 2.54 cm towards the end of the core continuing the control rods. This material was in the form of slabs, most of which were 40.6 cm wide. It took several of these slabs to go around the cavity and since they were rectangular pieces they did not form a perfect cylinder. The inner beryllium surface was at an average distance of 6.5 cm from the wet surface of the radial wall of the cavity. The distance from the center of each beryllium slab to a point tangent to the cavity wall was 5.8 cm. The 10.16 cm thick beryllium annulus contained about 4% D_2O, in the triangular gaps between the beryllium blocks.

Further description of the material within the cavity region for each configuration will be given in later sections of this report.

2.2 Experimental Procedures

The principal measurements made on these configurations were power and flux distributions and reactivity differences. Power distribution measurements were made with bare catcher foils. A catcher foil consists of a thin disc of aluminum, normally 1.429 cm (9/16 inch) in diameter, placed against a bare sheet of uranium and the two exposed in the reactor. The fission products from the surface of the fuel (outer 0.0006 cm layer) are embedded in the aluminum catcher foil and the activity of these fission products in the catcher foil are then beta counted for a measurement of activity which is proportional to power. Both bare and cadmium covered foils were used to map the cavity region. Cadmium covers were 0.0508 cm (0.020 in.) thick. The cadmium ratio is used to determine the ratio of total fissions to those occurring about the cadmium cutoff (nominally 0.45 ev).

Neutron flux measurements were made with bare and cadmium covered gold foils. The gold foils were the same diameter as the catcher foils. Foils of known thicknesses were used so that resonance integral self-shielding and thermal flux depression correction could be made. Thicknesses between 0.000508 and 0.00127 cm (0.0002 to 0.0005 inch) were used. The same cadmium thickness was used for gold as for catcher foils. Gold foils were exposed in the cavity and the reflector regions. The gold was counted on a 256-channel gamma-ray analyzer.

Control rods were remotely operated from the control room and rod positions were monitored on a digital voltmeter or ratiometer. Rod worth curves were not normally measured during each phase of testing. However, such measurements were obtained from the previous cavity reactors and the results were generally used for these experiments to evaluate k-excess and rod worths [1]. Tables 2.1 and 2.2 contain the tabular relative rod worth vs. ratiometer reading for a single actuator and for all rods operating as a "gang," respectively. Rod bumps were used as a measure of absolute rod worth and this was accomplished by leveling the reactor at a low power level and then pulling the rod or rods an increment and measuring the resulting period. The fractional worth of the total rod worth represented by the increment pulled was determined from Tables 2.1 or 2.2 and this value was divided into the reactivity worth of the period. The result was the total worth of the rod or rods pulled in the rod bump.

All periods were reduced to reactivity by using the normal inhour equation. The effective delayed neutron parameters used in the equation are given in Table 2.3. The ratio of β / β_{eff} for fission neutrons was assumed to be 1.0 for this system, since essentially all leakage occurred at low energies. Though the ratio of β / β_{eff} is slightly less than 1.0, this discrepancy is masked by the uncertainty in the gamma-neutron production. The calculated value of β / β eff. is 0.964. The value of the dollar, including gamma-neutron production was taken as 0.765% with a net uncertainty of about ±0.02%. The neutron lifetime was assumed to be 4.0 milliseconds.

Further description of the experimental procedures are given in Reference 1.

TABLE 2.1

Tabular Rod Worth - Actuator No. 4

Ratiometer Reading

Percent Inserted

	0	100	200	300	400	500	600	700	800	900
0	100.00	100.00	97.14	94.30	91.46	88.64	85.83	83.02	80.23	77.46
1000	74.72	72.00	69.29	66.61	63.94	61.32	58.72	56.15	53.63	51.16
2000	48.79	46.52	44.39	42.36	40.44	38.61	36.88	35.23	33.64	32.12
3000	30.65	29.23	27.87	26.55	25.27	24.04	22.84	21.69	20.57	19.50
4000	18.46	17.47	16.51	15.59	14.71	13.86	13.05	12.27	11.53	10.82
5000	10.14	9.50	8.88	8.29	7.73	7.21	6.71	6.23	5.77	5.34
6000	4.93	4.55	4.19	3.85	3.53	3.24	2.96	2.69	2.45	2.22
7000	2.01	1.81	1.63	1.47	1.32	1.18	1.05	.93	.82	.72
8000	.62	.54	.45	.37	.30	.24	.19	.15	.11	.08
9000	.06	.04	.02	00	00	00	00			

Difference Table

	0	100	200	300	400	500	600	700	800	900
0	0	0	2.86	2.84	2.84	2.82	2.81	2.81	2.79	2.77
1000	2.74	2.76	2.71	2.68	2.67	2.62	2.60	2.57	2.52	2.47
2000	2.37	2.27	2.13	2.03	1.92	1.83	1.73	1.65	1.59	1.52
3000	1.47	1.42	1.36	1.32	1.28	1.23	1.20	1.15	1.12	1.07
4000	1.04	.99	.96	.92	.88	.85	.81	.78	.74	.71
5000	.68	.64	.62	.59	.56	.52	.50	.48	.46	.43
6000	.41	.38	.36	.34	.32	.29	.28	.27	.24	.23
7000	.21	.20	.18	.16	.15	.14	.13	.12	.11	.10
8000	.10	.08	.09	.08	.07	.06	.05	.04	.04	.03
9000	.02	.02	.02	.00	.00					

TABLE 2.2

TABULAR

SUBCRITICAL ROD WORTH CURVE

CAVITY REACTOR

All Rods

Ratiometer Reading

	0	100	200	300	400	500	600	700	800	900
0	100.00	100.00	96.54	93.16	89.86	86.64	83.50	80.43	77.74	74.52
1000	71.68	68.92	66.23	63.62	61.08	58.61	56.22	53.90	51.64	49.45
2000	47.34	45.29	43.30	41.38	39.52	37.72	35.99	34.32	32.71	31.16
3000	29.66	28.21	26.82	25.48	24.19	22.95	21.77	20.63	19.53	18.48
4000	17.48	16.52	15.60	14.72	13.88	13.08	12.32	11.59	10.89	10.23
5000	9.59	8.99	8.42	7.87	7.34	6.85	6.38	5.93	5.50	5.10
6000	4.72	4.35	4.01	3.68	3.38	3.08	2.81	2.55	2.30	2.08
7000	1.86	1.66	1.47	1.30	1.14	.99	.85	.73	.62	.52
8000	.43	.35	.28	.22	.18	.14	.11	.09	.08	.08

DIFFERENCE TABLE

	0	100	200	300	400	500	600	700	800	900
0	0	0	3.46	3.38	3.30	3.22	3.14	3.07	2.99	2.92
1000	2.84	2.76	2.69	2.61	2.54	2.47	2.39	2.32	2.26	2.19
2000	2.11	2.05	1.99	1.92	1.86	1.80	1.73	1.67	1.61	1.55
3000	1.50	1.45	1.39	1.34	1.27	1.24	1.18	1.14	1.10	1.05
4000	1.00	.96	.92	.88	.84	.80	.76	.73	.70	.66
5000	.64	.60	.57	.55	.53	.49	.47	.45	.43	.40
6000	.38	.37	.34	.33	.30	.30	.27	.26	.25	.22
7000	.22	.20	.19	.17	.16	.15	.14	.12	.11	.10
8000	.09	.08	.07	.06	.04	.04	.03	.02	.01	.00

TABLE 2.3

Effective Delayed Neutron Parameters

Group	β_i	λ_i
1	0.000210	0.012400
2	0.001410	0.030500
3	0.00127	0.111000
4	0.002550	0.301000
5	0.000740	1.100000
6	0.000270	3.000000
7	0.000780	0.277000
8	0.000240	0.016900
9	0.000084	0.004810
10	0.000040	0.001500
11	0.000025	0.000428
12	0.000028	0.000117
13	0.000004	0.000044
14	0.000001	0.000004
	0.007652	

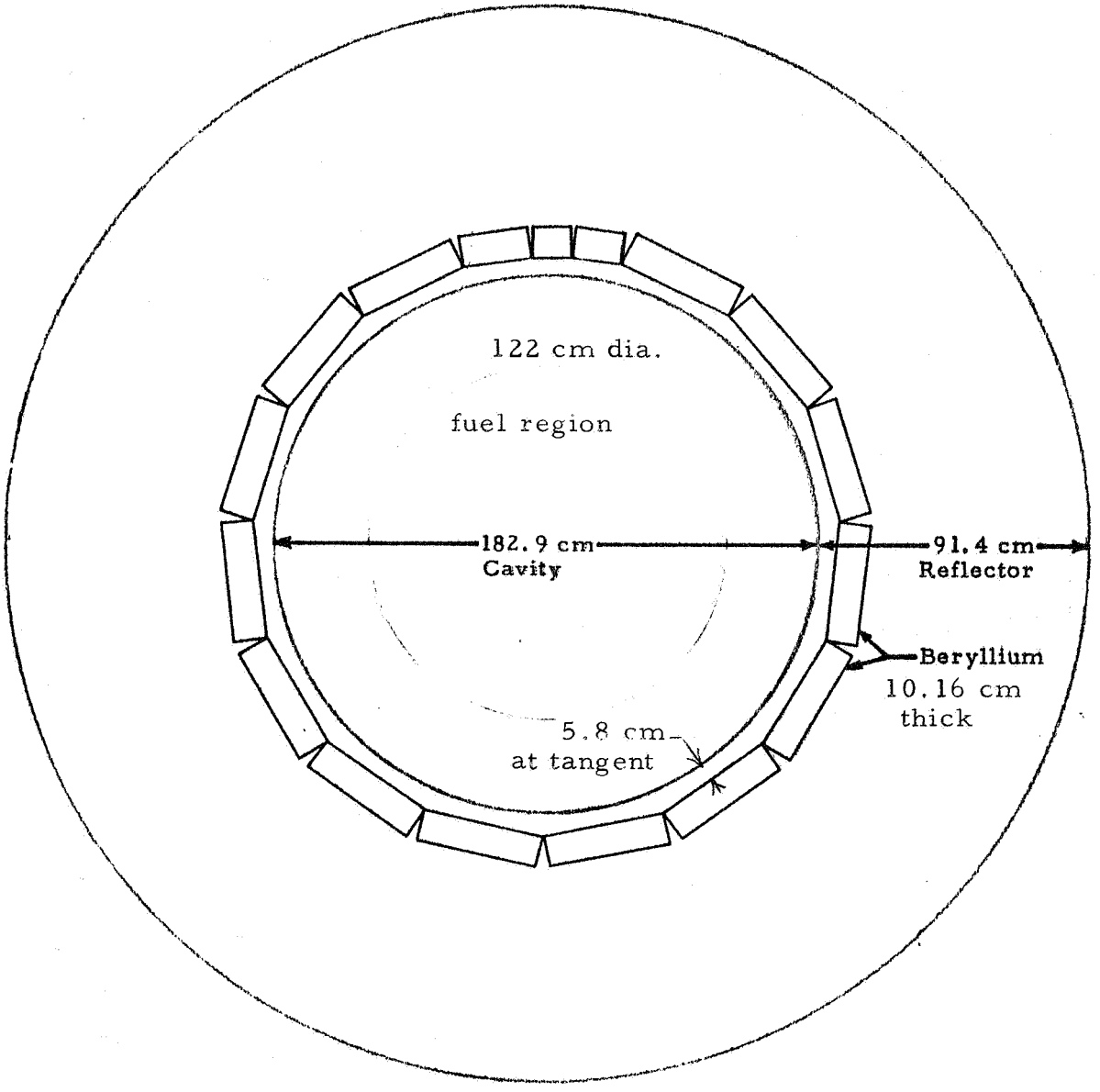


Fig. 2.1 Location of beryllium in the radial reflector

3.0 SUMMARY OF TEST RESULTS

The purpose of the gaseous UF_6 experiments and their equivalent sheet-fuel mockups was to determine the adequacy of the sheet fuel configuration. The orientation, distribution and arrangement of the sheets will affect the interaction probability of neutrons crossing the cavity. Since it is impractical to describe the sheet arrangement in a nuclear model for calculation, a uniform gaseous distribution is generally assumed. Therefore, the gas experiment represents the ultimate for correlation purposes, and a satisfactory foil mockup should closely duplicate its characteristics of reactivity, flux distribution, etc. Unfortunately, construction differences occurred between the gas experiment and its mockup, the most notable being the fact that the gaseous configuration contained fluorine (which fortunately was worth very little) while the mockup contained aluminum within the core region (which was worth several kg of uranium loading). The aluminum in the core of the mockup experiment was of considerable quantity (160 kg); the aluminum was not included in the gas experiment because it was desired to keep this configuration as "clean" and uniform as possible. Other differences occurred because it was not feasible to exactly duplicate the size and cylindrical configuration of the gas experiment when constructing the mockup experiment. Uranium foil sizes effectively quantize the dimensions that can be simulated, and a circular outer boundary was compromised by using a slightly irregular octagonal cross section in the second mockup experiment. However, the foil arrangement in mockup No. 2 allowed fewer irregularities in total nuclear path lengths through the core. The following sections summarizes these differences and present conclusions concerning the degree to which the mockup experiments differed from the UF_6 gas experiment.

3.1 Fundamental Characteristics

The characteristics of the cavity reactor are such that the absorption cross section of the materials of the reactor are extremely important. Even for those materials that have unusually small absorption cross sections, such as beryllium and deuterium, small impurities or minor changes in location may have an extremely significant effect on the multiplication factor. The aluminum, used for structure because of its relatively low cross section, accounts for about 30% of the neutron losses, while leakage from the system accounts for only nominally 20% of the losses. Thus, an accurate representation of the location and quantity of the aluminum is a prerequisite to an adequate understanding of the system. But the exact description is quite complex. Nevertheless, both cylindrical two dimensional and spherical one dimensional representations that can be employed for nuclear models are given in Section 10. The basic dimensions and masses of the configurations are given in Tables 3.1 to 3.3.

3.2 Geometry

The gas experiment was performed with a core that was perfectly cylindrical (121.9 cm in diameter by 108.6 cm long), except for the two flux traverse tubes penetrating the tank and accounting for 0.1% of the normal cylindrical volume.

The mockup No. 1 fuel, placed on screens, was confined to the same dimensions as the gas in the UF_6 experiment with a minor exception that the fuel length was probably, on the average, 0.6 cm longer in the mockup experiment. Another minor difference was the two "gray" gaps where the screen support rods passed through the screens. However, all these rods were not aligned, so that perfect streaming paths in which no fuel was encountered did not exist. This mockup is further described in Section 4.0 and by Figures 4.1 to 4.3.

The mockup No. 2 fuel volume was quantized into boxes (55.8 square cm frontal area and 109.5 cm long) as shown in Figure 7.3. The resulting volume of the fuel region was larger than in the gas experiment. To reduce the volume by reducing the area would have resulted in a geometry less circular than that adopted. Since data is available on the effect of a radial change in the fuel volume (Reference 1, p. 50) and none on the effect of uneven boundaries, the evenness of the boundary was selected as the more important factor.

Several approaches to the differences in interaction rates between the slightly different sized cores of the gaseous experiment and of the mockup No. 2 experiment are discussed in detail in Section 9. In summary, the conclusion is that the mockup No. 2 experiment had an effective fuel diameter of 130 cm compared to the gaseous diameter of 121.9 cm, but in the extra annular region, the fuel density was only 25% of that in the remaining core. This difference, plus the 0.9 cm longer length of the mockup should have resulted in an approximate 1% lower critical mass in the mockup, all other conditions and structural details being equivalent. Two method of computing this correction were employed; one in which the fuel density vs core radius data in Reference 1 was employed, and another in which this same data was converted to mean chord lengths and fuel densities in order to compute the correction to fuel mass.

3.3 Critical Mass Comparisons

All configurations were made critical with a slight amount of excess reactivity and the resulting multiplication factor was determined with an accuracy of approximately $\pm 0.01\%\Delta k$ using period measurements. Fine adjustments in fuel loading were impractical, so that k-excess was generally in the $0.5\%\Delta k$ range and was determined from rod worth and shape measurements. The resulting measured fuel masses* and excess reactivities are listed in Table 3.4, for the as-measured configurations. Also listed are the various measured corrections to these reactivities for effects which would be difficult if not impossible to evaluate analytically. As will be noted, the final excess reactivity of a convenient and analytically describable system without gap or end nozzle such as given in Section 10 is in the range of 2 to 2.5% excess reactivity.

---

* Since the fuel loading was adjusted to provide reactivity for various experimental measurements, critical mass values with excess reactivity around the value of $0.5\%\Delta k$ were selected.

Comparison between the gaseous core experiments and the mockups requires that an exchange correction of fuel for the aluminum in the core of the mockups be made. Other smaller corrections are for fluorine in the UF_6 and, in the case of mockup No. 2, a correction for a difference in fuel region dimensions. The sum of these corrections represents from 2 to 4 kg of uranium, or as much as 3% in reactivity. This difference is sufficient to affect perturbation worth values when extrapolated to such limits. Therefore, comparisons have been made in both directions; first, by removing aluminum from and adding fluorine to the mockup reactors, and second, by adding aluminum to and removing fluorine from the gas-core reactors. In each case, k-excess differences were applied after making these corrections. The resulting configuration was compared with its counterpart, on which the 1% fuel loading correction for outer boundary irregularities was made. These corrections and their uncertainties are discussed in detail in Section 9.0, and summarized in Table 3.5.

The comparison of the mockup No. 1 with the gaseous experiment shows a 15% bias in fuel loading, with the mockup having the higher loading. The bias is in the expected direction, for the mockup fuel sheets were oriented only in two directions on screens that were spaced about 3.8 cm apart. Axial streaming paths for neutrons and the interaction deficiencies in the screen gaps near the edge of the core were probably the principal reasons for the fuel loading bias. Since the volumes in which the fuel was confined were nominally identical, it appears that the deduced bias of 15% is almost entirely caused by the distribution of fuel sheets. Therefore, the revised fuel arrangement of Mockup No. 2 with fuel sheets oriented in three directions was constructed.

Since the mockup No. 2 with its effectively larger fuel volume requires both a geometric correction and a correction for the aluminum in the core, the uncertainty of the comparison to the gaseous experiment is larger. The resultant average ratio of mockup No. 2 to the gaseous fuel masses is 1.04 ± 0.02. The bias factor with the configuration having the beryllium and D_2O reflector is substantially less than on the all D_2O reflector case. The 23.5 kg loading of the beryllium configuration lies midway between configurations for which the aluminum worth had been measured. This was not the case for the all D_2O configuration, in which an extrapolation was required from the core loading of approximately 20 kg, where the aluminum worth data ends, back to a loading of 17 kg corresponding to the loading of the UF_6 reactor. The reason for the larger uncertainties and hence the ostensibly larger biases in the results for the all D_2O configuruation are apparent.

In summary, it appears as if the mockup No. 1 contained an experimental bias which was approximately 15% in fuel loading. Such a bias can be assumed to apply to all other experiments utilizing the mockup No. 1 core structure and reported in Reference 1. On the other hand, the mockup No. 2 core structure probably contained a bias in fuel loading of only about 4%, i.e., the mockup loadings contain 4% more fuel than the equivalent gaseous experiment.

3.4 General Flux and Power Distribution Comparisons

The cavity reactors, which have been tested up to and including the reactor assemblies discussed in this data report, cover a wide range of fuel loadings. In addition, the radial reflector has contained both pure D_2O and D_2O with Be. The bare catcher foil data, which represents relative total fission power per unit fuel mass, have been measured within the cavity region and reported either in Reference 1 or in this report for each of these configurations. In order to show the total change in fission power distribution over the range of core loadings, reported in this volume, comparative radial and axial power profiles were selected and plotted for the extreme fuel loadings. These are presented in Figures 3.1 and 3.2. The lightest loading represents the gas core with a pure D_2O reflector while the heaviest loaded core is the mockup with Be in the radial reflector. These two configurations therefore, have two major differences, the fuel loading and the reflector. Measurements have not been made which clearly separate the effects of these two variables on fission power distribution within the cavity region. It is strongly believed that the change in power profiles is primarily caused by differences in fuel loading, while the change in the radial reflector has very little effect.

As expected, the heavy fuel loadings caused considerably more flux attenuation than the higher loading, as will be noted from Figure 3.1. The radial outer edge of the fuel shows a 42.5% increase in power gradient with respect to the core center for a 56.6% increase in fuel loading (ignoring any minor effects of the reflector changes). The axial power profile showed similar effects at the ends of the core as seen on the outer radius. The two configurations shown in Figure 3.2 give a 21.6% difference at the separation plane (axial position of 205.9 cm) and 38.4% difference at the other end of the core. The change was less at the separation plane and it will also be noted that the power is higher at the separation plane than at the other end of the core. This latter effect was caused by the mockup exhaust nozzle, a 30.5 cm diameter hole at the separation plane through the end reflector tank which was used to mockup the exhaust nozzle.

Neutron flux measurements were obtained from the various configurations using bare and cadmium covered gold foils. The gold foils have been nominally 1.429 cm (9/16 inch) in diameter by 0.00127 cm (0.0005 inch) thick and the cadmium covers were 0.0508 cm (0.020 inch) thick. The average bare and cadmium covered gold foil activity per watt of reactor power, corrected to the 20 minute foil exposure shutdown, time, was obtained from Configurations 4, 5, 6 (Reference 1) and the two mockup and UF_6 reactors. These data are shown in Figures 3.3 and 3.4 for the radial and end reflectors, respectively. All of these data are with beryllium in the radial reflector. Each of these curves are labeled with the standard deviation among all the configutations. Configuration 5 and mockup No. 1 results from the end reflector were not used because of the suppressive effects of rods which were inserted near the measurement region on these two reactors. It will be noted that the spread in the bare gold data over the range of configurations included in the average was reasonably small, being only ±5% in the end reflector and ±8% in the radial reflector. The radial reflector showed the larger error primarily because of the different positions of the beryllium within the radial reflector.

The larger error or variations associated with the cadmium covered foils was due in part to the low counting rates for these foils, and the actual spread in activity between the various configurations may be significantly less.

The thermal flux within the reflector regions was calculated from the bare and cadmium covered gold foils for the above configurations and the average values for all the configurations are given in Figure 3.5. Here, again, the radial reflector shows a larger spread in results than the end reflector, due in part to the larger errors from the source data given in Figure 3.3. The thermal flux peaks around 20 cm from the cavity wall. The end reflector has the highest flux level, being about 38% above the radial reflector flux at the peak. This difference can likely be explained by the close proximity of the end reflector to the fueled region which resulted in a higher density of fast neutrons entering the end reflector at the cavity-reflector interface.

3.5 Material Worth Comparisons

Fuel worth measurements were obtained on each of the configurations and are summarized in Table 3.6. Included in this table are all the values reported in Reference 1 and two measurements obtained from experiments which were conducted following the mockup experiments. These values are also presented graphically in Figure 3.6 which gives a least squares curve fit to all of the data of:

$$\text{fuel worth } (\%\Delta k)/kg = 79.14 \left[\text{ fuel mass } (kg) \right]^{-1.472}$$

This fit has a standard deviation of ±12.2%. Considering the geometrical and minor spectral differences between the various configurations, this much deviation from a smooth functional dependence of fuel worth is to be expected. For instance, in every case the fuel worths for the mockup reactors were higher than for the UF_6 fueled reactors for comparable total fuel loadings. The reason for this difference, as explained in detail in Section 9.1.2, is principally because of geometrical differences in the outer core boundary. The irregular outer boundary of the mockup No. 2 reactor resulted in a significant amount of fuel jutting out beyond the otherwise smooth cylindrical boundary. This fuel was thus in a higher worth region, and the overall difference in average worth of fuel in the mockup reactors was 15 to 20% higher than in the gaseous core reactors (see Figure 9.1). The same difference observed with the mockup No. 1 reactor was more the result of the overall experimental bias caused by the orientation of the fuel sheets in the core. In neither case is the aluminum structure of the mockup considered a significant factor in the fuel worth differences. The absorption of the aluminum structure was only approximately 3% of the absorption of the fuel. Calculations of fuel worth also showed virtually no dependence on the amount of aluminum structure.

The worth of type 1100 aluminum within the active core region was also measured over a wide range of core loadings after construction of the second mockup fuel support structure. These results are presented in Figure 3.7 as a function of kg of aluminum per kg of uranium and in

Figure 3.8 as the reactivity worth per kg of aluminum. Included in these data are the stainless steel liner configurations shown at the end of Table 3.6 and also the aluminum worth for the hold-down straps on mockup No. 1 (type 6061 Al). Between a core fuel loading of about 20 to 50 kg, the ratio of aluminum to uranium worth is linear and follows the expression kg Al/kg U = 7.24 - 1.028 [core fuel loading (kg)]. The relationship then flattens out and changes only by 16% from a core fuel loading of 57 to 89 kg.

3.6 Temperature and Impurity Effects

Two minor corrections not considered in the previous comparisons between the various configurations are the effects on reactivity caused by the worth of fuel impurities and moderator temperature changes. The impurity content of the sheet fuel was nominally 3.3% by weight. Reported critical masses give only the uranium content. No reactivity correction has been made for these impurities. The impurities are mostly oxygen, fluorine, and carbon and their net effect is unknown. However, they should have less of a negative effect on reactivity than does the more highly absorbing aluminum In the 25 kg loading, the impurity content is 0.8 kg. If this were aluminum, the effect would be 23 gm of fuel or -0.015%Δk. Since both fluorine and carbon were measured to have a negative effect on reactivity, it is unlikely that the impurities would not also be negative. The above value, based on more poisonous aluminum, is not large enough to significantly affect the quoted critical mass results compared to the accuracy of those results.

The moderator temperature varied by 5 degrees Centigrade throughout the testing period. The mockup experiments were generally run in cold weather, and the cell and moderator temperatures were in the 22° to 24°C range. The UF_6 experiments for which heat was required were run in warm weather. Refrigerated cooling was not available for the cell and the moderator temperatures reached 27°C at times. Unfortunately the temperature coefficient is not accurately known at these low temperatures. In fact, one measurement indicated the coefficient was positive in this range. However, assuming the minimum negative coefficient shown on p. 367 of Reference 1, the effect of 5°C is approximately 40 gm of fuel of 0.024%Δk, a relatively insignificant effect.

TABLE 3.1

Characteristics of Cavity Reactor Critical Experiment

Total volume of heavy water (with 0.22% H_2O) (with no plug in exit nozzle)			27.8×10^6 cm^3
Total mass of type 6061 aluminum in D_2O tanks (excluding the cavity walls)			221 kg
Mass of aluminum (type 6061) walls that mate at table separation plane (does not include cavity walls)			529 kg
Radial cavity-wall thickness (aluminum)			0.952 cm
End cavity-wall thickness (aluminum)			1.27 cm
UF_6 tank -	total aluminum mass (type 6061)		245 kg
	Teflon insulation mass		7.9 kg
	Internal volume (1)		1.266×10^6 cm^3
	Inside diameter		121.9 cm
	Inside length		108.6 cm
Mockup fueled region (2)		Mockup 1	Mockup 2
	Fuel length (nominal)	109 cm	109.2 cm
	Fuel diameter	122 cm	(effective 125 cm)
	Fuel area	11.6×10^3 cm^2	12.3×10^3 cm^2
	Fuel volume	1.26×10^6 cm^3	1.34×10^6
	Mass of Al (type 6061)	40.8 kg	3.0 kg (3)
	Mass of Al (type 1100)	---	158 kg
	Mass of Al (type 3003H14)(4)	40.5 kg	---

NOTE: All values are accurate to the number of significant figures quoted.

(1) Does not include the volume of the flux measurement tubes.
(2) Includes all materials not used to simulate the 246 kg UF_6 tank.
(3) This material was miscellaneous pads, bolts, etc. and was mostly between the core and the cavity wall.
(4) This was the type of aluminum in the screen material and it contained the following nominal w/o impurities: Si, 0.6; Fe, 0.7; Cu, 0.2; Mn, 1.0 to 1.5; Zn, 0.1; other, 0.15. There was, therefore, a minimum of 0.4 kg Mn in the screens.

TABLE 3.2

Material Compositions of Cavity Reactor Critical Experiment

Uranium hexafluoride (UF_6 fuel)

	w/o	
Uranium composition	93.18	U^{235}
	0.62	U^{234}
	0.3	U^{236}
	5.9	U^{238}

UF_6 gas purity assumed to be 99.9%

Uranium metal foil fuel for mockup

	w/o	
Uranium	(96.7 ± 0.5)	
Impurities	(3.3 ± 0.5)	nominally carbon, oxygen and fluorine

(Note: all final critical mass specifications are given in terms of total uranium, not total fuel, since the latter would include impurities.)

	atom %	
Uranium composition	93.18	U^{235}
	0.98	U^{234}
	0.52	U^{236}
	5.32	U^{238}

Heavy Water

H_2O impurity content = (0.22 ± 0.02) mole %

TABLE 3.3

Beryllium Radial Reflector Characteristics

Length of beryllium (Refer to Figure 10.1 for Be axial position)	108.9 cm
Nominal thickness of beryllium slabs	10.16 cm
Total volume of beryllium	0.69×10^6 cm^3
Closest location of Be to cavity wall (inside tangent)	5.8 cm
Furthest location of Be from cavity wall (outside corner)	13.0 cm
Volume of supporting hardware *	
Stainless steel	1079 cm^3
Aluminum	26940 cm^3
Teflon	4290 cm^3

* Most of the supporting hardware is at the extreme ends of the beryllium

TABLE 3.4

"Critical" Configuration Data

Configuration	UF_6 All D_2O	Mockup No. 2 all D_2O	UF_6 Be-D_2O	Mockup Be-D_2O No. 1	Mockup Be-D_2O No. 2
Uranium [1] Mass (kg)	17.27	20.78	23.55	28.3	27.25
Fuel impurity mass (kg)	--	0.71	--	0.4	0.92
UF_6 Mass (kg)	25.65	--	34.97	--	--
Measured Excess Reactivity (%Δk)	0.65	0.23	0.50	0.61	0.56
Corrections to system [2] reactivity (%Δk)					
a. Teflon insulation	0.26	--	0.26	--	--
b. Valves and tubing	0.23	--	0.23	--	--
Total [2] excess reactivity (%Δk) on comparative basis	1.14	0.23	0.99	0.61	0.56

(1) Uranium masses are accurate to within an estimated ± 1%. The isotopic composition is listed in Table 3.2.

(2) The corrections to the excess reactivity do not include measured values of 0.70%Δk for the end nozzle and 0.55% for the approximately 1.14 cm air gap at the table separation plane. An additional 1.25%Δk should be added to the above excess reactivities if the gap and nozzle are not considered.

TABLE 3.5

Critical Loading Comparisons

Correction of Mockups to Equivalent Gaseous Reactors	All D_2O Reflector	Be and D_2O Reflector
UF_6 loading (uranium)	17.27 kg	23.55 kg
k-excess	1.14%Δk	0.99%Δk
Corrected loading to larger effective diam	17.1±0.2 kg	23.3±0.3kg
Mockup No. 1 loading	---	28.3 kg U
at k-excess of		0.61%Δk
Corrected for Al		-2.0 kg U
Corrected for F		+0.25 kg U
Corrected to UF_6 k-excess		+0.50 kg U
Corrected loading		27.1±0.3 kg U
Bias Mockup/UF_6		1.151±0.03
Mockup No. 2 loading	20.78 kg U	27.25 kg U
at k-excess of	0.23%Δk	0.56%Δk
Corrected for Al	-2.9 kg U	-3.5 kg U
Corrected for F	+0.10kg U	+0.23 kg U
Corrected to UF_6 k-excess	+0.74 kg U	+0.49 kg U
Corrected loading	18.7±0.4 kgU	24.4±0.3 kg U
Bias Mockup/UF_6	1.093±0.03	1.047±0.02
Mockup No. 2 average fuel loading bias		1.06 ± 0.02

Correction of Gaseous Reactors to Equivalent Mockups	Mockup No.1	Mockup No. 2	
	Be & D_2O Reflector	All D_2O Reflector	Be & D_2O Reflector
Mockup loading (U)	28.3 kg	20.78	27.25
k-excess (%Δk)	0.61	0.23	0.56
Mockup loading (U) corrected to UF_6 geometry	28.3kg	21.0 kg	27.5 kg
UF_6 loading (U)	23.5 kg	17.3 kg	23.5 kg
k-excess (%Δk)	0.99	1.14	0.99
Correction for Al	+2.0 kg U	+3.6 kg U	+4.9 kg U
Correction for F and k-excess	-0.9 kg U	-1.1 kg U	-1.2 kg U
Corrected loading (U)	24.6 kg	19.8 kg	27.2 kg
Bias (Mockup/UF_6)	1.151±0.03	1.061±0.03	1.011±0.002
Average bias	1.151±0.03	1.03±0.02	
Overall average bias	1.15±0.03	1.04±0.02	

TABLE 3.6

Summary of Fuel Worth

Configuration	Core Loading (kg U)	Uranium Worth (%Δk/kg U)	$\frac{\Delta k/k}{\Delta m/m}$
1	10.6	3.017 ± 0.275	0.349 ± 0.030
2B	19.7	0.902 ± 0.560	0.184 ± 0.114
3A	14.0	1.760 ± 0.296	0.255 ± 0.043
3B	14.5	1.681 ± 0.168	0.252 ± 0.025
4	20.8	0.837 ± 0.055	0.180 ± 0.012
5A	20.8	1.010 ± 0.106	0.217 ± 0.023
5B	19.4	0.826 ± 0.031	0.165 ± 0.006
6	19.1	1.074 ± 0.113	0.212 ± 0.022
7B	20.2	0.831 ± 0.055	0.174 ± 0.011
Mockup No. 1 - Be	27.8	0.644 ± 0.055	0.185 ± 0.016
Mockup No. 2 - Be	27.2	0.703 ± 0.034	0.187 ± 0.009
Mockup No. 2 - No Be	20.8	1.105 ± 0.055	0.222 ± 0.011
UF_6 - Be	23.4	0.766 ± 0.054	0.179 ± 0.013
UF_6 - Be	24.2	0.627 ± 0.015	0.152 ± 0.004
UF_6 - Be	24.9	0.598 ± 0.007	0.149 ± 0.002
UF_6 - Be	25.3	0.612 ± 0.035	0.155 ± 0.009
UF_6 - Be	26.0	0.588 ± 0.043	0.152 ± 0.011
UF_6 - No Be	17.7	1.060 ± 0.020	0.188 ± 0.004
SS liner in cavity	36.6	0.468 ± 0.023	0.172 ± 0.008
SS liner and polyethylene in cavity	57.3	0.208 ± 0.010	0.116 ± 0.006
SS liner andpolyethylene in cavity	89.6	0.116 ± 0.006	0.104 ± 0.005

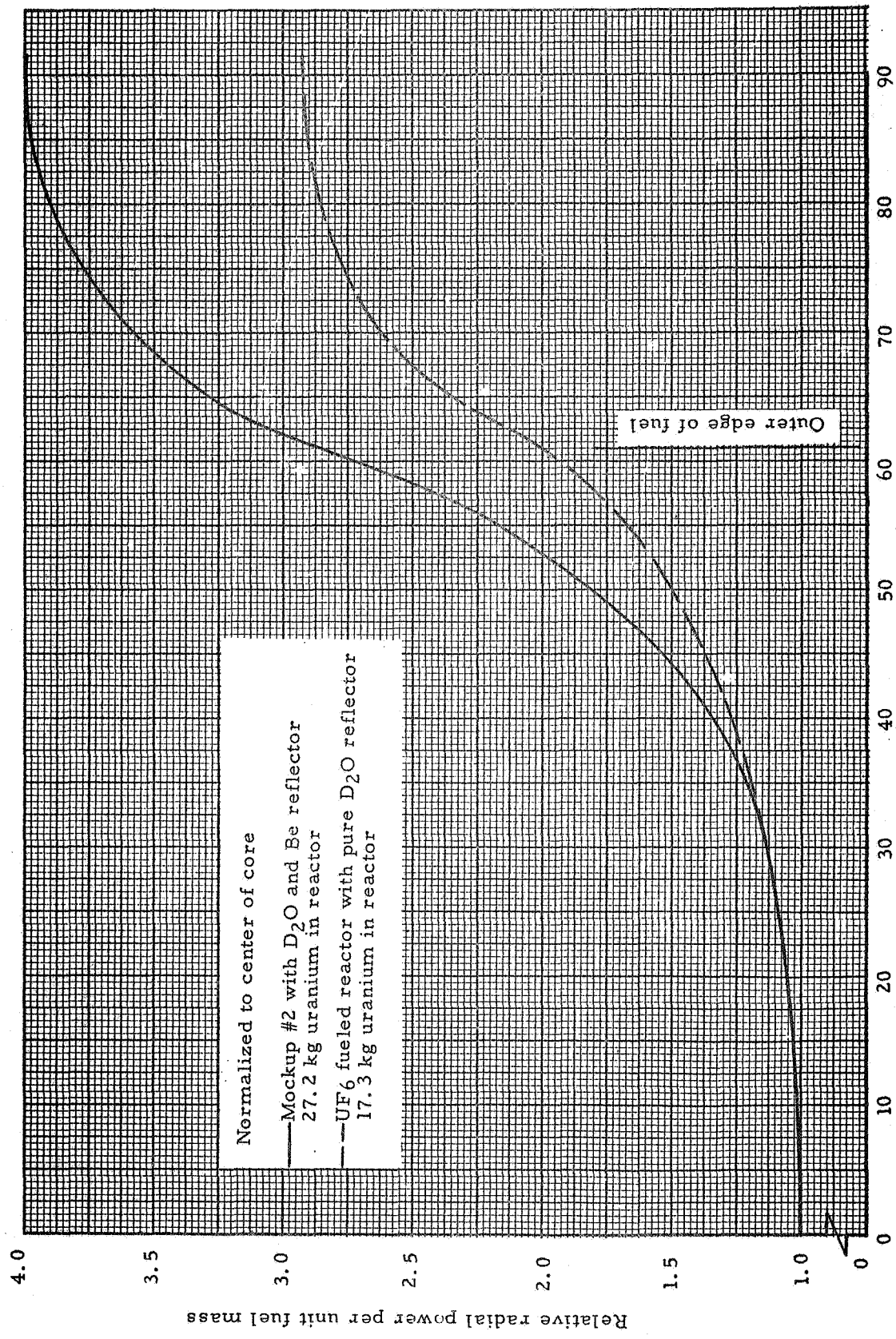


Fig. 3.1 Comparison of radial power distribution within the cavity between Mockup No. 2 with beryllium in the radial reflector and UF_6 reactor with pure D_2O reflector

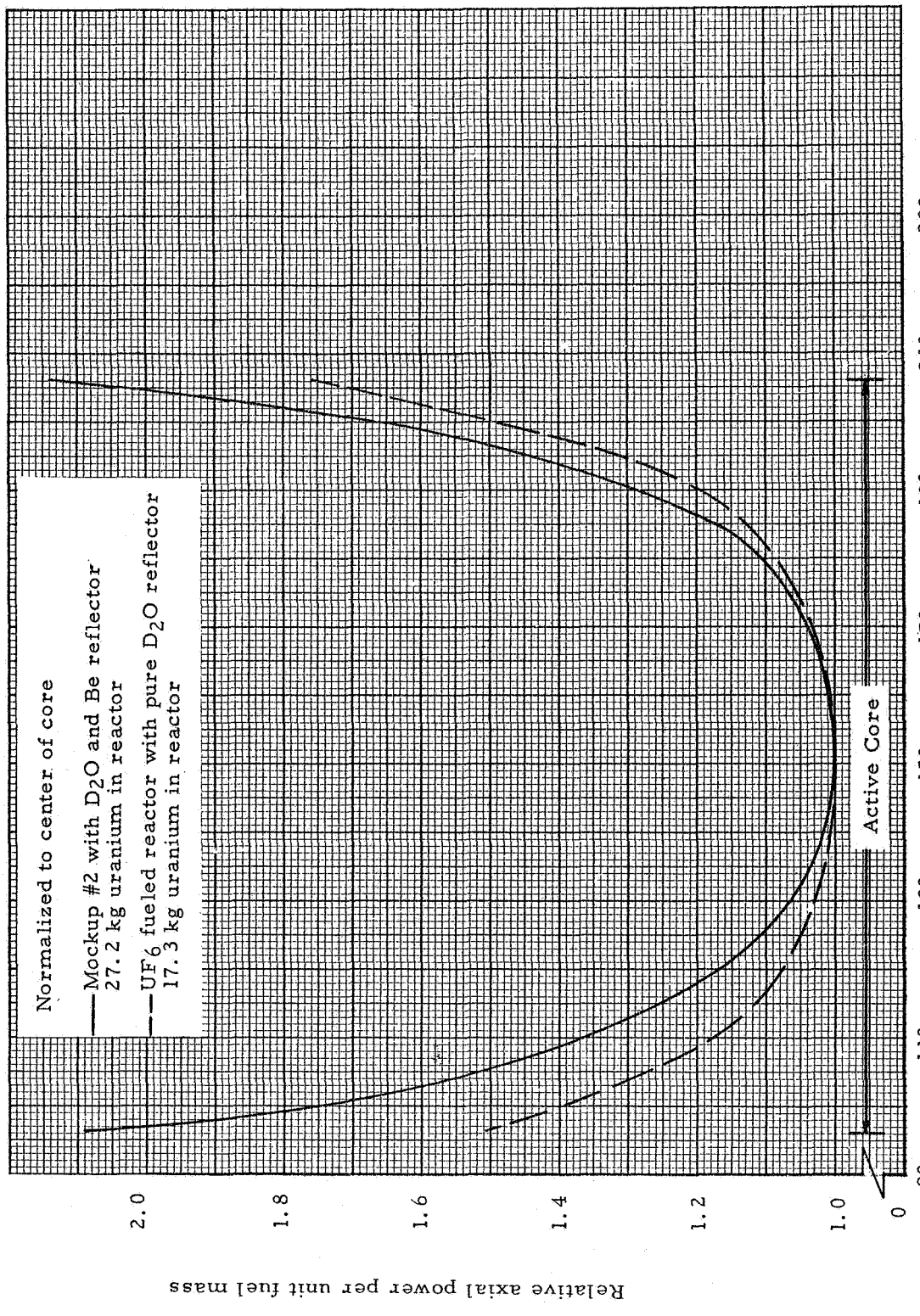


Fig. 3.2 Comparison of axial power distribution within the cavity between Mockup No. 2 with beryllium in the radial reflector and UF_6 reactor with pure D_2O reflector

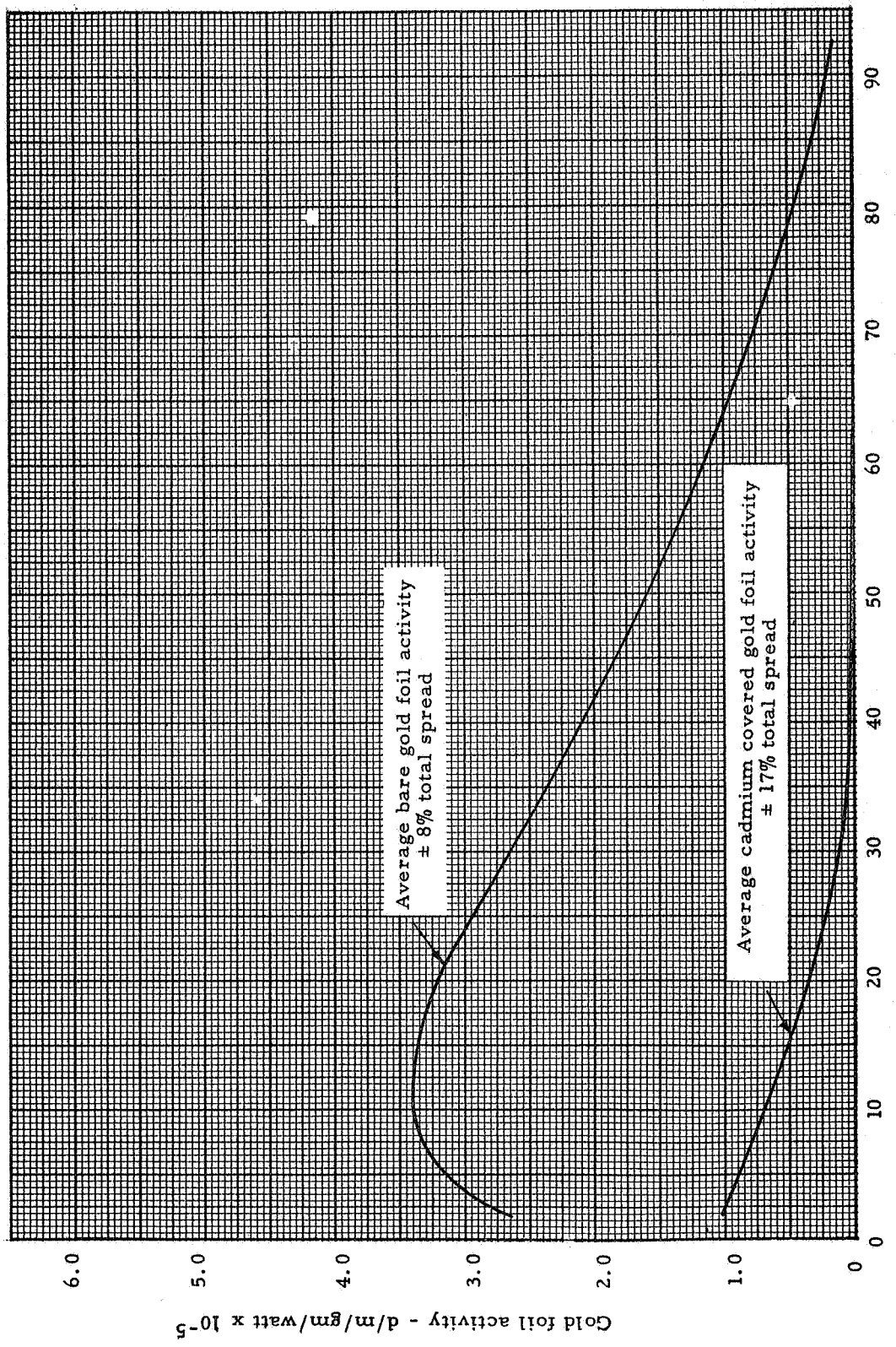


Fig. 3.3 Average gold foil activity per watt of reactor power in the radial reflector

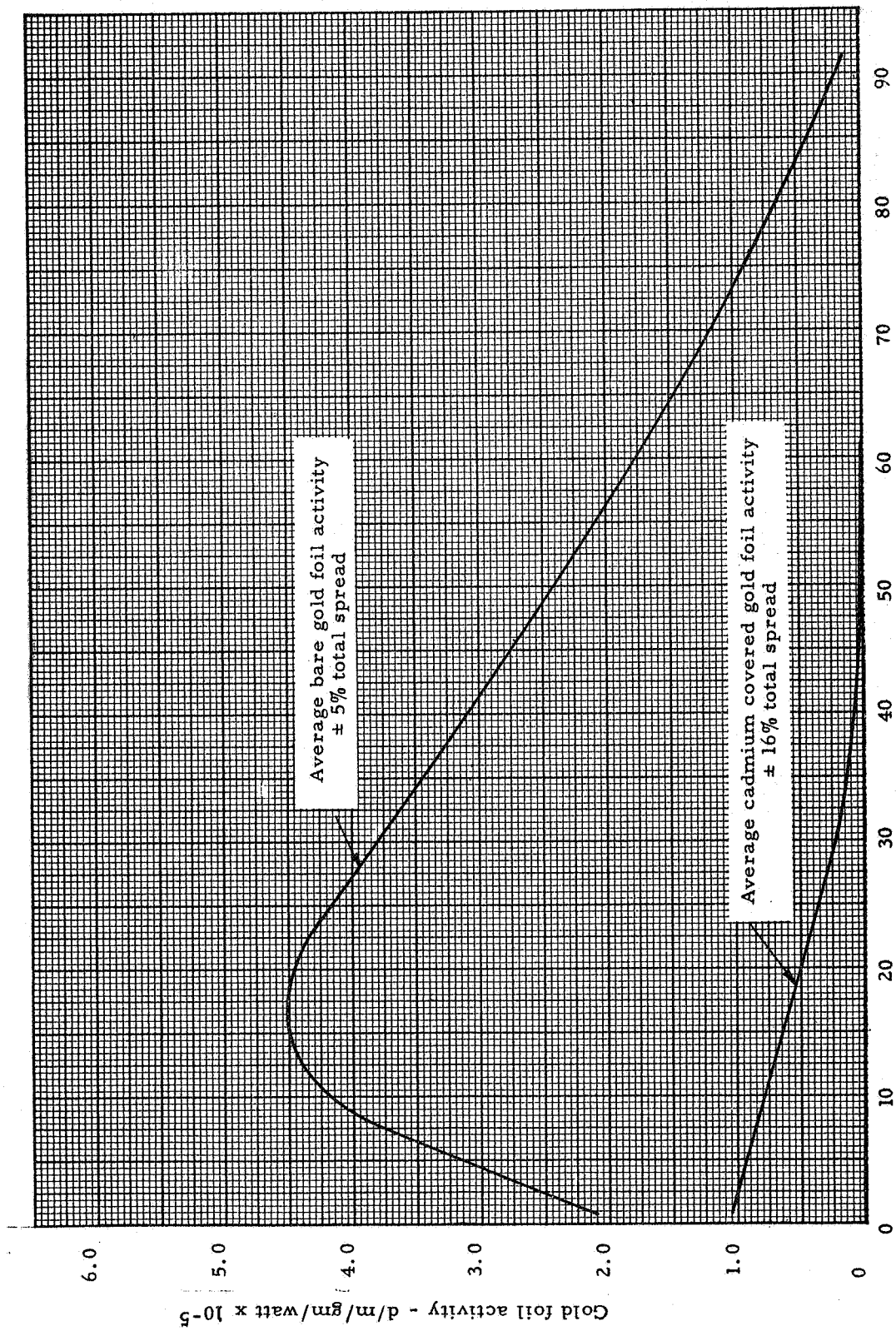


Fig. 3.4 Average gold foil activity per watt of reactor power in the end reflector

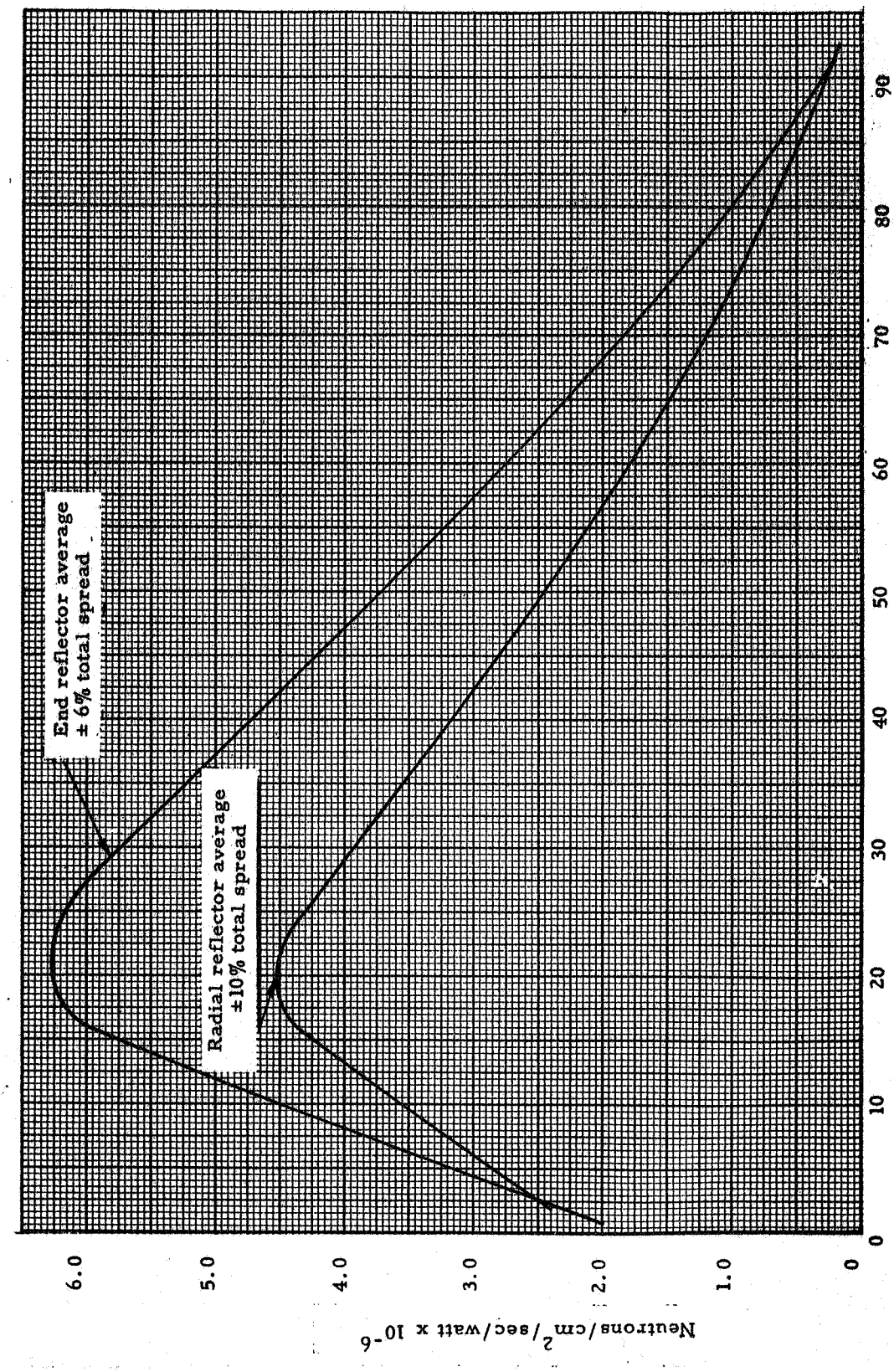


Fig. 3.5 Average thermal neutron flux per watt of reactor power in the reflector regions

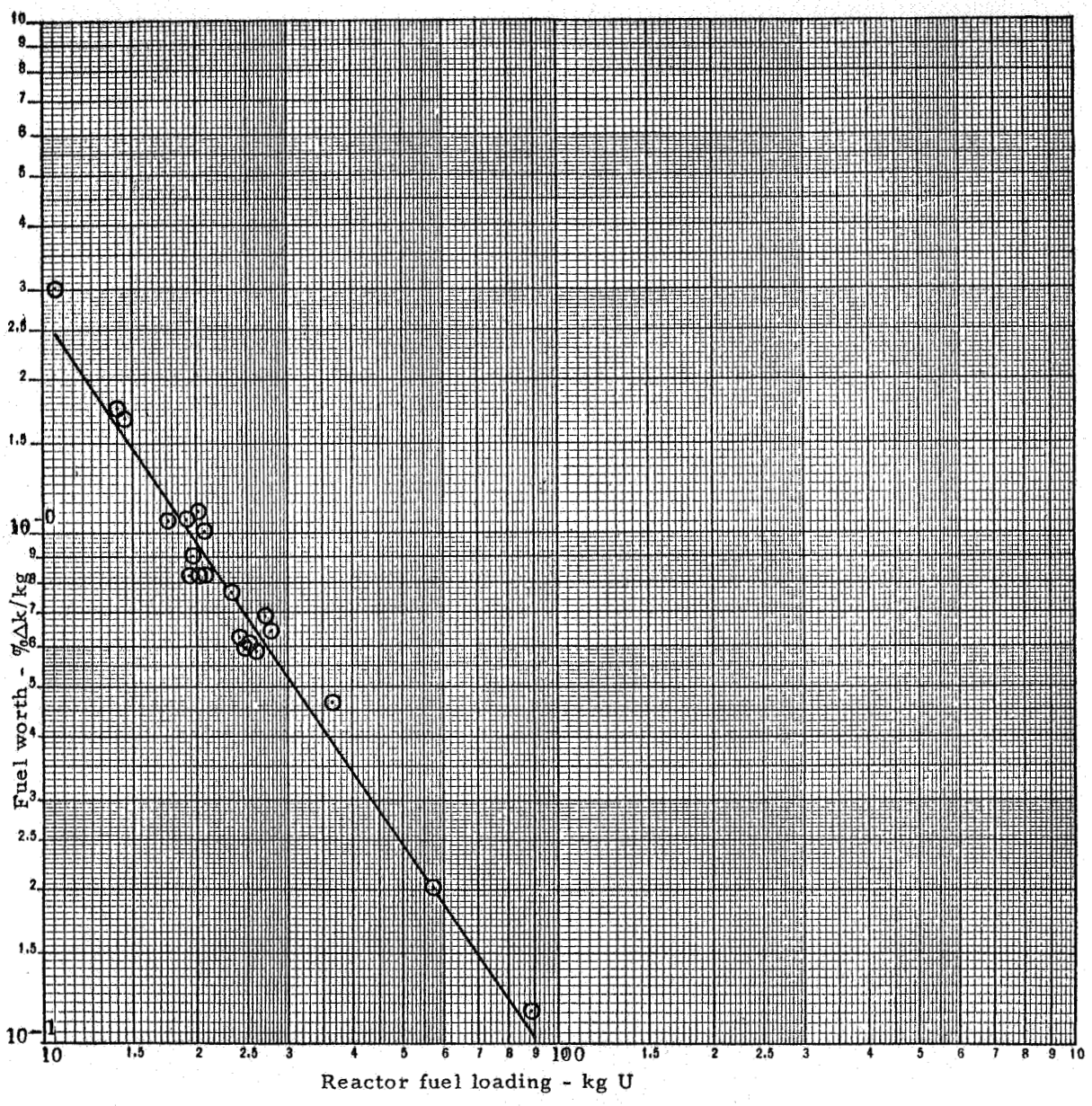


Fig. 3.6 Effect of core loading on fuel worth for all cavity reactor assemblies

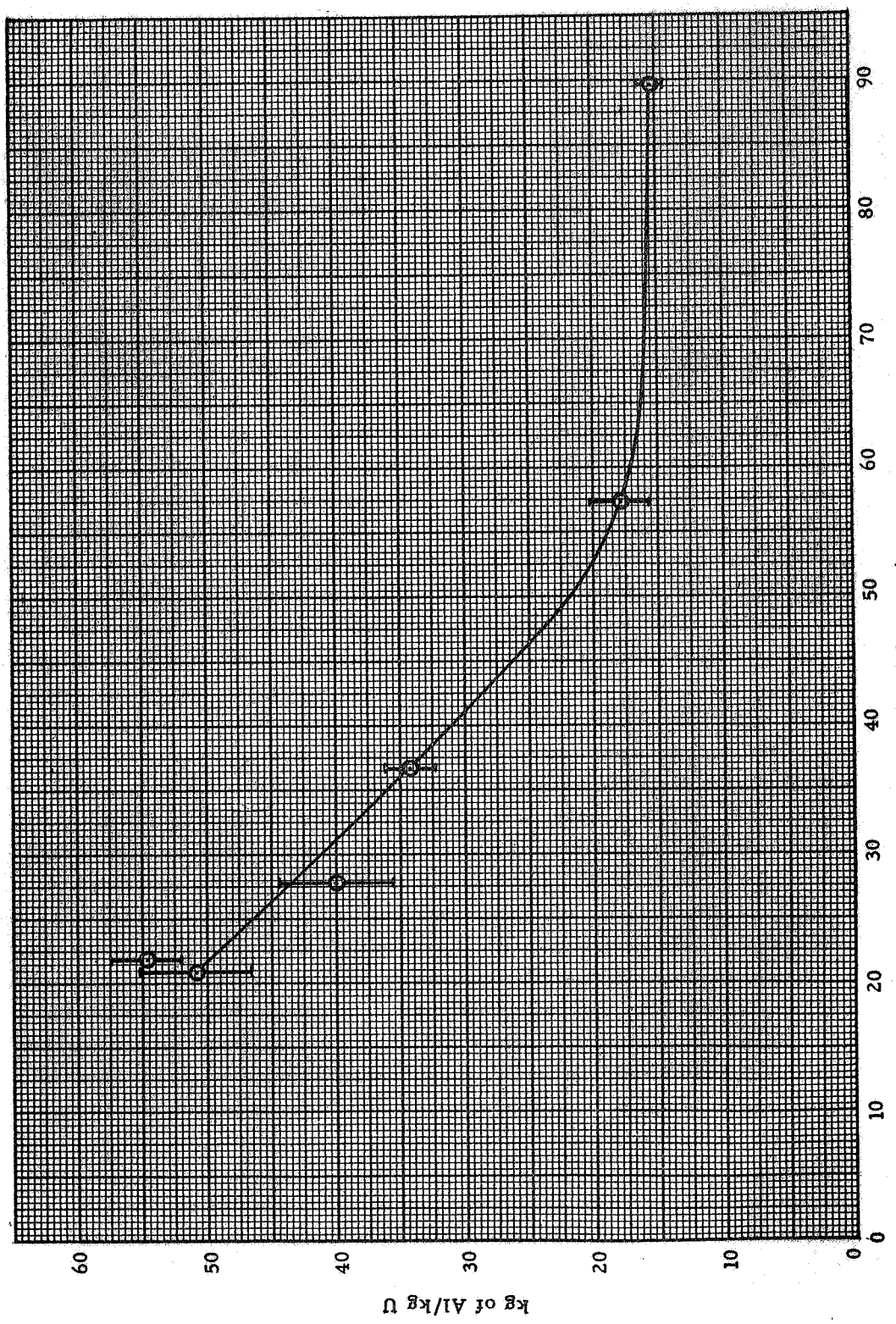


Fig. 3.7 Core loading effects on core average aluminum worth with respect to uranium worth

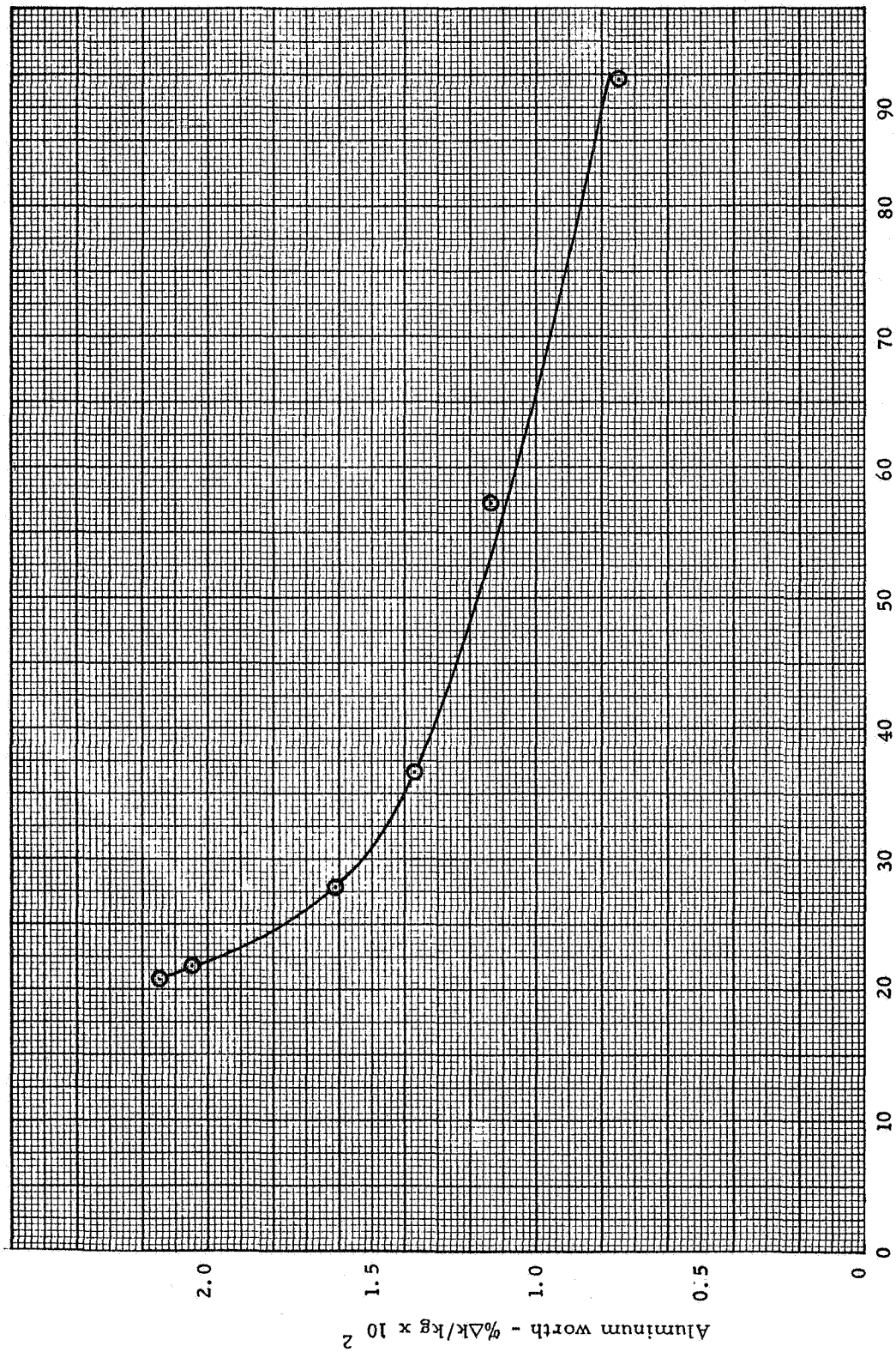


Fig. 3.8 Effects of core loading on core average worth of type 1100 aluminum

4.0 MOCKUP NO. 1 EXPERIMENT

The mockup reactors were loaded with metallic, thin, sheet fuel which was nominally 0.00254 cm thick. Two different sizes of sheets were available; these were 7.30 cm x 7.30 cm (size 1.0 sheets nominal U mass = 2.62 gm) and 7.30 cm wide by 10.95 cm long (size 1.5 sheets nominal U mass = 3.88 gm). The first mockup reactor contained a fuel screen support structure as shown in Figures 4.1 and 4.2. The fuel was loaded on the aluminum fuel trays and an aluminum strip (hold-down strap) was placed across each corrugation of the fuel tray to hold the fuel in place. The aluminum within the active core region was as follows:

Main Support Structure (Type 6061)	54.52 kg
Fuel Support Screens (Type 3003 H14)(*)	
Screen Support Tubes (Type 6061)	82.67
Hold-Down Straps (Type 6061)	
Total	137.19 kg

The fuel was dispersed over a radius of 61 cm thus giving a fuel to cavity radius ratio of 0.67, as illustrated in Figure 4.3.

4.1 Initial Loading

Initial loading of the first UF_6 mockup reactor began on January 11, 1967. This mockup contained the beryllium annulus in the reflector as described in Section 2.1. It was originally anticipated that it would take on the order of 24 kg of fuel to go critical or 18.5 fuel sheets per surface. Since this assembly, less the extra aluminum used to simulate the UF_6 tank, had been previously operated, initial loading began with approximately half the fuel loading of the earlier assembly. The inverse multiplication data obtained during the initial loading are given in Table 4.1. The average is shown in Figure 4.4. With 24.43 kg of uranium in the cavity, the reactor was still subcritical and the inverse multiplication curves extrapolated to between 26 and 27 kg to go critical. As will be seen from Table 4.1, 27.08 kg gave an excess reactivity of 0.181%Δk.

Since the fuel loading was heavier than anticipated, the design of the UF_6 containment tank and its mockup were altered so as to increase the thickness. This increase in thickness was due to the higher pressure requirements on the UF_6 containment tank. The following gives the total weights of aluminum used to mockup the final tank design.

	Required (kg) Al	Actual (kg) Al	Diff. (kg) Al
121.9 cm square plate on end of core in fixed table	55.61	54.66	-0.95
121.9 cm square on movable table	55.61	55.79	+0.18
Cage and side plates	133.68	131.86	-1.82
Total			-2.59

* There were 40.5 kg of screen material in the core. This type of aluminum contains the following nominal w/o impurities: Si 0.6, Fe 0.7, Cu 0.2, Mn 1.0 to 1.5, Zn 0.1, other 0.15.

As can be seen above, the mockup of the tank contained 2.59 kg less aluminum than the actual aluminum in the UF_6 tank. With 28.68 kg of fuel (total fuel sheet physical weight) 137 kg of aluminum to support the fuel, and 242.31 kg of aluminum in the reactor to mockup the UF_6 tank, k-excess was 0.610%Δk. This value is not corrected for the aluminum in the active core in the form of fuel support screen and hold-down straps which held the fuel sheet in place. These corrections will be discussed in the following section.

4.2 Reactivity Measurements

4.2.1 Rod Worths

Rod worth measurements were obtained for the three rods on actuators 5 and 7 and all seven actuators (20 rods) as a bank. These results are summarized below:

Actuator No.	Reactivity Worth (%Δk)
5 (3 rods)	-0.630 ± 0.002
7 (3 rods)	-0.664 ± 0.007
1 to 7 (20 rods)	-4.709 ± 0.240

Each of these values is an average of three separate measurements.

4.2.2 Material Worths

When changing the amount of aluminum around the fuel region to mockup the heavier UF_6 tank, a total of 30.53 kg of additional Al was placed in the cavity region. This reduced k-excess 0.937 ± 0.021%Δk and results in a worth-per-gram for aluminum of $-(3.07 \pm 0.07) \times 10^{-5}$ %Δk at the edge of the active core.

Material worth measurements were also required in the fueled region to give a core average worth for teflon (CF_2), carbon, aluminum fuel support screens and aluminum hold-down straps. The teflon measurement was to determine the effect of fluorine in the UF_6. The worth of carbon was needed to obtain the fluorine worth from CF_2. The aluminum in the fuel support screens and hold-down straps was not considered in the aluminum used to mockup the tank and this material was not included in the design of the UF_6 tank. It was, therefore, necessary to correct for this material. Table 4.2 summarizes these material reactivity worths.

In order to obtain a core average with the material available, the core was divided up into annular regions of given volumes. Five regions were used and the relative volumes of each were as follows:

Region	Relative Volume
1	1
2	2
3	3
4	3
5	3

These regions are shown in Figure 4.5. Representative positions were chosen in each region, as shown in the above figure, where the material to be evaluated was placed over the full length of the core. Equal amounts of material were placed on each of the 12 locations for each of the measurements shown in Table 4.2.

The mockup experiment contained a total of 34 kg of aluminum in hold-down straps. This material would, therefore, be worth -(0.55 ± 0.04) %Δk. Likewise, there was 40.5 kg in Al screens which would be worth -(0.77 ± 0.08)%Δk. Each fuel screen also contained two Al tubes which rested on the angles at the edge of the fueled region and provided support and proper spacing for the screen. This material amounted to 7.8 kg. Assuming these to be worth the same per gram as the hold down straps, they would be worth -(0.13 ± 0.01)%Δk. The total worth of these aluminum materials within the fueled region materials which were not to be included in the UF_6 tank, was -(1.45 ± 0.14)%Δk. After the assembly was removed from the core, all of the aluminum in the screens, hold-down straps and screen support tubes was weighed to check the above values and the total was 82.67 kg. Note, however, that there was a shortage of aluminum in the UF_6 tank mockup of 2.59 kg which is worth +0.080%Δk.

The total measured fuel loading was 28.68 kg as recorded during initial loading and k-excess was 0.610%Δk at 18.6°C, D_2O temperature. The fuel weight following the experiment was 28.75 kg. This was a 70 gm increase in weight. At this period of time, several fuel sheet samples were chemically analyzed to determine the total amount of uranium. The fluorocarbon coated fuel samples showed (96.7 ± 0.2)% by weight uranium whereas uncoated samples were (97.2 ± 0.7)% uranium. Two samples of uncoated and recently cleaned fuel measured to be (100.0 ± 0.5)% uranium. Oxidation occurs on the surface of uranium metal exposed to air. Although most of the uranium foil used in the reactor was all coated, it still oxidizes to some extent. The coating placed on the fuel represented less than 1.0% of the uranium foil weight.

Therefore, the remaining differences are other impurities. The 70 gm increase in fuel weight noted above could possibly be due to oxidation during the experiment. Note, however, that the apparent 70 gm increase has a nominent 30% error caused by weighing uncertainties. Other experiments with oxidation of bare fuel in a closed atmosphere (but not sealed) showed an increase in weight over one year of (0.11 ± 0.04)%. (The above 70 gm increase is a 0.25% weight gain). These data would, therefore, indicate that about (3.3 ± 0.2)% of the fuel weight is coating and oxygen, and that this increased by less than the uncertainty during the period of the experiment.

The correction of fuel mass to give a multiplication of 1.0 is as follows:

1.	k-excess	-0.610%Δk
2.	Aluminum correction	-1.37%Δk
3.	Equivalent fuel weight in -(0.610 + 1.37)%Δk	-2870 gm

4.	Base fuel loading - total fuel sheet weight	28680 gm
5.	Corrected fuel loading to k = 1.0 with aluminum correct as per above	25810 gm
6.	Correction impurities in the fuel sheets (3.3 ± 0.2)%	-850 gm
7.	Critical mass for multiplication of 1.0 = 25810 - 850	24960 ± 300 gm

These corrections were based on an average fuel worth of (0.690 ± 0.055) x 10^{-3}%Δk/gm which was obtained from a curve of fuel worths for the mockup experiments and is the average fuel worth at an average core loading of 27.25 kg U. See Figure 9.1. The total aluminum in the reactor simulating the UF_6 tank was 244.9 kg for the above critical mass.

4.3 Power Distribution Measurements

4.3.1 Bare Catcher Foil Results

Foil exposures were obtained with all rods (20) equally withdrawn about 38.3 cm and the D_2O at a temperature of 19°C. Each exposure run was for 20 minutes.

Bare catcher foils were exposed within the cavity to obtain a fine radial power profile at the axial center of the core and a detailed axial at the radial center of the core. The data obtained are given in Table 4.3 and it should be noted here that the axial data are referenced to the outer wet surface of the fixed D_2O tank. This table includes both bare and cadmium covered foil data. The relative radial and axial power profiles are shown in Figures 4.6 and 4.7. A radial profile was also measured on each end of the core, as shown in Figure 4.6. The specific power at the back end of the core (the end of the core containing the central rods) was consistently higher than at the separation plane. This is also obvious in the axial power curve. There were two possible reasons for at least part of this. The first, was that there were 100 extra fuel sheets (about 262 gm) at the separation plane, evenly dispersed over the end of the core. This extra fuel was used to increase excess reactivity to a desired level for power mapping. This would tend to reduce the power per unit fuel mass (specific power) in this region of the heavier loading. The second, (but less significant) compromise was that the fuel was not exactly centered in the core lengthwise. There was about a 7.62 cm space at the back end of the core between the aluminum end plates and the fuel. The reason for this was that the location of the studs in the support structure required that one set of the 1.27 cm diameter aluminum support tubes for the screens be placed at approximately the 7.62 cm (3-inch) location from the separation plane, since the width of the fuel sheet is 7.62 cm and these cannot be placed where the support rods go through the screens. Between the

two support rods, the fuel was overlapped slightly so that the total fuel length was maintained at 109.2 cm (compared to 108.6 cm in the actual UF_6 tank). However, because of the location of the studs and the screen support tubes, the fuel was not exactly centered longitudinally within the cavity. The center of the fuel was about 2.54 cm toward the open end of the cavity compared to the cavity center.

The volume weighted average relative radial power across the fuel region, as shown in Figure 4.6, was 1.563. The ratio of the power from the outer edge of the fuel to the core center was 2.89. It will also be noted from Figure 4.6 that the radial profile near the table separation plane at the end of the core (209.5 cm position) shows an increase in power as the axial centerline is approached. This was real and due to the 30.5 cm diameter hole (exhaust nozzle) in the center of the end reflector as described in Reference 1.

The average longitudinal relative power, shown in Figure 4.7, was 1.234. The data point location on the curve at 43 cm from the end of the core (axial position of 133.1 cm from the reference point) was above the curve. This point occurs at the location of the fuel screen support tubes. There were two rows of these tubes, one near the separation plane about 7.6 cm from one end of the screen and one about 43 cm from the other end of the screen. Since no fuel could be placed at these points where the support tubes passed through the screens, there was essentially a path through which neutrons could pass without encountering much fuel. These support tubes did not exactly line-up with each other, therefore, a perfect steaming path with no fuel encounters did not exist, and the effect on reactivity was minimized. Furthermore, there were other locations where fuel on a particular screen slightly overlapped tc account for the "gap" at the tubes. The "gap" did allow better penetration of the thermal flux, and for this reason, the point at 133.1 cm was higher than the curve. No anomalies were observed that could be attributed to the consequential occasional overlap of the fuel.

4.3.2 Cadmium Ratios

Uranium-235 cadmium ratios obtained from the bare and cadmium covered catcher foils are given in Table 4.4 and are plotted in Figures 4.8 and 4.9 showing the radial and axial distribution. The cadmium covers were 0.0508 cm thick. At the center of the core the cadmium ratio was around 6.5. This increased to 15.2 at the outer radius of the fuel. At the ends and radial center of the core the ratio averaged about 13.0. The cadmium ratio increased across the void region to 19.2 at the axial center of the core. At the ends of the cavity next to the radial reflector, the ratio was still higher, ranging from about 22 to 24. The cadmium ratios are "essentially" those of infinitely dilute U^{235} detectors because of the nature of the catcher foil process. Actually, the estimated corrections are to increase the direct result by about 5% to obtain infinitely dilute values, but this correction is so uncertain and so small compared to measurement accuracy that it has not been made.

4.4 Gold Foil Data

4.4.1 Bare Gold Foil Data

Gold foils, nominally 5.08×10^{-4} cm (0.2 mil) thick, were exposed in the reactor to produce a radial and axial flux profile within the cavity and to measure the flux within the end and radial reflector regions. Both bare and cadmium covered foils were used. As with the catcher foils, the cadmium covers were 0.0508 cm thick. The foil data, including both bare and cadmium covered results, are given in Table 4.5. The radial and axial profiles of total activity (bare foils) normalized to the core center are shown in Figures 4.10 and 4.11. The ratio of the foil activity from the outer edge of the fuel to the core center, as shown in Figure 4.10, was 1.73 and the volume weighted average was 1.224. The point at 15.2 cm (Figure 4.10) was above the smooth curve and appears to be a bad piece of data.

The relative normalized axial activity distribution shows the same flux variation between the two ends of the core as noted from the catcher foils. The flux at the back end of the core was higher than at the separation plane by about 21% which is about the same as for catcher foils. The point at 133.1 cm was also high as with the catcher foil data and the reason for this is explained in Section 4.3.1. The curve average was 1.117.

The relative total activity distribution within the reflector regions are presented in Figure 4.12. The data through the radial reflector were taken at the axial center of the core and the end reflector results were obtained at the radial center of the core. Because the rod positions noted in Section 4.3 caused significant flux depression in the end reflector, the flux in the end reflector dropped below the radial reflector beyond 47 cm from the cavity wall.

It will be noted that the gold foil activity was normalized to a total reactor power of 17.9 watts. Each foil exposure run contained power normalization catcher foils exposed outside of the cavity. Three one minute counts were obtained on six of these foils after shutdown and the activity decay corrected to 50 minutes after shutdown. The average activity at this time was then used to correct the gold foil activity to a common power base. The power normalization factors are given in Table 4.6. The factors given in this table were used to power normalize the foil data in Table 4.5.

4.4.2 Cadmium Ratios

The cadmium ratios obtained from gold data are given in Table 4.7. The ratios were corrected to infinitely dilute foil activities thus correcting for self-shielding and variations in foil weight. The following equation was used to make these corrections.

$$\text{corrected activity} = AK_1 + AK_2 \frac{I_\infty}{I_{eff}}$$

where A = bare foil activity

K_1 = fraction of activity due to subcadmium neutron

K_2 = fraction of activity due to epicadmium neutrons

I_∞ = infinitely dilute resonance integral

I_{eff} = effective resonance integral

and $\frac{I_\infty}{I_{eff}} = 1 \Big/ \sqrt{\frac{S/4NV}{S/4NV + \sigma_r \left(\frac{\Gamma_\gamma}{\Gamma}\right)}}$

where S = surface area of foil

N = atomic density

V = volume of foil

σ_r = theoretical cross section at resonance peak

Γ_γ = (n,γ) absorption width

Γ = total width

The value used for $\sigma_r \frac{\Gamma_\gamma}{\Gamma}$ was 3.3×10^4 barns.

The distribution of these ratios within the core are shown in Figures 4.13 and 4.14. At the core center the cadmium ratio was 1.18 and increased to 1.53 at the outer edge of the fuel on the radial distribution. The axial plot shows the cadmium ratio at the ends of the core to be about 1.4.

The cadmium ratios within the reflector regions are given graphically in Figure 4.15. The end reflector shows a harder spectrum than the radial reflector. This was due primarily to the presence of control rods in the end reflector. The rods were equally withdrawn about 38 cm during these measurements which caused a reduction in thermal flux in the end reflector and particularly near the outer portion of the reflector.

4.5 Neutron Flux Distribution

The gold foil data were converted to thermal neutron flux by subtracting the corrected epi-cadmium or resonance contribution (as outlined in Section 4.4.3 of Reference 1). The thermal fluxes obtained were for equivalent 2200 m/sec cross section, and thus are nominally 0.886 times the value of the Maxwell-Boltzmann averaged flux at 68°F. The calculated values are found in Table 4.8. These values are presented graphically in Figures 4.16 and 4.17 normalized to a watt of reactor power. All of the data appear to follow smooth curves as no points deviated appreciably from the curves.

TABLE 4.1

Inverse Multiplication

Initial Loading - UF_6 Mockup No. 1

Increment	Total Fuel Loading (kg) (1)	Channel 1 CPM	Channel 1 CRo/CR	Channel 2 CPM	Channel 2 CRo/CR	Channel 3 CPM	Channel 3 CRo/CR	Average CRo/CR	Rod Positions
Background		9		14		11			In
Background		9		15		14			Out
0	0	63		80		74			In
0	0	70		89		74			Out
1	9.89	309	.210	387	.214	340	.225	.218	In
1	9.89	411	.174	536	.170	441	.173	.173	Out
2	11.54	366	.176	473	.174	419	.181	.177	In
2	11.54	506	.141	662	.138	532	.143	.141	Out
3	13.96	474	.135	594	.138	516	.147	.140	In
3	13.96	677	.105	903	.100	749	.101	.102	Out
4	16.38	580	.110	751	.109	651	.116	.112	In
4	16.38	940	.075	1215	.074	1069	.070	.073	Out
5	18.81	742	.086	938	.087	832	.090	.088	In
5	18.81	1378	.051	1779	.050	1522	.049	.050	Out
6	21.52	994	.064	1263	.064	1089	.069	.066	In
6	21.52	2341	.030	3103	.029	2571	.029	.029	Out
7	22.49	1148	.055	1449	.062	1198	.062	.060	In
7	22.49	3035	.023	4021	.022	3443	.022	.022	Out
8	24.43	1436	.044	1855	.043	1436	.052	.047	In
8	24.43	6091	.0115	7733	.0115	6731	.0110	.0113	Out
9	27.08	1980	.032	2479	.032	1984	.038	.034	In
9	27.08	Critical with 0.181 %Δk excess							Out
10	27.35	2856	.022	2962	.022	2356	.032	.027	In
10	27.35	Critical with 0.432 %Δk excess							Out

(1) Total fuel weight represents total physical weight of the fuel sheets of which 96.8% is uranium and 3.2% is coating and oxide.

TABLE 4.2

Material Worth Measurements

UF_6 Mockup No. 1 - Core Average Values

Material	Worth per Gram (%Δk)
Teflon (CF_2)	$-(1.28 \pm 0.20) \times 10^{-5}$
Carbon	$-(2.30 \pm 1.05) \times 10^{-5}$
Fluorine (1)	$-(0.96 \pm 0.42) \times 10^{-5}$
Al Hold-down straps (6061 Al)	$-(1.61 \pm 0.11) \times 10^{-5}$
Al Screens	$-(1.89 \pm 0.20) \times 10^{-5}$
Fuel	$+(0.644 \pm 0.055) \times 10^{-3}$

(1) Calculated from worths of teflon and carbon

TABLE 4.3

Catcher Foil Data - UF_6 Mockup No. 1

Foil No.	Type	Location Radial (cm)	Location Axial (cm)(1)	Tray No.	Normalized Counts	Ratio Local To Core Center (Foil No. X)
Run 1065						
1	Cd	0	100.3	17	5876	
2	Cd	0	118.0	17	5228	
3	Cd	0	148.5	17	4815	
4	Cd	0	179.0	17	4856	
5	Cd	0	209.5	17	5091	
Run 1066						
1	Cd	30.5	148.5	17	5228	
2	Cd	61.0	148.5	17	5966	
Run 1067						
10	Cd	91.4	148.5	17	6357	---
11	Bare	76.2	209.5	17	118595	3.738
12	Bare	76.2	148.5	17	115056	3.627
13	Bare	76.2	100.3	17	133927	4.221
14	Bare	61.0	209.5	17	104203	3.284
15	Bare	61.0	148.5	17	90871	2.864
16	Bare	61.0	100.3	17	115847	3.651
17	Bare	45.7	209.5	17	72309	2.279
18	Bare	45.7	148.5	17	47169	1.487
19	Bare	45.7	100.3	17	83207	2.623
Run 1068						
1	Bare	0	209.5	17	63686	2.007
2	Bare	0	194.3	17	36827	1.161
3	Bare	0	179.0	17	31630	0.997
4	Bare	0	163.8	17	30541	0.963
5	Bare	0	148.5	17	31730	1.000 (X)
6	Bare	0	133.3	17	37418	1.179
7	Bare	0	118.1	17	42055	1.326
8	Bare	0	102.8	17	71844	2.265
9	Bare	0	100.3	17	77804	2.452
10	Bare	15.2	209.5	17	59618	1.879

(1) Axial distances are referenced to the wet surface of the outer D_2O tank wall of the end reflector containing the control rods. This will be true of both gold and catcher foils.

TABLE 4.3
(Continued)

Foil No.	Foil Type	Location Radial (cm)	Location Axial (cm)[1]	Tray No.	Normalized Counts	Ratio Local to Core Center (Foil No. X)
Run 1068 (Cont'd)						
11	Bare	15.2	148.5	17	31110	0.981
12	Bare	15.2	100.3	17	79851	2.517
13	Bare	30.5	209.5	17	58516	1.844
14	Bare	30.5	148.5	17	37574	1.184
15	Bare	30.5	100.3	17	85022	2.680
16	Bare	91.4	209.5	17	113779	3.586
17	Bare	91.4	148.5	17	121958	3.844
18	Cd	91.4	100.3	17	5847	---
19	Cd	91.4	209.5	17	4783	---
20	Bare	91.4	100.3	17	127462	4.018

TABLE 4.4

Catcher Foil Cadmium Ratios

UF_6 Mockup No. 1

Location					
Radial (cm)	Axial (cm)	Tray No.	Normal. Bare Foil Activity	Normal. Cd Foil Activity	Cd Ratio
0	100.3	17	77804	5876	13.24
0	118.1	17	42055	5228	8.04
0	148.5	17	31730	4815	6.59
0	179.0	17	31630	4856	6.51
0	209.5	17	63686	5091	12.51
30.5	148.5	17	37574	5228	7.19
61.0	148.5	17	90871	5966	15.23
91.4	148.5	17	121958	6357	19.18
91.4	100.3	17	127462	5847	21.80
91.4	209.5	17	113779	4783	23.79

TABLE 4.5

Gold Foil Data

UF_6 Mockup No. 1

Run 1065 Foil No.	Type	Location Radial (cm)	Location Axial (cm)	Foil Weight (gm)	Specific Activity d/m/gm [1] x 10^{-6}
6	Bare	30.5	148.5	.0211	2.146
7	Bare	45.7	148.5	.0193	2.497
8	Bare	76.2	148.5	.0171	4.068
9	Bare	0	82.5	.0163	6.310
10	Bare	0	67.2	.0177	6.560
11	Bare	0	52.0	.0200	4.163
12	Bare	100.1	151.1	.0159	5.712
13	Bare	115.4	151.1	.0154	5.189
14	Bare	130.6	151.1	.0134	3.689
Run 1066					
3	Bare	0	209.5	.0188	2.782
4	Bare	0	194.2	.01555	2.416
5	Bare	0	179.0	.0162	2.214
6	Bare	0	163.8	.0172	2.162
7	Bare	0	148.5	.0178	2.116
8	Bare	0	133.3	.0156	2.416
9	Bare	0	118.0	.0159	2.448
10	Bare	0	102.8	.0199	3.043
11	Cd	0	89.4	.0221	1.797
12	Cd	0	59.6	.0212	0.3054
13	Cd	0	29.1	.0169	0.0080
14	Cd	91.4	148.5	.0186	1.941
15	Cd	61.0	148.5	.0179	1.850
16	Cd	30.5	148.5	.0180	1.667
17	Cd	93.2	148.5	.0205	1.977
18	Cd	123.0	148.5	.0186	0.1480
19	Cd	153.5	148.5	.0122	0.00347
Run 1067					
1	Cd	0	209.5	.0186	1.605
2	Cd	0	179.0	.0145	1.680
3	Cd	0	148.5	.0171	1.625
4	Cd	0	118.1	.0160	1.746
5	Cd	0	100.3	.0182	1.836
6	Cd	0	74.9	.0176	1.376
7	Cd	0	44.4	.0161	0.0536
8	Cd	107.7	151.1	.0170	0.976
9	Cd	138.2	151.1	.0151	0.0241

TABLE 4.5

(Continued)

Foil No.	Type	Location Radial (cm)	Location Axial (cm)	Foil Weight (gm)	Specific Activity d/m/gm (1) x 10^{-6}
Run 1068					
21	Bare	91.4	148.5	.0198	4.137
22	Bare	61.0	148.5	.0183	3.611
23	Bare	15.2	148.5	.0158	2.297
24	Bare	0	148.5	.0204	2.087
25	Bare	0	100.3	.0190	3.180
26	Bare	0	89.4	.0156	4.075
27	Bare	0	74.9	.0178	7.296
28	Bare	0	59.6	.0173	5.467
29	Bare	0	44.4	.0167	3.063
30	Bare	0	29.1	.0161	1.388
31	Bare	0	13.9	.0152	0.572
32	Bare	0	0.0	.0164	0.0880
33	Bare	93.2	151.1	.0160	4.793
34	Bare	107.7	151.1	.0164	5.655
35	Bare	123.0	151.1	.0184	4.342
36	Bare	138.2	151.1	.0193	2.961
37	Bare	153.5	151.1	.0171	1.770
38	Bare	168.7	151.1	.0177	0.828
39	Bare	183.9	151.1	.0187	0.109

(1) Specific activity is the disintegrations per minute per gram at shutdown normalized for power to Run 1065 (17.9 watts).

TABLE 4.6

Power Normalization Factors

UF_6 Mockup No. 1

Run No.	Count Time	Decay Time (min)	Decay Factor	Activity (cpm)	Corrected Activity (cpm) (1)	Norm. Factor
1065	1206.22	29.70	0.55	529426	291184	
	1207.53	31.01	0.58	502758	291600	
	1208.79	32.27	0.60	483162	289897	
					290894	1.000
1066	1417.15	20.10	0.39	741377	289137	
	1418.36	21.31	0.41	705046	289069	
	1419.57	22.52	0.43	672795	289302	
					289169	1.006
1067	1227.64	53.36	1.08	275522	297564	
	1228.88	54.60	1.10	270639	297703	
	1230.10	55.82	1.13	260638	294521	
					296596	0.981
1068	1525.94	41.86	0.81	362199	293381	
	1527.65	43.57	0.85	345982	294085	
	1528.89	44.81	0.87	334523	291035	
					292834	0.993

(1) Activity decay corrected to 50 minutes after shutdown.

TABLE 4.7

Gold Cadmium Ratios

UF_6 Mockup No. 1

Location Radial (cm)	Location Axial (cm)	Bare d/m/gm x 10^{-6}	Cd d/m/gm x 10^{-6}	Cd Ratio	Corrected (1) Cd Ratio
0	100.3	3.180	1.836	1.657	1.412
0	118.1	2.448	1.746	1.402	1.230
0	148.5	2.116	1.625	1.302	1.178
0	179.0	2.214	1.680	1.318	1.210
0	209.5	2.782	1.605	1.733	1.403
30.5	148.5	2.146	1.667	1.287	1.189
61.0	148.5	3.611	1.850	1.952	1.532
91.4	148.5	4.137	1.941	2.131	1.631
0	89.4	4.075	1.797	2.268	1.585
0	74.9	7.296	1.376	5.302	3.401
0	59.6	5.467	0.3054	17.90	9,784
0	44.4	3.063	0.0536	57.15	33.28
0	29.1	1.388	0.0080	173.5	98.85
93.2	151.1	4.793	1,977	2.424	1.705
107.7	151.1	5.655	0.976	5.794	3.698
163.0	151.1	4.342	0.1480	29.34	16.50
138.2	151.1	2.961	0.0241	122.9	72.59
153.5	151.1	1.770	0.00347	510.0	321.0

(1) Corrected to infinitely dilute foil activities.

TABLE 4.8

Thermal Neutron Flux Distribution

UF_6 Mockup No. 1

Location		$n/cm^2/sec$ at 17.9 watts $\times 10^{-6}$	$n/cm^2/sec/watt$
Radial (cm)	Axial (cm)		
0	209.5	18.38	1.027
0	179.0	9.23	0.516
0	148.5	7.97	0.445
0	118.1	10.85	0.606
0	100.3	21.31	1.191
0	89.4	31.77	1.775
0	74.9	92.05	5.143
0	59.6	79.83	4.460
0	44.4	46.76	2.612
0	29.1	21.44	1.198
0	13.9	8.84	0.494
0	0.0	1.36	0.076
0	148.5	7.97	0,445
30.5	148.5	8.86	0.495
61.0	148.5	27.58	1.541
91.4	148.5	34.77	1.943
93.2	151.1	40.98	2.290
107.7	151.1	72.50	4.051
123.0	151.1	65.15	3.640
138.2	151.1	45.65	2.550
153.5	151.1	27.45	1.534
168.7	151.1	12.85	0.718
183.9	151.1	1.691	0.094

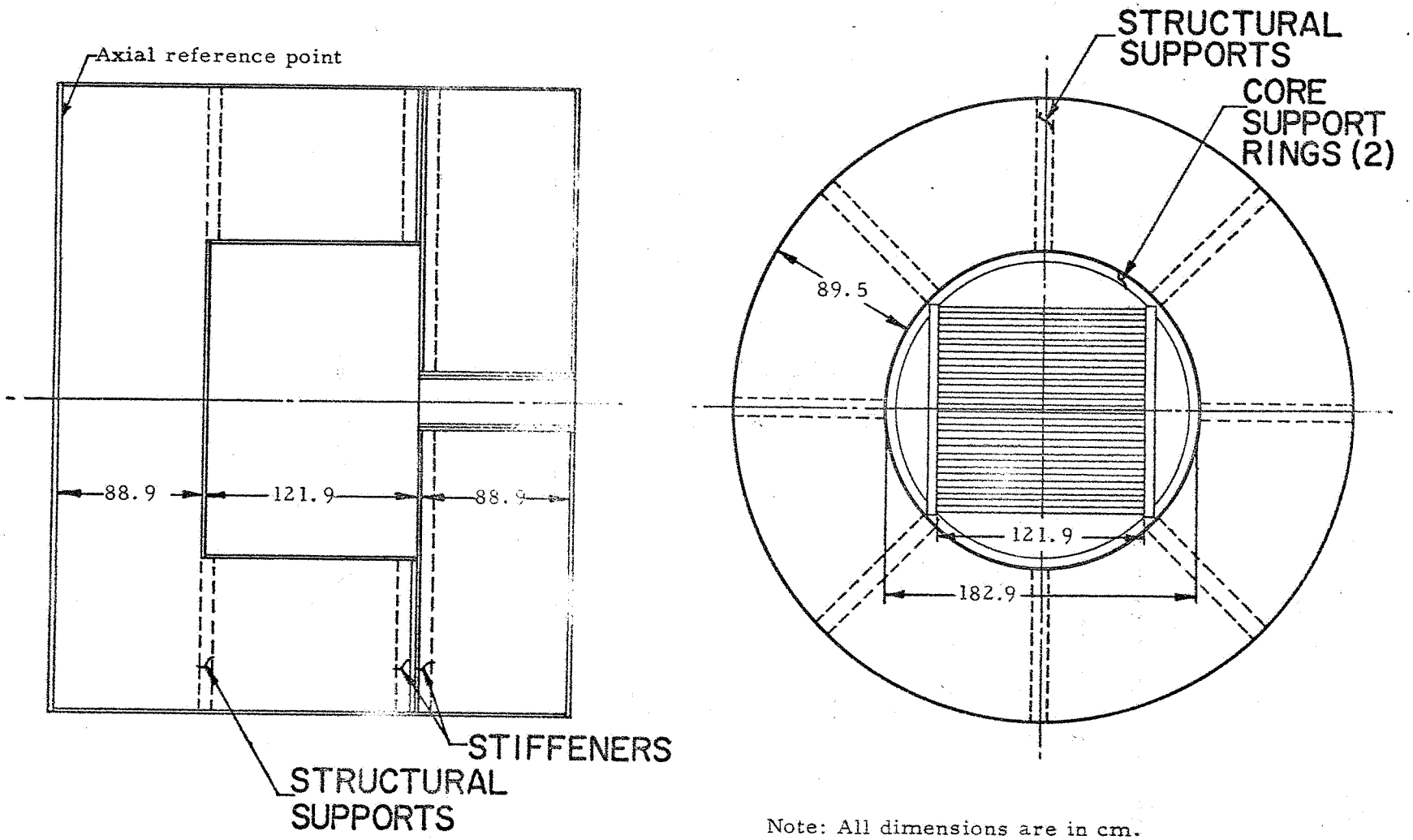


Fig. 4.1 Core layout - Mockup No. 1 reactor

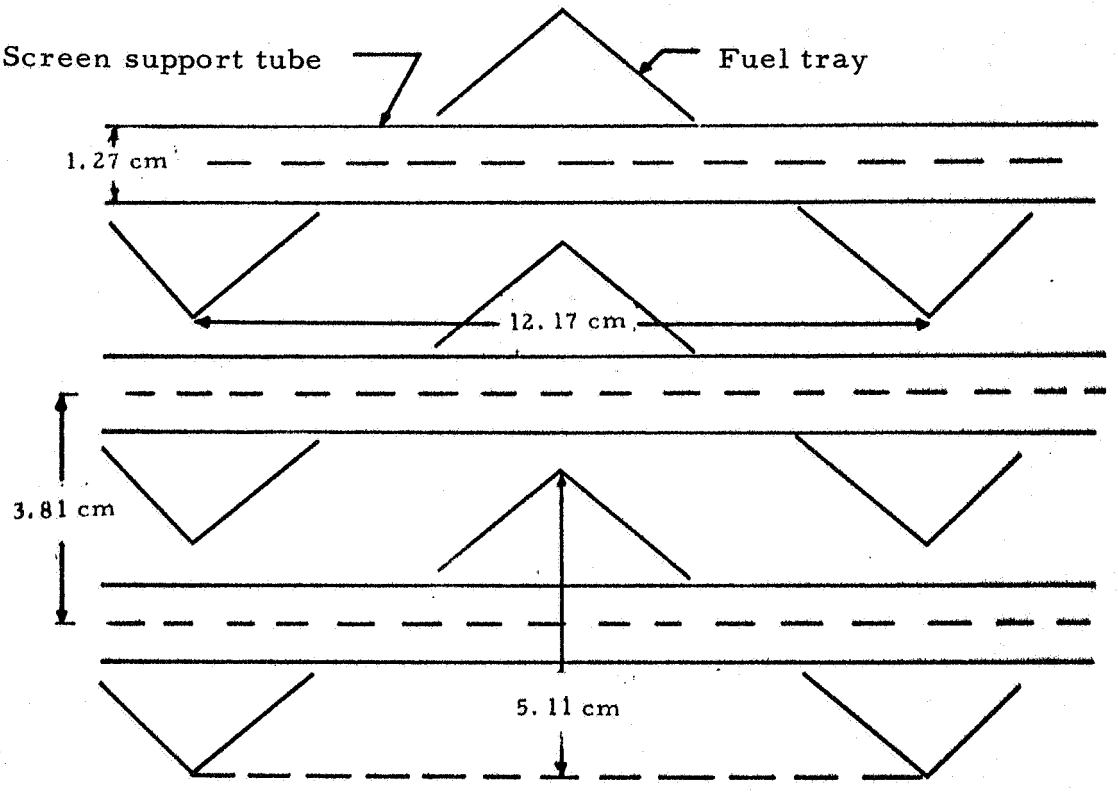


Fig. 4.2 Fuel sheet support screen layout on Mockup No. 1

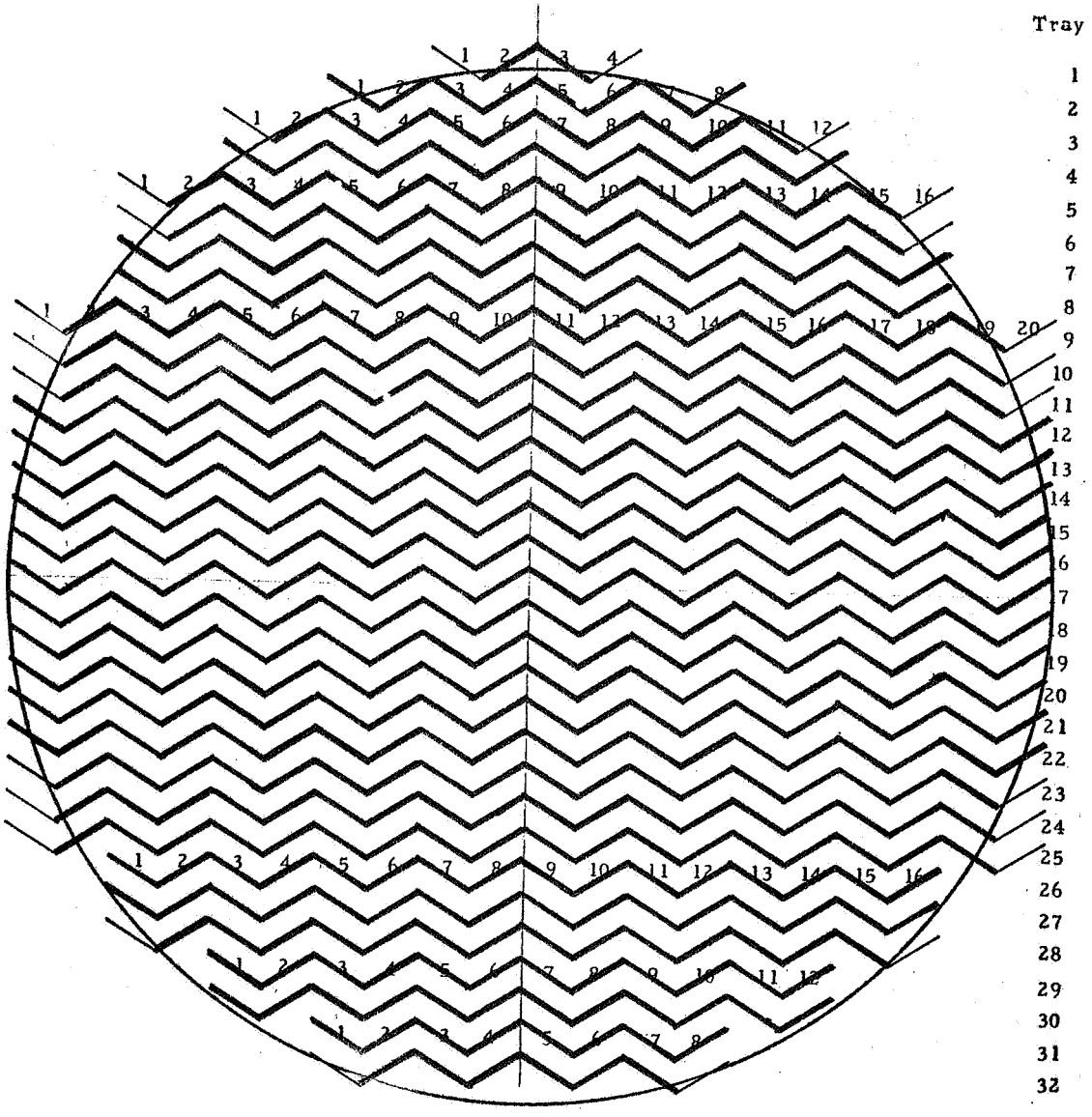


Fig. 4.3 Fuel tray installation pattern and nomenclature - Mockup No. 1

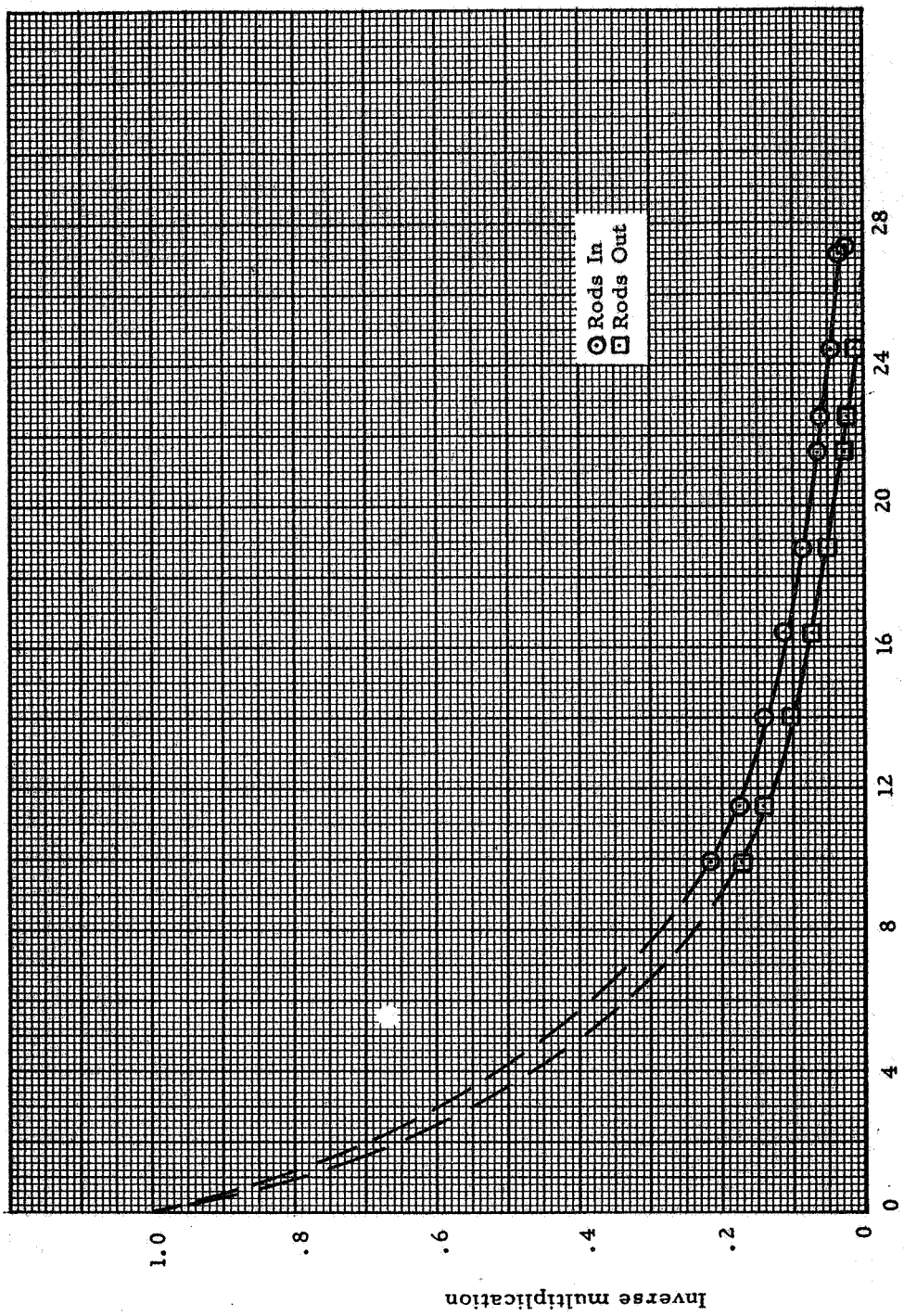


Fig. 4.4 Inverse multiplication curve, average of three channels - Mockup No. 1

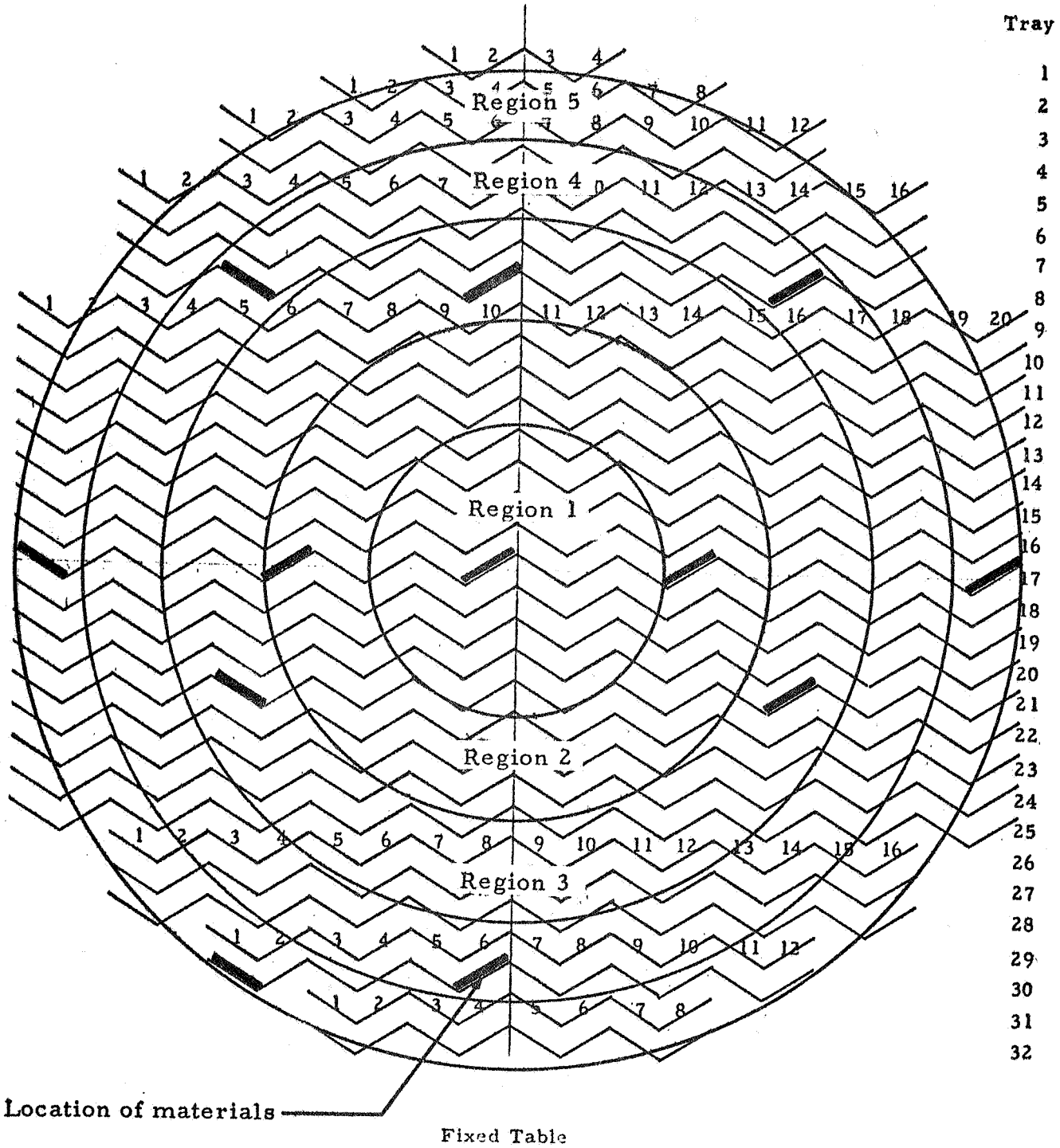


Fig. 4.5 Material locations for aluminum, teflon, carbon reactivity measurements - Mockup No. 1

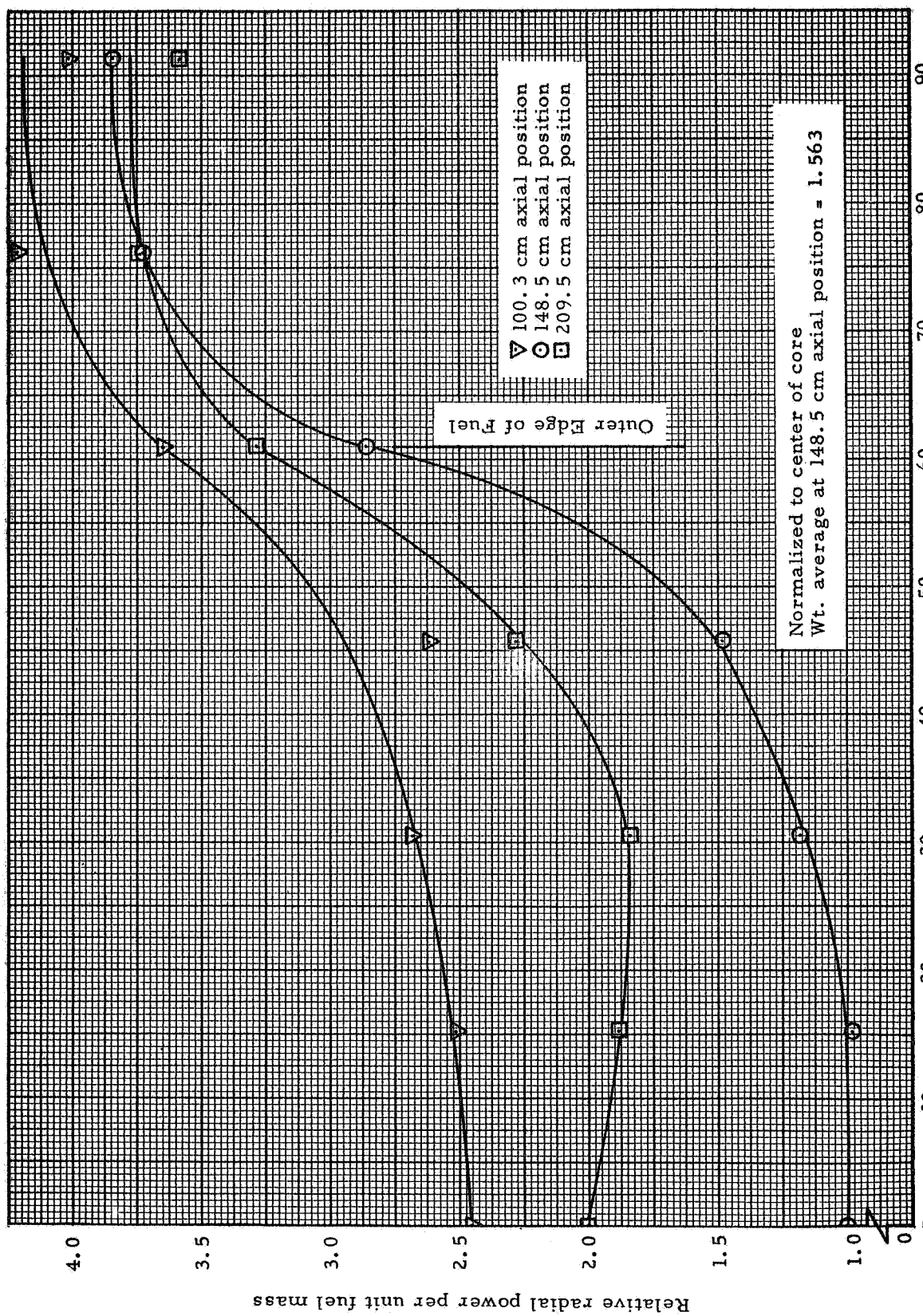


Fig. 4.6 Radial power distribution from bare catcher foils - Mockup No. 1

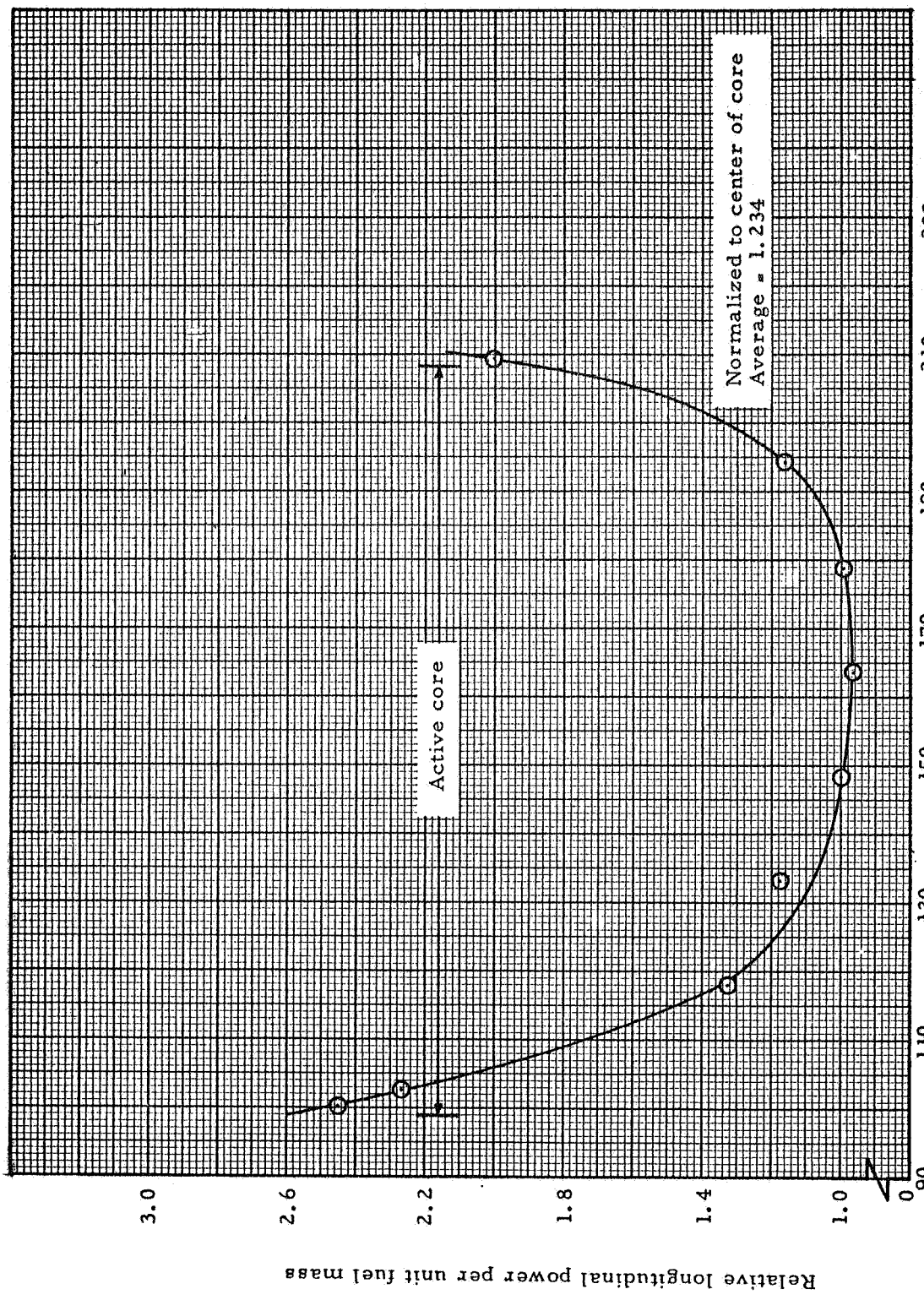


Fig. 4.7 Axial power distribution from bare catcher foils at core center - Mockup No. 1

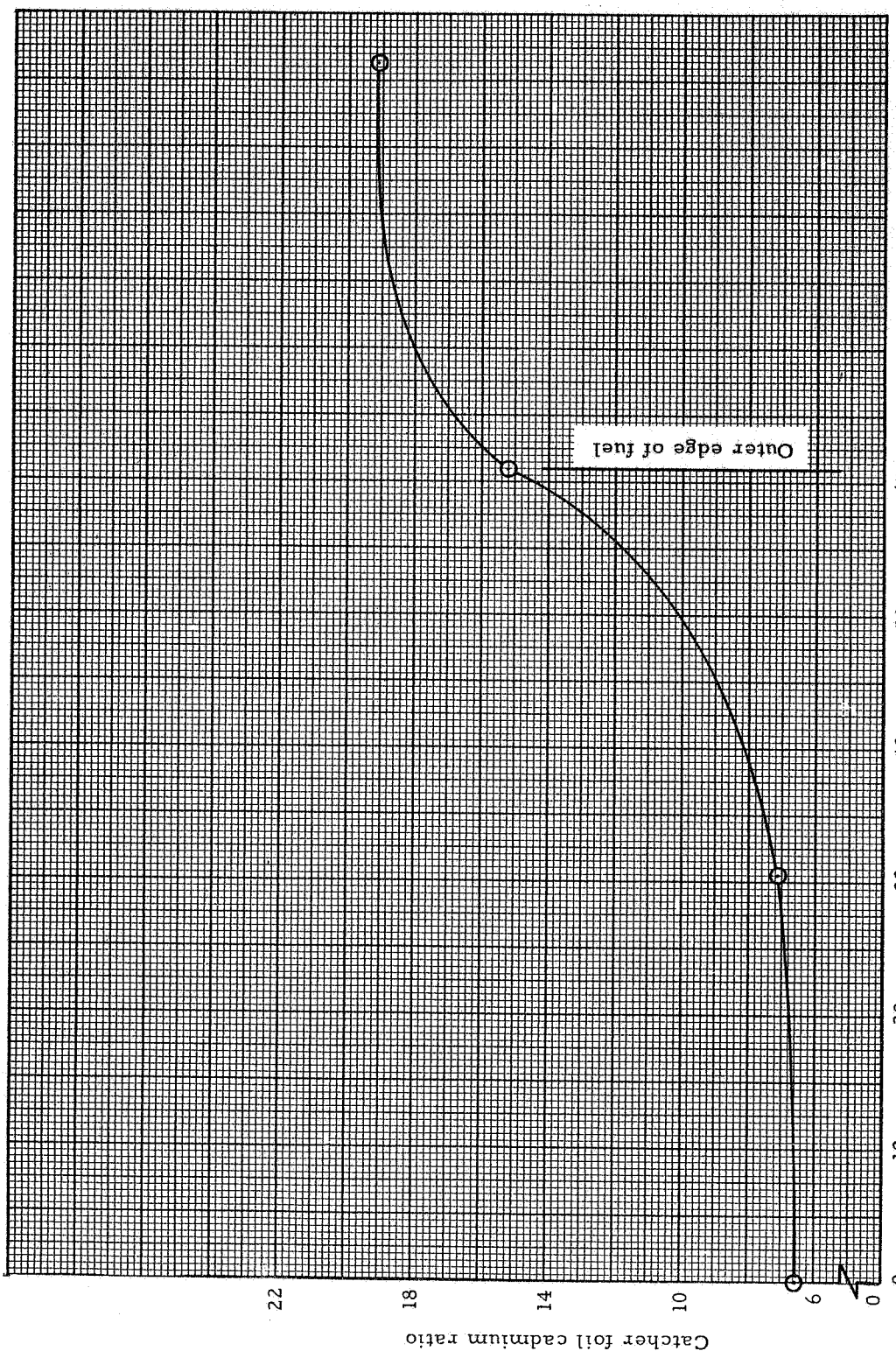


Fig. 4.8 Catcher foil cadmium ratio radial profile - Mockup No. 1

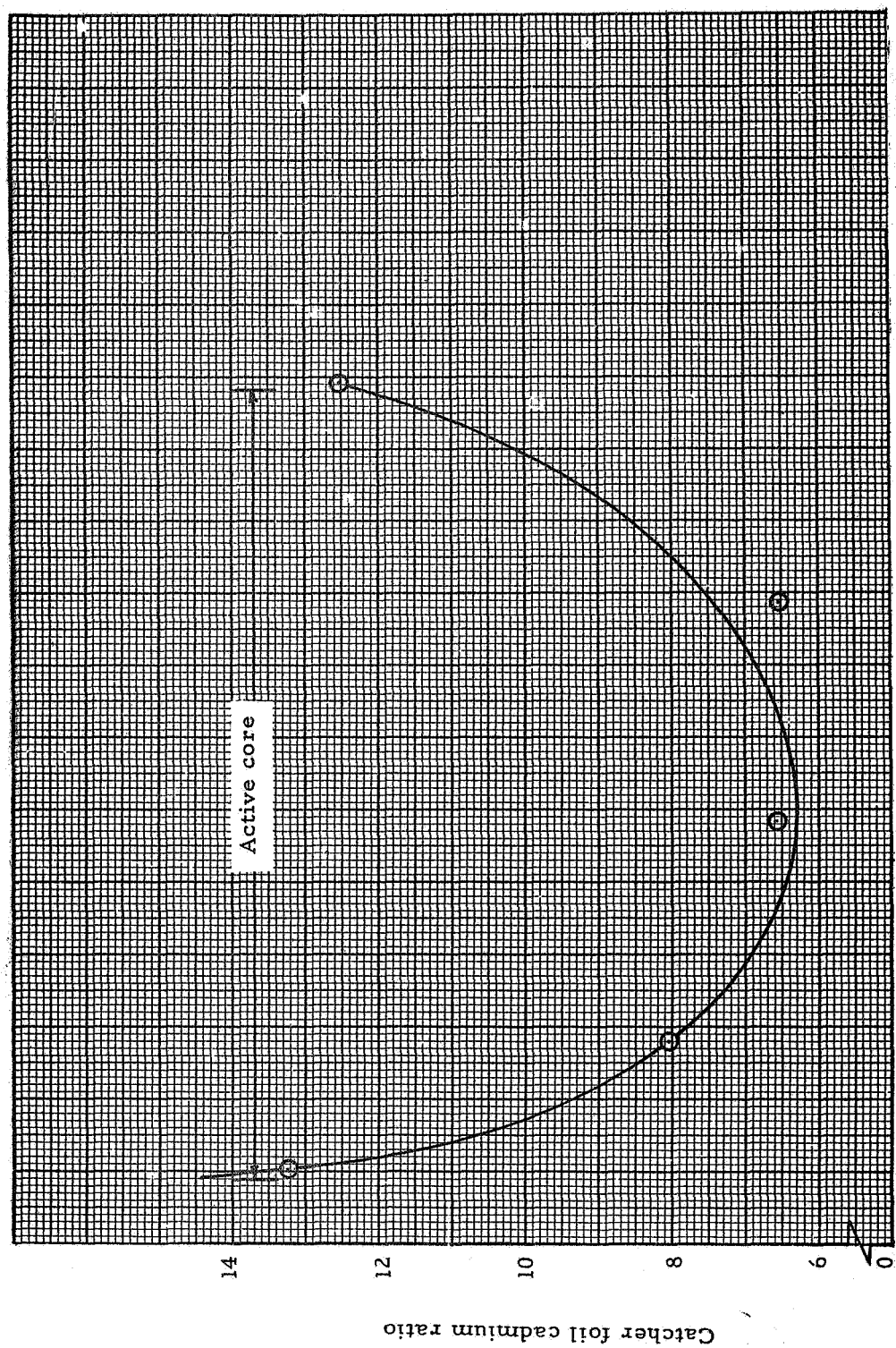


Fig. 4.9 Catcher foil cadmium ratio axial profile - Mockup No. 1

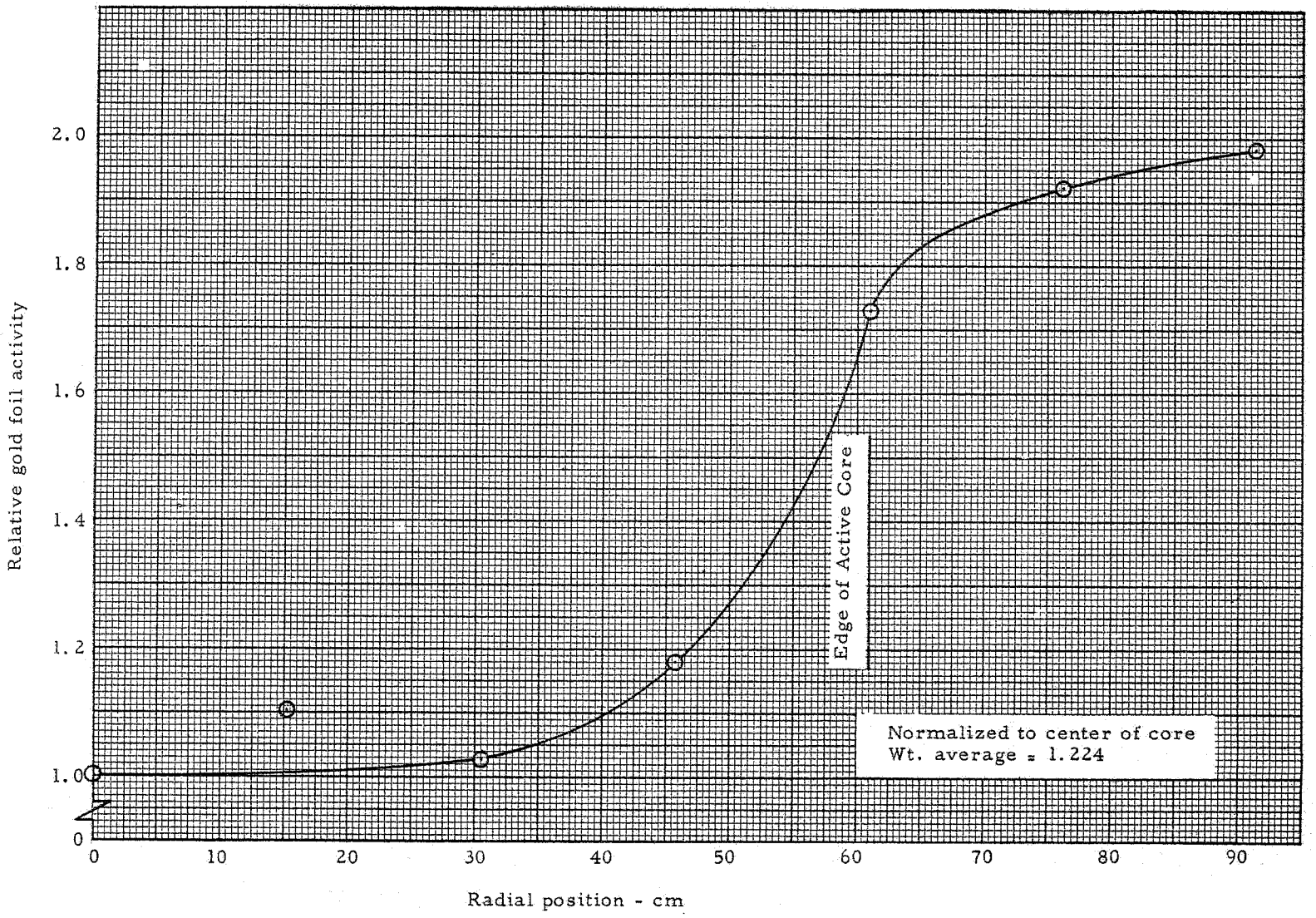


Fig. 4.10 Radial distribution of bare gold foil activity - Mockup No. 1 .

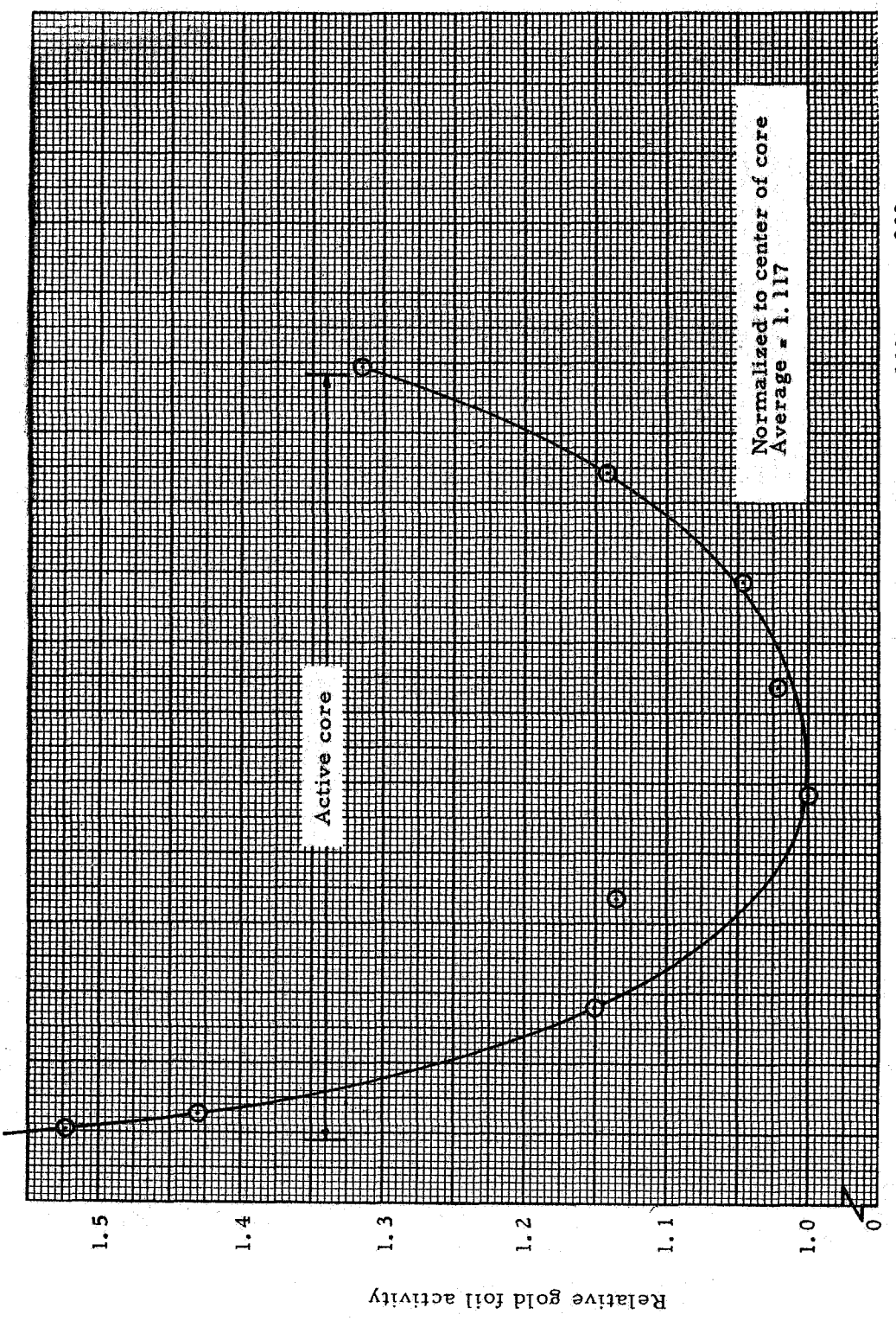


Fig. 4.11 Axial distribution of bare gold foil activity - Mockup No. 1

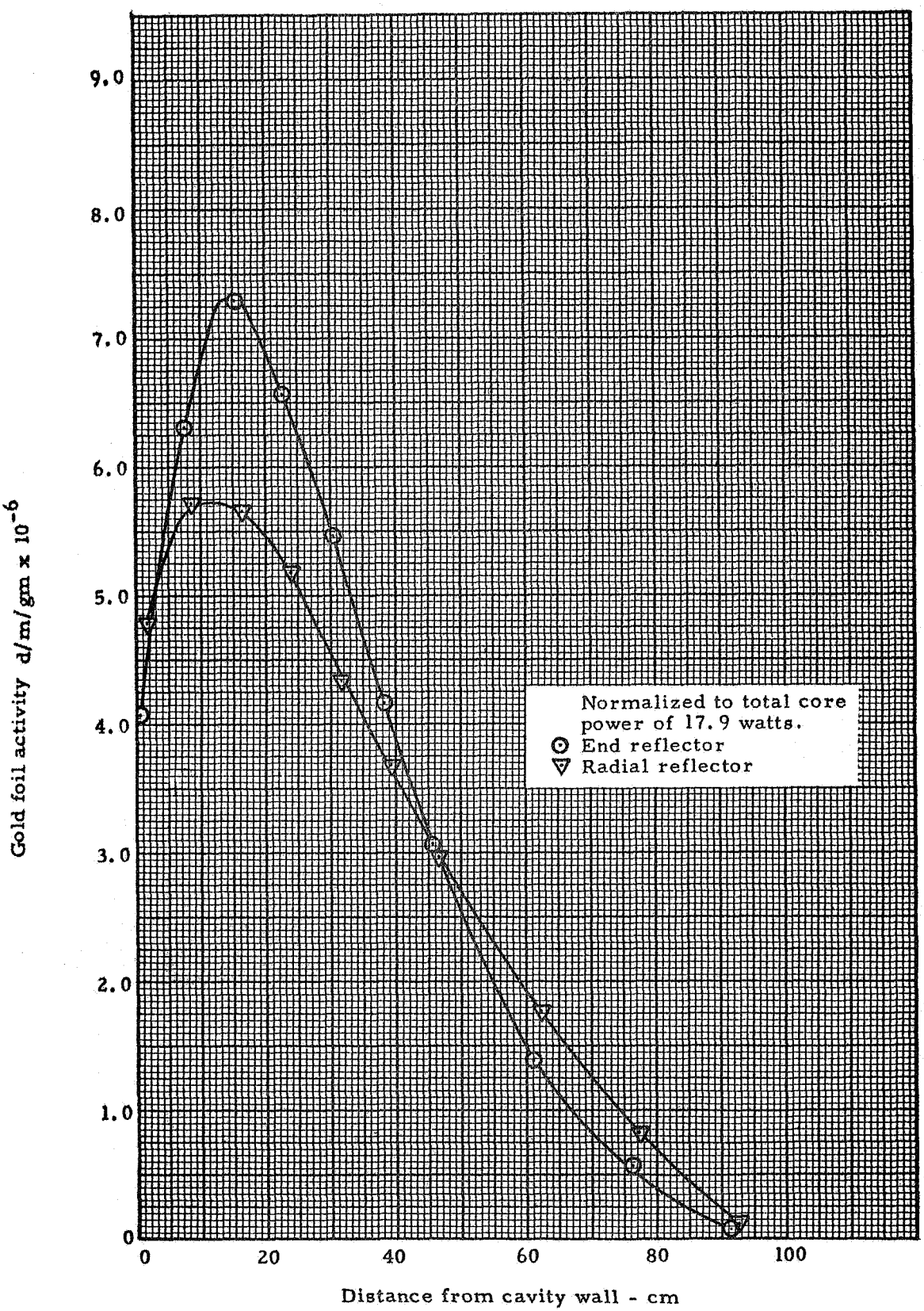


Fig. 4.12 Bare gold foil activity distribution in the reflectors - Mockup No. 1

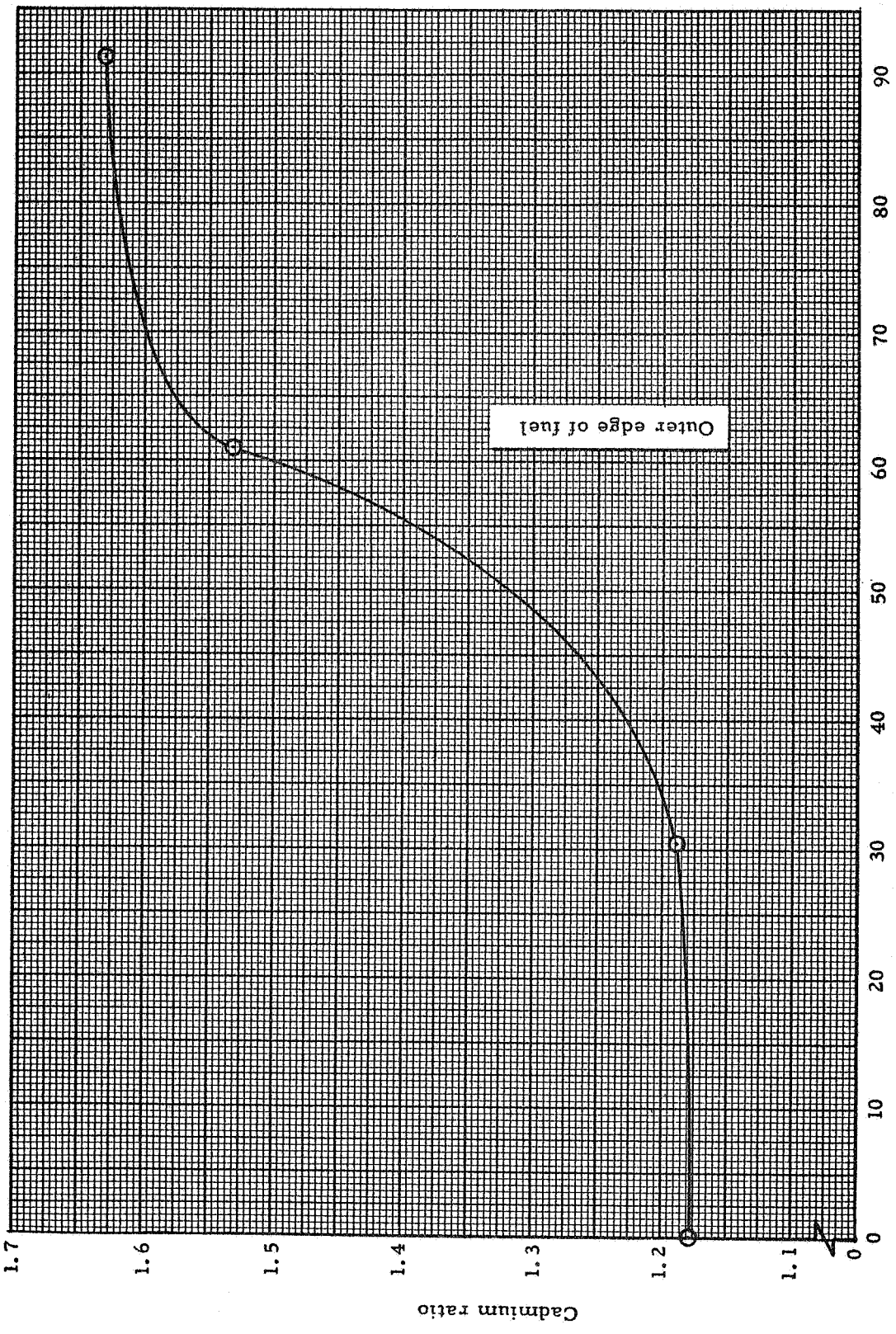


Fig. 4.13 Gold foil cadmium ratio radial profile - Mockup No. 1

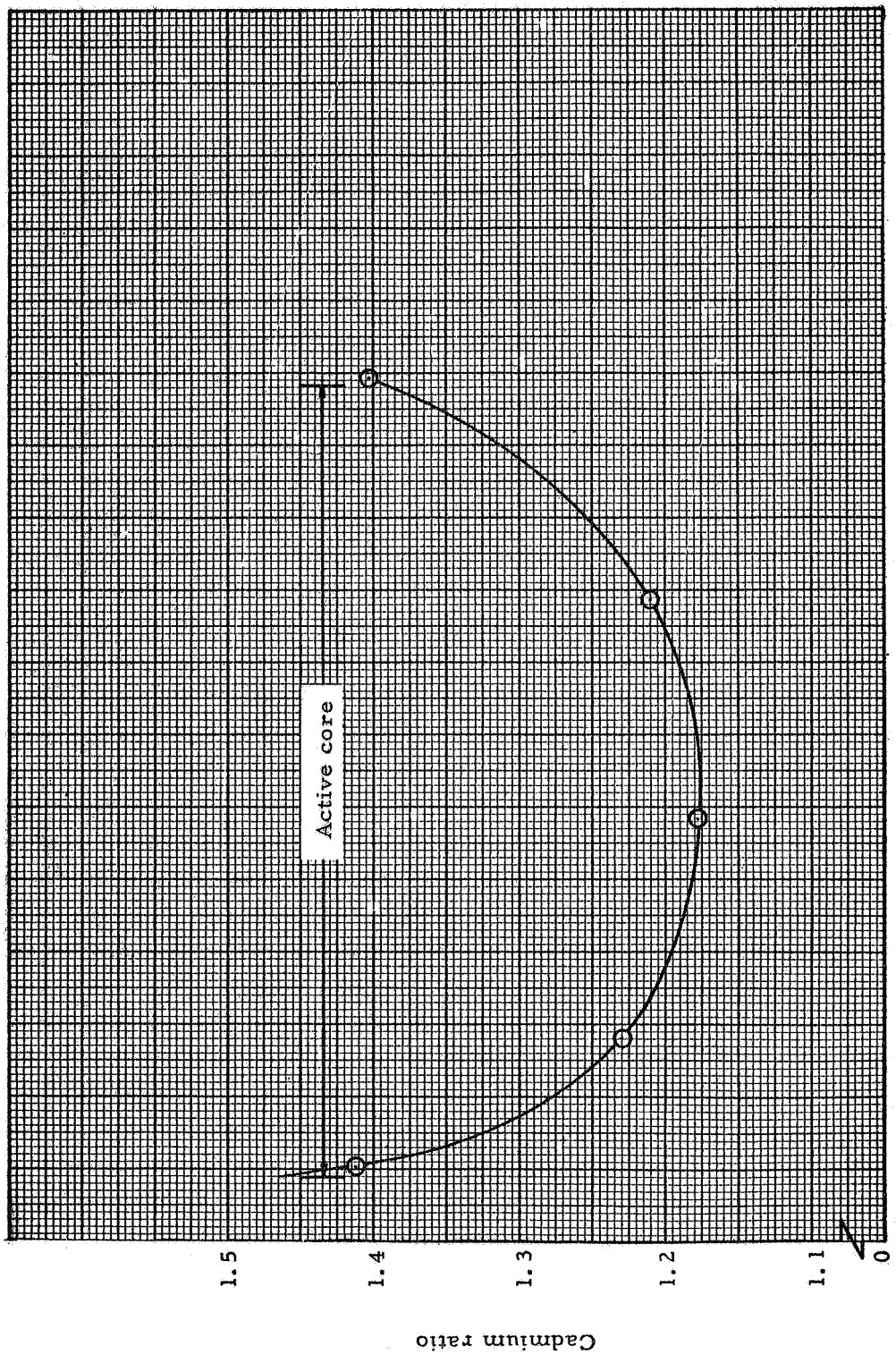


Fig. 4.14 Gold foil cadmium ratio axial profile - Mockup No. 1

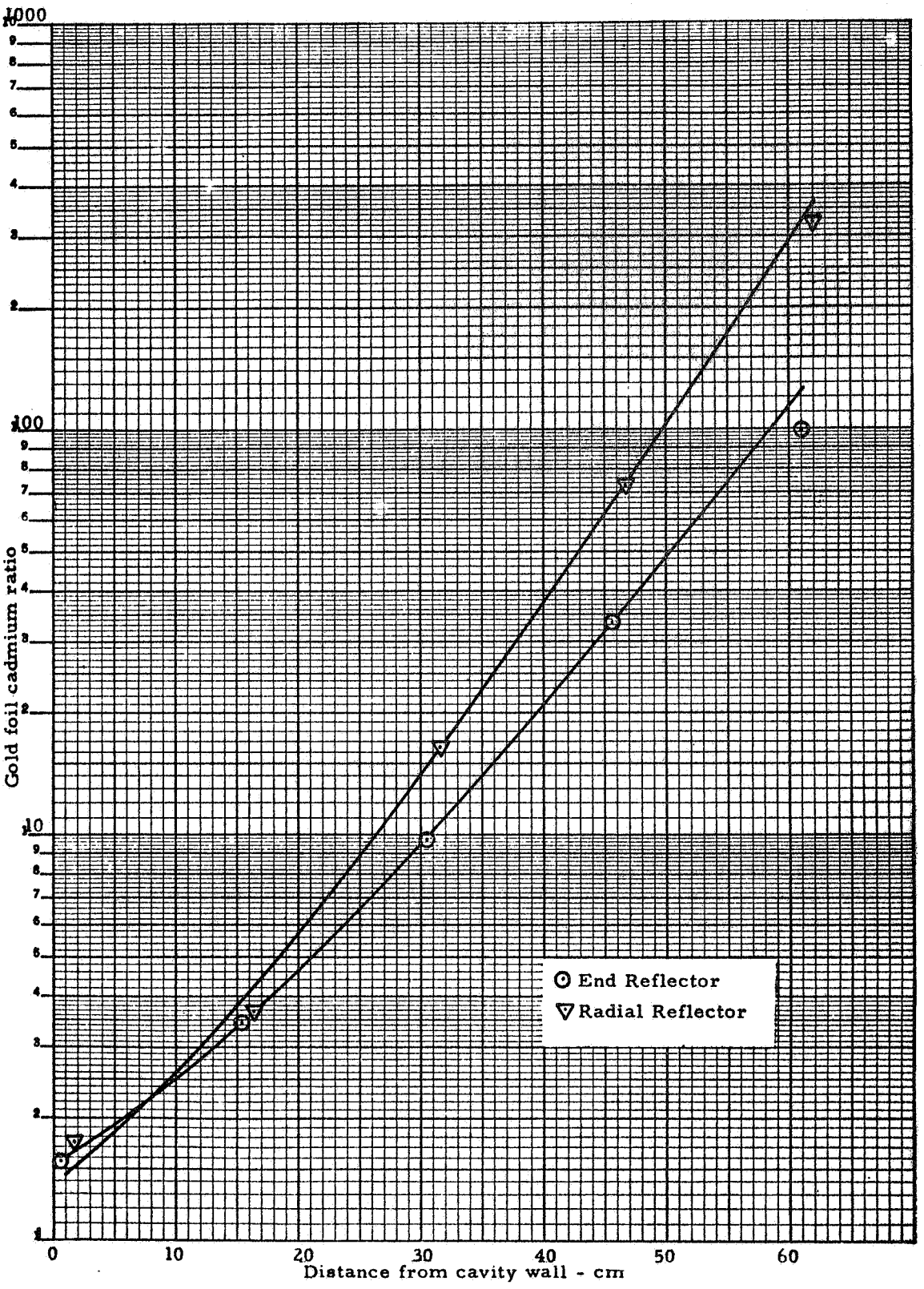


Fig. 4.15 Gold foil cadmium ratios in the radial and end reflectors - Mockup No. 1

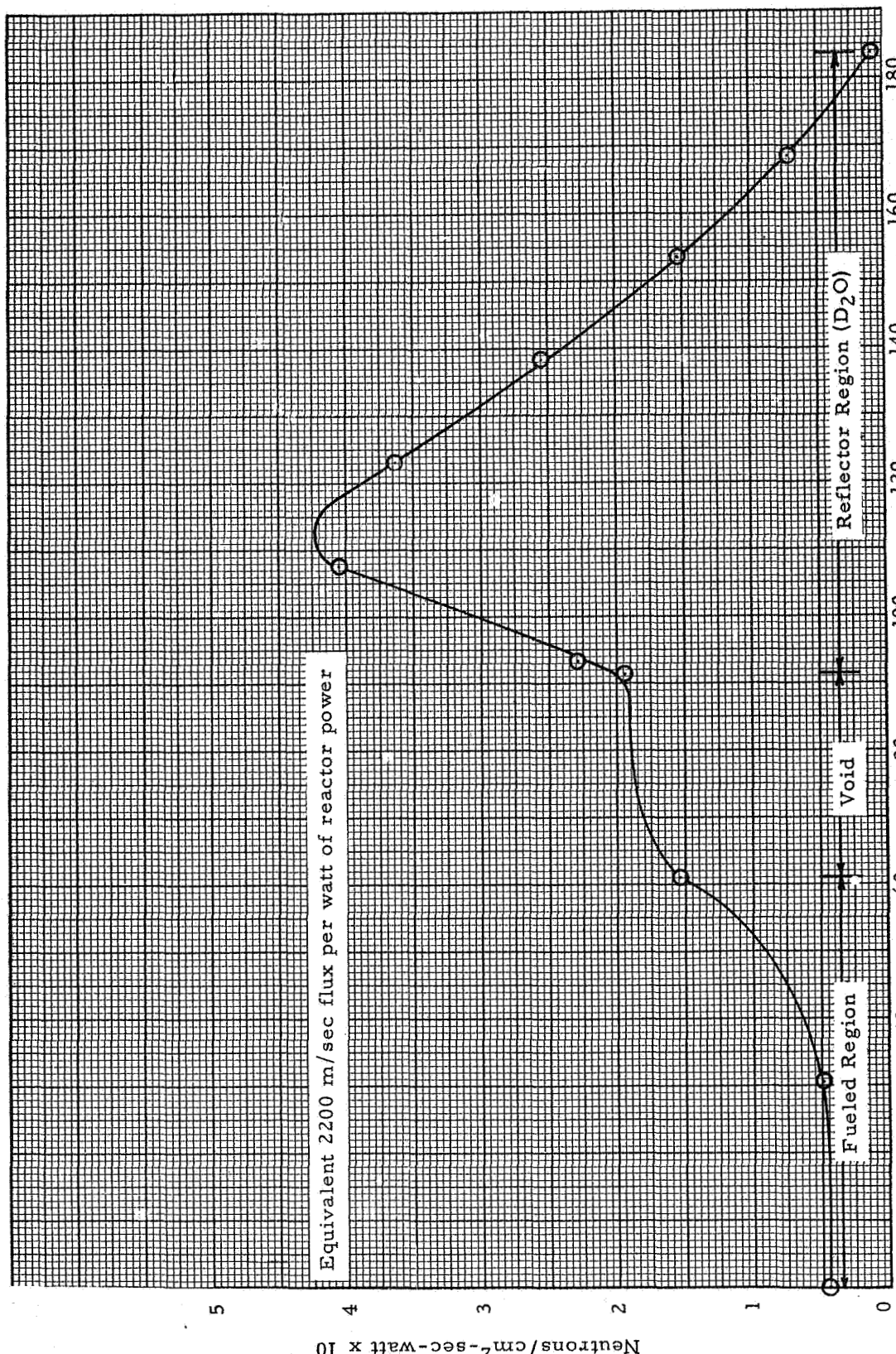


Fig. 4.16 Thermal neutron flux distribution radially through axial center of core - Mockup No. 1

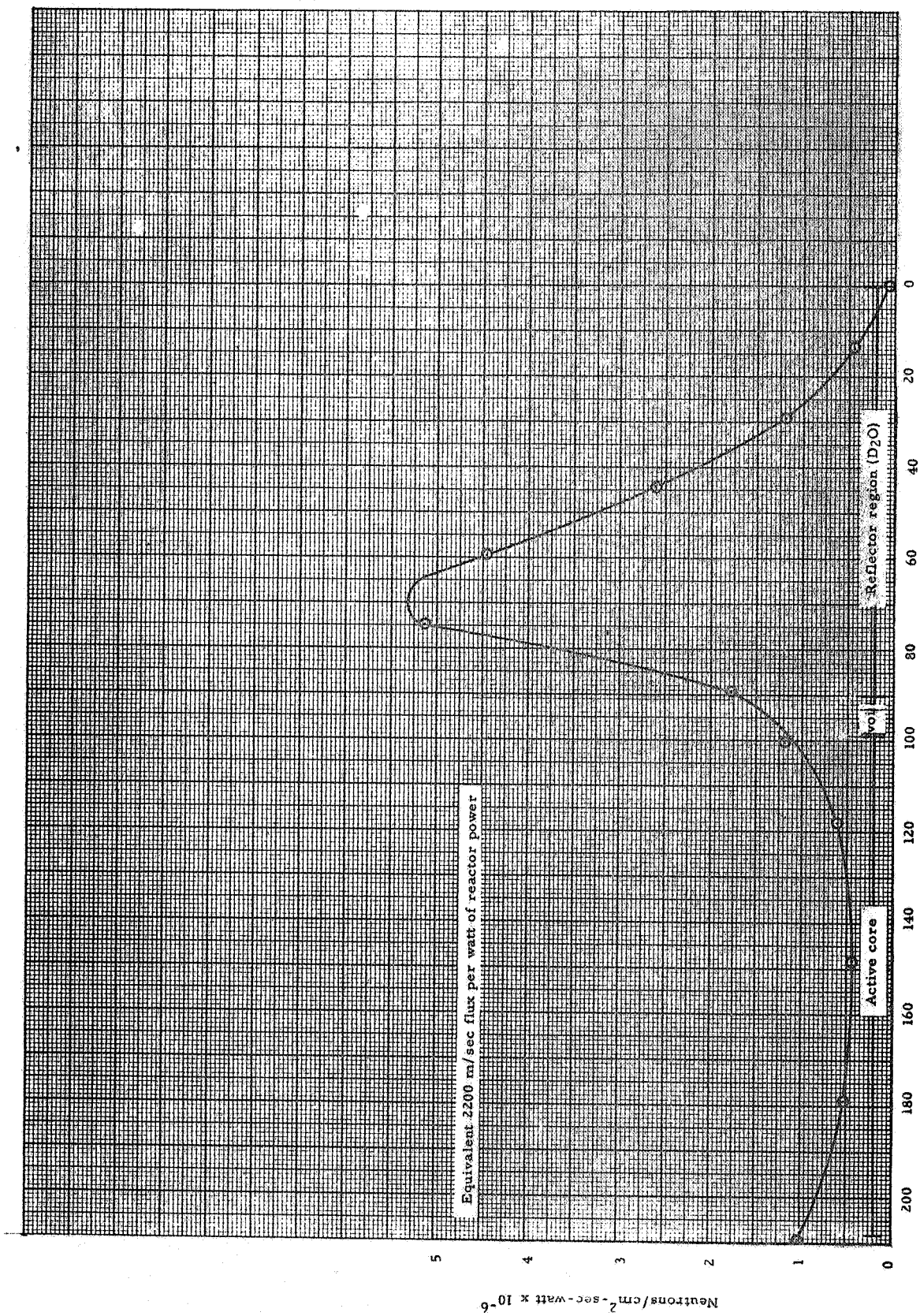


Fig. 4.17 Thermal neutron flux distribution axially through radial center of core - Mockup No. 1

5.0 UF_6 EXPERIMENT - BERYLLIUM AND D_2O REFLECTOR

An overall view of the UF_6 reactor assembly used for this experiment is shown in Figure 5.1. The core vessel which contained the UF_6 had inner dimensions of 108.6 cm long and 121.9 cm in diameter. The radial wall thickness was 0.635 cm thick and the end plates on the tank were 0.952 cm thick. Completely surrounding the tank was an air-flow annulus which was 7.08 cm wide on the ends of the tank and 0.635 cm wide over the radial walls. Ducting connected to the tank at the separation plane passed through the 30.5 cm diameter hole in the end reflector to a blower and electric heaters. Hot or cold air could then be sucked around the UF_6 tank to either heat or cool the UF_6 as needed to perform the experiments. Baffles were built into the tank structure to force the air to pass from the inlet line over the bottom half of the tank and then return to the exhaust duct over the top half of the tank. The tank was insulated on the ends with a 0.152 cm thick sheet of teflon and on the sides with crushed aluminum foil. There were two small (2.54 cm) diameter aluminum tubes inside the tank, one running along the full-length axial center-line, and the other on the radius from the center to the top of the tank at the midplane. These were used for inserting flux detectors into the tank and the tubes did not contain UF_6. Their volume was 2/3% of the total UF_6 volume.

The material weights in the tank assembly were as follows:

Material	Weight (kg)
Teflon	7.93
Aluminum	244.9
Brass covered, steel screws	0.075

The aluminum weight includes insulation around the UF_6 tank and the flow skirt but not the hot air ducting through the 30.5 cm hole.

The UF_6 was transferred to and from the reactor tank through monel tubing which is nominally 64 w/o Ni, 32 w/o Cu with small amounts of Mn and Fe. There were also two valves on the reactor tank which were monel. The total weight of this material was about 974 grams and there was an additional 91 cm of tubing extending from the UF_6 tank through the end reflector (with the table closed) and this tubing weighed about 190 gm. The reactivity effect of this miscellaneous material was separately determined, and therefore, it is unnecessary to simulate it in a nuclear calculation model.

Thermocouples were used to monitor tank and air temperatures throughout the system and were remotely monitored in the control room. A pressure gauge was also mounted in the UF_6 transfer line leading to the UF_6 tank and could be observed through a closed circuit TV.

Figure 5.2 shows the tank and ducting inside the cavity with the table separated. Both inlet and outlet air ducting were attached to one end of the tank with the inlet pipe inside the outlet duct. The UF_6 transfer line was inside the inlet pipe. The heaters, UF_6 transfer control valves and the box in which the UF_6 bottles were heated to force the gas into the large

reactor tank were located on the floor next to the dolly on which the reactor was supported as shown in Figure 5.3.

The inside of the UF_6 tank had been treated with a fluoridizing process by Oak Ridge National Laboratory. Nevertheless, about 45 gm of uranium was not recovered in the form of UF_6. Some of this (12 gm) was washed from the walls. It seems reasonable to assume that as much as 45 grams of uranium had been absorbed into the walls of the tank early in the experiment and remained there throughout.

5.1 Initial Loading

The standard incremental loading procedure to load the fuel into the UF_6 tank was used starting from an initial increment of 16.11 kg UF_6. The inverse multiplication data obtained during this phase of the experiment are given in Table 5.1 with a single representative inverse multiplication curve shown in Figure 5.4 which is for channel No. 2. No unusual difficulties were encountered during initial loading. It normally took about three hours to vaporize the UF_6 in the large tank. It was noted, however, that reactivity continued to change slightly with time thus making it somewhat difficult to measure small reactivity differences. With 34.97 kg of UF_6 in the reactor and at an indicated* average tank temperature of 88°C, k-excess was 0.501 ± 0.015%Δk. The D_2O reflector temperature was 27°C and all rods were withdrawn except Actuator 7 which was 8.2 cm withdrawn. The above k-excess was based on an average worth for actuator 7 of (0.675 ± 0.020)%Δk.

5.2 Reactivity Measurements

5.2.1 UF_6 Effects on Reactivity Due to Heating and Cooling

UF_6 may be in the form of liquid, solid or gas depending on the temperature and pressure. These characteristics are shown in Figure 5.5 and the operating points normally held during reactor testing are given for the two major configurations (the beryllium and D_2O and the pure D_2O reflected reactors). It will be noted that these operating points were well within the required temperature and pressure to assure that the fuel was in a gaseous state.

During the operation of the UF_6 fueled reactor, it was noted that reactivity changed to some extent after the minimum temperature and pressure levels were attained to vaporize the UF_6 and after sufficient time had elapsed to allow complete vaporization. Some startups were conducted prior to full vaporization of the fuel with all control rods withdrawn. The reactor was controlled as it approached critical by gradually inserting the control rods until full vaporization was achieved. This type of startup was accomplished with comparative ease as the rate of increase in reactivity was slow enough to be handled by the control system without any difficulty.

---

* The nominal "tank temperature," unless otherwise noted, is an average of 4 thermocouples, one on each end, one on the radial wall, and one inside the radial flux tube near the tank center.

Two separate measurements were also made to evaluate the reactivity fluctuations which might be encountered as the UF_6 tank was cooled and the vaporized fuel began to solidify on the wall of the tank. The results of these measurements appear in Figures 5.6 and 5.7. The first measurement produced only a single reactivity spike of about 0.05%Δk whereas the second measurement, with an all D_2O reflector and 25 kg of UF_6, shows two reactivity swings with the magnitude of the first reactivity peak being about 0.04%Δk or approximately the same as observed on the first measurement. The second reactivity peak followed a large negative swing of about -0.53%Δk but the second peak was approximately 0.09%Δk below the level of the first reactivity peak. It will be noted from both sets of data that the reactivity changes due to cooling the tank occurred at an indicated * temperature level above the vaporization temperature for the specific fuel loading. Since only three or four thermocouples monitored the tank temperature, the complete temperature distribution was not known. The reason for the initial increase in reactivity as the reactor tank was cooled is believed to be due to condensation of fuel on the wall of the UF_6 tank. The neutron flux level was highest at the outer edge of the fueled region thus causing an increase in reactivity. As the fuel migrated from the center to the cavity wall, the probability of neutron capture in the fuel also increased. This effect, however, was only positive for small amounts of fuel movement or collection of fuel on the cavity wall and thus lasted only for short periods of time before producing a negative effect caused by self-shielding of the accumulated fuel deposits. The reason for the second peak in Figure 5.7 is theorized to be caused by overall condensation on all tank walls, following the initial (first peak) condensation which occurred only at the cool spot where the inlet air first contacted the tank wall. The measurement shown in Figure 5.6 allowed only natural convective and radiation cooling without forced air. Thus, the cool spot at the inlet did not occur, but once the entire tank wall reached condensation temperature, a single reactivity spike developed. After the spike appeared, only then were the blowers turned on.

5.2.2 Rod Worths

Several rod worth measurements were made during the course of the experiment with the following average values:

Actuator Number	Reactivity Worth (%Δk)
1 to 7 (20 rods)	-4.674 ± 0.049
3 (3 rods)	-0.861 (single measurement)
6 (3 rods)	-0.654 ± 0.022
7 (3 rods)	-0.675 ± 0.020

---

* The data in Figure 5.7 averaged only three thermocouples, those on the tank walls, to obtain the apparent tank temperature.

5.2.3 Material Worths

Various material worths were measured during this experiment. These are summarized in Table 5.2, and are all based on the above rod worths and include the standard errors associated with the rod worths.

The teflon was used as insulation over the ends of the UF_6 tank. If it is assumed that all 7.928 kg of teflon used in the reactor was worth the same as measured at the separation plane, its total worth was $-(0.259 \pm 0.033)\%\Delta k$.

The stainless steel worth was obtained by placing a sheet 91.4 cm wide by 121.9 cm long by 0.0965 cm thick against the cavity wall with a 57.3 degree pie sector on each end of the cavity. If the worth of stainless steel thus measured is extrapolated to a completed stainless steel lined cavity using the same thickness of material (0.0965 cm), it would reduce reactivity $(12.76 \pm 0.14)\%\Delta k$. This is 1/6 lower than results on Configuration 3B (Reference 1) which were an extrapolation from material worth on the radial wall only.

The polyethylene measurements in the reactor consisted of 12 sheets approximately 30.5 cm wide by 121.9 cm long by 0.0762 cm thick. These sheets were spaced across the void region between the cavity wall and the fueled section of the cavity by using five corrugated aluminum screens as spacers. A strip of stainless steel about 45.7 cm wide by 121.9 cm long by 0.0965 cm thick was placed between the first layers of polyethylene and the cavity wall. A 29 degree sector of stainless steel was also placed at each end of the cavity over the region containing the polyethylene. This was done to evaluate the hydrogen worth with a stainless steel liner in place. The worth of polyethylene was $-(0.253 \pm 0.009) \times 10^{-3}\%\Delta k$ compared to $-(0.283 \pm 0.009) \times 10^{-3}\%\Delta k/gm$ as determined from Configuration 5B (Reference 1) with no steel on the cavity wall. Therefore, the steel liner may have caused a decrease (11%) in hydrogen worth according to these data, but differences in fuel loading and those caused by the UF_6 tank may have been just as significant.

The exchange of beryllium for BeO involved a 55 degree sector over a length of 109.2 cm of the radial reflector. The beryllium was 6.5 cm (average distance) from the cavity wall. From the weights noted in Table 5.2, it will be seen that the BeO was a little short (0.9%) in weight based on the densities of 1.85 for Be and 3.025 for BeO. Replacing Be with BeO caused k-excess to decrease by $(0.330 \pm 0.031)\%\Delta k$. The same measurements on a previously tested configuration (1) gave $-(0.314 \pm 0.050)\%\Delta k$ when BeO was placed in the radial reflector in place of Be over the same sector and the same distance from the cavity wall. Compared to the most recent measurement, there is no apparent difference within the standard error of the two measurements.

In order to evaluate a ring of beryllium 10.16 cm thick around the cavity in the radial reflector at an average distance of 6.5 cm from the wet side of the cavity wall, it was necessary to reduce the fuel loading and evaluate the total worth from the worth of fuel removed from the reactor. Therefore, several fuel worth measurements were obtained to

establish a curve of fuel worth vs. core loading and these results are given in Table 5.2. The resulting curve is shown in Figure 5.8. Included in this figure is the point measured after removing the beryllium from the radial reflector. The error bars show large variations from a very small error to as much as ±7%. The primary reason for the different error values was that quite different quantities of uranium were involved in the several measurements and the error on the worth-per-gram of uranium was inversely proportional to the amount of fuel involved.

The critical loading for the UF_6 fueled reactor required corrections for aluminum, teflon, fluorine and k-excess in order to compare directly to the mockup reactor. These are as follows:

1.	Teflon (7.928 kg)	$-(0.259 \pm 0.033)\%\Delta k$
2.	Fluorine (11.4 kg)	$-(0.180 \pm 0.020)\%\Delta k$
3.	k-excess	$-(0.501 \pm 0.015)\%\Delta k$
	Total	$-(0.940 \pm 0.040)\%\Delta k$

The base fuel loading was 34.972 kg of UF_6 or 23.554 kg of uranium and according to Figure 5.8 uranium is worth $0.728\%\Delta k/kg$ at this loading. The value used, however, should be an average value between uncorrected and corrected loading. (The corrected fuel loading is that loading for which k = 1.00.) Interpolating this value gives a fuel worth of $0.77 \times 10^{-3}\%\Delta k/gm$ of uranium. Based on this value, $-(0.940 \pm 0.040)\%\Delta k$ is worth (1.220 ± 0.080) kg of uranium. A 5% standard error is assumed for uranium worth. The critical loading corrects to 22.33 kg of U only or 33.50 kg of UF_6 (correcting for the fluorine reactivity) with an estimated possible error of about 1.0%.

After this test series was completed, a measurement was made in Mockup No. 2 with the pure D_2O reflector to determine the worth of the hot air ducting, the monel tubing and the two values which were not a part of the mockup experiments. This material reduced k-excess $0.227\%\Delta k$. If it is assumed that the beryllium in the D_2O had no effect on this value, which is a fairly reasonable assumption, the critical loading would have to be reduced 337 gm of UF_6 for a total loading of 33.16 kg of UF_6 (22.30 kg of U). This compares with the value of 25.0 kg given in Section 4 for the corrected mockup loading. This 11% fuel loading difference is discussed further in Section 9.

5.3 Power Distribution Measurements

5.3.1 Bare Catcher Foil Results

The UF_6 tank was provided with a tube running axially through the radial center of the core into which foils could be placed to measure power and flux distribution. A similar tube also traversed the tank radially at the axial midplane of the tank. All foil exposures on the UF_6 reactor with a Be and D_2O reflector were conducted with all but Actuator 7 withdrawn. Actuator 7 was withdrawn nominally 17 cm and the D_2O temperature averaged about 25°C. The average UF_6 temperature varied from 83 to 88°C during these measurements.

Catcher foils were exposed in the cavity region to obtain radial power at the center and end of the core and axial power at the center and outer edge of the fueled region. Both bare and cadmium covered foils were used and the data are given in Table 5.3. The radial power distribution from bare catcher foils normalized to the core center is shown in Figure 5.9. The figure shows the distributions at the axial center of the active core and at the separation plane. The volume weighted average at the axial center was 1.523. The power hump in the distribution near the radial center of the reactor as the separation plane is approached is due to the 30.5 cm diameter hole in the tank in the end reflector. At the separation plane, the radial power curve goes through a minimum at 23 cm from the center.

The axial power profile is presented in Figure 5.10 which gives both the axial profile at the core center and at the outer surface of the UF_6 tank. In order to check the detailed power profile over the ends of the reactor where the power gradient was steep, small (0.635 cm diameter) catcher foils were used. These are presented in Figure 5.10 and it will be noted that there is excellent agreement between the two sizes of catcher foils. The average axial power over the length of the active core at the radial center of the reactor was 1.224.

5.3.2 Cadmium Ratios

The cadmium ratios resulting from the bare and cadmium covered catcher foil activities are given in Table 5.4 and the resulting distributions are shown in Figures 5.11 and 5.12. There was some data scatter from a smooth curve distribution; as will be noted; however, the data normally fall within 5% or less of a smooth curve. The cadmium ratio at the core center was 6.9 and this increased to 15.1 at the outer edge of the fuel. At the outer edge of the cavity next to the D_2O the cadmium ratio was about 21.5 on the average.

5.4 Gold Foil Data

5.4.1 Bare Gold Results

All of the gold data obtained during this experiment are contained in Table 5.5 and the power normalization factors are given in Table 5.6. The radial and axial activity profiles from the bare foil data within the cavity region normalized to the center of the core are shown in Figures 5.13 and 5.14, respectively. As shown in Figure 5.13, the ratio of the foil activity at the outer edge of the fuel to the core center was 1.57 compared to 2.47 for catcher foils. The normalized axial distribution given in Figure 5.14 shows the activation flux level at the separation plane to be about 4% higher than at the other end of the active core. The catcher foil data also showed the power at the separation plane to be higher than the other end but the magnitude of the difference was about 16%. This difference between the two ends of the reactor at the radial center of the core was due primarily to the 30.5 cm diameter hole in the center of the movable table which allows streaming of high thermal flux into the cavity from the reflector region.

The relative activation distribution within the radial and the end reflectors is presented in Figure 5.15. The end reflector data were obtained by placing foils in a rod guide tube hole at the radial center of the reactor. The radial reflector results came from foils inserted into a small aluminum pipe which extended from the top of the hatch on the fixed D_2O reflector tank to the wet surface of the cavity wall. This pipe was at the axial center of the reactor.

The foil activity was considerably higher in the end reflector than in the radial reflector except at the cavity wall. This was due to the close proximity of the end reflector region to the heavily loaded fueled region, which suppressed the low energy flux at the cavity-reflector interface but provided a greater source for the slowing down of neutrons that ultimately lead to a higher peak thermal flux in the D_2O.

5.4.2 Cadmium Ratios

The gold foil cadmium ratios obtained with the cavity region are given in Table 5.7. The corrected cadmium ratios are based on calculated infinitely dilute foil activity from the measured foil weight and count rate as explained in Section 4.4.2. The distribution of these ratios within the cavity is shown in Figures 5.16 and 5.17. At the core center the cadmium ratio was 1.22 and increases to 1.47 at the outer edge of the fuel and 1.69 at the cavity wall as shown in Figure 5.16. At the ends and radial center of the active core the cadmium ratios were 1.37 at the back end and 1.45 at the separation plane of the cavity. The increase in cadmium ratio at the separation plane was due to the 30.5 cm hole in the movable end reflector of the movable table.

The cadmium ratios in the reflector regions are shown in Figure 5.18. The end reflector cadmium ratios were consistently lower than the radial reflector, as will be noted, which gives a "harder" spectrum (more slowing down flux, less thermal flux) for this region of the reflector than was shown in the radial reflector. This is believed to be due primarily to the close proximity of the end reflector to the fuel in the cavity resulting in less thermal flux relative to the slowing down flux than exists in the radial reflector. The presence of control rods in the end reflector also tends to harden the spectrum in this region.

5.5 Neutron Flux Distribution

The thermal neutron flux was calculated from the bare and cadmium covered foil data and the results are given in Table 5.8 and Figures 5.19 and 5.20. As in the other configuration, thermal flux level in the end reflector was higher than in the radial reflector beyond about 10 cm from the cavity wall. It was also noted in the previous section that the neutron spectrum was harder in the end reflector than in the radial reflector; therefore, the entire neutron flux (as measured with 0.5 cm bare gold) was higher in the end reflector. As stated before, this difference was caused by the physical locations of the two reflector regions with respect to the fueled region of the cavity, the end reflector being against the fueled region and the radial reflector being 30.5 cm from the fuel.

5.6 Noise Measurements

A set of noise measurements were made using two large boron detectors placed inside the cavity. Principally, these measurements were to determine if there was a cyclical motion to the gas in the cavity. Though not necessarily from the same cause, it was hoped that any cyclical motion might relate to the steady but small drift in the system reactivity observed after an apparent steady state operating temperature is reached (Figures 5.6 and 5.7). The two large chambers each had an active volume of approximately 700 cm^3. The exact boron loading is not known, but the effective amount probably did not exceed 0.1 gm B^{10} in each chamber. This would give each chamber a relative efficiency with respect to the total fission rate, of 10^{-3}. Thus, at 1 cycle/second, the ratio of reactor neutron noise to the electronic white noise of the chamber is about 2/1 (Reference 4, p. 122) too low a ratio to expect to arrive at any definite conclusions concerning reactor behavior, unless the effects of gas motion on reactivity were substantial. Indeed, the smothering effect of background electronic noise was confirmed by the analysis of a single chamber, which exhibited only random white noise half a decade in amplitude at frequencies above 0.3 cycle/second. Elimination of this chamber noise by cross correlation [5] of the output from the two chambers gave the results shown in Figure 5.21.

It is apparent from the appearance of the spectral density of the cross correlation function that it is essentially a zero power reactor transfer function, except for some minor perturbations at 0.05, 0.08, 0.18, and 0.75 cycles per second. Beyond about 5 cycles per second, there is considerable variation in the amplitude of the spectral density function, a condition that may or may not be caused by effects in the reactor, i.e., the variations may be the result of "correlated" electronic noise. For this cavity reactor, the zero power transfer function amplitude vs. frequency plot does not have a well defined break point for prompt neutrons (Reference 1, p. 369) because the prompt neutron lifetime is so long and merges with the delayed neutrons to give a monotonically decreasing function (10 db/decade). Thus, the general trend of a decrease of 1 decade per decade in frequency was expected over the entire frequency range shown.

The two-detector cross correlation function, when fitted to a single exponential plus a background and thus ignoring the longer lived exponentials from delayed neutrons (6), gave a decay constant of 2.8 ± 0.3 sec^{-1}, which corresponds to a neutron generation time of approximately $(3.0 \pm 0.4) \times 10^{-3}$, (the reactor was less than 0.1%Δk sub-delayed critical when the measurements were taken). This neutron lifetime compares favorably with the values obtained on previous configurations using pulsed neutron techniques (Reference 1, p. 361).

The results of the noise analysis did not show any significant effects of the UF_6 gas motion. The few small resonances observed at low frequencies may be caused by gas motion which may affect reactivity and/or the flux in the vicinity of the chambers. These small effects imply that small density variations seem to exist in the gas, and that there is probably circulation of the gas (these conclusions are not

certain, however). The very low frequency of these effects (20 seconds per cycle) would imply that if the density variations have an increasing or decreasing trend with time, then very slow effects such as shown in Figures 5.6 and 5.7 would be consistent with the slow cyclical effects deduced from noise analysis. Thus, it is possible that the gas distribution was not entirely uniform (as the result of non-uniform wall temperatures perhaps) when these measurements were made. But the non-uniformities probably were such that they had an insignificant effect on the reactivity of the system. It is concluded that the reported multiplication factor, which implies a uniform gas distribution, is uncertain by less than $0.1\%\Delta k$ as a result of possible non-uniformities in the gas.

TABLE 5.1

Inverse Multiplication

Initial Loading - UF_6 Reactor with Be and D_2O Reflector

Increment	Fuel kg, UF_6	Channel 1 CPM	Channel 1 CRo/CR	Channel 2 CPM	Channel 2 CRo/CR	Channel 3 CPM	Channel 3 CRo/CR	Average CRo/CR	Rod Positions
0	0	1248	1.000	1920	1.00	1380	1.000	1.000	In
0	0	1270	1.000	1991	1.000	1375	1.000	1.000	Out
1	16.11	4943	0.252	4479	0.429	5050	0.273	0.318	In
1	16.11	6226	0.204	5311	0.375	6337	0.217	0.265	Out
2	20.38	6627	0.188	5629	0.341	6680	0.207	0.245	In
2	20.38	9411	0.135	7525	0.265	9486	0.145	0.182	Out
3	24.46	8667	0.144	6998	0.274	8875	0.155	0.191	In
3	24.46	14916	0.085	11353	0.175	15109	0.092	0.117	Out
4	28.64	11956	0.104	9253	0.208	12138	0.114	0.142	In
4	28.64	29568	0.043	21171	0.094	28920	0.048	0.062	Out
5	32.87	17526	0.071	12919	0.149	17262	0.080	0.100	In
5	32.87	145642	0.009	94296	0.021	129992	0.011	0.014	Out

TABLE 5.2

Material Worths

UF_6 Experiment

Material	Location	Material Weight (kg)	Material Worth %Δk per gram
Teflon	Separation plane	3.454	$-(3.27\pm0.41)\times 10^{-5}$
Stainless Steel	Cavity Wall	14.910	$-(0.136\pm0.002)\times 10^{-3}$
Polyethylene	Between Stainless Steel and Fuel	3.064	$-(0.253\pm0.009)\times 10^{-3}$
Be replaced with BeO	Radial Reflector 55 degree sector	184.8 Be 299.5 BeO	-0.330±0.031 total worth
Be	10.16 cm of Be 6.5 cm from the cavity wall in the radial reflector	not weighed	-3.003±0.260 total worth

Fuel Worths

Average Core Loading (kg uranium)	Worth per gram of uranium (%Δk)	$\frac{\Delta k/k}{\Delta m/m}$
17.66	$(1.081\pm0.020)\times 10^{-3}$	0.191±0.004 (1)
23.40	$(0.788\pm0.054)\times 10^{-3}$	0.184 ± 0.013
24.26	$(0.647\pm0.015)\times 10^{-3}$	0.157 ± 0.004
24.88	$(0.618\pm0.007)\times 10^{-3}$	0.154 ± 0.002
25.32	$(0.633\pm0.035)\times 10^{-3}$	0.160 ± 0.009
26.01	$(0.608\pm0.043)\times 10^{-3}$	0.158 ± 0.011

(1) Fuel worth measurement after removing the beryllium from the radial reflector.

TABLE 5.3

Catcher Foil Data

UF_6 Experiment

Foil No.	Foil Type	Location Radial (cm)	Location Axial (cm)	Normalized Counts	Ratio of Local to Core Center (Foil No. X)
Run 1070					
1	Bare	0	92.1	86826	2.390
2	Bare	0	106.6	52089	1.434
3	Bare	0	121.9	41869	1.153
4	Bare	0	137.1	37235	1.025
5	Bare	0	152.3	36314	1.000 X
6	Bare	0	167.6	37659	1.037
7	Bare	0	182.8	41393	1.140
8	Bare	0	188.7	60408	1.663
9	Bare	0	213.3	115540	3.181
10	Bare	0	228.5	157657	4.340
11	Bare	0	243.8	168834	4.648
12	Bare	0	259.0	143334	3.946
13	Bare	15.2	151.4	38172	1.051
14	Bare	30.5	151.4	42680	1.175
15	Bare	45.7	151.4	54394	1.497
16	Bare	61.0	151.4	89706	2.470
17	Bare	76.2	151.4	124212	3.420
18	Bare	91.4	151.4	128309	3.532
Run 1072					
1	Cd	30.5	151.4	5268	
2	Cd	0	98.1	6254	
3	Cd	0	158.4	5239	
4	Cd	0	219.3	5133	
Run 1073					
1	Cd	0	121.9	5391	
2	Cd	0	182.8	5246	
3	Bare	0	208.2	88602	2.440
4	Cd	61.0	151.4	5922	
5	Cd	91.4	151.4	6254	
Run 1074					
1	Cd	45.7	151.4	5079	
2	Bare	0	99.0	61401	1.706
3	Bare	0	151.1	35990	1.000 X
4	Bare	0	208.2	85352	2.372

TABLE 5.3
(Continued)

Foil No.	Foil Type	Location Radial (cm)	Location Axial (cm)	Normalized Counts	Ratio of Local to 6988
Run 1075 (0.635 cm diameter foils)					
1	Bare	0	91.8	16764	2.400
2	Bare	0	92.5	16560	2.370
3	Bare	0	93.3	15804	2.262
4	Bare	0	94.0	15358	2.198
5	Bare	0	94.8	14914	2.135
6	Bare	0	95.6	14464	2.070
7	Bare	0	96.3	13785	1.973
8	Bare	0	97.1	13174	1.886
9	Bare	0	97.8	12798	1.832
10	Bare	0	98.6	11593	1.659
11	Bare	0	99.4	12211	1.748
12	Bare	0	100.1	11815	1.691
13	Bare	0	100.9	11442	1.638
14	Bare	0	101.7	11332	1.622
15	Bare	0	102.4	10997	1.574
16	Bare	0	103.2	10825	1.549
17	Bare	0	103.9	10658	1.526
					Ratio of Local to Core Center (Foil No. X)
Run 1075					
18	Bare	0	104.7	10483	1.501
19	Bare	0	105.5	10233	1.465
20	Bare	0	148.1	6938	0.993
21	Bare	0	148.8	6914	0.990
22	Bare	0	149.6	7002	1.002
23	Bare	0	150.3	6999	1.002
24	Bare	0	151.1	7035	1.007
25	Bare	0	151.9	7028	1.006
26	Bare	0	152.6	6990	1.001
27	Bare	0	154.1	6979	0.999
28	Bare	0	154.9	6988	1.000 X
29	Bare	0	198.4	10820	1.549
30	Bare	0	199.1	11165	1.598
31	Bare	0	199.9	11597	1.660
32	Bare	0	200.7	11874	1.700
33	Bare	0	201.4	12305	1.761
34	Bare	0	202.2	12883	1.844
35	Bare	0	202.9	13330	1.908

TABLE 5.3
(Continued)

Foil No.	Foil Type	Location Radial (cm)	Location Axial (cm)	Normalized Counts	Ratio of Local to Core Center (Foil No. X)
Run 1075 (Cont'd)					
36	Bare	0	203.7	13831	1.980
37	Bare	0	204.5	14118	2.021
38	Bare	0	205.6	14023	2.007
39	Bare	0	206.0	15584	2.231
40	Bare	0	206.7	16572	2.372
41	Bare	0	207.5	17441	2.497
42	Bare	0	208.3	17930	2.567
43	Bare	0	209.0	18493	2.647
44	Bare	0	209.8	19265	2.758
45	Bare	0	210.6	19326	2.766
46	Bare	0	211.3	19758	2.828
47	Bare	0	212.1	18757	2.685
Run 1076					
1	Bare	0	151.4	37535	1.000 X
2	Cd cov.	0	208.2	5360	---
3	Bare	15.2	212.7	87883	2.341
4	Bare	30.5	212.7	88457	2.356
5	Bare	45.7	212.7	106781	2.845
6	Bare	61.0	212.7	127313	3.392
8	Bare	91.4	212.7	135438	3.608
9	Bare	63.2	90.8	136216	3.629
10	Bare	63.2	105.3	122029	3.251
11	Bare	63.2	120.6	112410	2.995
12	Bare	63.2	135.8	111827	2.979
13	Bare	63.2	151.1	111705	2.976
14	Bare	63.2	166.3	46921	---
15	Bare	63.2	181.5	109457	2.916
16	Bare	63.2	196.8	115959	3.089
17	Bare	63.2	212.0	129505	3.450
18	Cd cov.	76.2	151.4	6335	---

TABLE 5.4

Catcher Foil Cadmium Ratios

UF_6 Experiment

Location				
Radial (cm)	Axial (cm)	Normal. Bare Foil Activity	Normal. Cd Foil Activity	Cd Ratio
0	92.1	86826	6254	13.88
0	121.9	41869	5391	7.77
0	152.4	36314	5239	6.93
0	182.8	41393	5246	7.89
0	208.2	86977	5360	16.23
0	213.3	115540	5133	22.51
30.5	151.4	42680	5268	8.10
45.7	151.4	54394	5079	10.71
61.0	151.4	89706	5922	15.15
76.2	151.4	124212	6335	19.61
91.4	151.4	128309	6254	20.52

TABLE 5.5

Gold Foil Data

UF_6 Experiment

Foil No.	Foil Type	Location Radial (cm)	Axial (cm)	Foil Weight (gm)	Specific Activity d/m/gm x 10^{-6}	Normalized to Core Center (X)
Run 1069						
1	Bare	0	89.4	0.04055	3.157	1.53
2	Bare	0	74.9	0.03230	7.960	3.86
3	Bare	0	59.6	0.03340	6.607	3.20
4	Bare	0	44.4	0.04210	4.822	2.33
5	Bare	0	29.1	0.02793	3.047	1.48
6	Bare	0	13.9	0.03430	1.558	0.755
7	Bare	0	0	0.03913	0.225	0.109
8	Bare	0	92.1	0.04170	3.153	1.53
9	Bare	0	106.6	0.03524	2.484	1.210
10	Bare	0	121.9	0.02930	2.335	1.140
11	Bare	0	137.1	0.03900	2.115	1.030
12	Bare	0	152.3	0.04140	2.051	1.000 (X)
13	Bare	0	167.6	0.040445	2.064	1.005
14	Bare	0	182.8	0.03610	2.200	1.070
15	Bare	0	198.1	0.03670	2.580	1.26
16	Bare	0	213.3	0.03330	3.716	1.81
17	Bare	0	228.5	0.04250	4.161	2.025
18	Bare	0	263.8	0.03070	3.971	1.93
19	Bare	0	259.0	0.04750	3.164	1.54
20	Bare	15.2	151.1	0.04325	2.024	0.986
21	Bare	30.5	151.1	0.03760	2.200	1.07
22	Bare	45.7	151.1	0.03250	2.564	1.25
23	Bare	61.0	151.1	0.03600	3.223	1.57
24	Bare	76.2	151.1	0.03560	4.110	2.00
25	Bare	91.4	151.1	0.03190	4.256	2.07
26	Bare	93.2	151.1	0.032215	4.681	2.27
27	Bare	107.7	151.1	0.0388	5.737	2.78
28	Bare	123.0	151.1	0.0360	4.695	2.27
29	Bare	138.2	151.1	0.0414	3.168	1.53
30	Bare	153.5	151.1	0.0399	1.914	0.927
31	Bare	168.7	151.1	0.0368	0.887	0.330
32	Bare	183.9	151.1	0.0318	0.120	0.058
Run 1070						
1	Bare	100.1	151.1	0.033845	5.686	
2	Bare	115.4	151.1	0.03648	5.058	
3	Bare	130.6	151.1	0.037077	3.740	
4	Cd	153.5	151.1	0.0339	0.002696	
5	Bare	0	82.5	0.0348	6.259	
6	Bare	0	67.2	0.032170	7.296	
7	Bare	0	52.0	0.033515	5.552	
8	Cd	0	29.1	0.02756	0.006371	

TABLE 5.5
(Continued)

Foil No.	Foil Type	Location Radial (cm)	Location Axial (cm)	Weight (gm)	Specific Activity d/m/gm x 10^{-6}
Run 1071					
1	Au-Cd	93.2	151.1	0.0280	1.744
2	Au-Cd	123.0	151.1	0.03450	0.140
3	Au-Cd	45.7	151.1	0.03976	1.382
4	Au-Cd	0	59.6	0.0354	0.288
5	Au-Cd	0	89.4	0.0381	1.597
6	Au-Cd	0	121.9	0.0282	1.572
7	Au-Cd	0	152.3	0.03745	1.396
8	Au-Cd	0	182.8	0.03657	1.408
9	Au-Cd	0	213.3	0.035415	1.381
Run 1072					
1	Au-Cd	0	74.9	0.041265	1.134
2	Au-Cd	0	44.4	0.0406	0.0506
3	Au-Cd	107.7	151.1	0.0338	0.758
4	Au-Cd	138.2	151.1	0.04177	0.0172
5	Au-Cd	61.0	151.1	0.0380	1.489
Run 1073					
1	Au-Cd	30.5	151.1	0.0421	1.366
2	Au-Cd	0	92.1	0.0337	1.652
3	Au-Cd	0	52.0	0.0337	0.121
4	Au-Cd	130.6	151.1	0.0379	0.050
Run 1074					
1	Au-Cd	91.4	151.1	0.03126	1.696
Run 1076					
1	Bare	0	92.1	0.0410	3.392
2	Bare	0	106.6	0.0409	2.466
3	Bare	0	121.9	0.0402	2.245

TABLE 5.6

Power Normalization Factor

Run	Count Time	Decay Time (min)	Decay Factor	Foil Activity (CPM)		Corrected Foil Activity (CPM) (1)	Norm. Factor
1069	2303.50	59.73	1.23	229172		281882	
	2305.75	61.98	1.28	219535		281005	
	2308.00	64.23	1.36	209479		284891	
	2310.30	66.53	1.41	200949		283338	
	2312.35	68.58	1.46	193843		283011	
	2314.40	70.63	1.51	186938		282276	
					Avg	282749	1.029
1070	1843.00	51.65	1.03	291474		289918	
	1845.70	54.35	1.10	264496		290945	
	1849.00	57.65	1.18	246570		290953	
					Avg	290605	1.001
1071	2144.27	46.06	0.90	325077		292569	
	2146.80	48.59	0.96	305452		293234	
	2149.02	50.81	1.01	289632		292528	
					Avg	292777	0.997
1072	1344.35	44.86	0.87	338183		294219	
	1347.10	47.61	0.94	315087		296182	
	1350.90	51.41	1.02	287778		293534	
					Avg	294645	0.987
1073	1629.35	63.62	1.33	220262		292948	
	1631.60	65.87	1.39	211021		293319	
	1633.80	68.07	1.44	202168		291122	
					Avg	292463	0.995
1074	1904.30	50.07	1.00	292984		292984	
	1906.60	52.37	1.05	277690		291574	
	1908.70	54.47	1.10	264426		290869	
					Avg	291809	0.997
1075	1426.50	27.90	0.52	517940		269329	
	1428.90	30.30	0.57	477745		272315	
	1431.25	32.65	0.61	444473		271129	
					Avg	270924	1.074
1076	1553.91	18.49	0.36	768667		276720	
	1556.17	20.75	0.40	698686		279474	
	1557.91	22.49	0.43	653604		281050	
					Avg	279081	1.042

TABLE 5.7

Gold Foil Cadmium Ratios - UF_6 Reactor

Location		Bare Foil Activity	Cd Foil Activity	Cadmium	Infinitely Dilute Cadmium
Radial (cm)	Axial (cm)	d/m/gm x 10^{-6}	d/m/gm x 10^{-6}	Ratio	Ratio
0	29.1	3.047	0.006371	478.3	226.7
0	44.4	4.822	0.0506	95.3	39.1
0	52.0	5.552	0.121	45.9	20.6
0	59.6	6.607	0.288	22.9	10.4
0	74.7	7.960	1.134	7.02	3.38
0	89.4	3.157	1.597	1.98	1.42
0	92.1	3.153	1.652	1.91	1.43
0	121.9	2.335	1.572	1.49	1.23
0	152.3	2.051	1.396	1.47	1.21
0	182.8	2.200	1.408	1.56	1.24
0	213.3	3.716	1.381	2.69	1.71
30.5	151.1	2.200	1.366	1.61	1.22
45.7	151.1	2.564	1.382	1.86	1.31
61.0	151.1	3.223	1.489	2.16	1.47
91.4	151.1	4.256	1.696	2.51	1.68
93.2	151.1	4.681	1.744	2.68	1.82
107.7	151.1	5.737	0.758	7.57	3.89
123.0	151.1	4.695	0.140	33.5	15.1
130.6	151.1	3.740	0.050	74.8	31.7
138.2	151.1	3.168	0.0172	184.2	74.2
153.5	151.1	1.914	0.002696	709.9	309.9

TABLE 5.8

Thermal Neutron Flux Distribution

UF_6 Reactor - Be and D_2O Reflector

Location		$n/cm^2/sec$ at 17 watts $\times 10^{-7}$	$n/cm^2/sec/watt$ $\times 10^{-6}$
Radial (cm)	Axial (cm)		
0	0	0.349	0.205
0	13.9	2.414	1.420
0	29.1	4.724	2.778
0	44.4	7.414	4.361
0	52.0	8.437	4.962
0	59.6	9.806	5.768
0	74.9	10.418	6.127
0	89.4	2.487	1.463
0	92.1	2.548	1.499
0	121.9	1.222	0.719
0	152.3	1.106	0.651
0	182.8	1.219	0.717
0	213.3	3.573	2.102
30.5	151.1	1.193	0.702
45.7	151.1	1.651	0.971
61.0	151.1	2.642	1.554
91.4	151.1	3.988	2.352
93.2	151.1	4.709	2.770
107.7	151.1	7.800	4.588
123.0	151.1	7.080	4.164
130.6	151.1	5.732	3.371
138.2	151.1	4.895	2.879
153.5	151.1	2.969	1.747
168.7	151.1	1.378	0.810
183.9	151.1	0.186	0.110

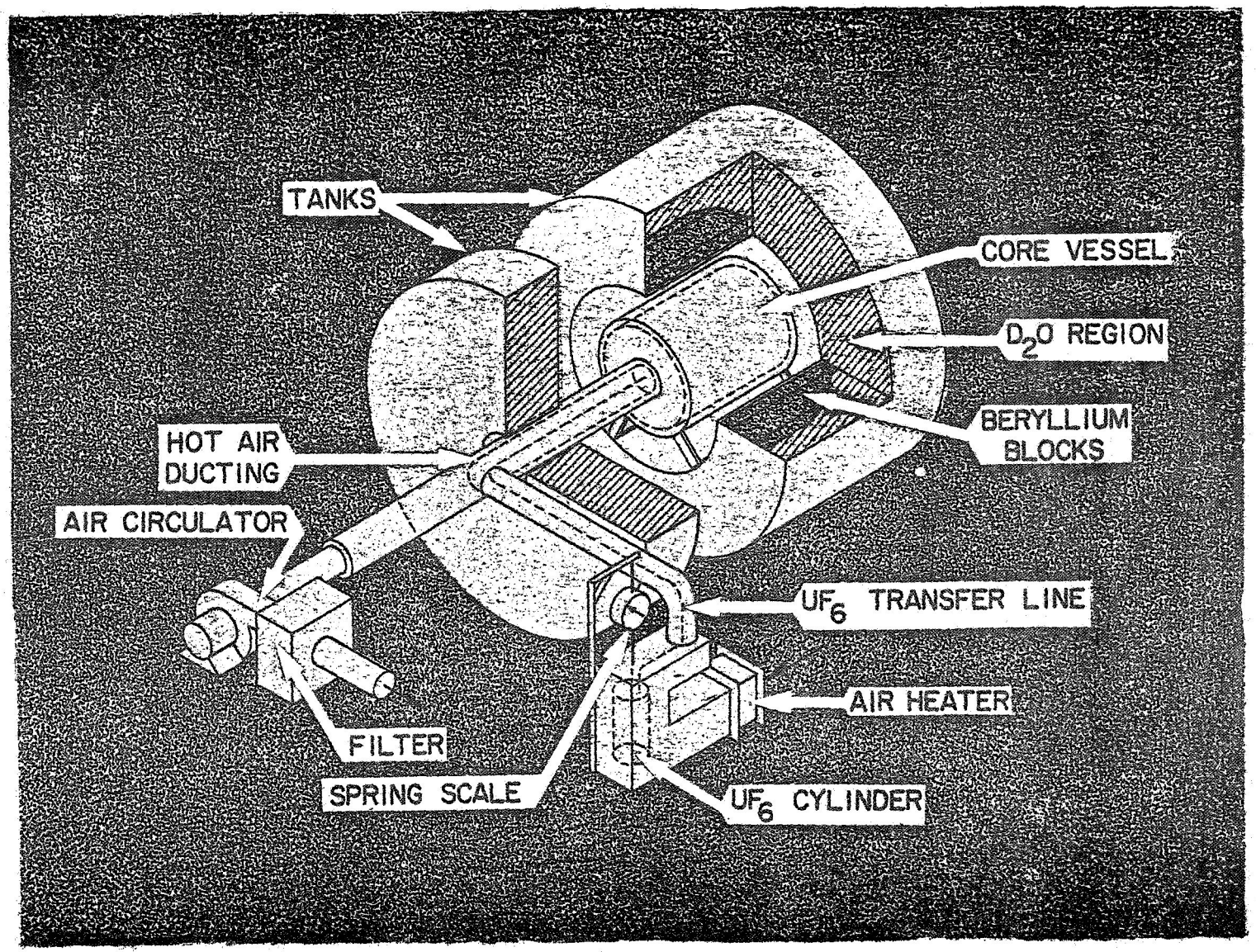


Fig. 5.1 General arrangement of cavity reactor showing heating equipment and UF_6 transfer system

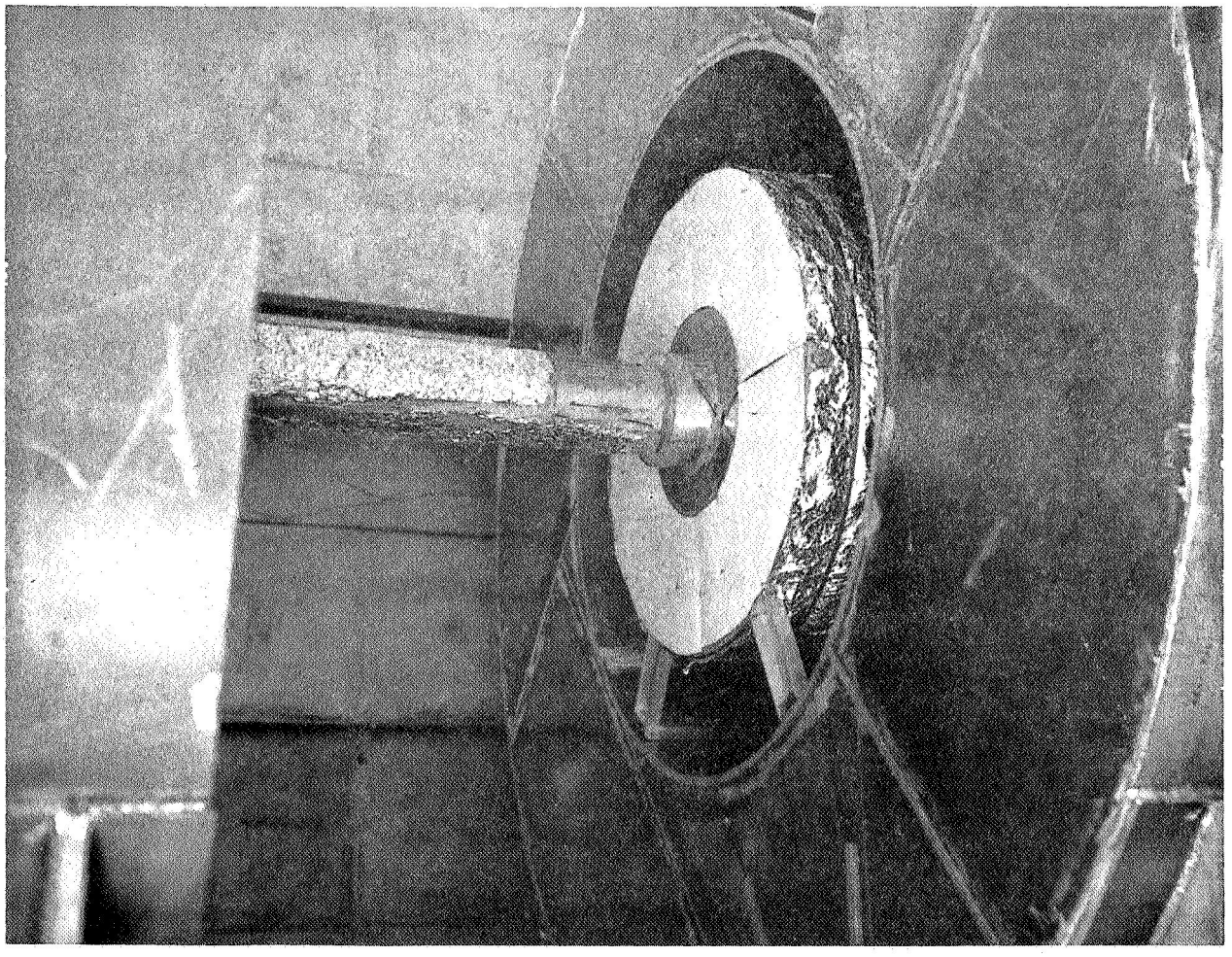
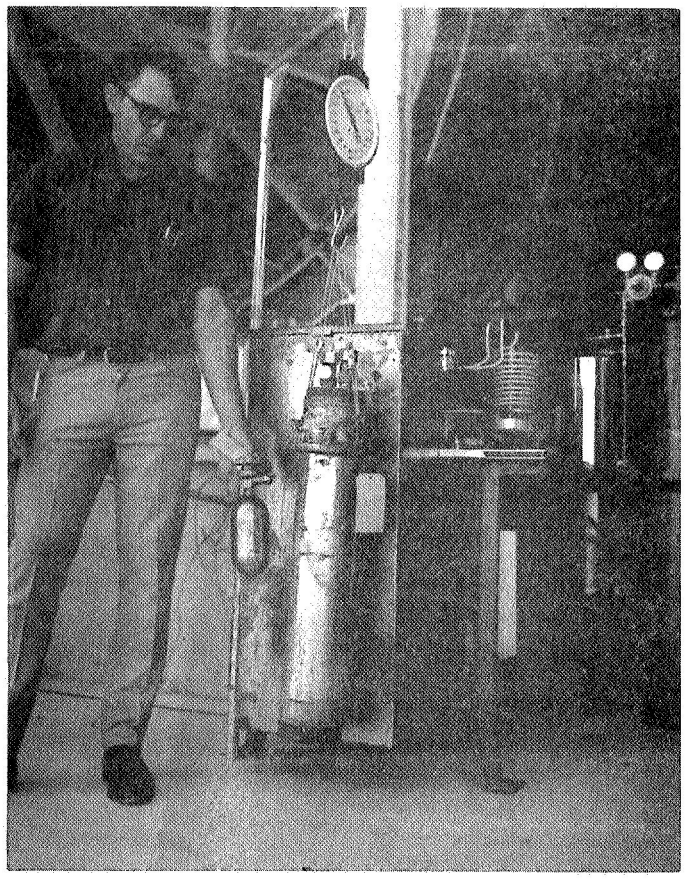


Fig. 5.2 View of separation plane with UF_6 tank in reactor



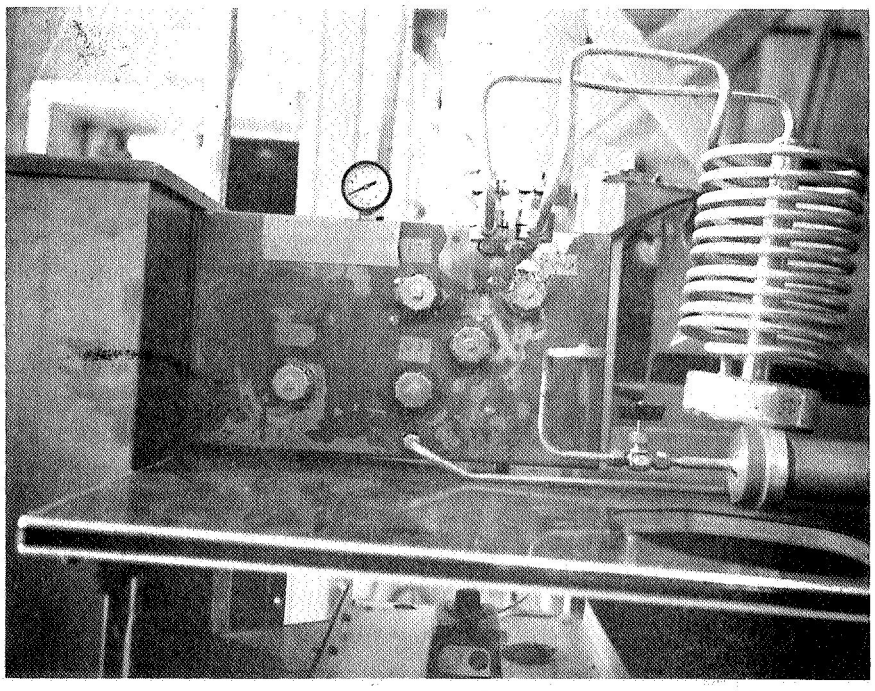


Fig. 5.3 UF_6 transfer control panel

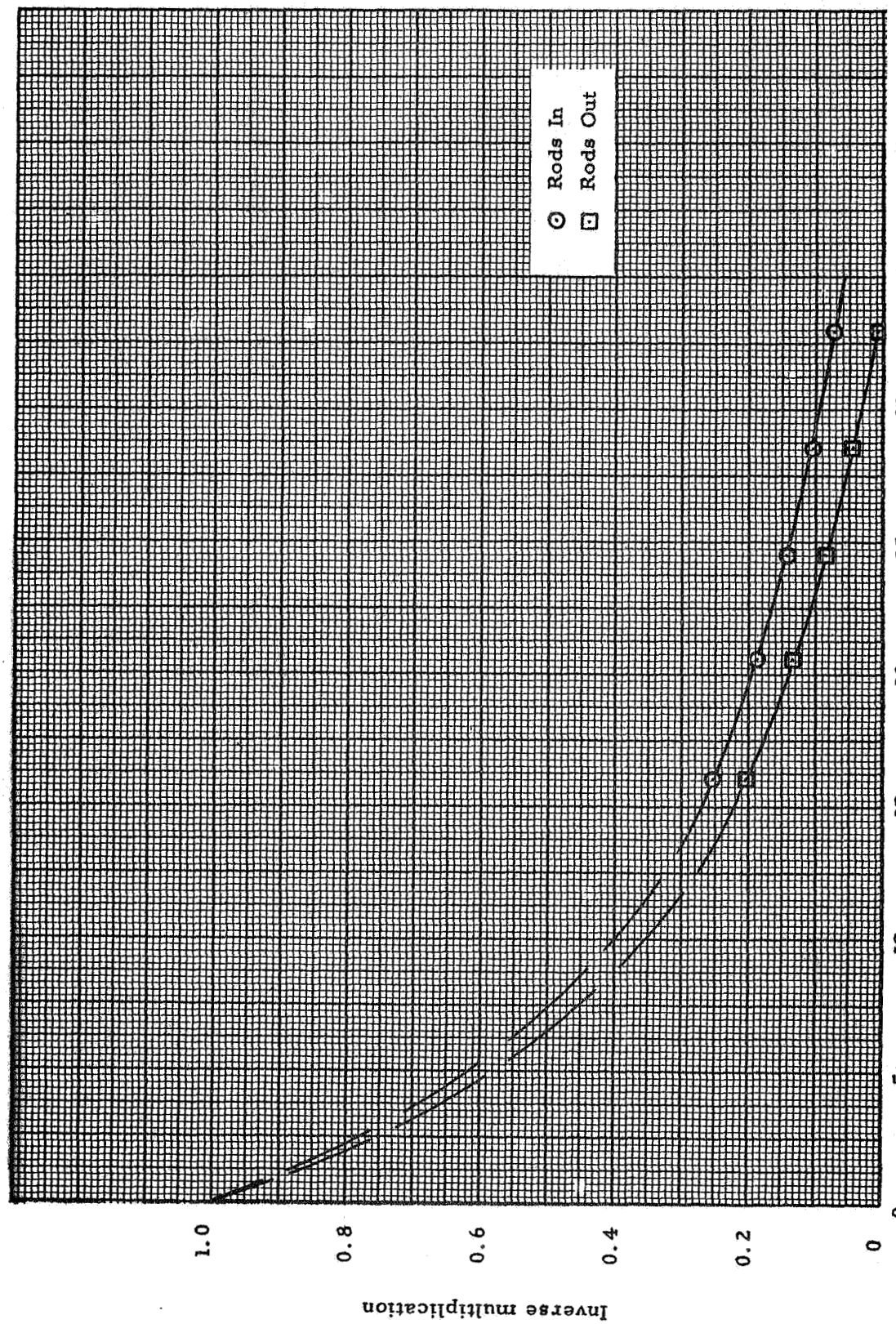


Fig. 5.4 Inverse multiplication curve - Channel No. 2 - UF_6 reactor with beryllium in reflector

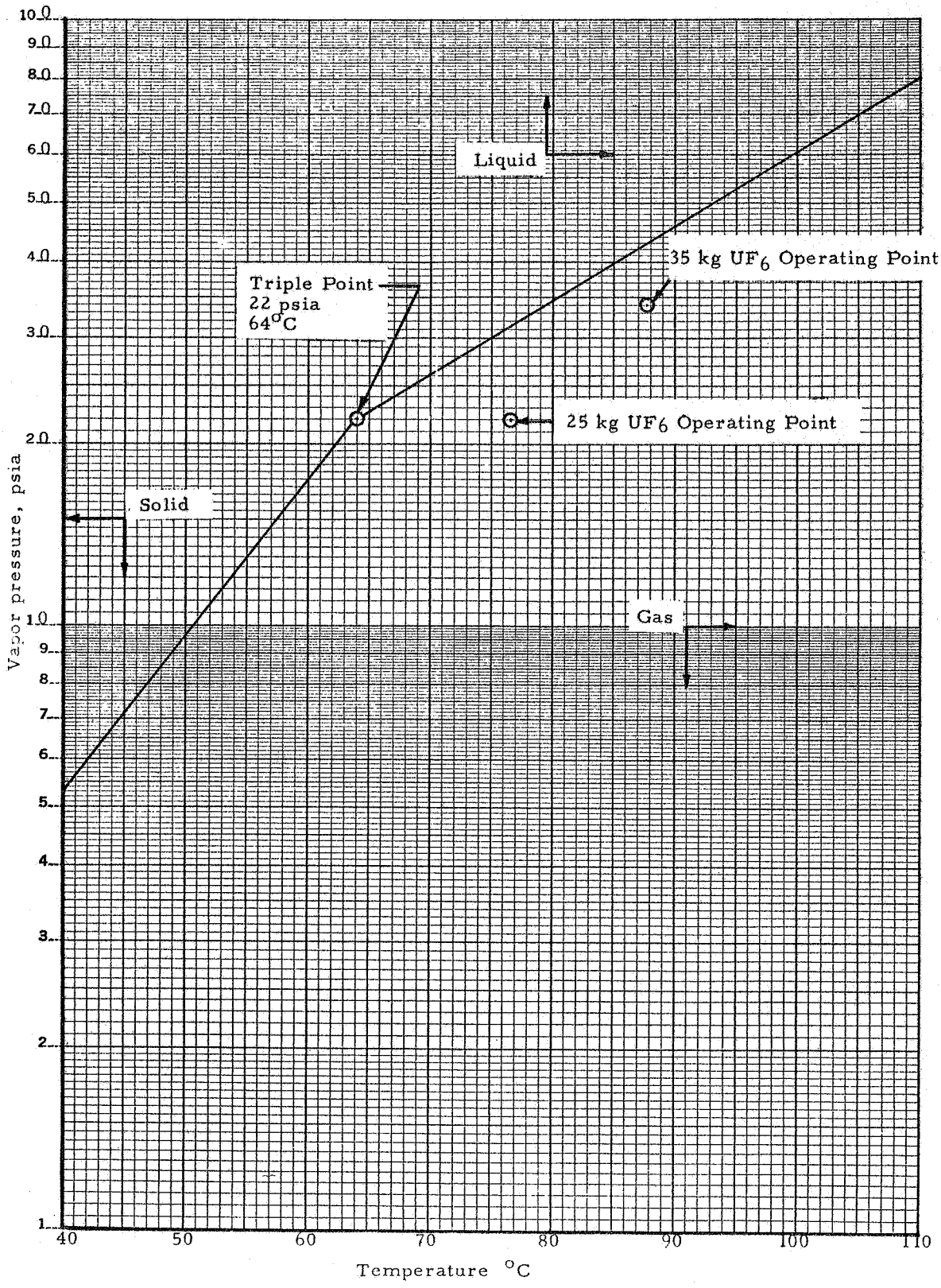


Fig. 5.5 UF_6 physical characteristics

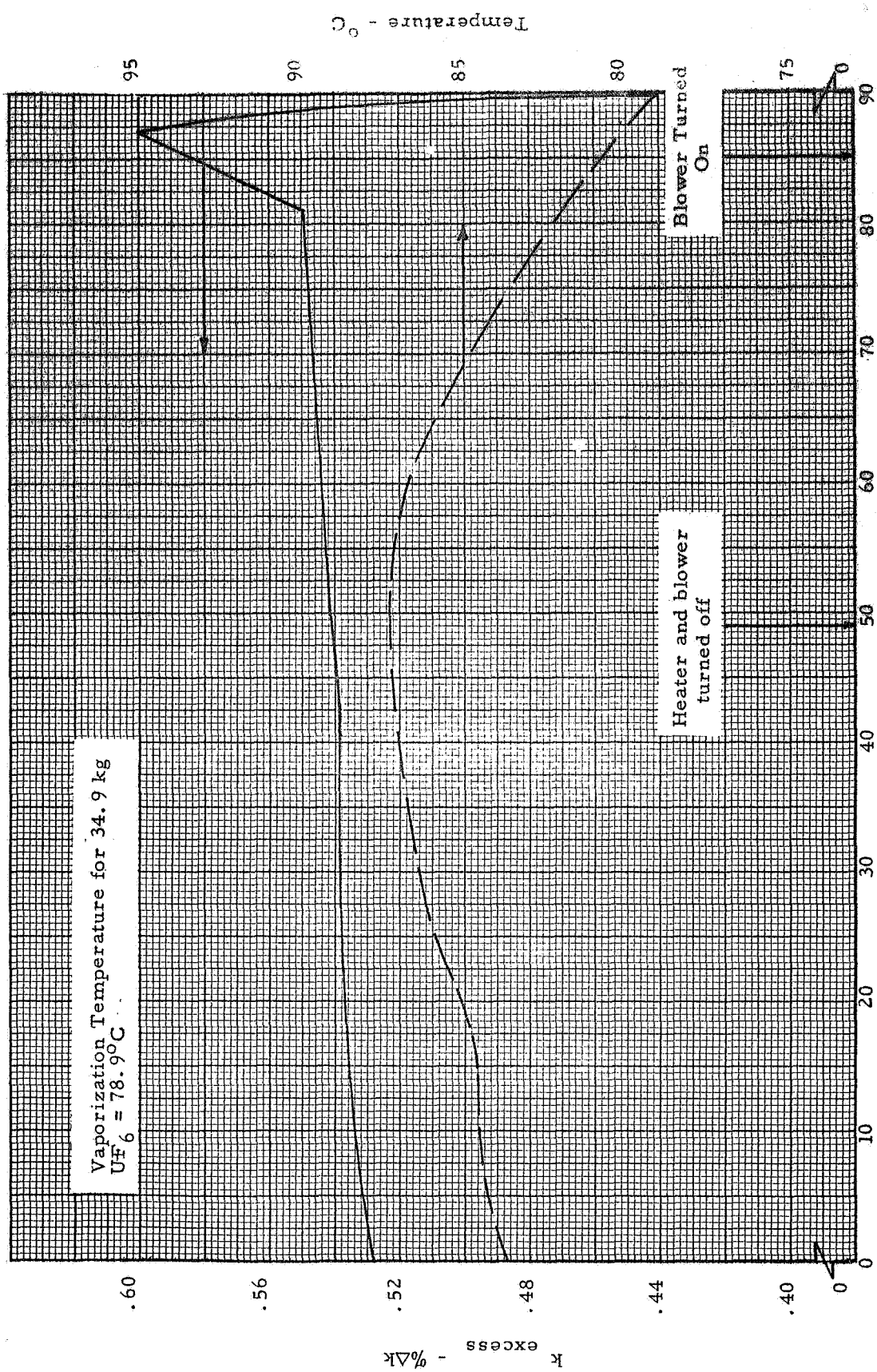


Fig. 5.6 Reactivity effect of cooling the UF_6 tank - UF_6 reactor with beryllium in reflector

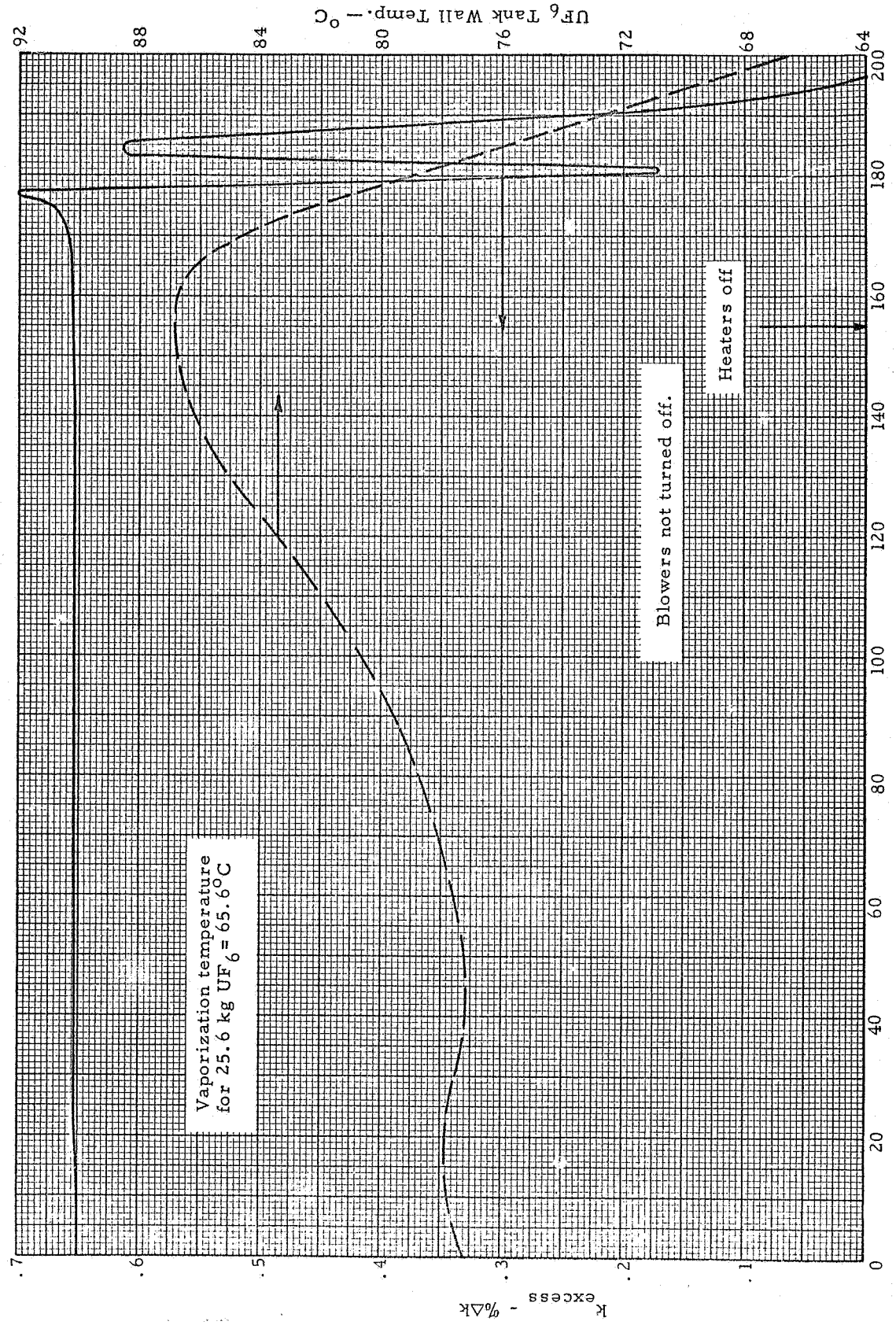


Fig. 5.7 Reactivity effect of cooling the UF_6 tank, second measurement - UF_6 reactor with beryllium in reflector

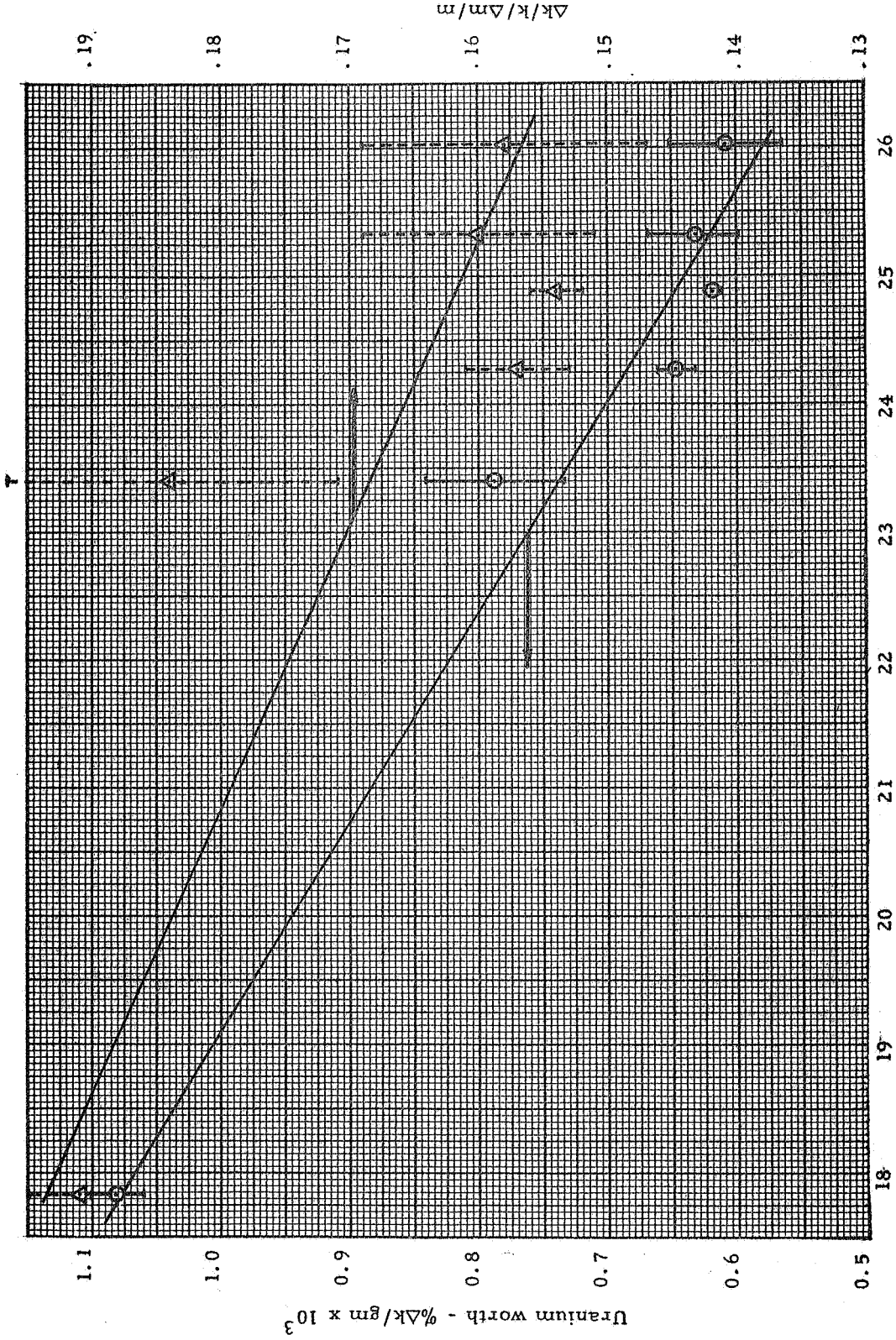


Fig. 5.8 Effects of core loading on uranium worth - UF_6 reactor with beryllium in reflector

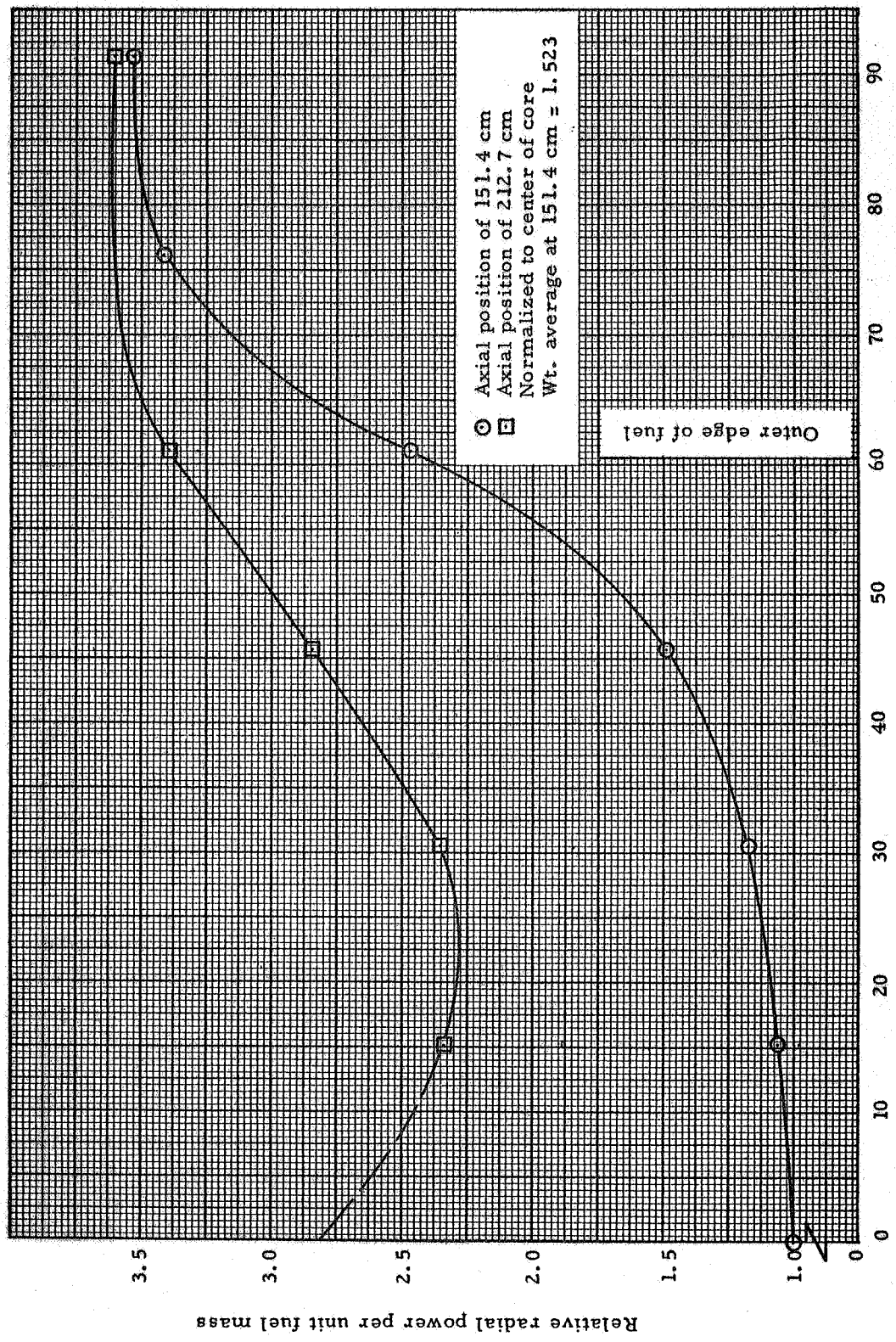


Fig. 5.9 Radial power distribution from bare catcher foils - UF_6 reactor with beryllium in reflector

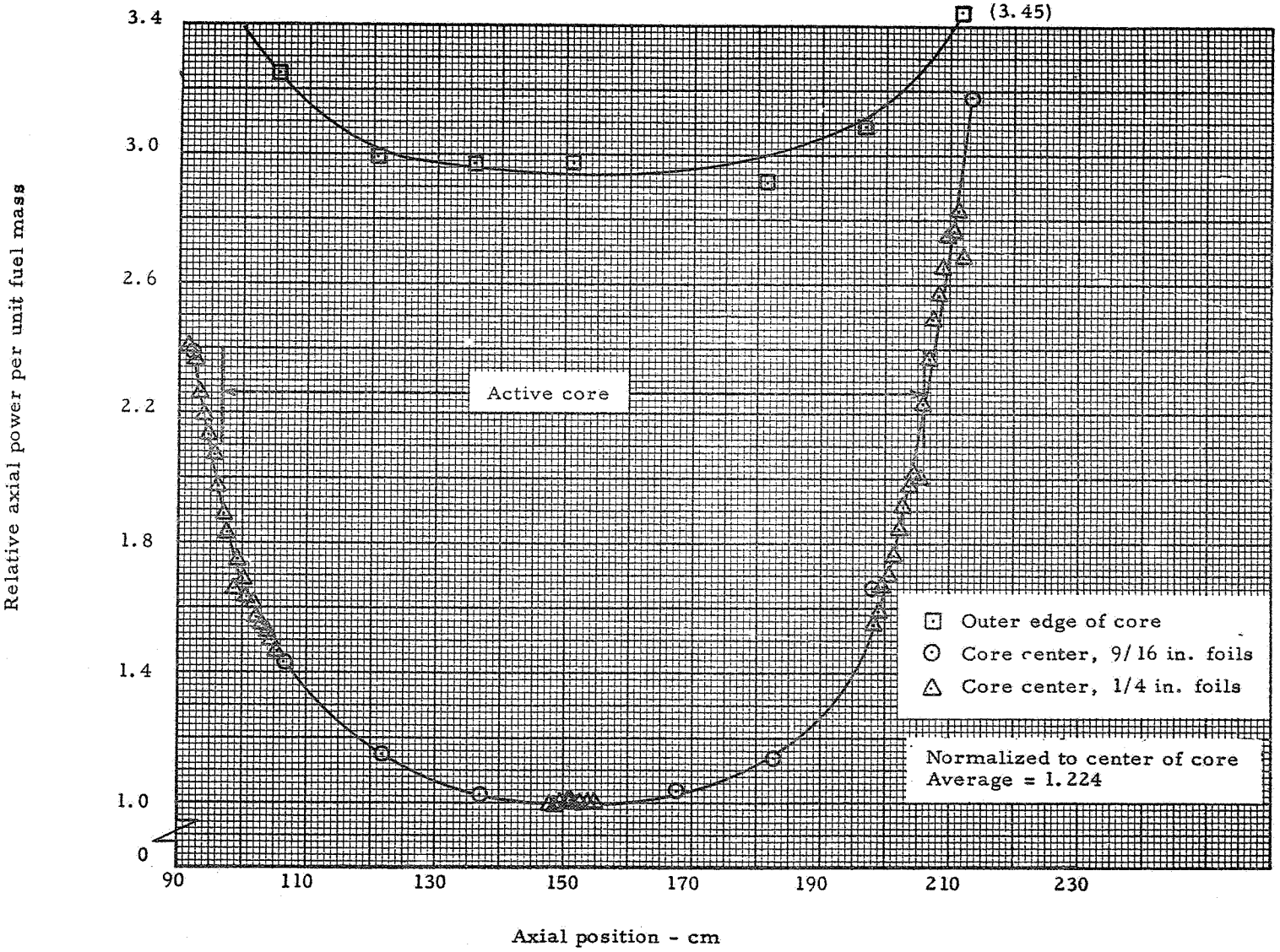


Fig. 5.10 Axial power distribution from bare catcher foils - UF_6 reactor with beryllium in reflector

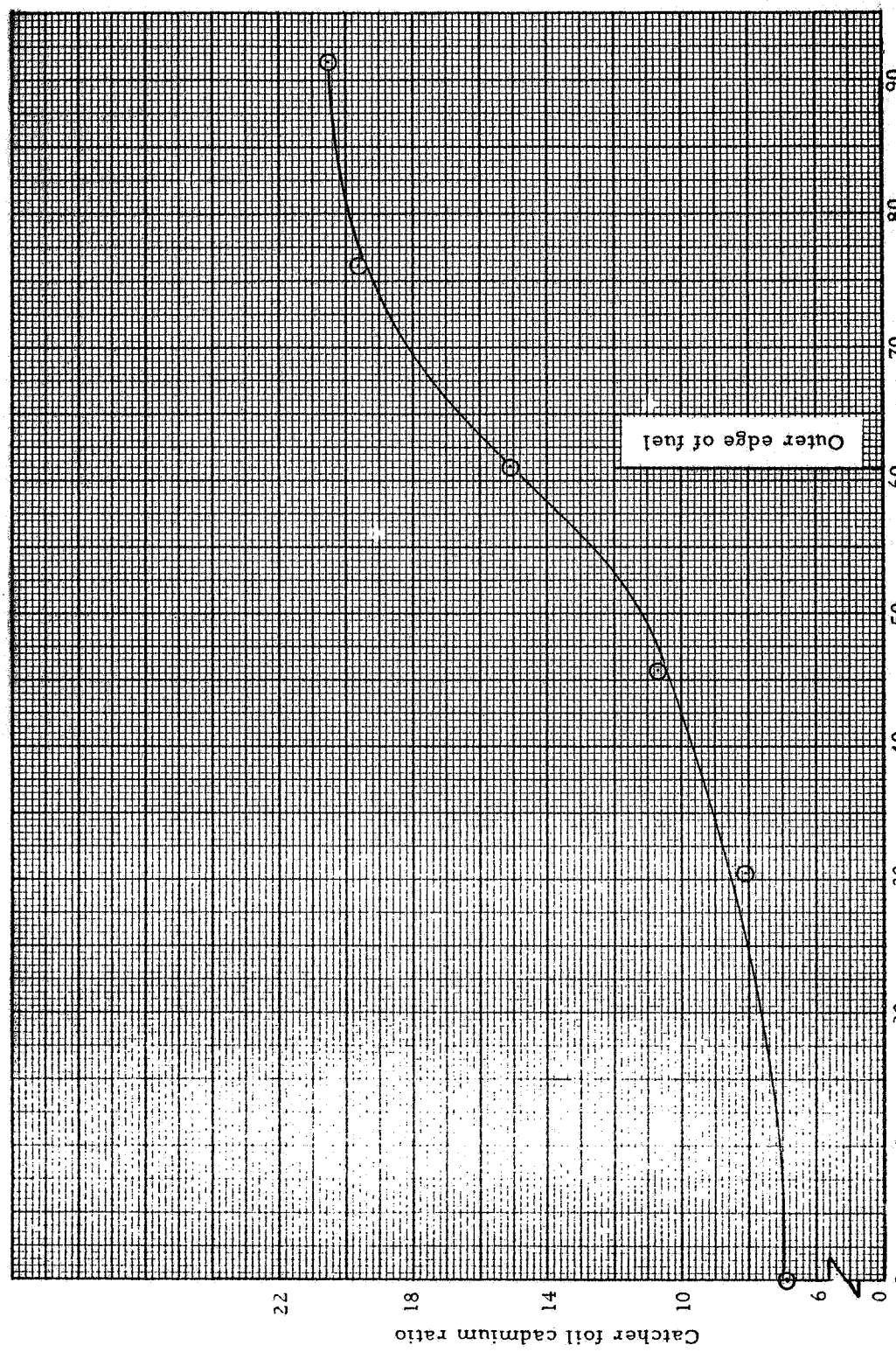


Fig. 5.11 Catcher foil cadmium ratio radial profile - UF_6 reactor with beryllium in reflector

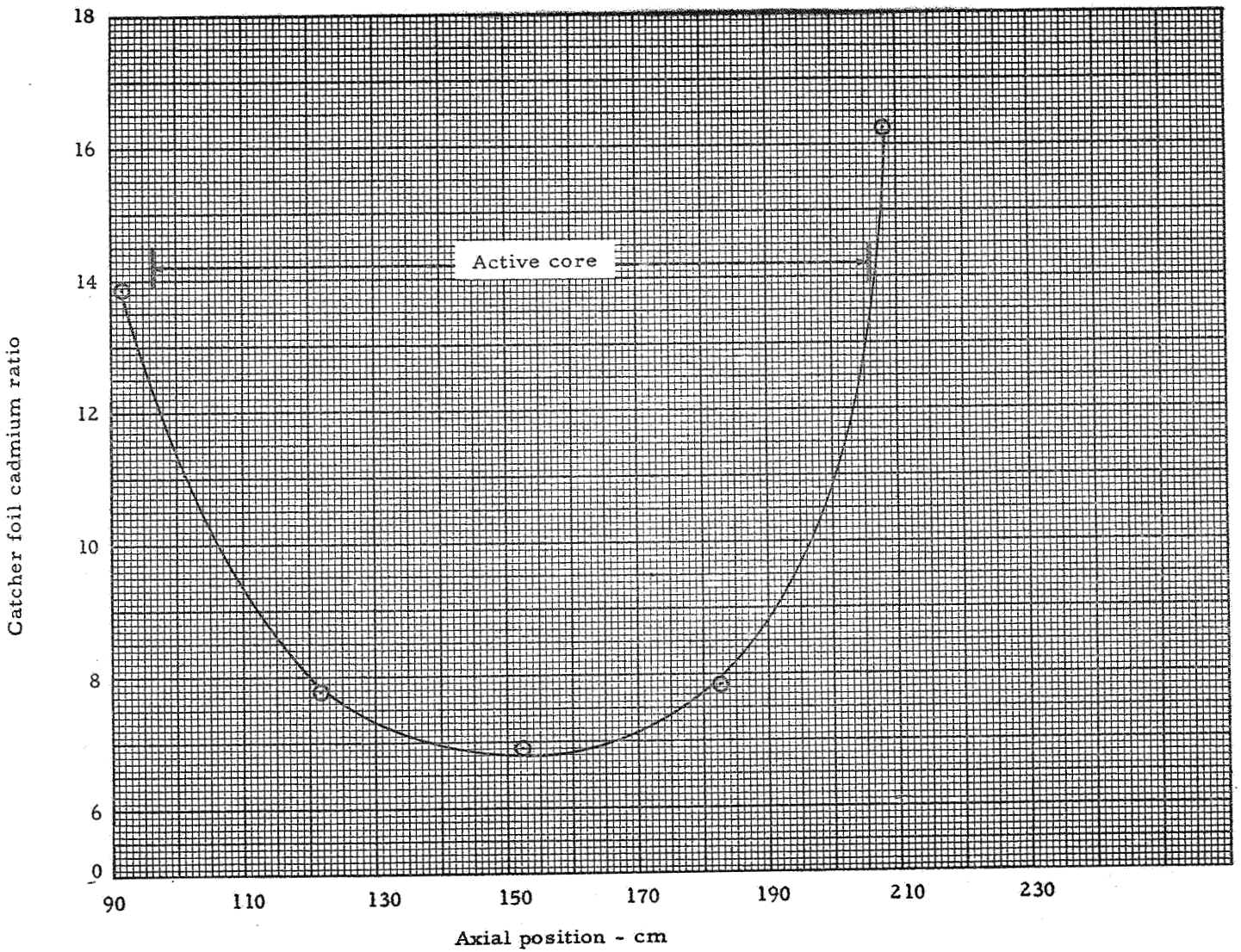


Fig. 5.12 Catcher foil cadmium ratio axial profile - UF_6 reactor with beryllium in reflector

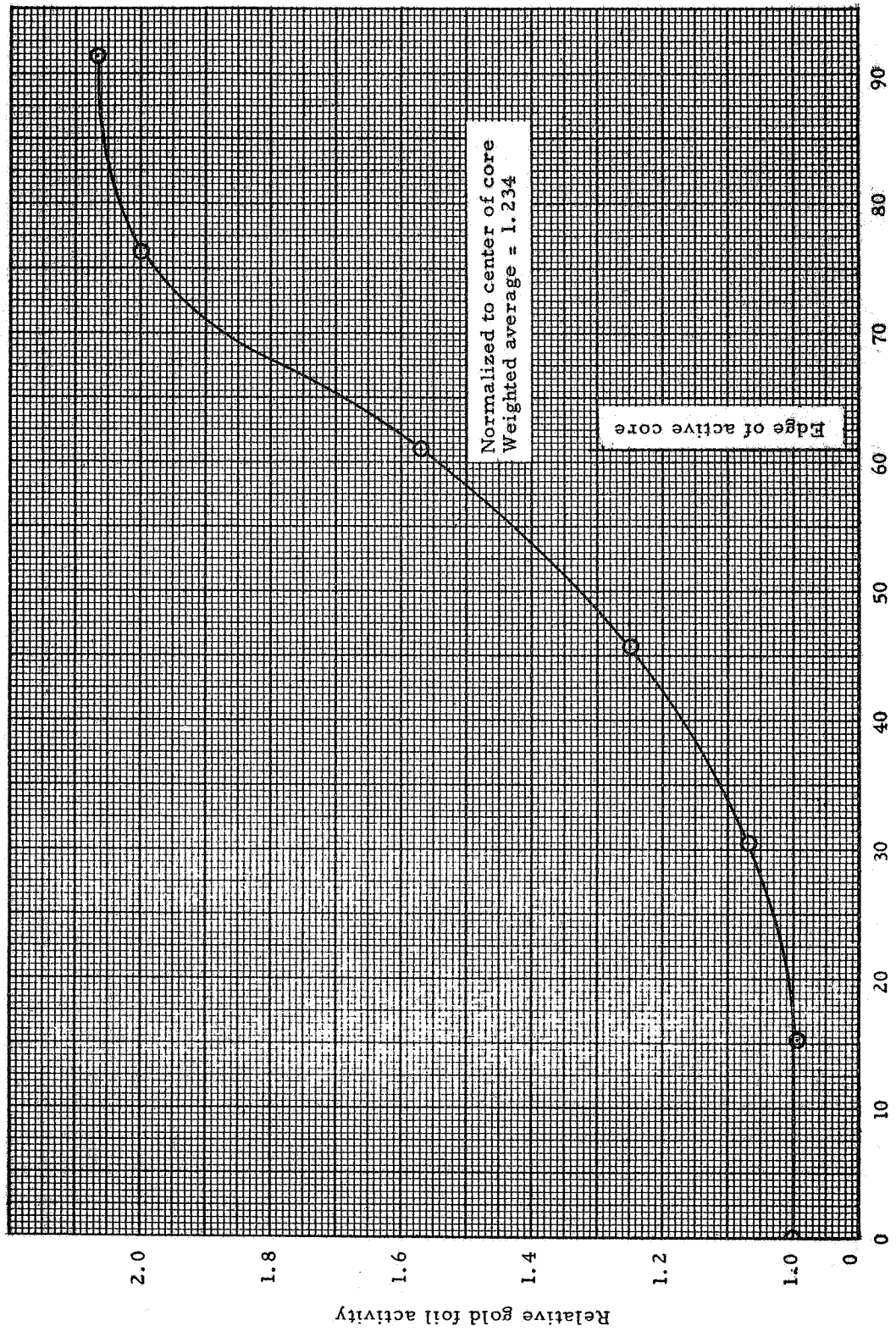


Fig. 5.13 Radial distribution of bare gold foil activity - UF_6 reactor with beryllium in reflector

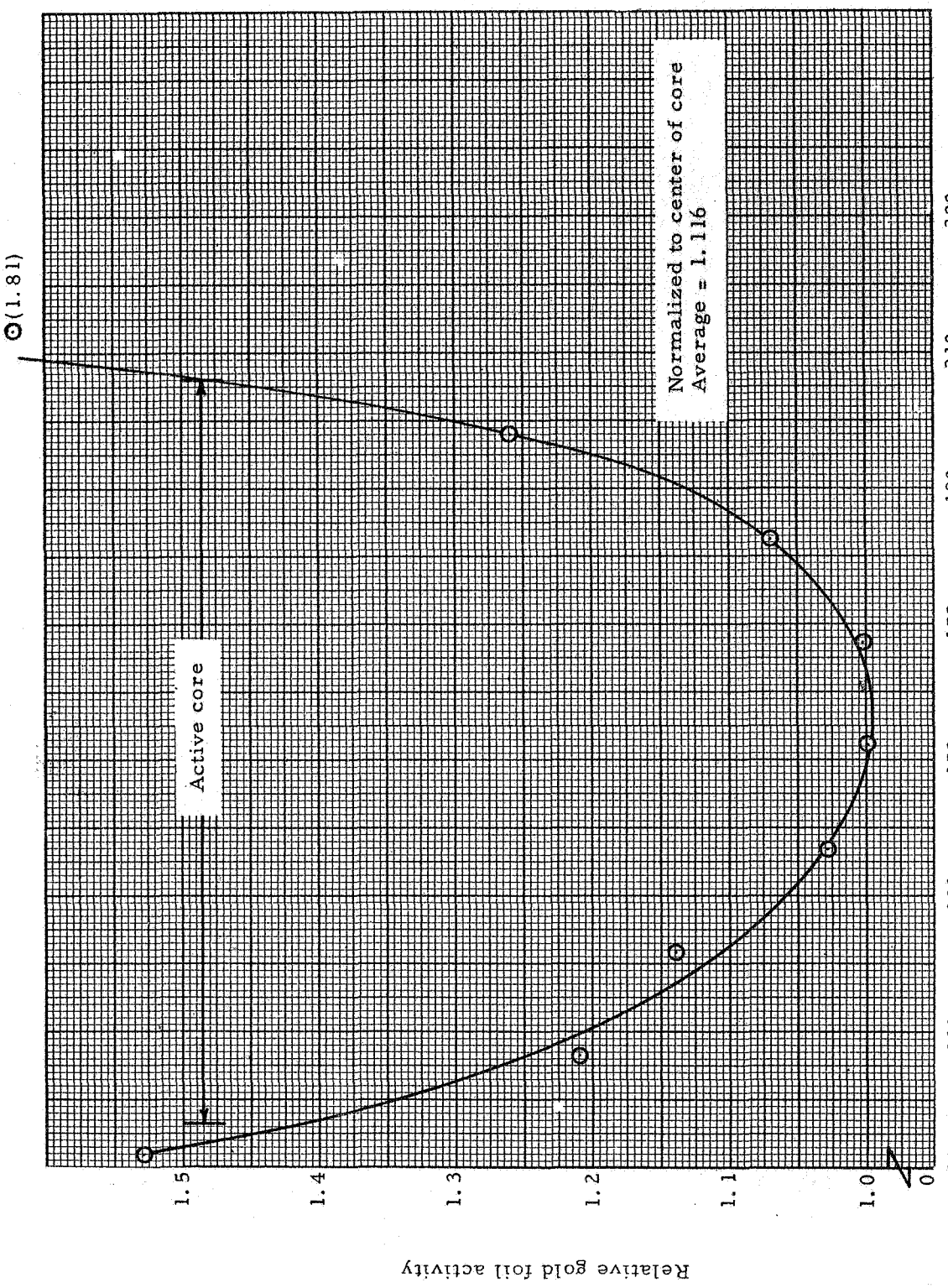


Fig. 5.14 Axial distribution of bare gold foil activity - UF_6 reactor with beryllium in reflector

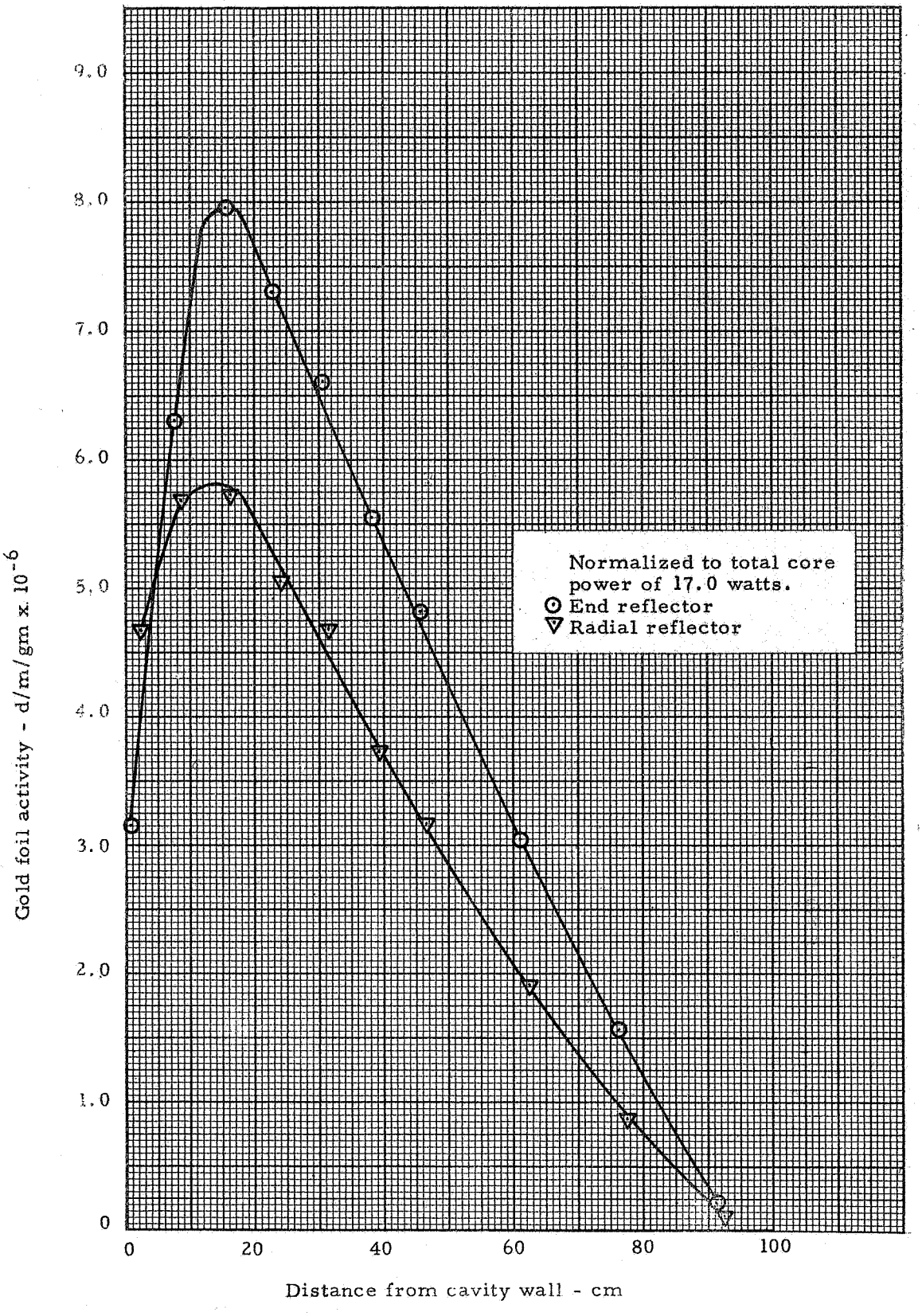


Fig. 5.15 Bare gold foil activity distribution in the reflectors - UF_6 reactor with beryllium in reflector

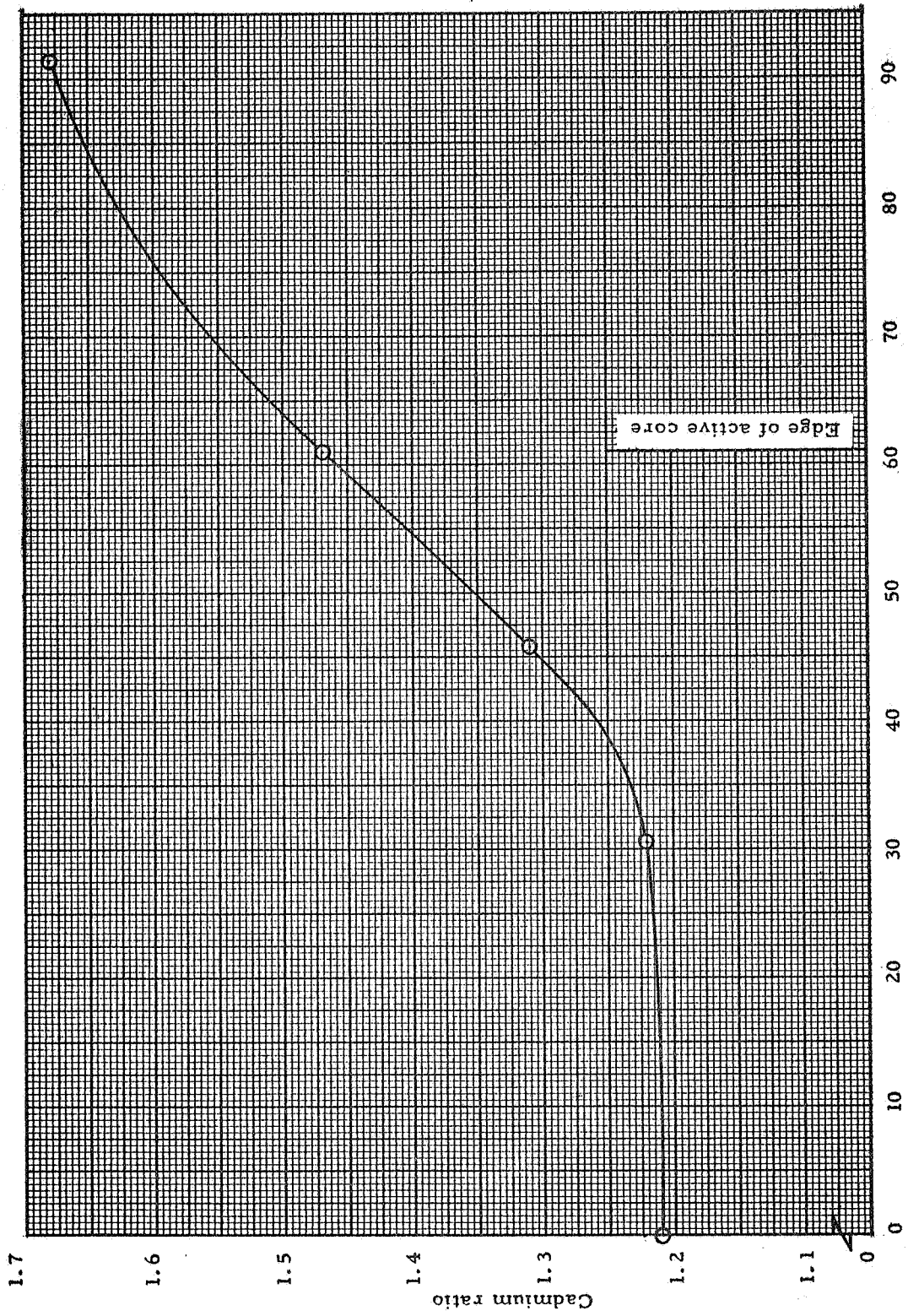


Fig. 5.16 Gold foil cadmium ratio radial profile - UF_6 reactor with beryllium in reflector

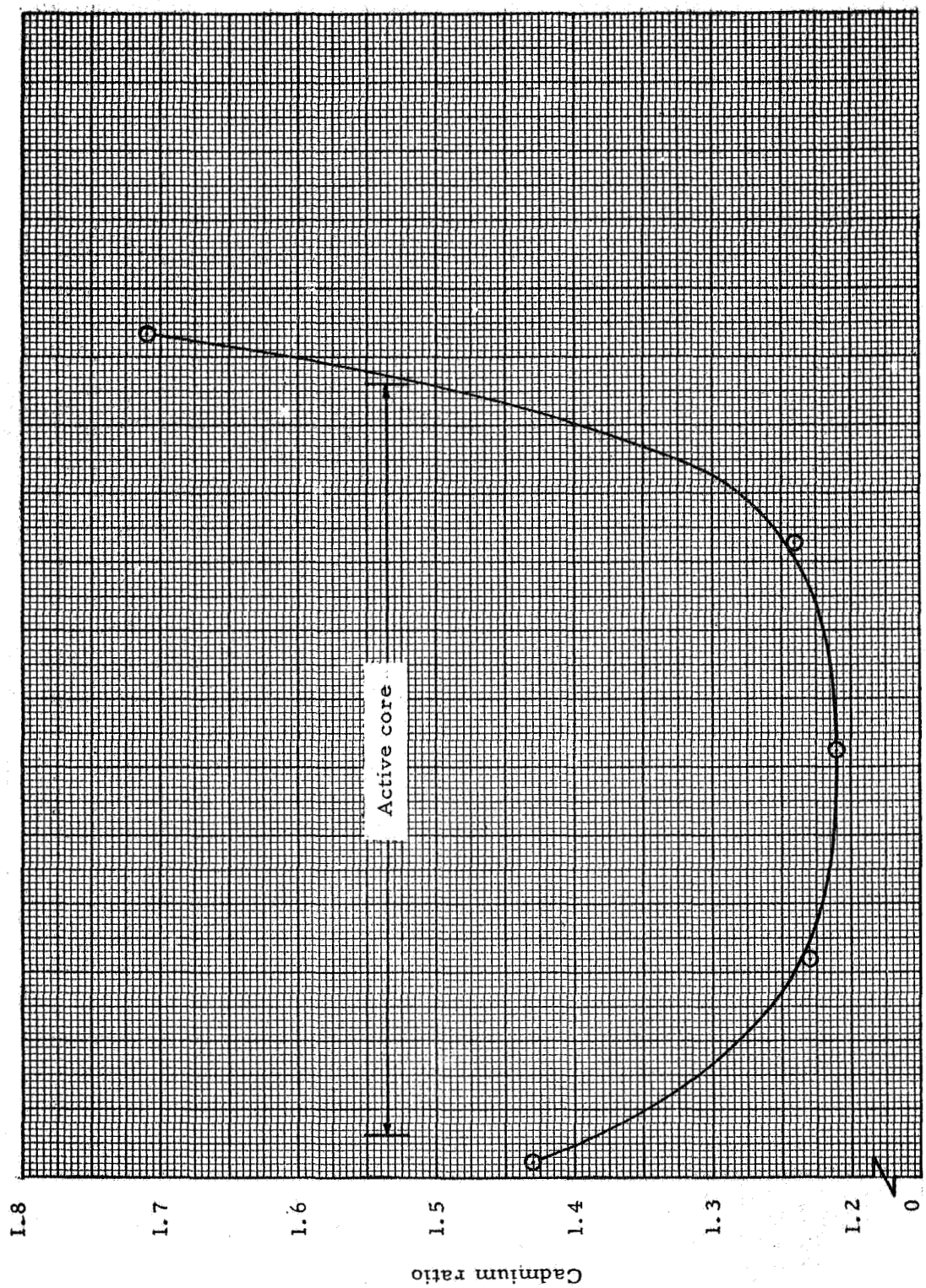


Fig. 5.17 Gold foil cadmium ratio axial profile - UF_6 reactor with beryllium in reflector

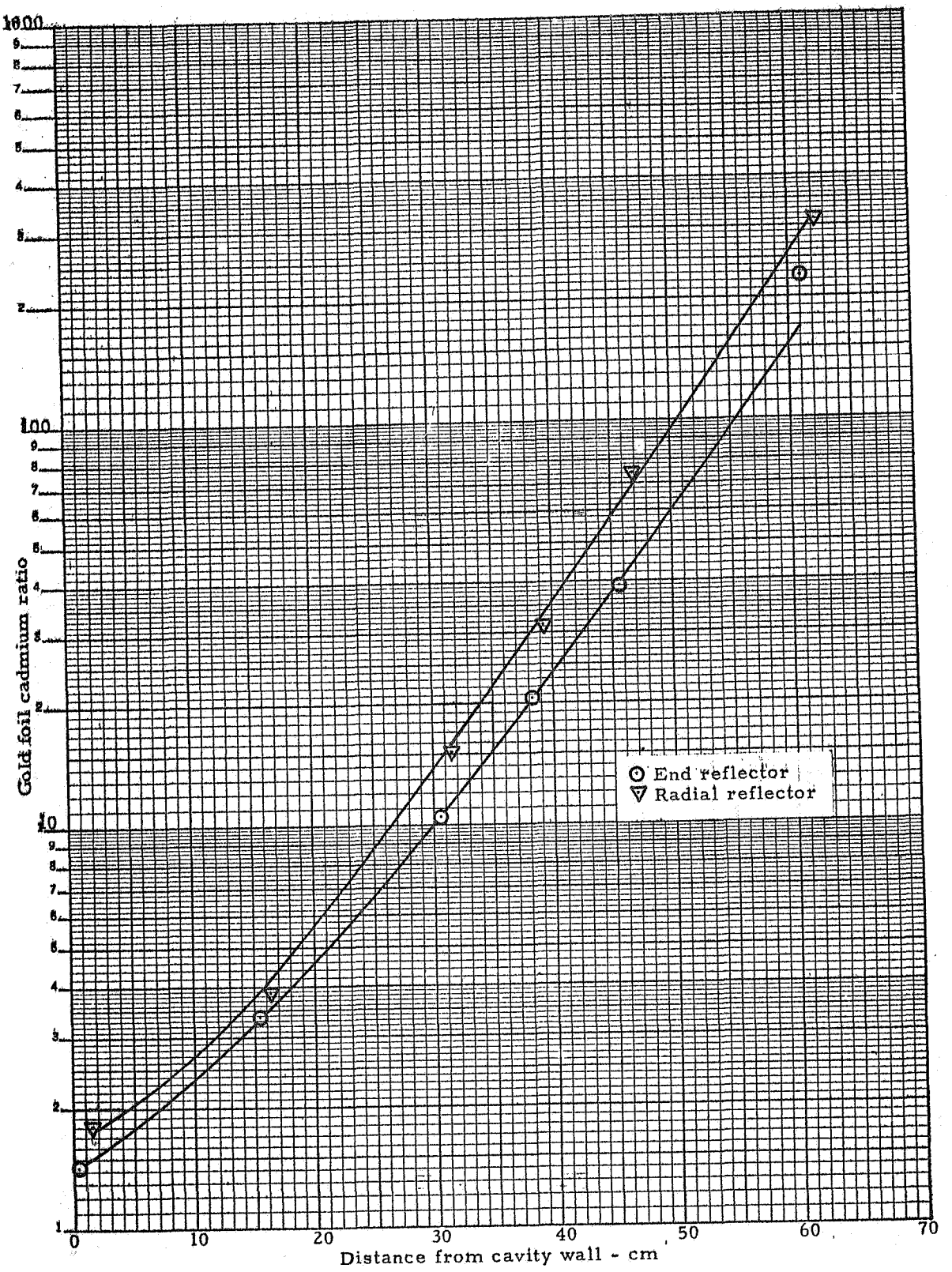


Fig. 5.18 Gold foil cadmium ratios in the radial and end reflectors - UF_6 reactor with beryllium in reflector

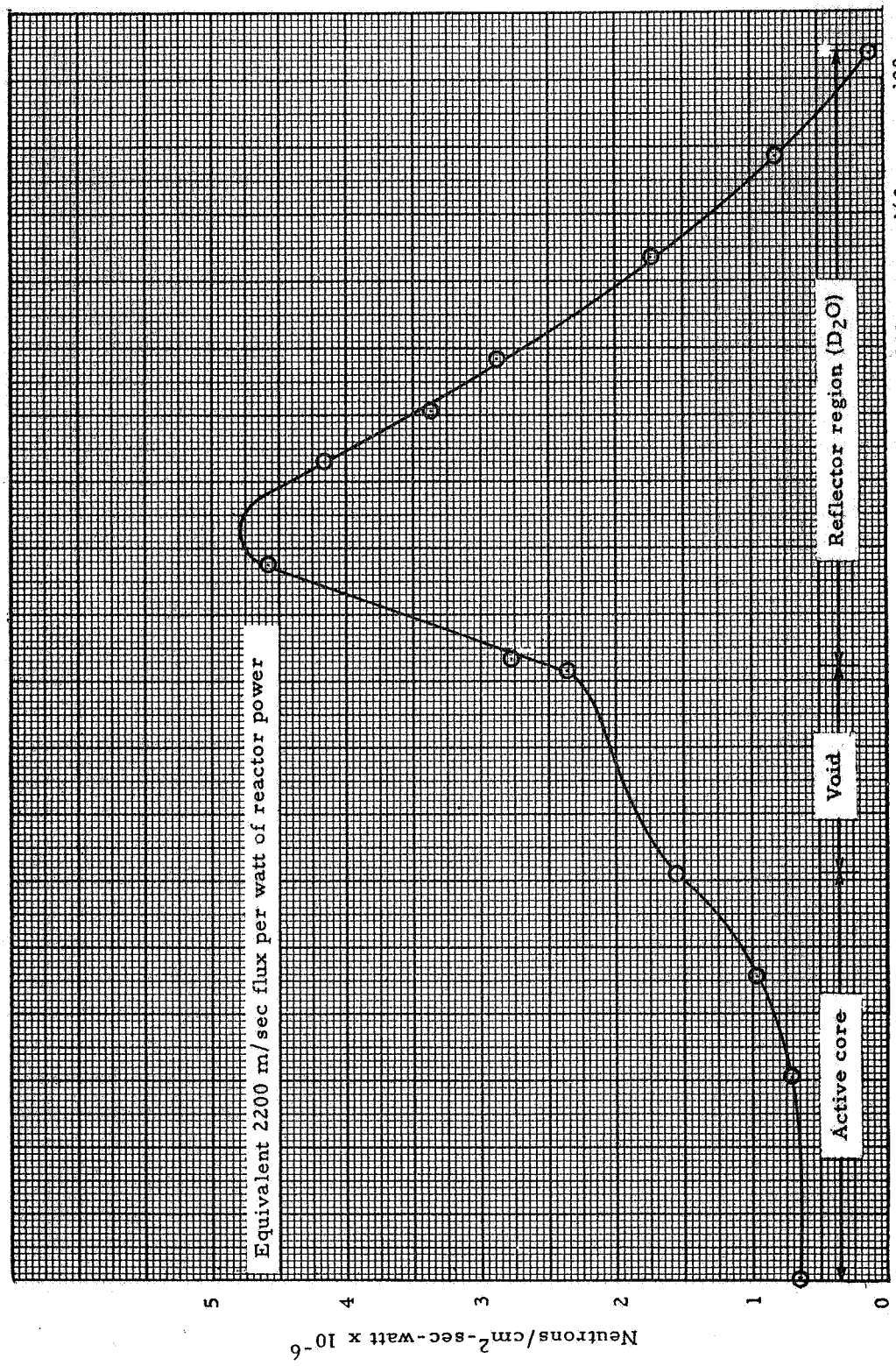


Fig. 5.19 Thermal neutron flux distribution radially through axial center of core UF_6 reactor, Beryllium in the reflector

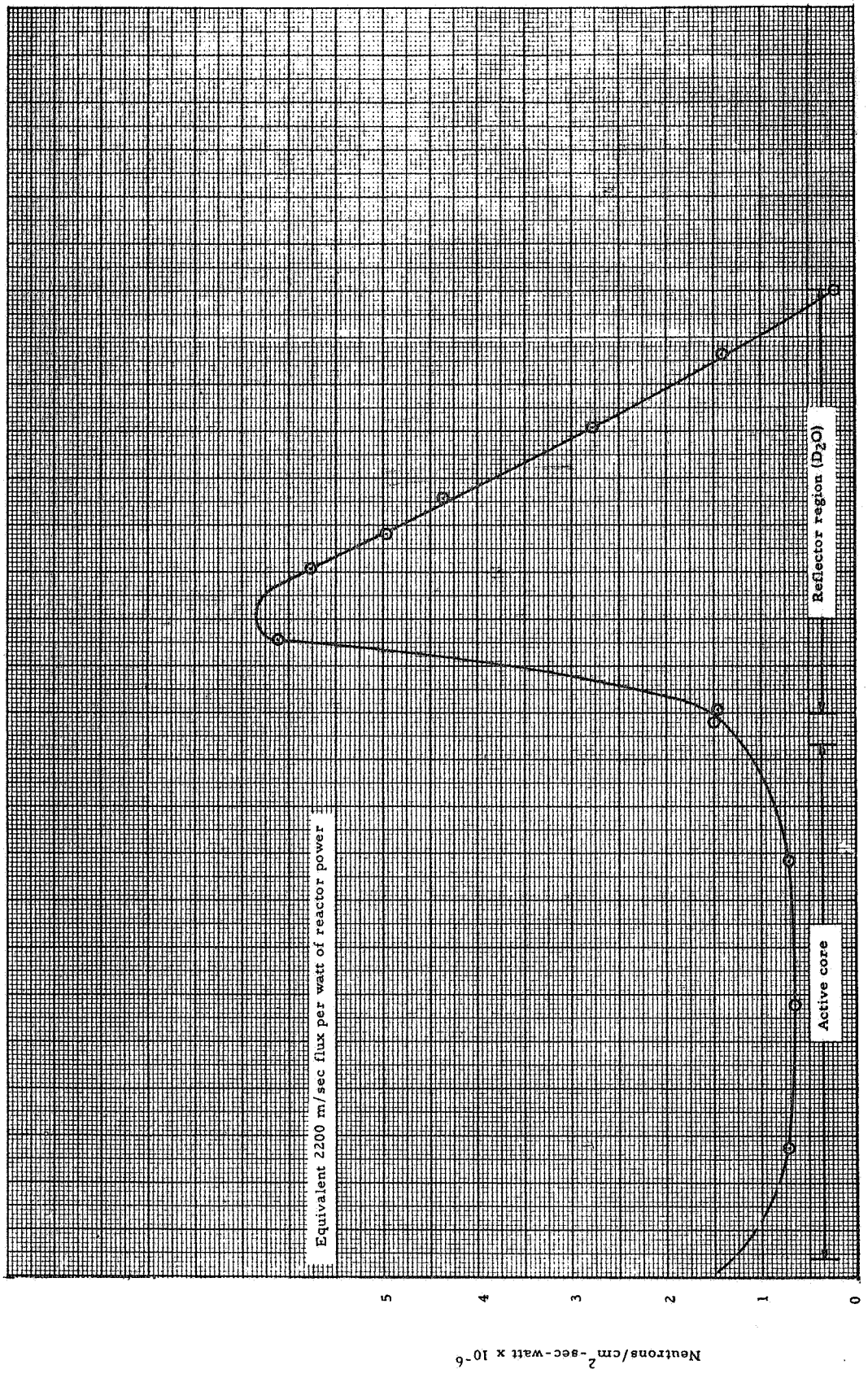


Fig. 5.20 Thermal neutron flux distribution axially through radial center of core UF_6 reactor, Beryllium in the reflector

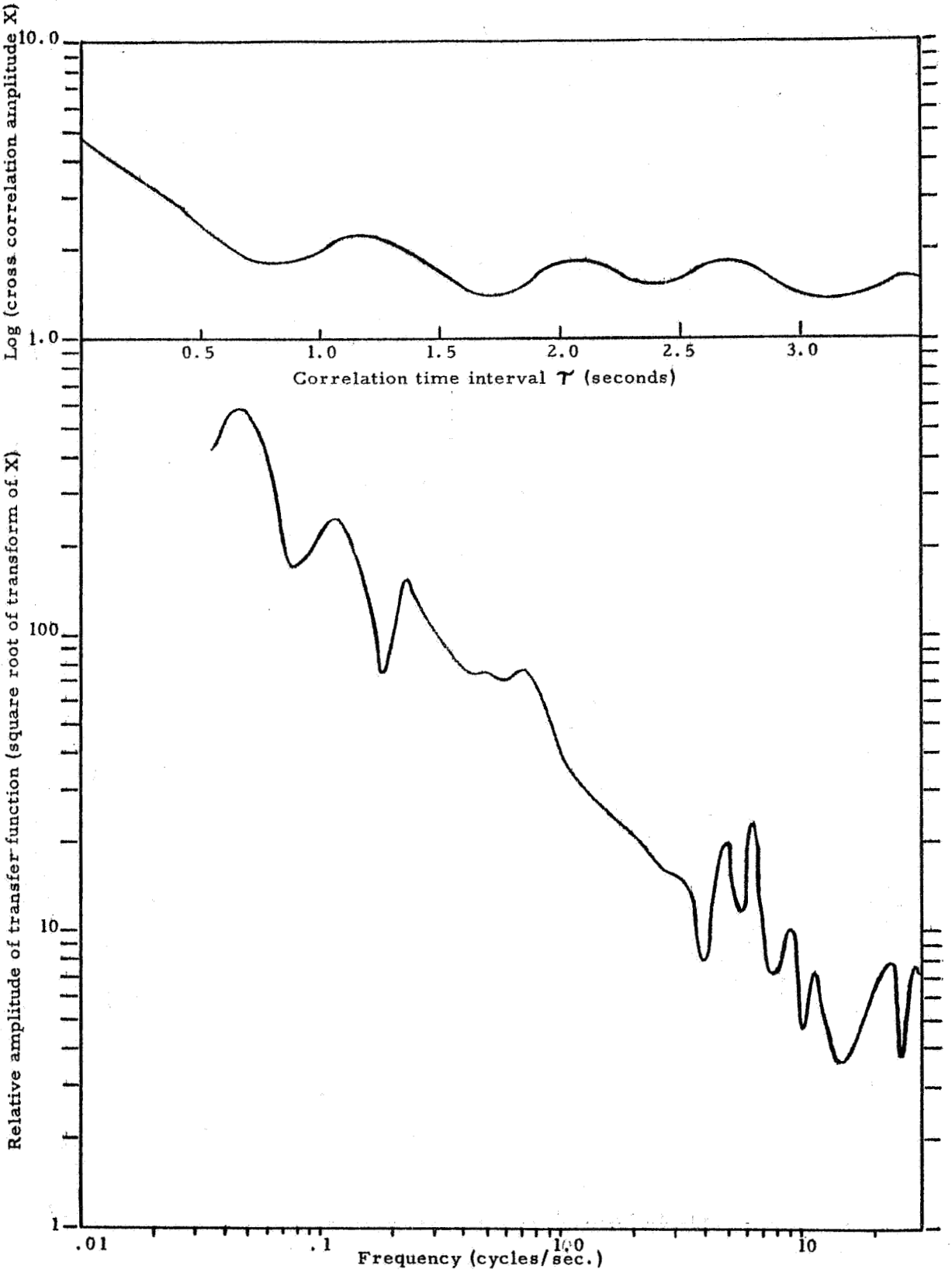


Fig. 5.21 Results of noise analysis on UF_6 reactor

6.0 UF_6 EXPERIMENT - PURE D_2O REFLECTOR

This reactor configuration was attained simply by removing fuel from the reactor and the beryllium from the radial reflector. Sufficient fuel was removed to compensate for the expected increase in reactivity caused by the absence of the beryllium. Outside of these changes, the reactor and associated components were exactly the same as described under Section 5.0.

6.1 Reactivity Measurements

6.1.1 Rod Worths

All of the rod worth measurements for the UF_6 experiments were reduced to a single set of average values. These are given in Section 5.2.

6.1.2 Material Worths

The basic core configuration before removing any beryllium contained 34.75 kg of UF_6 or 23.41 kg of uranium and k-excess was 0.111%Δk. The 55 degree sector of BeO was still in the radial reflector so this would factor k-excess up to (0.441±0.031)%Δk if this sector were Be. A total of 7946.66 gm of UF_6 was then removed from the reactor tank and the Be and BeO taken from the radial reflector. The resulting fuel loading was 26.81 kg of UF_6 or 18.05 kg of uranium and excess reactivity was (1.499±0.016)%Δk. The k-excess difference was, therefore, (1.058±0.035)%Δk. The average fuel loading between these two configurations was 20.73 kg which, according to Figure 5.7, gave a fuel worth of 0.900%Δk/gm. The following values constitute the worth of the beryllium.

1.	5.35 kg of uranium	-4.815±0.235%Δk
2.	2.59 kg of fluorine	+0.039±0.006%Δk
3.	Be end plates and other positioning	+2.726±0.100%Δk
4.	k-excess difference	-1.058±0.035%Δk
	Worth of beryllium	-3.108±0.26%Δk

The error associated with the worth of 5.35 kg of uranium was based on a possible 5% error of the worth-per-gram value and fluorine was figured using a measured worth of $-(0.016\pm0.002)\times10^{-3}$%Δk/gm. The hardware and Be end plates include only that material which was removed when the Be was removed from the reactor and is based on measured values.

Stainless steel worth on the cavity wall and ends was measured with approximately half the material used in the measurement reported in Table 5.2 for the UF_6 reactor with the Be and D_2O reflector. The worth of 7.371 kg of stainless steel was -(1.126±0.019)%Δk for a worth-per-gram of $-(0.153\pm0.003)\times10^{-3}$%Δk. This value is 12.5% higher than with Be and D_2O in the radial reflector. The total worth of a stainless steel liner 0.0965 cm thick extrapolates to be -(14.33 ± 0.28)%Δk.

Fuel worth was also measured for this configuration. A total of 1158.92 grams of UF_6 was removed from the reactor tank starting with the base loading given above of 26.81 kg. The resulting fuel worth was (1.081±0.020)%Δk/kg uranium and a Δk/k/Δm/m of 0.191±0.004. This is plotted in Figure 5.7 at an average uranium loading of 17.66 kg.

The critical mass for this reactor assembly requires essentially the same corrections as the UF_6 reactor with Be in the radial reflector. These corrections are as follows:

1.	Teflon (7.928 kg)	-(0.259±0.033)%Δk
2.	Fluorine (8.752 kg)	-(0.140±0.037)%Δk
3.	k-excess	-(1.499±0.016)%Δk
4.	Air ducting, monel lines and valves	-(0.227±0.010)%Δk
		-(2.125±0.053)%Δk

The interpolated fuel worth for this correction in multiplication was 1.095×10^{-3}%Δk/gm of uranium and so the above reactivity correction respresents (1.915±0.098) kg of uranium. An assumed 5% error was assigned to the fuel worth-per-gram in calculating this correction. The lowest loading obtained with the UF_6 experiment, was 25.65 kg of UF_6 or 17.27 kg U with an excess reactivity of 0.65%Δk. The critical mass thus calculates to be 16.13 kg of uranium (or 24.14 kg of UF_6 if the fluorine correction is not included) with an uncertainty of about 1.0%. *

6.2 Power Distribution - Bare Catcher Foils

With the beryllium removed from the radial reflector and the fuel loading reduced from 34.97 to 25.65 kg of UF_6, bare catcher foils were exposed within the cavity region to determine the radial and axial power profiles. All data were obtained with all control rods withdrawn except No. 7 actuator, which was nearly fully inserted. These data are given in Table 6.1 and Figures 6.1 and 6.2. This weighted radial average normalized to the center of the core was 1.380 compared to 1.523 with beryllium in the radial reflector and the heavier fuel loading. This is a 9% reduction. The ratio of the power at the outer edge of the fuel to the core center went from 2.47 for the Be and D_2O reflector to 2.01 for the pure D_2O reflector for a 19% decrease. It is obvious that the radial power was considerably flatter for the pure D_2O reflector than for the Be and D_2O reflector. Although two major changes occurred, that is the removal of both beryllium from the reflector and fuel from the active core, the change in fuel loading was the main contributor to the flatter power distribution for the pure D_2O system.

The average relative power (compared to the core center) over the axial profile (Figure 6.2) was 1.143 which compares to 1.224 for the Be and D_2O reflected reactor, a 7% decrease.

---

*When the UF_6 was removed from the reactor tank, about 40 gm of uranium remained in the tank. It was assumed to be absorbed in the tank wall, having changed from UF_6 to some other compound.

6.3 Gold Foil Data - Bare Foils

Bare gold foils were also exposed in the cavity and reflector regions with the pure D_2O reflector. The data are contained in Table 6.2 and Figures 6.3 and 6.4. The power normalization factors for the two foil exposures are given in Table 6.3. The weighted radial average out to the outer edge of the fuel was 1.169. The ratio of the foil activity at the outer edge of the fuel to the core center was 1.46. Prior to removing the beryllium from the reflector region the weighted radial was 1.234 and the ratio of the foil activity at the outer edge of the fuel to the core center was 1.57. Therefore, removing the beryllium from the reflector and reducing the fuel loading by about 23% caused a 6% decrease in the weighted average radial and a 7% decrease in the activation at the edge of the fuel with respect to the core center. These changes in neutron activation are attributed primarily to the change in fuel loading. Note that the changes in the power distribution were more pronounced than for the gold activity, principally because so much of the gold activity was caused by epithermal flux which readily passes through both the cores of light and heavy loadings with very little attenuation.

The average relative axial flux distribution compared to the core center and shown in Figure 6.4, was 1.052. This compares with an average of 1.155 for the Be and D_2O reflected reactor which is a difference of nearly 10%. A comparison at the ends of the active core show about the same percentage change.

The gold foil activity distributions in the reflector regions are shown in Figure 6.5. It will be noted that it was necessary to shift some of the data (represented by the solid symbols) in the radial reflector in order to give a flux distribution which was reasonable based on previous results. What apparently happened was that the aluminum wand on which the foils were taped was not fully inserted into the aluminum tube which extends into the radial reflector. The foil positions given in Table 6.2 for Run 1076 for foils 8 to 14 are, therefore, assumed to be in error by about 31 cm.

The bare gold data from the reflector regions, per unit reactor power are compared in Table 6.4 and it will be observed that the pure D_2O reflector gave a higher foil activation all the way through than did the system containing beryllium. In the end reflector the ratio of the bare gold foil data for the Be and D_2O reflected reactor to that of the pure D_2O system averaged 0.833 ± 0.050. The same ratio in the radial reflector averaged 0.685 ± 0.021, if the point at 183.9 cm which appears to be poor data is ignored.

TABLE 6.1

Bare Catcher Foil Data

Pure D_2O Reflector - UF_6 Reactor

Foil No.	Location Radial (cm)	Location Axial (cm)	Normalized Counts	Ratio of Local to Core Center (Foil No. X)
1	0	95.9	68574	1.535
2	0	105.4	56831	1.272
3	0	120.6	48297	1.081
4	0	135.9	46053	1.031
5	0	151.1	44692	1.000 X
6	0	166.3	46465	1.040
7	0	181.6	47545	1.064
8	0	196.8	61615	1.379
9	0	205.1	77001	1.723
10	15.2	151.1	46644	1.044
11	30.5	151.1	51327	1.149
12	45.7	151.1	61617	1.379
13	61.0	151.1	89730	2.008
14	76.2	151.1	129018	2.887
15	91.4	151.1	124594	2.788

TABLE 6.2

Bare Gold Foil Data

UF_6 Reactor - Pure D_2O Reflector

Foil No.	Location Radial (cm)	Location Axial (cm)	Foil Weight (gm)	d/m/gm at S. D. (2) x 10^{-6}	Activity Normalized to Run 1065 d/m/gm at S. D. (2) x 10^{-6}	Relative Flux Level Compared to Core Center
Run 1076						
1	0	89.4	0.0400	3.215	3.395	
2	0	74.9	0.0411	6.469	6.831	
3	0	59.6	0.0418	5.355	5.655	
4	0	44.4	0.0418	4.038	4.264	
5	0	29.1	0.0392	2.592	2.737	
6	0	13.9	0.0385	1.314	1.388	
7	0	0	0.0390	0.190	0.201	
8	93.2 (1)	151.1	0.0380	4.710	4.974	
9	107.7	151.1	0.0381	3.193	3.372	
10	123.0	151.1	0.0379	1.966	2.076	
11	138.2	151.1	0.0369	0.829	0.875	
12	153.5	151.1	0.0364	0.117	0.124	
13	168.7	151.1	0.0357	0.096	0.101	
14	183.9	151.1	0.0417	0.063	0.0665	
Run 1077						
1	0	95.9	0.0366	2.578	2.717	1.284
2	0	105.4	0.0374	2.272	2.395	1.132
3	0	120.6	0.0398	2.040	2.150	1.017
4	0	135.9	0.0356	1.998	2.106	0.995
5	0	151.1	0.0352	2.007	2.115	1.000
6	0	166.3	0.0388	1.964	2.070	0.978
7	0	181.6	0.0367	2.045	2.155	1.019
8	0	196.8	0.0361	2.259	2.381	1.126
9	0	205.1	0.0376	2.678	2.823	1.334
10	15.2	151.1	0.0360	2.023	2.132	1.008
11	30.5	151.1	0.0368	2.124	2.239	1.058
12	45.7	151.1	0.0399	2.323	2.448	1.157
13	61.0	151.1	0.0379	2.942	3.101	1.466
14	76.2	151.1	0.0390	3.612	3.807	1.800
15	91.4	151.1	0.0414	3.662	3.860	1.824
16	100.1	151.1	0.0392	5.788	6.101	
17	115,4	151.1	0.0357	5.596	5.898	
18	130.6	151.1	0.0402	3.994	4.210	
19	0	82.5	0.0404	5.397	5.688	
20	0	67.2	0.0414	6.269	6.608	
21	0	52.0	0.0417	4.713	4.968	

(1) The radial position for foils 8 to 14 appears to be in error by about 31 cm due to failure to fully insert foils in the radial reflector.

(2) S. D. stands for reactor shutdown time.

TABLE 6.3

Power Normalization Factors

UF_6 Reactor - Pure D_2O Reflector

S.D.	Run No.	Count Time	Decay Time (min)	Decay Factor	CPM	Corr. CPM	Norm. Factor
1446.41	1076	1531.15	44.74	0.87	315456	274447	
		1533.12	46.71	0.91	300472	273430	
		1536.90	50.49	1.01	275816	278574	
						275484	1.056
1143.96	1077	1233.80	49.84	0.99	280246	277444	
		1235.79	51.83	1.03	266688	274689	
		1237.80	53.84	1.08	255207	275624	
						275919	1.054

TABLE 6.4

Comparison of Gold Foil Data in Reflector Regions

UF_6 Reactor Assemblies

Location		Be and D_2O Reflected Reactor counts/min/gm/watt x 10^{-5}	D_2O Reflected Reactor counts/min/gm/watt x 10^{-5}	Ratio of Be & D_2O to D_2O Reflected Reactors
Radial (cm)	Axial (cm)			
0	0	0.132	0.157	0.841
0	13.9	0.916	1.084	0.845
0	29.1	1.792	2.138	0.838
0	44.4	2.836	3.331	0.851
0	52.0	3.266	3.881	0.842
0	59.6	3.886	4.418	0.880
0	67.2	4.292	5.162	0.831
0	74.9	4.682	5.336	0.877
0	82.5	3.682	4.443	0.829
0	89.4	1.857	2.652	0.700
93.2	151.1	2.753	--	--
100.1	151.1	3.345	4.766	0.702
107.7	151.1	3.375	5.039 (1)	0.670
115.4	151.1	2.975	4.608	0.646
123.0	151.1	2.762	3.945 (1)	0.700
130.6	151.1	2.200	3.289	0.669
138.2	151.1	1.863	2.695 (1)	0.691
153.5	151.1	1.126	1.617 (1)	0.696
168.7	151.1	0.522	0.742 (1)	0.704
183.9	151.1	0.071	0.052 (1)	1.356

(1) These are extrapolated values from the curve shown in Figure 6.5.

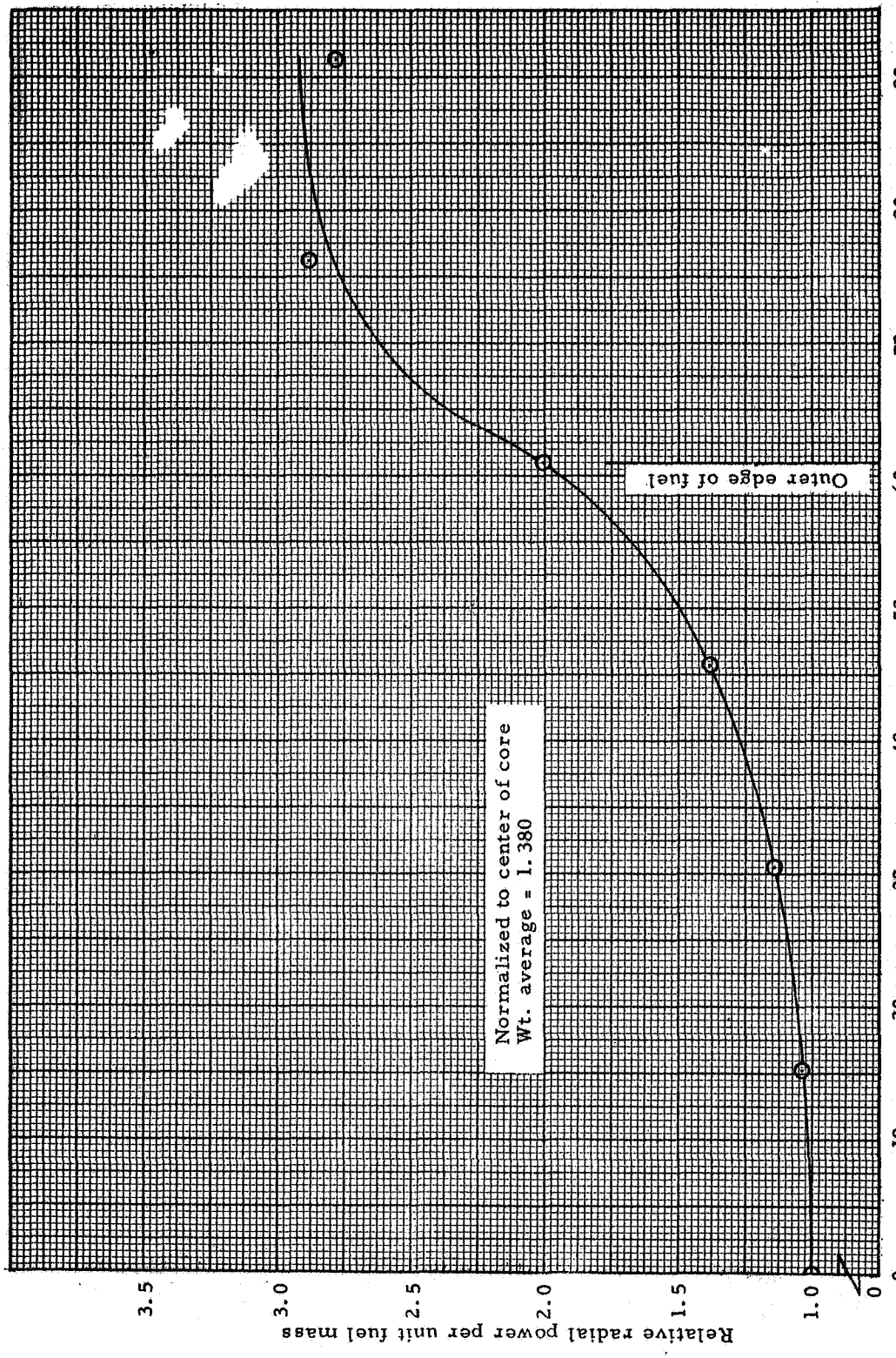


Fig. 6.1 Radial power distribution from bare catcher foils - UF_6 reactor with pure D_2O reflector

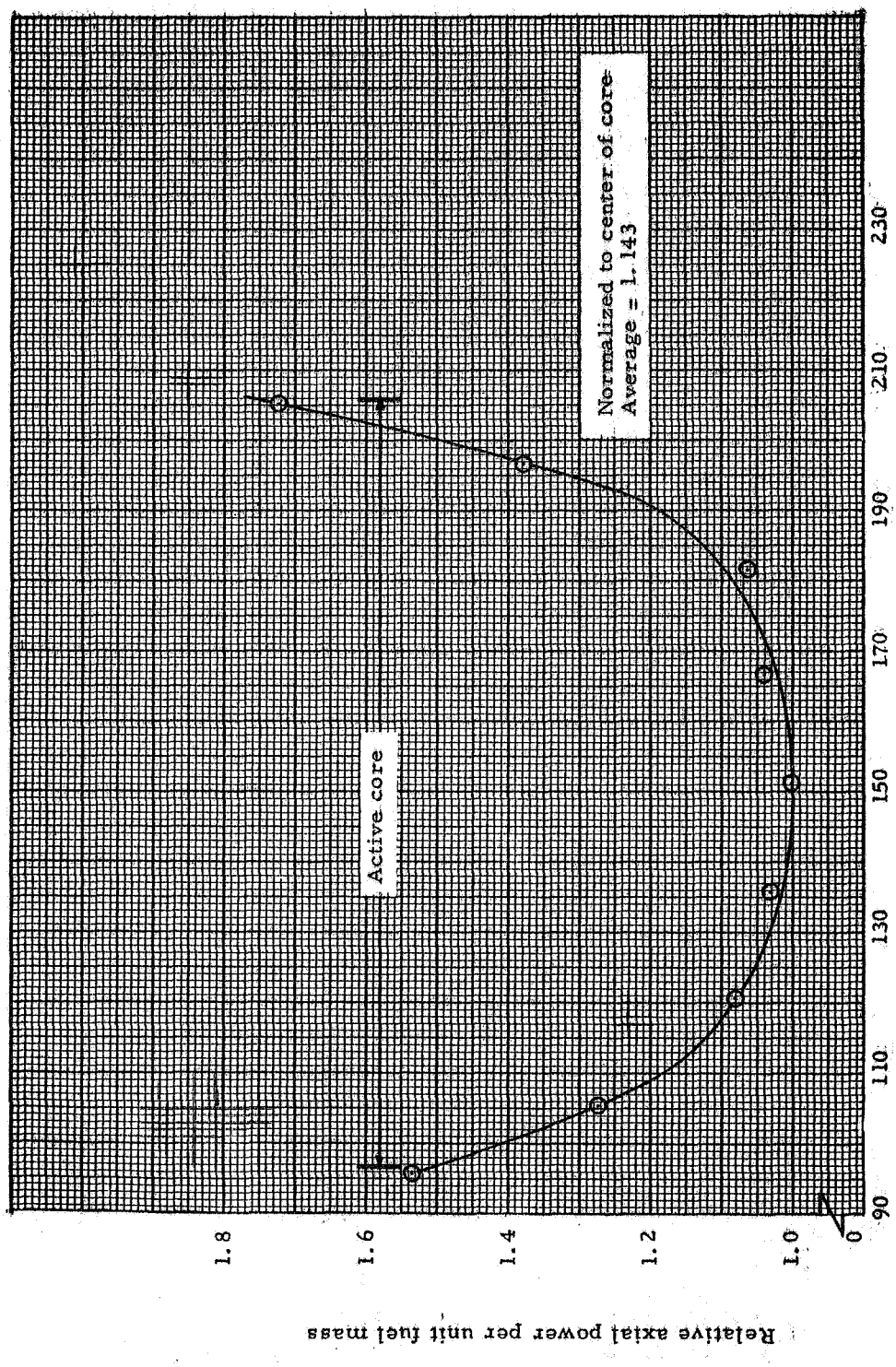


Fig. 6.2 Axial power distribution from bare catcher foils - UF_6 reactor with pure D_2O reflector

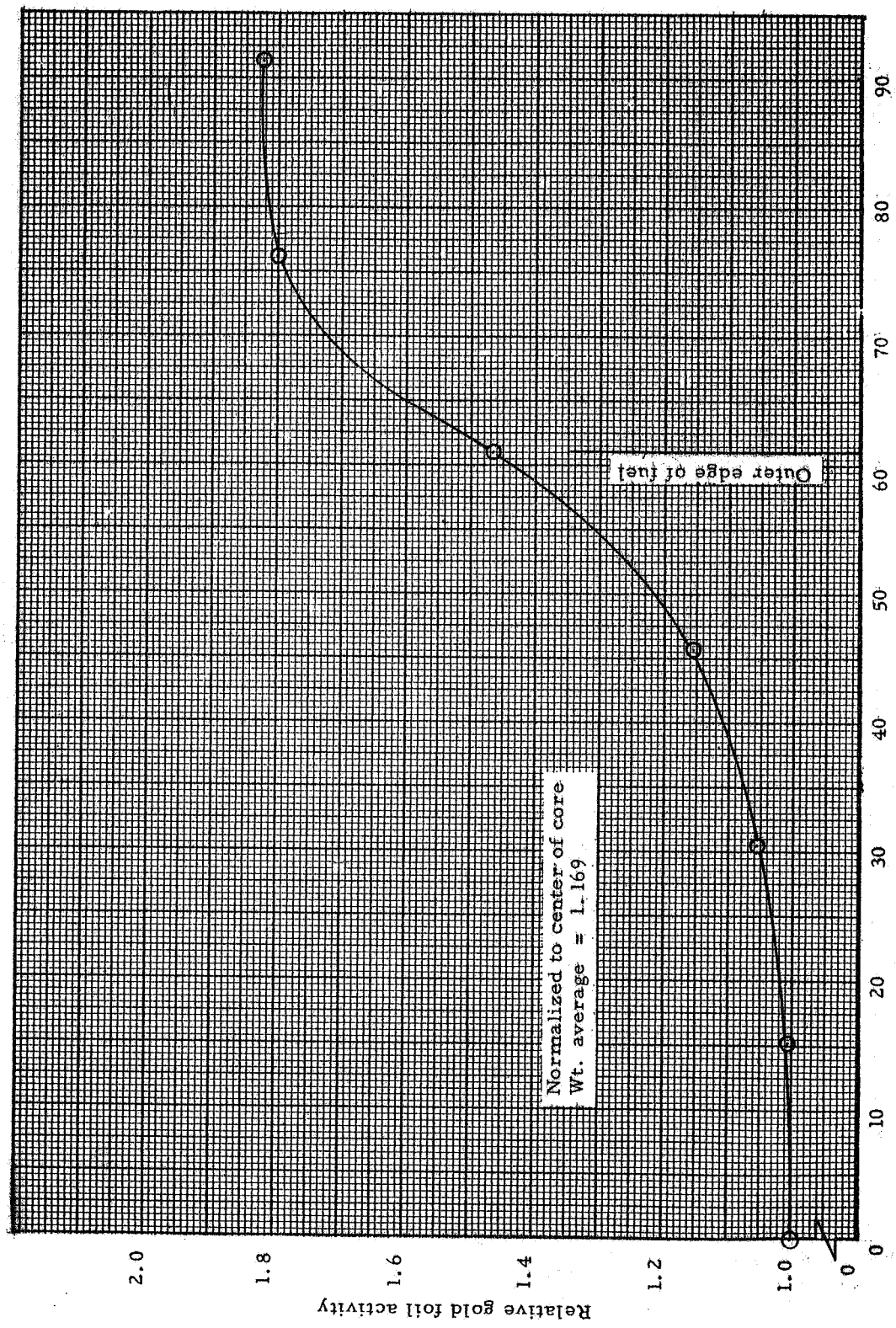


Fig. 6.3 Radial distribution of bare gold foil activity - UF_6 reactor with pure D_2O reflector

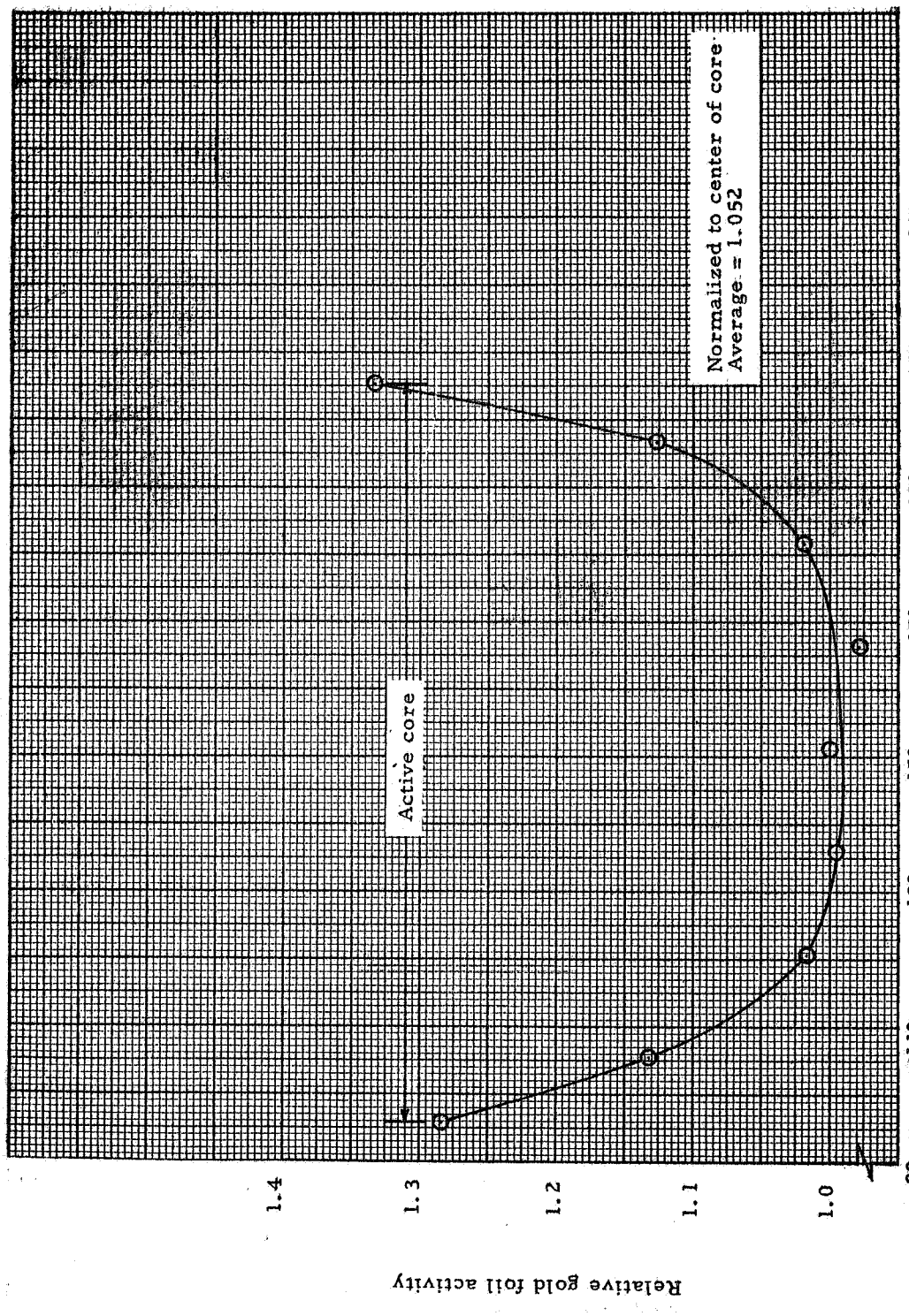


Fig. 6.4 Axial distribution of bare gold foil activity - UF_6 reactor with pure D_2O reflector

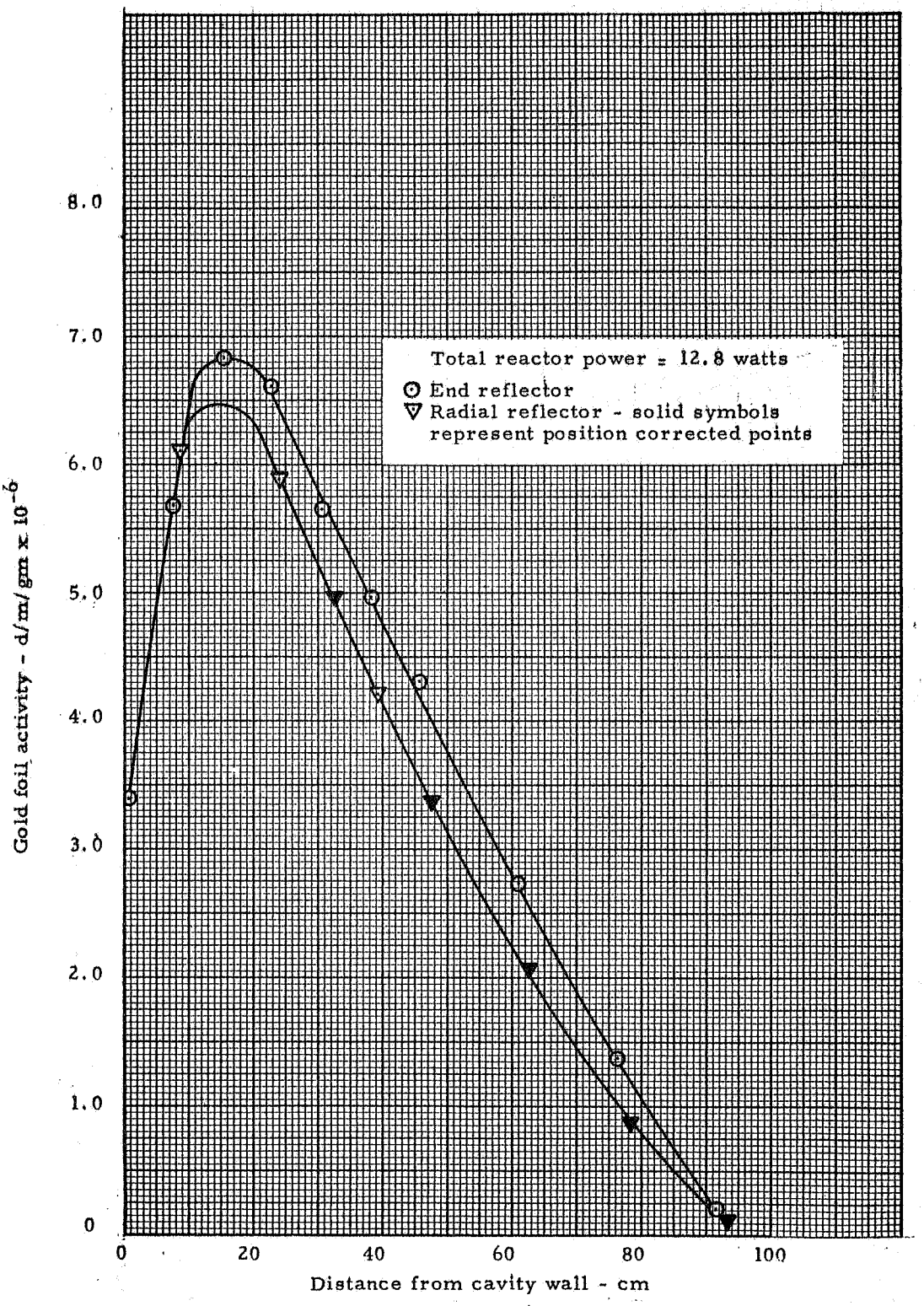


Fig. 6.5 Bare gold foil activity distribution in the reflectors UF_6 reactor with pure D_2O reflector

7.0 MOCKUP NO. 2 EXPERIMENT - PURE D_2O REFLECTOR

A new fuel support structure was constructed with the intention of minimizing the low neutron absorption paths through the fueled region of the cavity which existed in the fuel support screen arrangement used for Mockup No. 1 experiments. This new core support structure is shown in Figure 7.1, and consisted of 12 rectangular and 4 triangular cells into which fuel elements were placed. Each of the rectangular cells held 16 fuel elements and the triangular cells each contained 6 fuel elements. The cells and fuel elements were numbered so as to specify any particular location within the reactor. This numbering arrangement is presented in Figure 7.2.

In order to produce a more nearly circular fueled region and thus simulate the UF_6 reactor geometry, the fuel element positions in the 8 corner positions did not contain any fuel. These positions were 2-1, 3-4, 5-1, 8-4, 9-13, 12-16, 14-13, 15-16. This left 208 fuel-containing locations within the active core region. The equivalent circular diameter of the core was 125.2 cm, based on equivalent area. This was the most appropriate circular arrangement available, even though the "circle" was larger than the 121.9 diameter cross section of the UF_6 gas experiment. This difference in diameter is equivalent to a 2.6% difference in critical mass (Reference 1, p. 50). For further discussions see Section 3 and 9.

The fuel elements were square boxes nominally 7.47 cm square by 116.8 cm long (3 in. square by 46 in. long). They were, therefore, designed to accept the size 1.0 fuel sheets which were 7.30 cm square. The fuel was loaded into the fuel trays in three orientations as illustrated in Figure 7.3. As can be seen from this figure, the proper dispersion of the three fuel orientations throughout the active fueled region would eliminate any zero absorption paths for neutrons that cross the fuel region near its center and therefore would more accurately mockup a UF_6 fueled core.

In order to mockup the UF_6 reactor experiment, it was necessary to surround the fueled region with sufficient aluminum to mockup the UF_6 tank. This is summarized in Table 7.1. Included in this table are the weights of the aluminum in the support structure and the eight corner (unused) fuel elements. These were included as part of the mockup of the UF_6 tank. These corrections will, of course, be discussed in subsequent sections. It should be noted from the table that the UF_6 tank was accurately simulated. A ratio of 1.09 was used to correct type 1100 Al to type 6061 Al. The aluminum in the core region in the form of support structure, fuel elements, spacer rings and lids which was not included in the UF_6 tank mockups amounted to 159.94 kg type 1100 Al.

The pure D_2O reflector configuration was tested first, since this was the condition of the reflector when the UF_6 reactor experiment was terminated. It was anticipated that it would require about 21 kg of fuel to produce the critical mass. This required 40 sheets per fuel element for a total loading of 8320 sheets of fuel. The fuel elements (six types) were loaded according to the loading schedule given in

Figure 7.4. Fifteen stages of fuel per element were used which gave an active core length of 109.2 cm (0.6 cm longer than the UF_6 tank). As seen from Figure 7.4, there was a 1/2 stage gap or void at each end of the fuel elements containing a single spacer ring. The six types of fuel elements were then dispersed throughout the fueled region as shown in Figure 7.5.

7.1 Initial Loading

The fuel elements were loaded into the reactor in 11 increments as given in Table 7.2. The resulting inverse multiplication data obtained for rods in and rods out are presented in Table 7.3, and the average values are shown graphically in Figure 7.6. The loading proceeded without any fuel adjustments being required and the final k-excess was 1.282±0.033%Δk at a D_2O temperature of 26°C. There were 8320 size 1.0 fuel sheets in the reactor at this point which amounted to 21.8 kg of uranium (using an average weight of 2.62 gm of U per sheet). The measured physical weight of the fuel, including coating and oxygen, was 22896.2 gm.

7.2 Reactivity Measurements

7.2.1 Rod Worths

Several rod worth measurements were made during the course of these mockup experiments. It was noted early in the test that there was some inconsistency in the worth of Actuators 3 and 6 when using the old rod worth curve data. During the fuel worth measurements to be discussed later, these two rods traveled from a critical position of 788 (ratiometer reading) to all the way withdrawn and the computed rod worths varied from -1.410%Δk to -1.719%Δk. This was considered to be far too much spread and it was assumed that the rod worth shape curve was in error. A new rod shape curve was generated from the above mentioned "rod-bump" data. The curve is given in Figure 7.7 along with the two curves that were already in use. From this new curve, the average worth of Actuators 3 and 6 was -(1.572±0.016)%Δk for six separate measurements over the above rod travel. This, of course, is excellent agreement, showing a standard error of only 1.0%. This new curve was reduced to tabular form as shown in Table 7.4 and these data were used to evaluate all of the reactivity data for the Mockup No. 2 reactor.

In addition to measuring the total worth of Actuators 3 and 6 together, the total worths of all six actuators (17 rods) and of single Actuator 2 were found to be -4.088%Δk and -0.775%Δk, respectively. These values are from single measurements.

7.2.2 Material Worths

One of the initial reactivity measurements performed was to evaluate the worth of aluminum within the active core region so that a fuel loading correction could be applied to the reactor for the 160 kg of aluminum in the support structure and fuel element assemblies. With

a total of 7.757 kg of aluminum placed in the reactor as shown in Figure 7.8, k-excess decreased 0.1566±0.0011%Δk. The aluminum placed in the reactor for this measurement was distributed proportional to the aluminum in a 90° sector, of the active core. Since all of the aluminum in the outer surface of the fuel support structure was used as part of the UF_6 tank simulation, proportionately less aluminum was placed in the cells at the core edge as will be noted from Figure 7.8.

This aluminum worth measurement was repeated again after the fuel loading had been reduced by 390 sheets of fuel. The fuel was uniformally reduced and k-excess was 0.2295%Δk. The worth was -(0.1680±0.0120)%Δk for the same amount of aluminum (7.757 kg). This represents a (7±7)% increase in worth for a 4.7% decrease in fuel loading.

7.2.3 Uranium Foil Weight Analysis

At this point of the experiment, it was decided that a more detailed fuel worth measurement should be made and that chemical analyses would be made on several samples of fuel. In addition, 235 sheets of fuel were cleaned in boiling water and the solutions from this cleaning were analyzed for total uranium. Table 7.5 gives the weights before and after cleaning along with the amount of uranium found in the water after cleaning. Batch 1 and 2 were deliberately selected to represent light and heavy sheets, respectively. Batch 3 sheets were a random selection and, when reduced to an average fuel sheet weight for all 215 sheets, the weight was (2.756±0.070)gm/sheet. This value times the weight percent uranium for batch 3 (Table 7.6) gives (2.618± 0.066) grams of uranium per fuel sheet. The light fuel sheets give a uranium weight per sheet of 2.470 gram and for the heavy sheets this value is 2.715 gm for an average of (2.593±0.173) gm/sheet. This, of course, is within the standard deviation of the value given above. The total weight of 8320 size 1.0 fuel sheets was 22896.2 gm giving 2.752 gm/sheet which agrees very well with the random selection of 215 sheets noted above. The first two solid, uncleaned uranium samples which were analyzed for uranium content were from the same fuel sheet and give an average percent uranium of (88.00±4.20)%. The next two samples, samples 3 and 4, were also from one sheet of fuel and the average uranium was (87.53±2.76)%. These values times the weight of the fuel sheet before the sample was punched, gives an average uranium weight of (2.684±0.128) gm/sheet and (2.643±0.0834) gm/sheet. Although there was considerable spread in these results, they do not contradict the average fuel sheet mass of 2.62 gm. In the case of the samples obtained to represent extremes in the distribution, the spread between the uncleaned light samples and heavy samples was 0.46 gm (2.50 to 2.96 gm per sheet). After cleaning, the spread was only 0.25 gm (2.47 to 2.72 gm per sheet).

Statistical averaging was performed on many groupings of mass data obtained during the various loadings of the 208 fuel elements in these mockup experiments and for other experiments that followed. These results indicate that the fuel sheets in general fit a Gaussian distribution, with a most probable uncleaned weight of 2.75 gm/sheet, with a standard

devaition of 0.15 gm. There did appear to be local probability peaks at 2.66, 2.75 and 2.84 grams. These probably indicated slightly different coating thickness applied to three different batches of fuel, or possibly a different number of cleanings having been applied to these batches. Nevertheless, these groupings were only minor, and the distribution of weights of groups of sheets in the actual mockup reactor was centered about the value of 2.75 gm per uncleaned sheet.

The average weight of uranium in a fuel sheet is 2.62 grams as obtained from the several sets of data cited above. The 95% confidence range of this average value is estimated ±0.02 grams. The actual Gaussian distribution of the weight per sheet has a standard deviation of approximately 0.10 gm. But, for the loading of the reactor containing 8320 sheets of fuel, there is less than a 1% probability that the selection of sheets chosen has an average weight differing from the mean of the entire sampling of sheets by as much as 0.004 grams using the t-test of significance on statistics on 50-sheet samples. Thus, the uranium mass of the mockup reactors is based on an average weight of 2.62 gm/sheet, and the total mass thus calculated is accurate to within 1% with a confidence of greater than 95%.

It is concluded from these data that on the average the size 1.0 fuel sheets contain (2.62 ± 0.007) grams of uranium for selecting a single sheet. The total weight of each size 1.0 sheet is (2.75±0.007) grams on the average, including uranium and impurities and that 95% of the uncleaned weight is uranium. The quoted standard deviation is based on randomly selected sheets, and represents the variance of the Gaussian distribution. Using the t-test of significance, the mean mass of 8000 randomly selected fuel sheets has only a 1% probability (t = 2.6) of differing from 2.618 gm by 0.002 grams or more.

7.2.4 Uranium Worth Measurements

Considerable time was devoted to an accurate measurement of fuel worth in this mockup reactor. The first set of measurements involved the removal of 390 sheets of fuel in three increments. Each increment of fuel was removed from various fuel elements (13) in a one-quarter sector of the core as shown in Figure 7.9. Ten sheets of fuel were removed from each of the 13 fuel elements which reduced the fuel loading. It should be remembered that the regular fuel elements contained 40 size 1.0 fuel sheets and these were distributed over 15 stages with two sheets per stage in five stages. There were two sheets in all stages in the lighter loaded elements involved in the fuel worth measurements.

The results obtained from these measurements are shown in Table 7.7. It was originally hoped that the other quadrant could also have been changed but there was not sufficient k-excess as noted from this table. The average fuel worth was (1.015±0.014) x 10^{-3}%Δk/gm of uranium. These data were based on an average fuel sheet weight of 2.62 grams uranium.

Other fuel worth measurements followed by taking the cleaned fuel and assembling fuel elements with 3 sheets of fuel per stage for a total loading of 45 sheets. The fuel content in these elements was known and they were interchanged for 30 fuel sheet elements in the core containing uncleaned fuel. The weight of the fuel in the 40-sheet elements was assumed to be 2.62 grams of uranium per fuel sheet. Sufficient measurements were made to produce a radial profile of fuel worth from the center to outer edge of the fueled region and these data are given in Table 7.8 and Figure 7.10. A further set of fuel worth measurements was made using clean fuel in both heavy and light loaded fuel elements. In general, these data agreed very well except for the point at 49.7 cm which was below the smooth curve. Each of the measurements involved the interchange of four fuel elements at the same radial position as illustrated in Figure 7.11. The volume weighted average fuel worth from these data was $1.105 \times 10^{-3}\%\Delta k/gm$ at a fuel loading of 20.8 kg of uranium. The error associated with this fuel worth is about 5% as indicated by the average uncertainty of the values given in Table 7.8. The above value is 8.9% above the fuel worth given in Table 7.5. The earlier measurements were obtained with an average fuel loading of 21.3 kg uranium which is a 2.3% higher loading than for the above fuel worth measurements.

A critical mass for this mockup reactor without aluminum in the core can be deduced at this point by factoring in the following corrections, assuming that the ratio of aluminum to uranium worth is constant:

1. k-excess (20.74 kg U) - 0.230%Δk

2. $$\frac{7.757 \text{ kg Al}}{0.168\%\Delta k} \times \frac{1.105\%\Delta k}{\text{kg U}} = 51.0 \frac{\text{kg Al}}{\text{kg U}}$$ 159.94 kg Al/

$$51.0 \frac{\text{kg Al}}{\text{kg U}} = 3.14 \text{ kg U}$$

The excess reactivity of 0.230%Δk is worth 208 gm of uranium based on a worth of 1.105%Δk/kg. The total fuel correction, therefore, amounts to -3.35 kg of uranium which gives a critical mass of (20.74 - 3.35) = 17.39 kg. This compares to 16.11 kg of uranium for the UF_6 reactor for a 7.9% difference. Note, however, this result does not account for differences in core geometry between the mockup and gas configurations. These are discussed in Sections 3 and 9.

7.3 Power Distribution

7.3.1 Bare Catcher Foils

Sufficient catcher foil data were obtained for radial and axial power profiles. The radial was at the axial center of the core and the axial at the radial center of the core. The data are given in Table 7.9 and included in this table are both bare and cadmium covered foils. These bare foil data are presented graphically in Figures 7.12 and 7.13. The ratio of the power at the outer edge of the fuel to the core center was 2.15 and the volume weighted average was 1.430 as shown in the radial profile (Figure 7.12). The axial distribution from Figure 7.13

shows the power at the separation plane to be a factor of 1.76 above the core center and the other end of the core to be a factor of 1.95 above the core center. The curve average was 1.177.

7.3.2 U^{235} Cadmium Ratios

The catcher foil cadmium ratios are given in Table 7.9 and Figures 7.14 and 7.15. At the core center, the ratio was 8.2 and this increased to 17.4 at the radial edge of the fuel. At the ends and the radial center of the active core, the cadmium ratio ranged from 14.7 to 15.2 with the highest value being at the separation plane where there was a 30.5 cm hole in the end reflector. The cadmium ratio on the surface of the cavity wall was 25.0.

7.4 Gold Foil Data

7.4.1 Bare Gold

Both bare and cadmium covered gold foils were exposed within the cavity and the reflector regions for this configuration. These data are given in Table 7.10. The foil activities were power normalized to Run 1065 by using the normalization factors given in Table 7.11 so as to have the foil data corrected to a uniform power base. The results within the cavity region from the bare gold foils normalized to the center of the core are shown in Figures 7.16 and 7.17. The radial distribution gives a weighted average of 1.204 and the ratio of the foil activity from the outer edge of the fuel to the core center of 1.535. The axial profile shows considerable data scatter which cannot be accounted for. However, the scatter is generally within 5% of the drawn curve, which is about two standard deviations for typical thin (0.1 to 0.2 mil thick) gold foil data. The curve average was 1.088.

The bare gold data from the end and radial reflector regions are presented in Figure 7.18. These data contain two points which deviate from the smooth curve. The point at 2.3 cm from the cavity wall in the radial reflector appears to be too high which may be due to a positioning error. The low point on the end reflector curve was believed to be due to a cadmium cover which was accidentally placed on this foil instead of the usual aluminum covers that protect the foils.

7.4.2 Gold Cadmium Ratios

The cadmium ratios obtained from the bare and cadmium covered gold foil data given in Table 7.10 are presented in Table 7.12. The corrected cadmium ratios are based on infinitely dilute foil activity and were calculated according to the procedure given in Section 4.4.2.

The cadmium ratios within the cavity region are shown in Figures 7.19 and 7.20. At the core center, the ratio was 1.27 and this increased to 1.56 at the outer edge of the fuel. At the cavity wall and axial center of the cavity, the cadmium ratio was 1.72. The axial profile shows a ratio of 1.52 at the separation plane and 1.43 at the opposite end of the core.

The cadmium ratios in the reflector regions are presented in Figure 7.21. The two points which were bad, as shown in Figure 7.18 from the bare gold foils, were corrected to fit the smooth curve and the resulting cadmium ratios were used in plotting the data in Figure 7.21.

7.5 Thermal Neutron Flux Distribution

Where both bare and cadmium covered gold foil data were available, thermal neutron flux was calculated using procedures already given in this report. The results thus obtained are presented in Table 7.13 and Figures 7.22 and 7.23. The corrected bare foil activity for the two points in the reflector region which did not fall on the curve (Figure 7.18) were used in calculating the flux at these points. In general, the data are consistent and deviate very little from the smooth curves drawn through the measured points.

TABLE 7.1

Material Weights in Mockup No. 2

	Total Weight (kg)
Fuel element support structure	
Type 6061 aluminum	15.15
Support sheets, type 1100 aluminum	38.60
Fuel elements, type 1100 aluminum	110.4
Spacer rings in fuel elements, type 1100 aluminum	23.03
Fuel element lids, type 1100 aluminum	6.16
Total	193.34

UF_6 Tank Mockup Aluminum (Type 6061 Al)

	Required (kg)	Measured (kg)	Difference (kg)
Back Plate	55.61		
Fuel element ends		2.60*	
Support structure (arch)		15.15	
Added Al plates		35.83	
Total	55.61	53.58	-2.03
Separation Plane Plate	55.61		
Fuel element ends		2.60*	
Added Al plates		55.79	
Total	55.61	58.39	+2.78
Sides	133.68		
Fuel element support sheets		11.55*	
Added Al plates		121.38	
Total	133.68	132.93	+0.75
Total Difference			+0.00
Totals of all above (kg)	244.9	244.9	

Active core aluminum required in k excess correction

Total in structure	193.34
Aluminum used in UF_6 tank mockup (periphery of structure)	-33.40
Difference (internal portions of structure)	159.94 kg (Type 1100 Al)

*Equivalent Type 6061 Al.

TABLE 7.2

Fuel Loading Increments - Mockup No. 2 With Pure D_2O Reflector

Number of Elements	Increment										
	1	2	3	4	5	6	7	8	9	10	11
	Fuel Element Location										
1	1-4	1-6	1-2	2-11	1-1	2-6	2-8	2-2	3-3	2-4	12-4
2	1-5	2-15	2-9	3-11	1-3	2-7	3-7	2-3	6-4	5-4	14-4
3	2-13	2-16	3-9	4-3	2-12	3-8	5-8	3-1	8-3	7-4	15-4
4	2-14	3-15	4-2	6-11	3-12	5-6	6-1	3-2	9-2	11-4	
5	3-13	3-16	5-9	7-11	4-1	5-7	6-8	5-2	9-3	15-4	
6	3-14	4-4	6-9	8-10	5-5	6-6	7-1	5-3	10-3		
7	4-4	5-15	6-16	8-11	5-11	6-7	7-8	6-2	10-4		
8	4-5	6-15	7-9	9-11	6-5	7-6	8-7	6-3	11-3		
9	5-13	7-15	7-16	10-10	6-12	9-6	8-8	7-2	12-2		
10	5-14	8-15	8-9	11-10	7-5	9-7	9-8	7-3	12-3		
11	6-13	9-16	8-16	12-11	7-10	10-6	10-1	8-1	13-2		
12	6-14	10-16	9-9	14-11	8-5	10-7	10-8	8-2	13-3		
13	7-13	11-15	10-9	15-10	9-5	11-6	11-1	9-1	14-3		
14	7-14	11-16	10-16	15-12	9-12	11-7	11-8	10-2	15-3		
15	8-13	14-16	5-16	2-5	10-11	12-6	12-8	11-2	16-2		
16	8-14	15-15	2-10	3-5	11-5	12-7	14-1	12-1	16-3		
17	9-14		3-10	5-12	11-11	14-6	14-8	13-1			
18	9-15		5-10	7-12	12-5	14-7	15-1	14-2			
19	10-13		6-10	8-12	12-12	15-6	15-8	15-2			
20	10-14		9-10	10-5	13-4	15-7		16-1			
21	11-13		11-9	10-12	14-10						
22	11-14		12-9	11-12	14-12						
23	12-13		12-10	13-5	15-5						
24	12-14		14-9	14-5	15-11						
25	12-15		15-9	16-5	16-4						
26	13-6			3-6							
27	14-14			7-7							
28	14-15			8-6							
29	15-13										
30	15-14										
31	16-6										

TABLE 7.3

Inverse Multiplication

Initial Loading - Mockup No. 2 With Pure D_2O Reflector

Increment No.	Fuel Elements in Reactor	Channel 1		Channel 2		Channel 3		Rod Positions
		CR	CRo/CR	CR	CRo/CR	CR	CRo/CR	
0	0	1947	1.000	2315	1.000	1651	1.000	In
0	0	2239	1.000	2688	1.000	1875	1.000	Out
1	31	3827	0.509	4356	0.531	3187	0.518	In
1	31	4661	0.480	5270	0.510	3875	0.484	Out
2	47	5039	0.386	5668	0.408	4186	0.394	In
2	47	6333	0.354	7088	0.379	5216	0.359	Out
3	72	7107	0.274	8016	0.289	6061	0.272	In
3	72	9822	0.228	10600	0.254	8053	0.233	Out
4	100	11085	0.176	12029	0.192	9080	0.182	In
4	100	16041	0.140	17298	0.155	13204	0.142	Out
5	125	15943	0.122	17331	0.134	13058	0.126	In
5	125	26508	0.084	28426	0.095	21207	0.088	Out
6	145	21475	0.091	23002	0.101	17271	0.096	In
6	145	41573	0.054	43744	0.061	32847	0.057	Out
7	164	28534	0.068	30351	0.076	22995	0.072	In
7	164	72130	0.031	74583	0.036	55978	0.033	Out
8	184	44549	0.044	45344	0.051	34077	0.048	In
8	184	245970	0.009	245258	0.011	177329	0.011	Out
9	200	63847	0.030	65460	0.035	49219	0.034	In
9	200	Critical with about 0.56%Δk excess reactivity						

TABLE 7.4

Actuator 3 and 6 Tabular Rod Worth Curve - Mockup No. 2

	0	100	200	300	400	500	600	700	800	900
					Fraction of Rod Worth Inserted					
Ratiometer Reading										
0	1.000	1.000	.9714	.9428	.9142	.8857	.8574	.8293	.8014	.7738
1000	.7465	.7198	.6937	.6682	.6432	.6190	.5955	.5723	.5498	.5278
2000	.5064	.4856	.4653	.4457	.4266	.4082	.3903	.3729	.3561	.3399
3000	.3241	.3090	.2943	.2802	.2666	.2536	.2411	.2291	.2176	.2066
4000	.1960	.1859	.1763	.1671	.1583	.1498	.1416	.1341	.1268	.1198
5000	.1131	.1067	.1007	.0949	.0895	.0843	.0793	.0745	.0700	.0658
6000	.0617	.0579	.0542	.0508	.0474	.0443	.0413	.0384	.0357	.0331
7000	.0306	.0282	.0259	.0237	.0216	.0197	.0179	.0161	.0145	.0130
8000	.0115	.0102	.0089	.0078	.0067	.0058	.0049	.0040	.0033	.0026
9000	.0020	.0015	.0011	.0008	.0005	.0003	.0001	.0000	.0000	.0000
					Difference Table					
Ratiometer Reading										
0	0.0	0.0	.0286	.0286	.0286	.0285	.0283	.0281	.0279	.0276
1000	.0273	.0267	.0261	.0255	.0250	.0242	.0235	.0232	.0225	.0220
2000	.0214	.0208	.0203	.0196	.0191	.0184	.0179	.0174	.0168	.0162
3000	.0158	.0151	.0147	.0141	.0136	.0130	.0125	.0120	.0115	.0110
4000	.0106	.0101	.0096	.0092	.0088	.0085	.0082	.0075	.0073	.0070
5000	.0067	.0064	.0060	.0058	.0054	.0052	.0050	.0048	.0045	.0042
6000	.0041	.0038	.0037	.0034	.0034	.0031	.0030	.0029	.0027	.0026
7000	.0025	.0024	.0023	.0022	.0021	.0019	.0018	.0018	.0016	.0015
8000	.0015	.0013	.0013	.0011	.0011	.0009	.0009	.0009	.0007	.0007
9000	.0006	.0005	.0004	.0003	.0003	.0002	.0002	.0001	.0000	.0000

TABLE 7.5

Fuel Weights Before and After Cleaning in Boiling Water

Batch	Number of Size 1.0 Sheets	Wt. Before Cleaning (gm)	Wt. After Cleaning (gm)	Wt. of U in Solution (gm)
1	10	25.02	22.77	1.976
2	10	29.63	23.10	4.088
3	20	54.30	48.45	
3	20	57.49	45.80	
3	20	57.00	47.80	
3	20	55.40	45.19	
3	20	55.19	44.60	
3	20	53.35	46.76	
3	20	53.83	46.09	
3	20	54.26	46.51	
3	20	54.70	45.73	
3	20	54.03	45.81	
3	15	43.00	34.40	
Totals for Batch 3	215	592.55	497.14	66.52

TABLE 7.6

Fuel Sheet Weight Percent Uranium from Chemical Analyses

Solid Uncleaned Sheets			
Sample Number	Total Sheet Weight (gm)	Sample Wt. Used In Analysis (gm)	Weight % U
1	3.05	0.0905	92.19
2	3.05	0.1002	83.80
3	3.02	0.0888	84.77
4	3.02	0.0882	90.29
Results from Cleaned Fuel			
1	2.11	0.0676	99.46
2	2.51	0.0782	100.08
3	2.49	0.0758	99.94
4	2.26	0.0652	99.81
		Avg.	99.82

Results from Fuel Cleaning			
Batch Number	Weight Before Cleaning (gm)	Weight After Cleaning (gm) (1)	Weight % U
1	25.02	24.705	98.74
2	29.63	27.146	91.62
3	592.55	562.77	94.97

(1) Corrected for 0.9982 uranium factor in cleaned fuel

TABLE 7.7

Fuel Worth Results - Mockup No. 2 - All D_2O Reflector

Run Number	Reduced Fuel Loading Positions	k ex (%Δk)	Δk ex (%Δk)	Fuel Worth (%Δk/gm) x 10^3 (1)
254	Base reactivity	1.267	--	--
255	3-3, 3-5, 3-10, 3-15, 4-2, 7-6, 7-8, 7-14, 7-16, 8-2, 8-8, 8-9, 8-11	0.918	0.349	1.025
256	1-2, 1-6, 2-3, 2-6, 2-9, 2-16, 5-7, 5-9, 5-15, 6-1, 6-3, 6-10, 6-12	0.573	0.345	1.013
257	11-6, 11-8, 11-9, 11-15, 12-2, 12-4, 12-10, 12-13, 15-1, 15-10, 15-12, 16-3, 16-4	0.230	0.343	1.007
			(2) Avg.	1.015 ± 0.014

(1) It was assumed in this measurement that each size 1.0 fuel sheet contained 2.62 gm of uranium.

(2) The error on this value is the error in rod worth used to calculate k excess. The three points by themselves show slightly less error than this.

The average fuel loading for this measurement was 21.3 kg of uranium.

TABLE 7.8

Fuel Worth Measurements Radially Across Active Core

Radius (cm)	Fuel Weight Difference (gm)	Change In k excess (%Δk) (1)	Fuel Worth (%Δk/kg)
5.4	101.52	0.0655±0.0053	0.645±0.052
16.2	98.49	0.720	0.731
26.9	98.49	0.825±0.0091	0.838±0.092
37.7	100.48	0.0902±0.0053	0.898±0.053
39.2	101.52	0.1047±0.0053	1.031±0.052
49.8	101.56	0.1176±0.0039	1.158±0.038
56.3	98.49	0.1398±0.0053	1.419±0.054
57.3	101.52	0.1504±0.0039	1.481±0.038
59.2	98.49	0.1568	1.592
60.2	100.54	0.1722±0.0091	1.713±0.091
Clean Sheet Element Interchange			
57.3	137.67	0.1976±0.0039	1.435±0.028
39.2	137.67	0.1336±0.0053	0.970±0.038
49.8	138.58	0.1475±0.0039	1.064±0.028
26.9	135.58	0.1027±0.0091	0.757±0.067
26.9	137.75	0.1017	0.738
49.8	136.75	0.1409	1.030

(1) The error values are the measured variations in the base reactivity values with no 45-sheet elements in the reactor. Where only a single base was available no error value is given.

TABLE 7.9

Catcher Foil Data - Mockup No. 2 - Pure D_2O Reflector

Foil No.	Foil Type	Location Radial (cm)	Location Axial (cm)	Normalized Counts	Ratio of Local to Core Center (Foil No. X)
Run 1078					
1	Bare	0	93.3	74250	1.954
2	Bare	0	96.5	73849	1.944
3	Bare	0	105.3	52314	1.377
4	Bare	0	120.6	43529	1.146
5	Bare	0	135.8	38996	1.026
6	Bare	0	151.1	37994	1.000 X
7	Bare	0	166.3	38564	1.015
8	Bare	0	181.5	43872	1.155
9	Bare	0	196.8	49646	1.307
10	Bare	0	205.8	66835	1.759
11	Bare	0	209.5	76137	2.004
12	Bare	15.2	151.1	36829	0.969
13	Bare	30.5	151.1	42135	1.109
14	Bare	45.7	151.1	53612	1.411
15	Bare	61.0	151.1	81684	2.150
16	Bare	76.2	151.1	103094	2.713
17	Bare	91.4	151.1	118609	3.122
Run 1080					Cd Ratio
1	Cd cov.	0	96.5	5018	14.7
2	Cd cov.	0	120.6	4169	10.4
3	Cd cov.	0	151.1	4654	8.2
4	Cd cov.	0	181.5	4633	9.5
5	Cd cov.	0	205.8	4403	15.2
6	Cd cov.	30.5	151.1	4404	9.6
7	Cd cov.	61.0	151.1	4685	17.4
8	Cd cov.	91.4	151.1	4744	25.0

TABLE 7.10

Gold Foil Data

Mockup No. 2 Pure D_2O Reflector

Foil No.	Foil Type	Location Radial (cm)	Location Axial (cm)	Foil Weight (gm)	Specific Activity d/m/gm x 10^{-6}
Run 1078					
1	Bare	0	83.3	0.0426	2.717
2	Bare	0	96.5	0.0349	2.595
3	Bare	0	105.3	0.0409	2.195
4	Bare	0	120.6	0.0483	1.901
5	Bare	0	135.8	0.0302	2.019
6	Bare	0	151.1	0.0328	1.918
7	Bare	0	166.3	0.0298	2.048
8	Bare	0	181.5	0.0323	2.051
9	Bare	0	196.8	0.0417	2.003
10	Bare	0	205.8	0.0348	2.626
11	Bare	0	209.5	0.0416	2.651
12	Bare	15.2	151.1	0.0339	1.968
13	Bare	30.5	151.1	0.0432	1.971
14	Bare	45.7	151.1	0.0373	2.337
15	Bare	61.0	151.1	0.0333	2.943
16	Bare	76.2	151.1	0.0385	3.428
17	Bare	91.4	151.1	0.0302	3.861
18	Bare	0	89.4	0.0399	3.206
19	Bare	0	74.9	0.0385	6.825
20	Bare	0	59.6	0.0385	4.252
21	Bare	0	44.4	0.0313	4.099
22	Bare	0	29.1	0.0371	2.529
23	Bare	0	13.9	0.0365	1.274
24	Bare	0	0	0.0413	0.180
25	Bare	93.2	151.1	0.0406	5.980
26	Bare	107.7	151.1	0.0337	6.479
27	Bare	123.0	151.1	0.0348	4.946
28	Bare	138.2	151.1	0.0402	3.376
29	Bare	153.5	151.1	0.0389	1.989
30	Bare	168.7	151.1	0.0322	0.866
31	Bare	183.7	151.1	0.0410	0.127
Run 1079					
1	Cd cov.	0	89.4	0.0397	1.326
2	Cd cov.	0	59.6	0.0418	0.263
3	Cd cov.	0	96.5	0.0369	1.268
4	Cd cov.	0	120.6	0.0364	1.164
5	Cd cov.	0	151.1	0.0357	1.142

TABLE 7.10

(Continued)

Foil No.	Foil Type	Location Radial (cm)	Location Axial (cm)	Foil Weight (gm)	Specific Activity d/m/gm x 10^{-6}
Run 1079 (Cont'd)					
6	Cd cov.	0	181.5	0.0417	1.098
7	Cd cov	0	205.8	0.0381	1.150
8	Cd cov.	30.5	151.1	0.0379	1.164
9	Cd cov.	61.0	151.1	0.0390	1.213
10	Cd cov.	91.4	151.1	0.0380	1.320
11	Cd cov.	93.2	151.1	0.0392	1.363
12	Cd cov.	123.0	151.1	0.0385	0.134
Run 1080					
1	Cd cov.	0	44.4	0.0398	0.0490
2	Cd cov.	0	74.9	0.0376	1.174
3	Cd cov.	107.7	151.1	0.0398	0.800
4	Cd cov.	138.2	151.1	0.0374	0.0212

TABLE 7.11

Power Normalization Factors - UF_6 Mockup No. 2

Run	Time	Decay Time (min)	Decay Factor	Activity (CPM)	Corrected Activity (CPM) (1)	Normalization Factor (2)
1078	1212.75	65.95	1.39	195684	272001	
	1214.65	67.85	1.43	189136	270464	
	1216.40	69.60	1.49	182856	272455	
					271640	1.071
1079	1439.00	64.5	1.36	203372	276586	
	1442.76	68.26	1.45	189866	275306	
	1444.95	70.45	1.51	182280	275243	
					275712	1.055
1080	1610.23	19.98	0.39	635900	248001	
	1611.85	21.60	0.42	599026	251591	
	1613.45	23.20	0.45	564267	253920	
					251171	1.158
1081	1229.59	64.02	1.35	212970	287510	
	1231.75	66.18	1.40	204484	286278	
	1232.57	68.00	1.44	197735	284738	
					286175	1.016
1082	1433.85	44.5	0.87	327378	284819	
	1436.35	47.0	0.93	306938	285452	
	1438.85	49.5	0.99	289214	286322	
					285531	1.019
1083	1548.50	34.03	0.65	438998	285349	
	1550.50	36.03	0.69	410874	283503	
	1552.50	38.03	0.73	392401	286453	
					285102	1.020

(1) Decay corrected to 50 minutes after shutdown.
(2) Normalized to Run 1065 with an average foil activity of 290894 counts per minute at 50 minutes after shutdown.

TABLE 7.12

Gold Foil Cadmium Ratios

Mockup No. 2 - Pure D_2O Reflector

Location		Bare Foil Activity	Cd Foil Activity		
Radial (cm)	Axial (cm)	d/m/gm x 10^{-6}	d/m/gm x 10^{-6}	Cadmium Ratio	Corrected Cadmium Ratio
0	44.4	4.099	0.049	83.7	34.7
0	59.6	4.252	0.263	16.2	7.05 (1)
0	74.8	6.825	1.174	5.81	3.01
0	89.4	3.206	1.326	2.42	1.58
0	96.5	2.595	1.268	2.05	1.43
0	120.6	1.901	1.164	1.63	1.32
0	151.1	1.918	1.142	1.68	1.27
0	181.5	2.051	1.098	1.87	1.30
0	205.8	2.626	1.150	2.28	1.52
30.5	151.1	1.971	1.164	1.69	1.31
61.0	151.1	2.943	1.213	2.43	1.56
91.4	151.1	3.861	1.320	2.92	1.76
93.2	151.1	5.980	1.363	4.39	2.40 (2)
107.7	151.1	6.479	0.800	8.10	3.87
123.0	151.1	4.946	0.134	36.9	14.4
138.9	151.1	3.376	0.0212	159.2.	67.2

(1) The bare gold data for this point appears to be low. If corrected to fit the curve, the cadmium ratio is 8.72.

(2) The bare gold data for this point was too high. If corrected to fit the curve, the cadmium ratio is 1.78.

TABLE 7.13

Thermal Neutron Flux

Mockup No. 2 - Pure D_2O Reflector

Location		
Radial (cm)	Axial (cm)	$n/cm^2/sec/watt \times 10^{-6}$
0	0	0.19
0	13.9	1.35
0	29.1	2.68
0	44.4	4.30
0	59.6	5.39
0	74.9	6.02
0	89.4	2.00
0	96.5	1.38
0	120.6	0.92
0	151.1	0.78
0	181.5	0.88
0	205.8	1.52
30.5	151.1	0.92
61.0	151.1	1.75
91.4	151.1	2.57
93.2	151.1	2.74
107.7	151.1	5.98
123.0	151.1	4.64
138.2	151.1	3.57
153.5	151.1	2.11
168.7	151.1	0.92
183.9	151.1	0.14

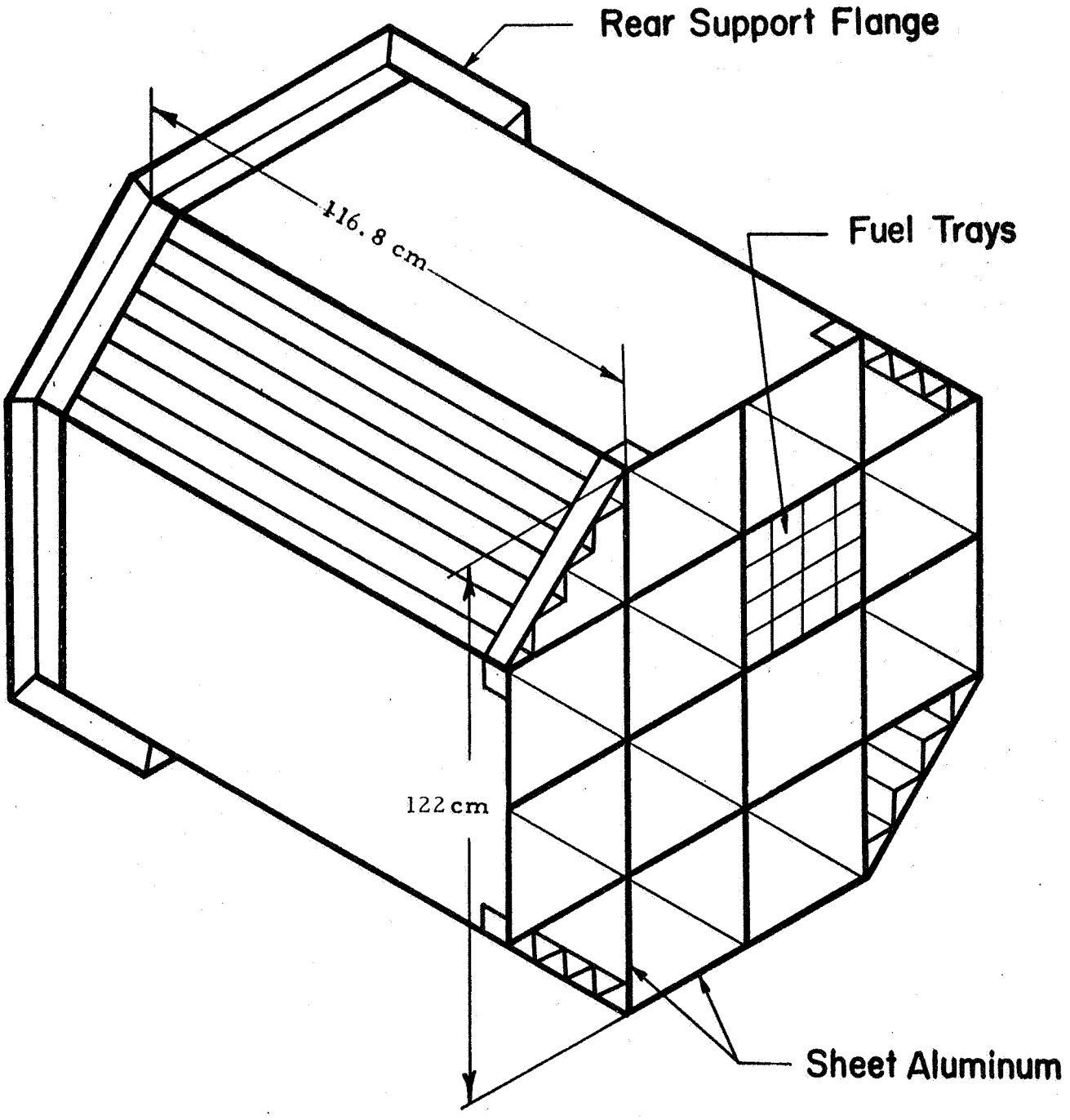


Fig. 7.1 Core support structure

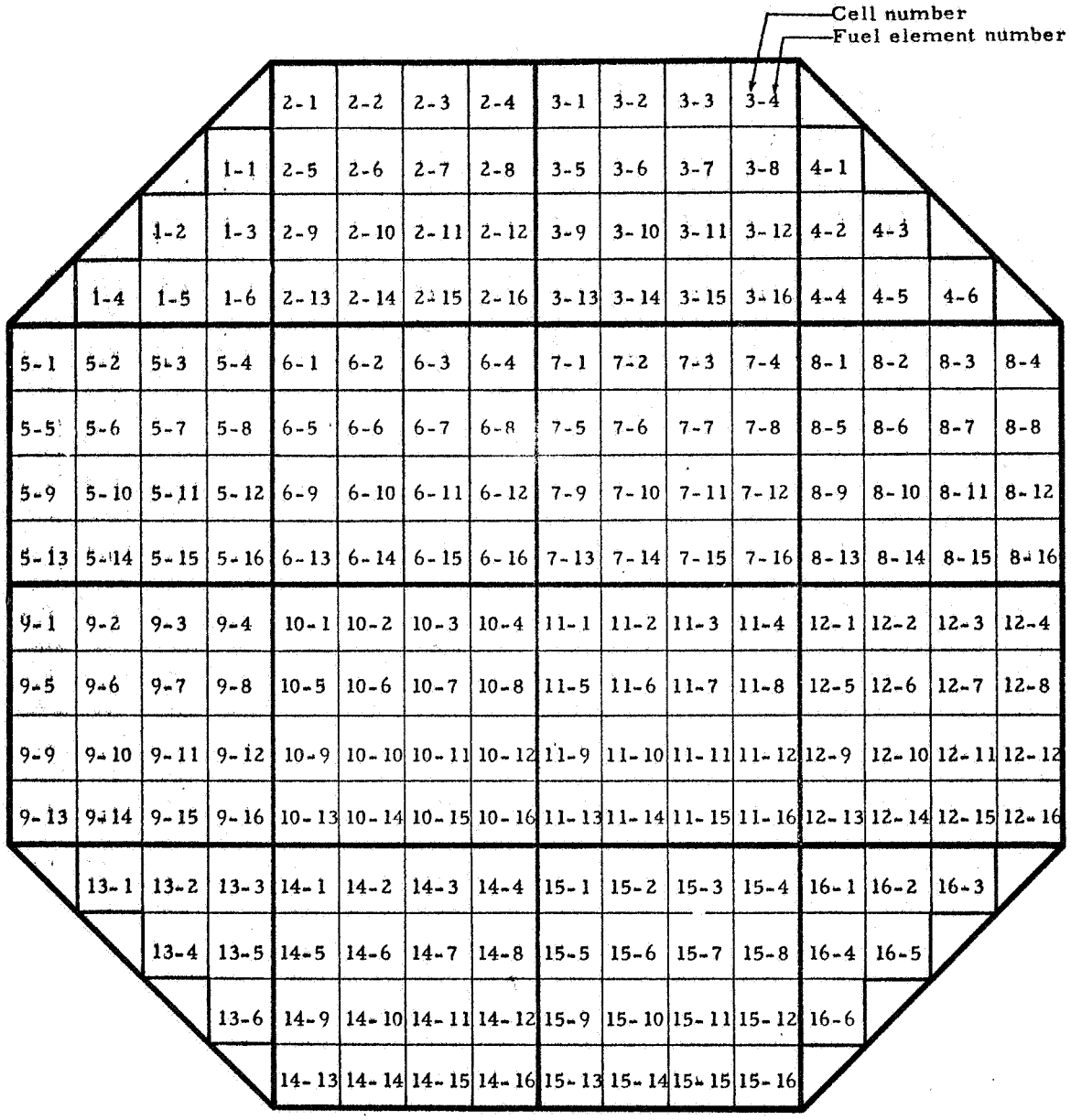


Fig. 7.2 Fuel element numbering system within the active core

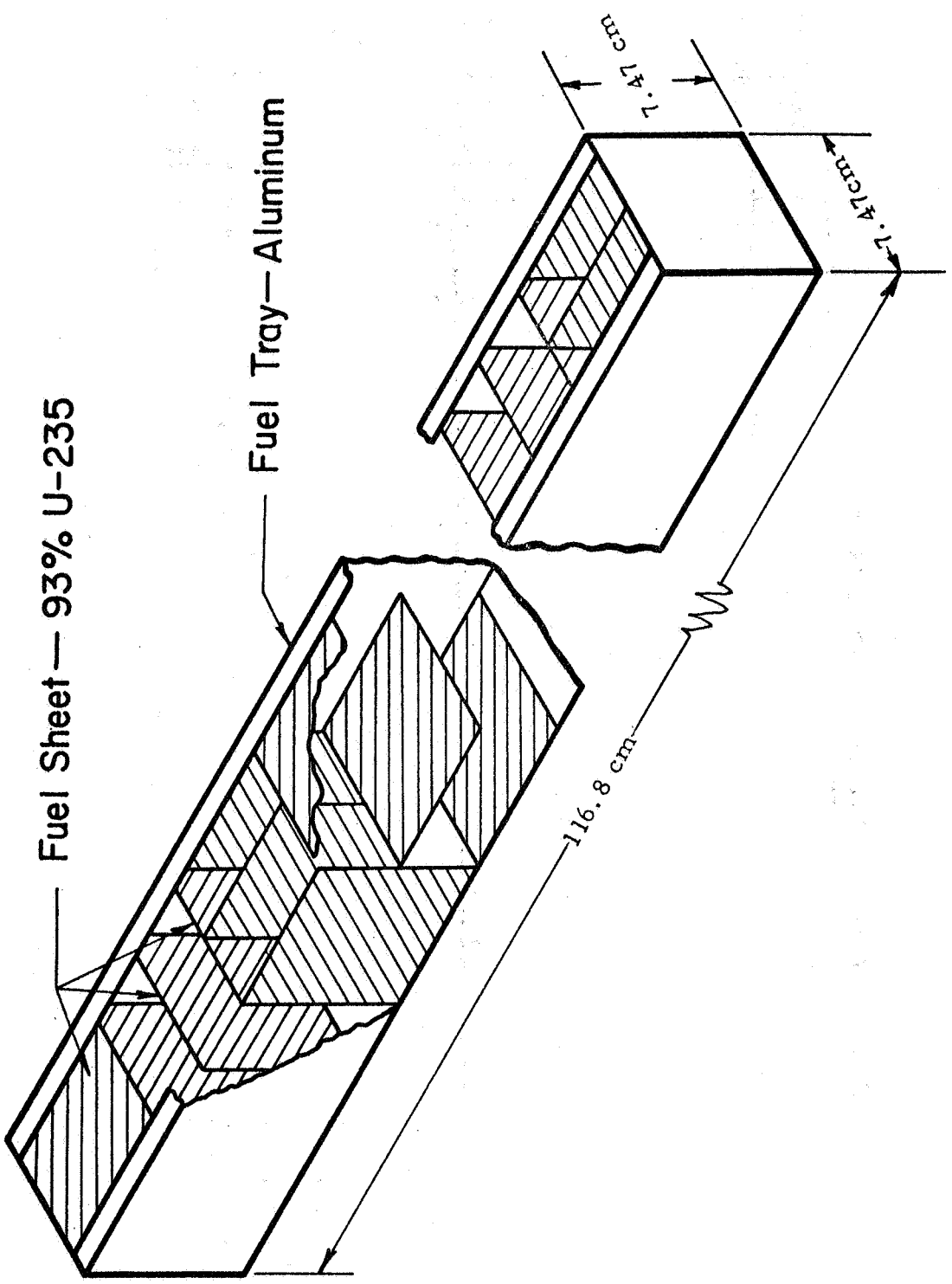


Fig. 7.3 Fuel tray and fuel sheet orientation

Separation Plane

TYPE 1 Fuel Element. When turned around is a TYPE 1A Fuel Element.

	1	2	3	4	5	6	7	8	9	10	11	12	13	14	15	
	1	2	3	1	2	3	1	2	3	1	2	3	1	2	3	Stage Number / Fuel Orientation
	3	3	2	3	3	2	3	3	2	3	3	2	3	3	2	Fuel Sheets/Stage

TYPE 2 Fuel Element. When turned around is a TYPE 2A Fuel Element.

	1	2	3	4	5	6	7	8	9	10	11	12	13	14	15	
	2	3	1	2	3	1	2	3	1	2	3	1	2	3	1	Stage Number / Fuel Orientation
	2	3	3	2	3	3	2	3	3	2	3	3	2	3	3	Fuel Sheets/Stage

TYPE 3 Fuel Element. When turned around is a TYPE 3A Fuel Element.

	1	2	3	4	5	6	7	8	9	10	11	12	13	14	15	
	3	1	2	3	1	2	3	1	2	3	1	2	3	1	2	Stage Number / Fuel Orientation
	3	2	3	3	2	3	3	2	3	3	2	3	3	2	3	Fuel Sheets/Stage

Fig. 7.4 Cavity reactor fuel element loading schedule

Type 1 - 1, 2, 3, 1, 2, 3 etc., its reverse - Type 1A - 1, 3, 2, 1, 3, 2 etc.
Type 2 - 2, 3, 1, 2, 3, 1 etc., its reverse - Type 2A - 2, 1, 3, 2, 1, 3 etc.
Type 3 - 3, 1, 2, 3, 1, 2 etc., its reverse - Type 3A - 3, 2, 1, 3, 2, 1 etc.

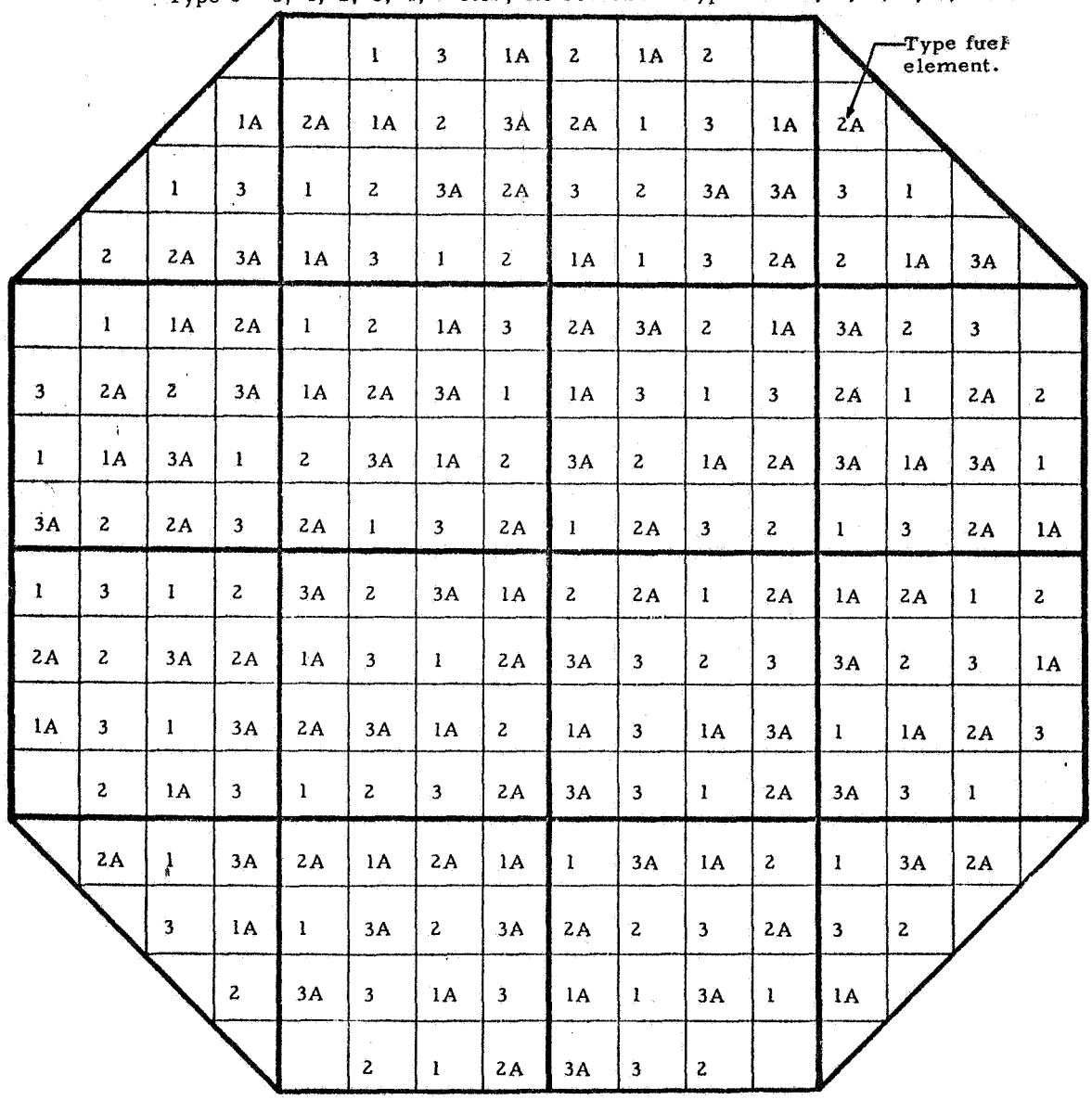


Fig. 7.5 Fuel element loading schedule - Mockup No. 2
Pure D_2O reflector

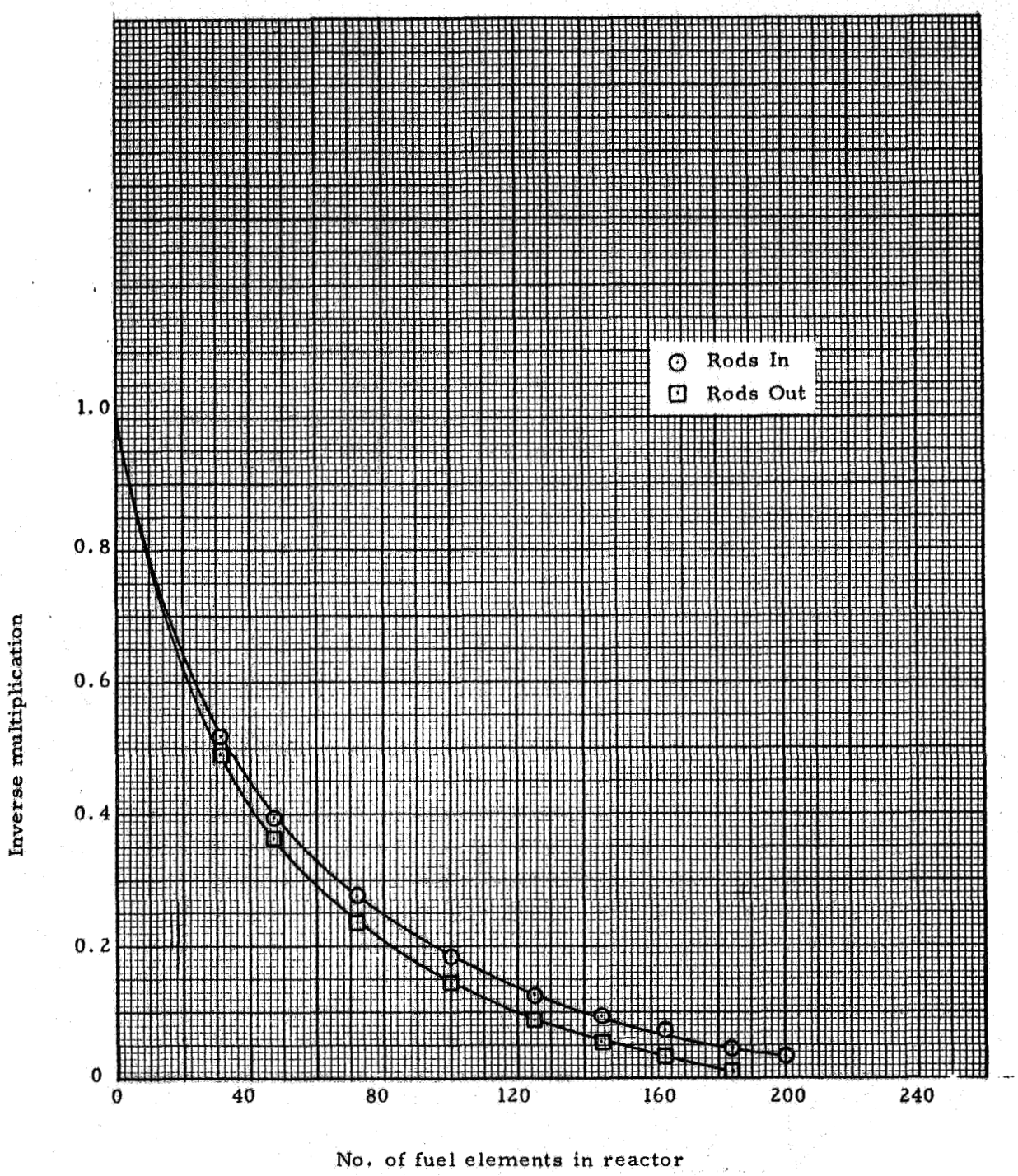


Fig. 7.6 Inverse multiplication - Mockup No. 2, pure D_2O reflector. Average of three channels

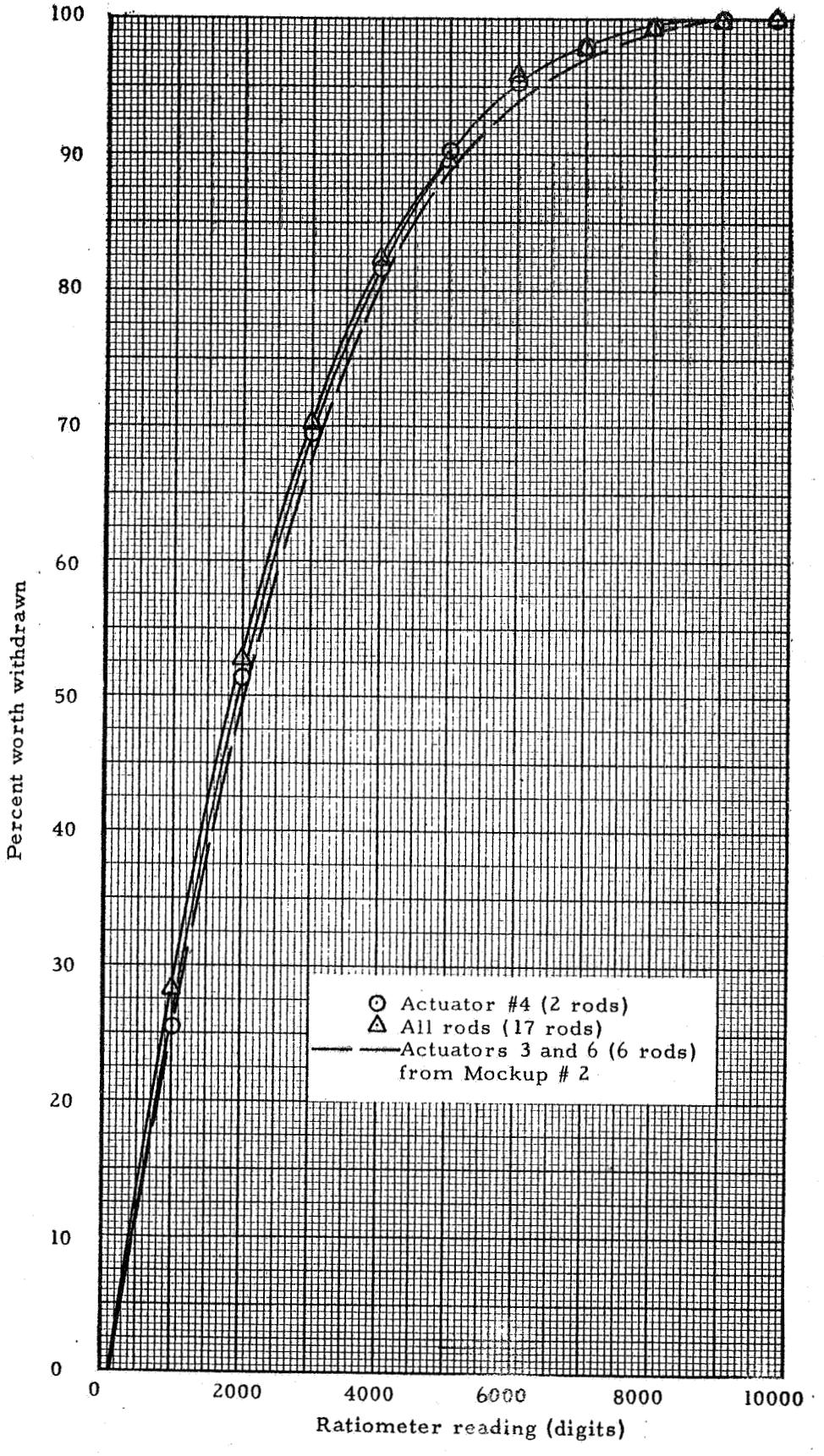


Fig. 7.7 Control rod worth curves

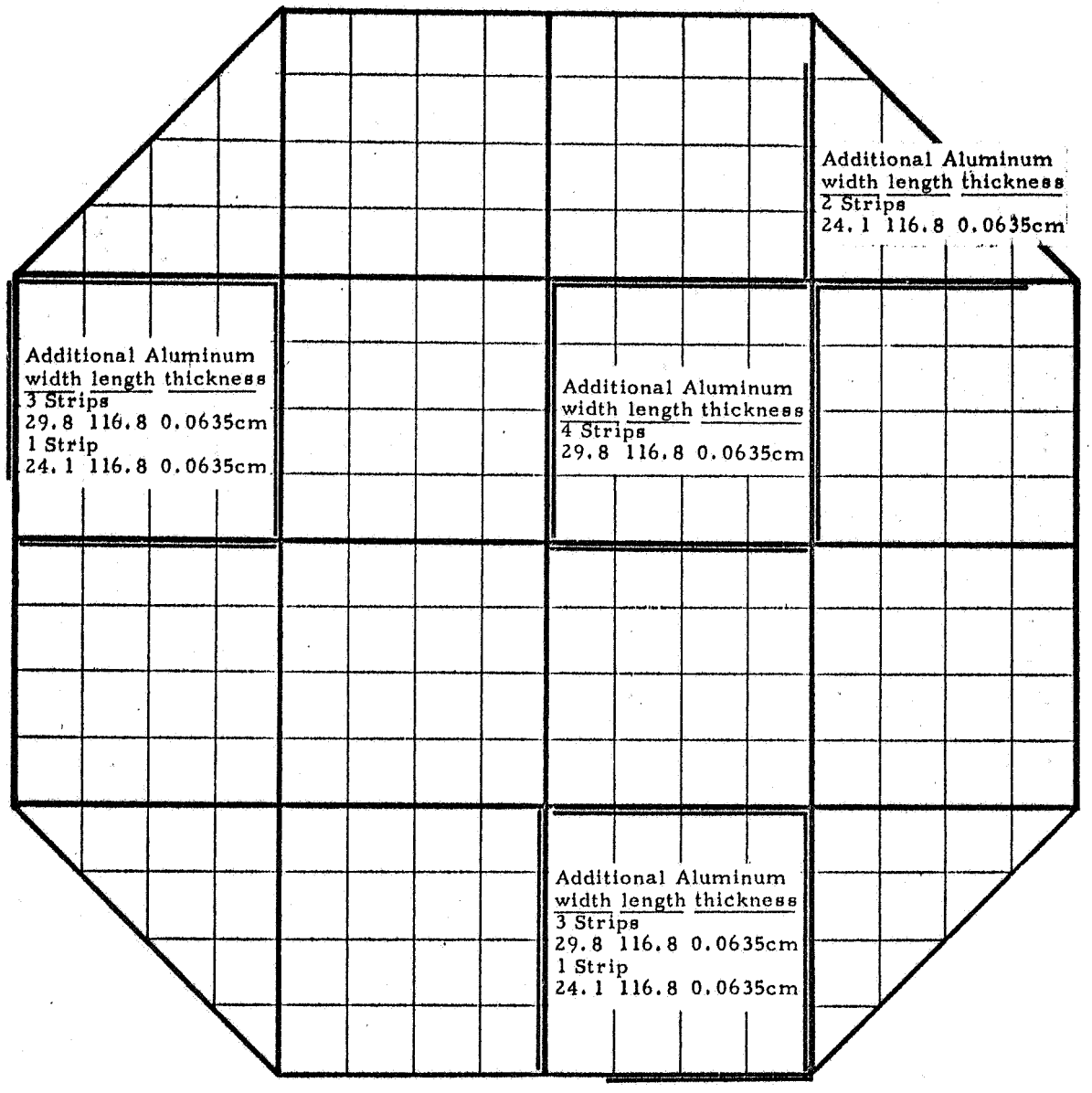


Fig. 7.8 Aluminum locations for reactivity measurements

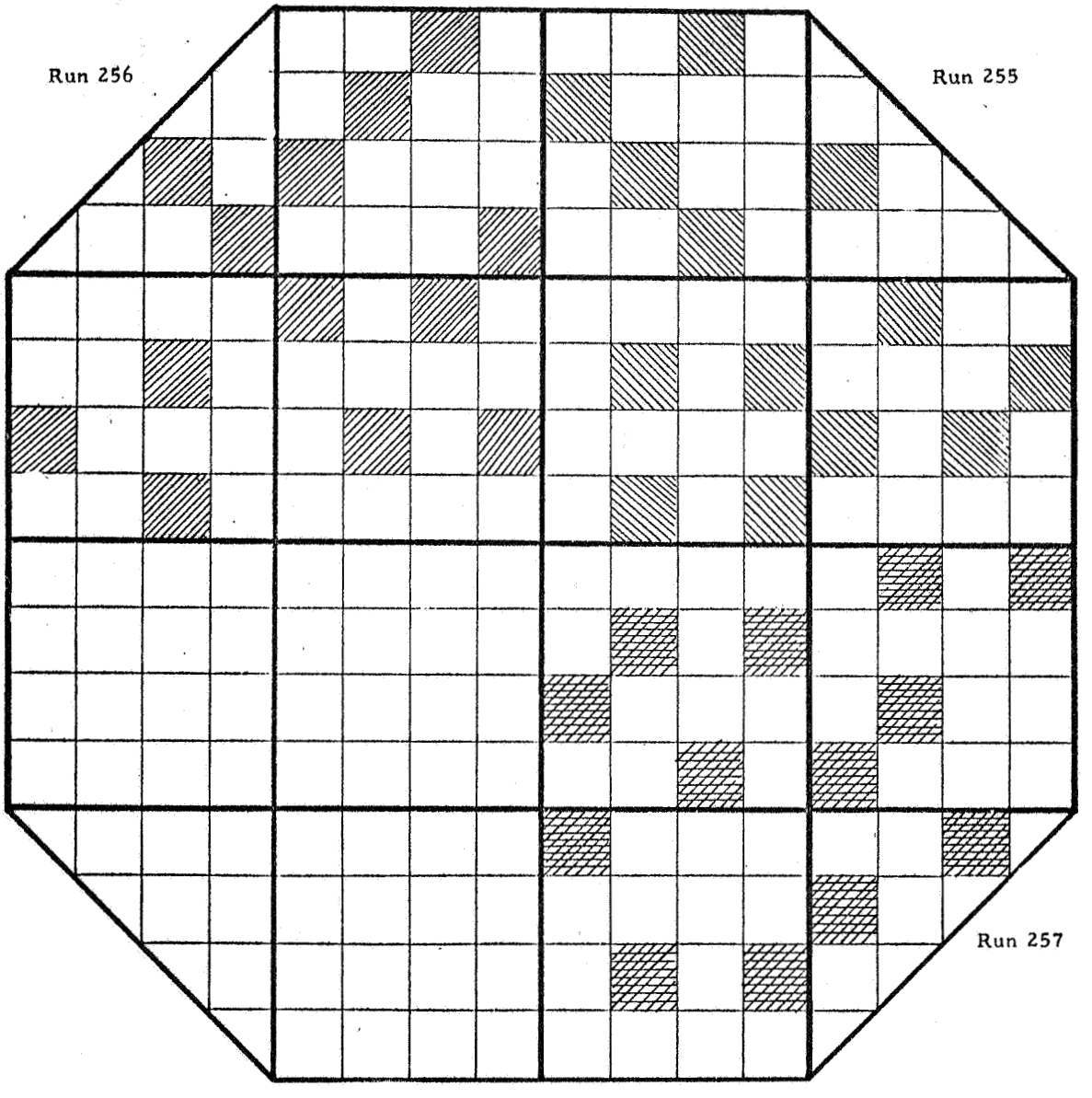


Fig. 7.9 Location of fuel elements which were reduced in loading by 10 sheets of fuel to measure the reactivity worth of fuel

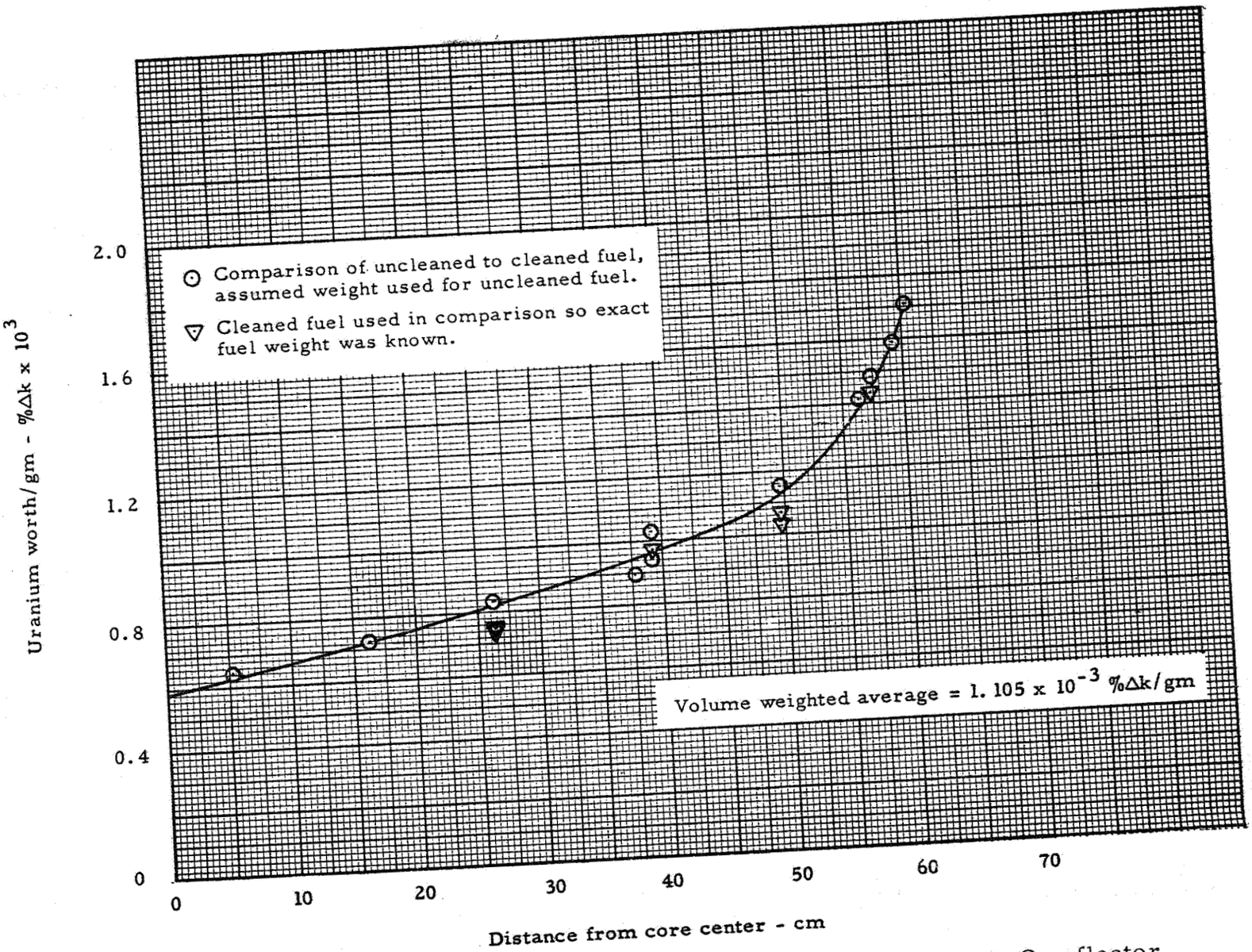


Fig. 7.10 Uranium worth within the active core - Mockup No. 2, pure D_2O reflector

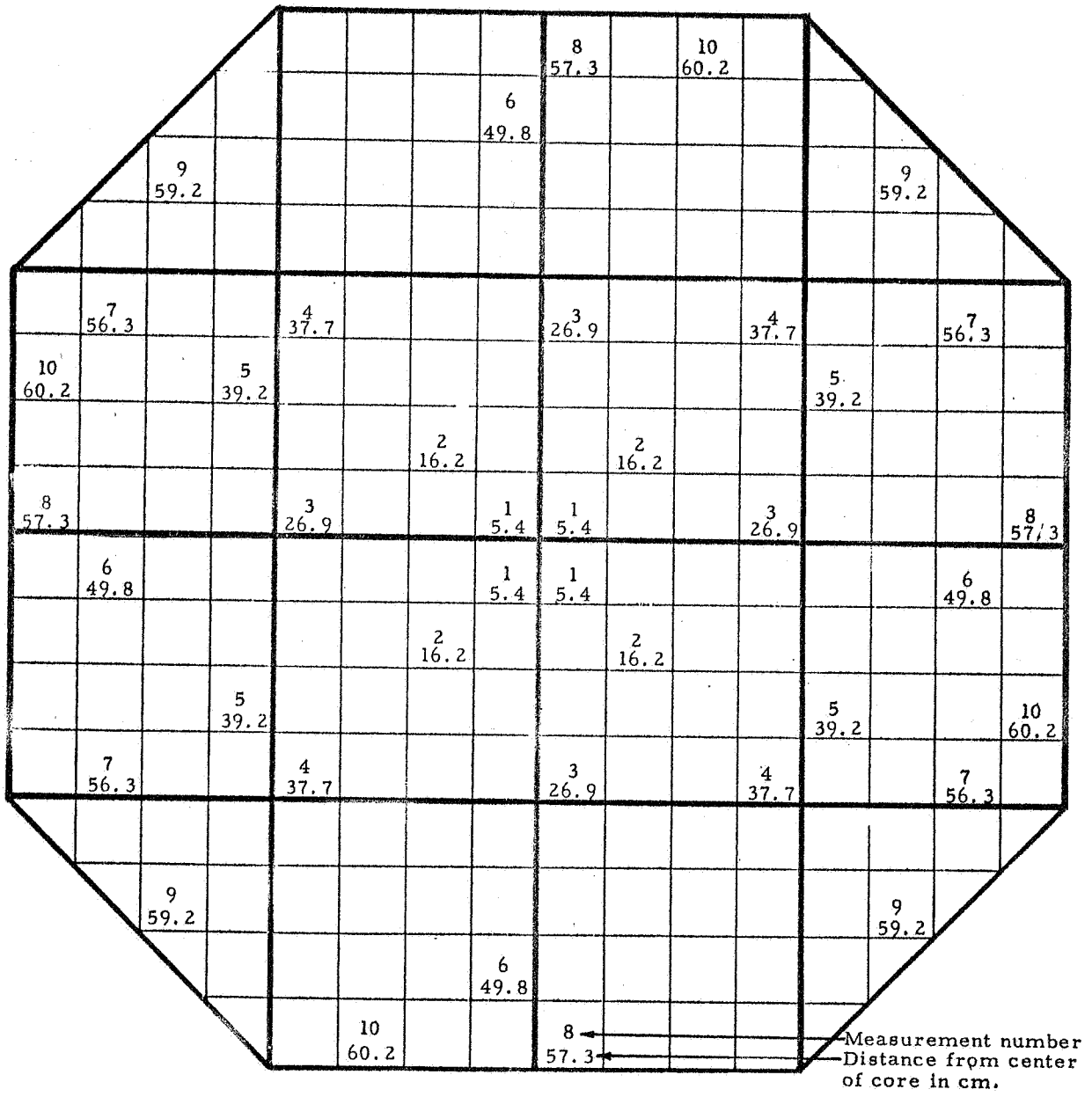


Fig. 7.11 Location of fuel elements involved in fuel worth measurements Mockup No. 2, pure D_2O reflector

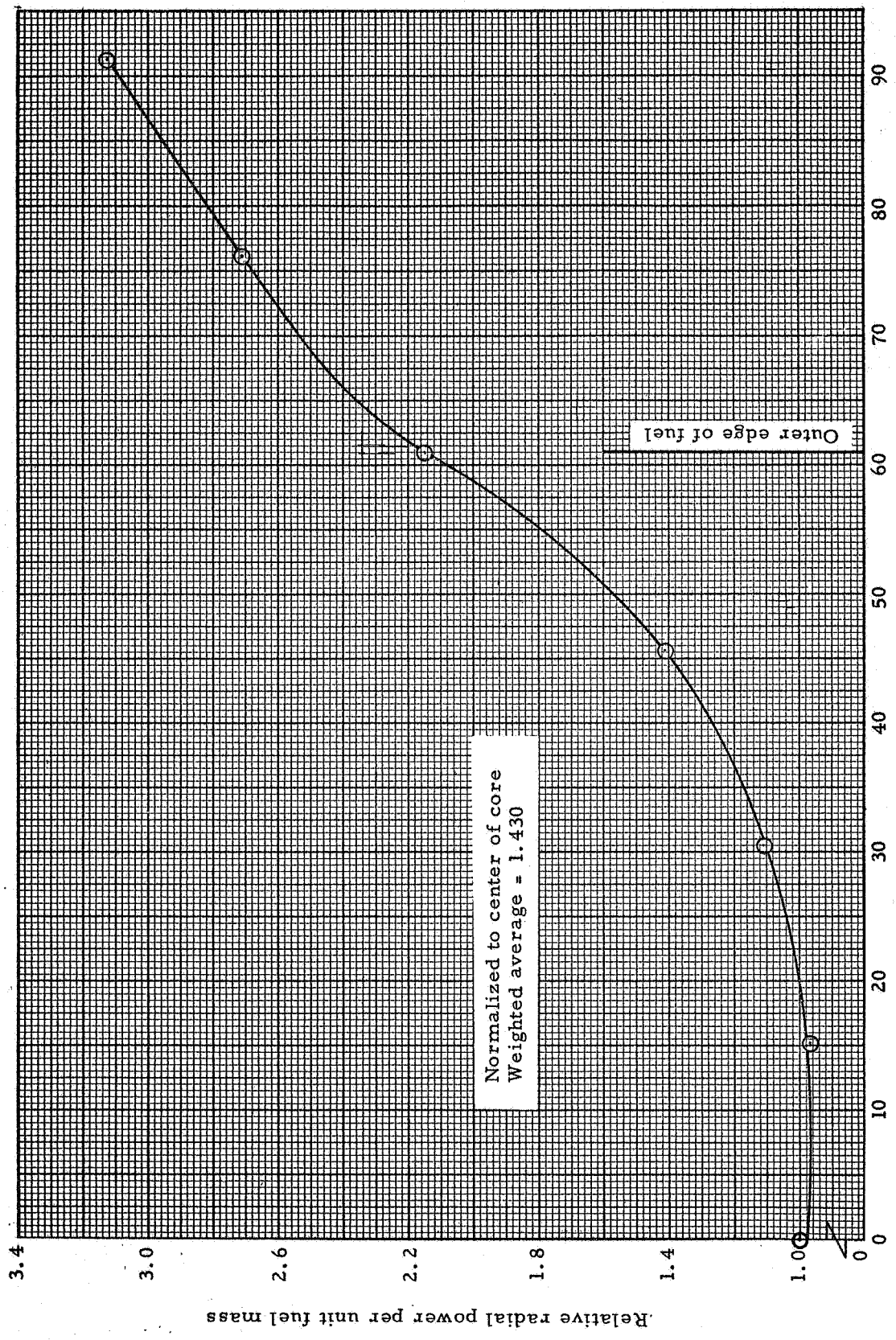


Fig. 7.12 Radial power distribution from bare catcher foils - Mockup No. 2, pure D_2O reflector

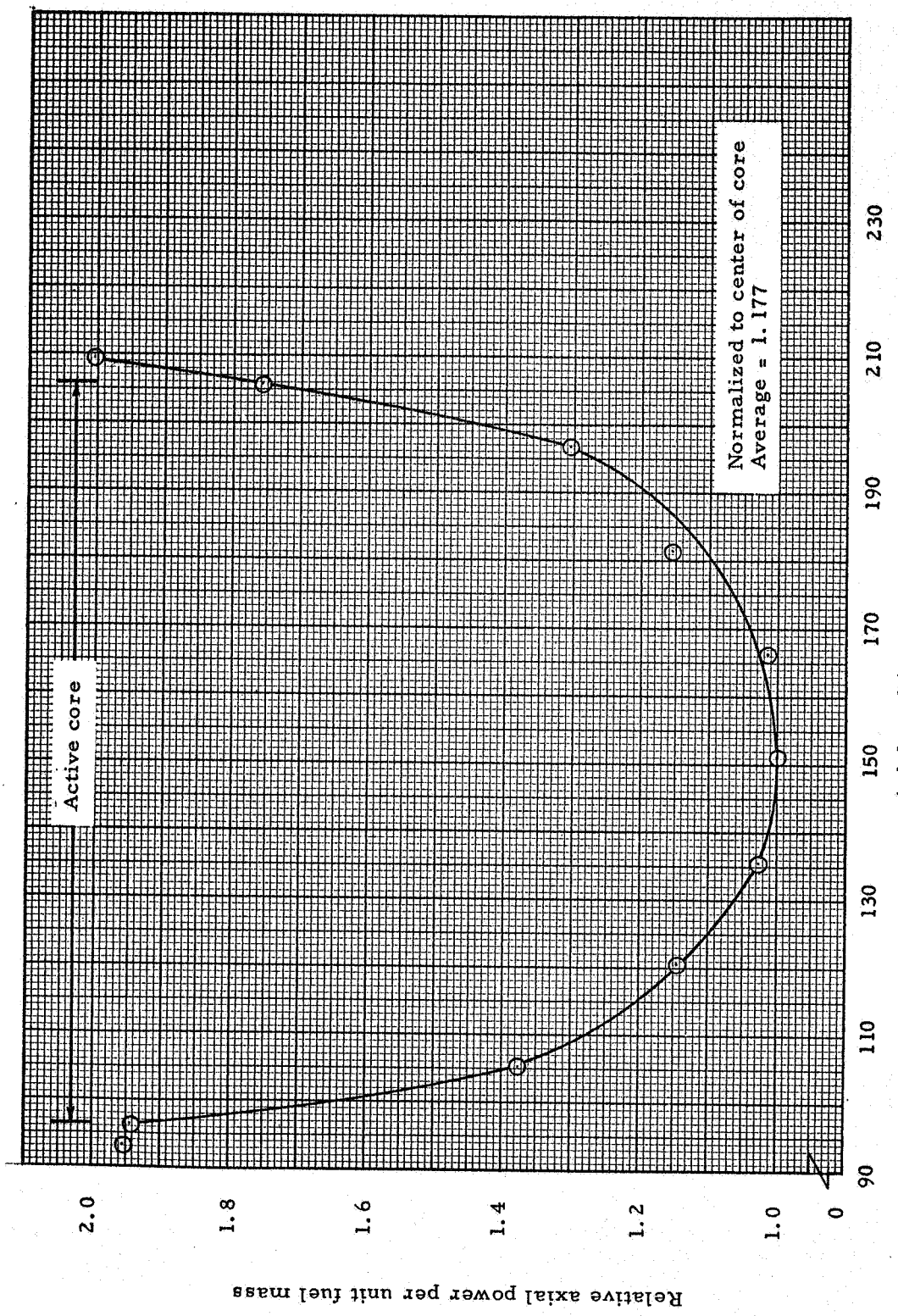


Fig. 7.13 Axial power distribution from bare catcher foils - Mockup No. 2, pure D_2O reflector

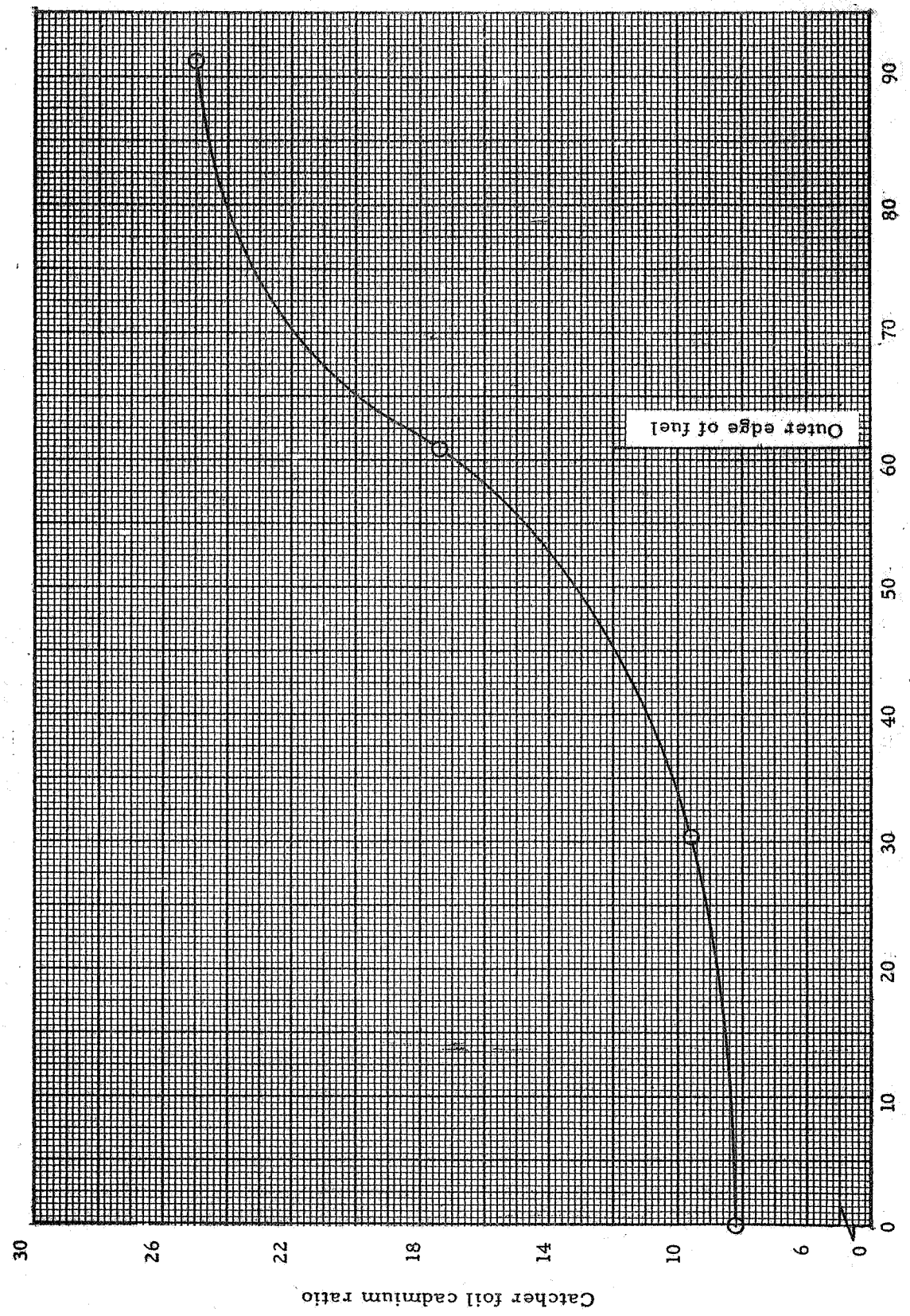


Fig. 7.14 Catcher foil cadmium ratio radial profile - Mockup No. 2, pure D_2O reflector

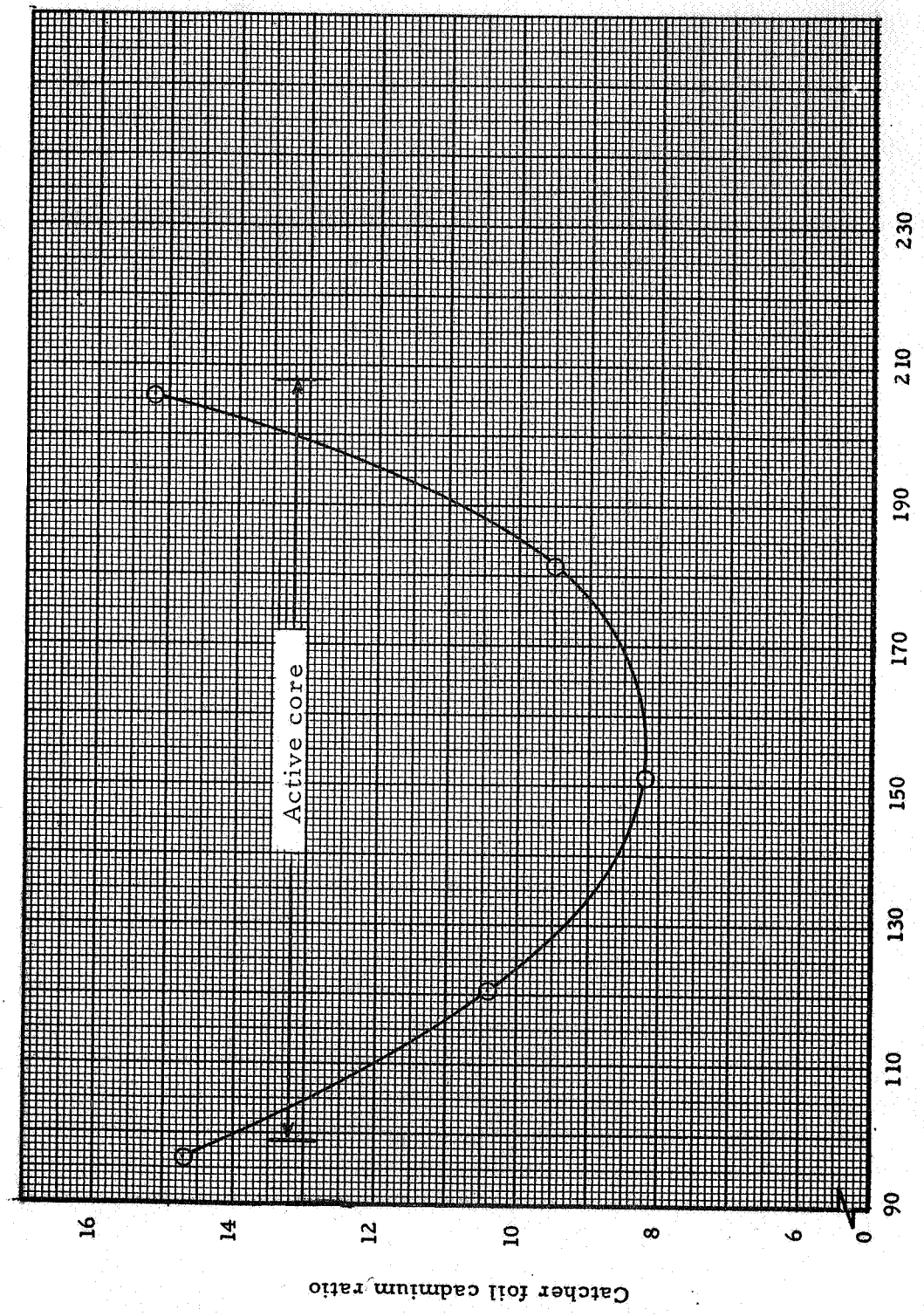


Fig. 7.15 Catcher foil cadmium ratio axial profile - Mockup No. 2, pure D_2O reflector

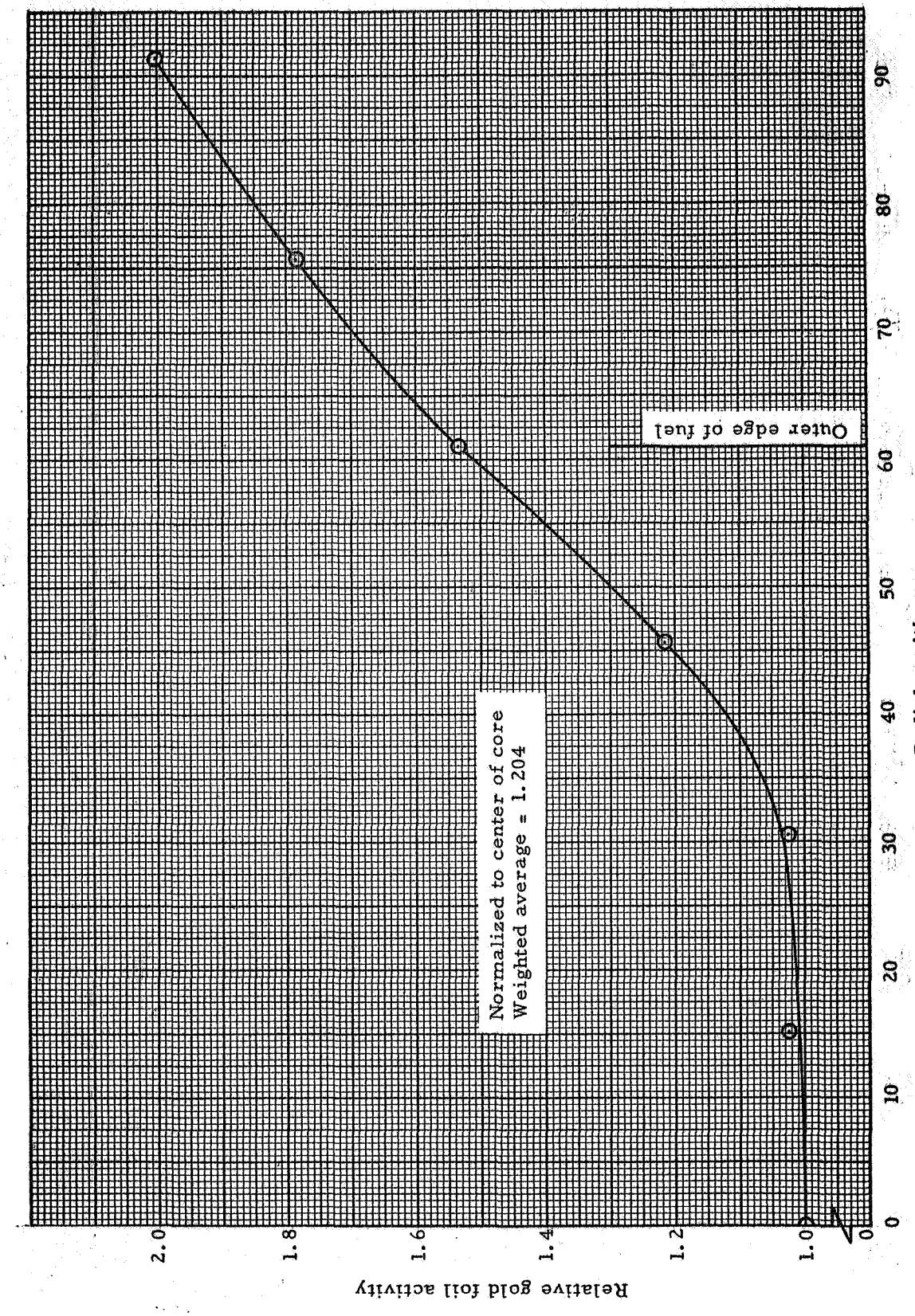


Fig. 7.16 Radial distribution of bare gold foil activity - Mockup No. 2, pure D_2O reflector

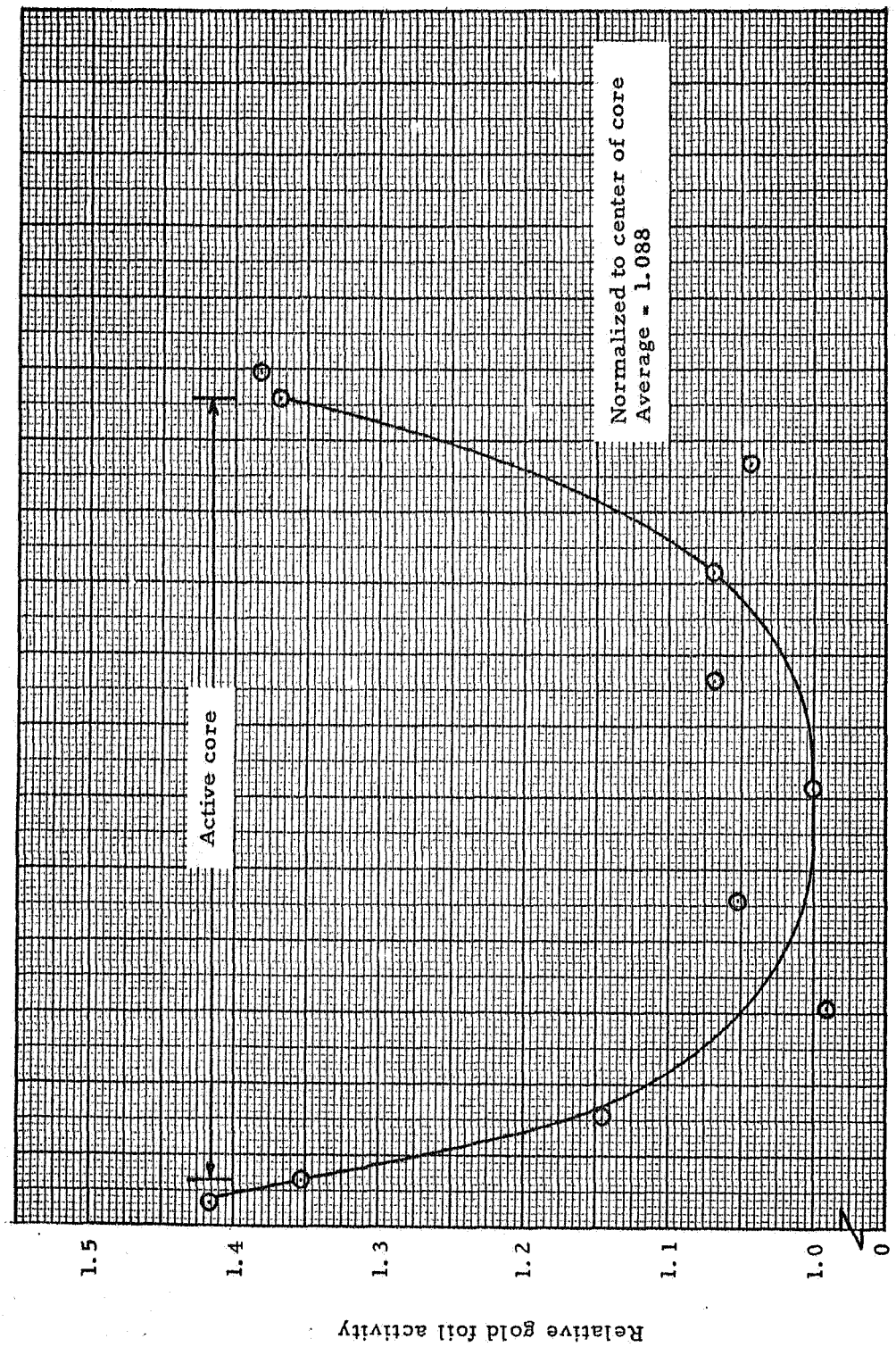


Fig. 7.17 Axial distribution of bare gold foil activity -Mockup No. 2, pure D_2O reflector

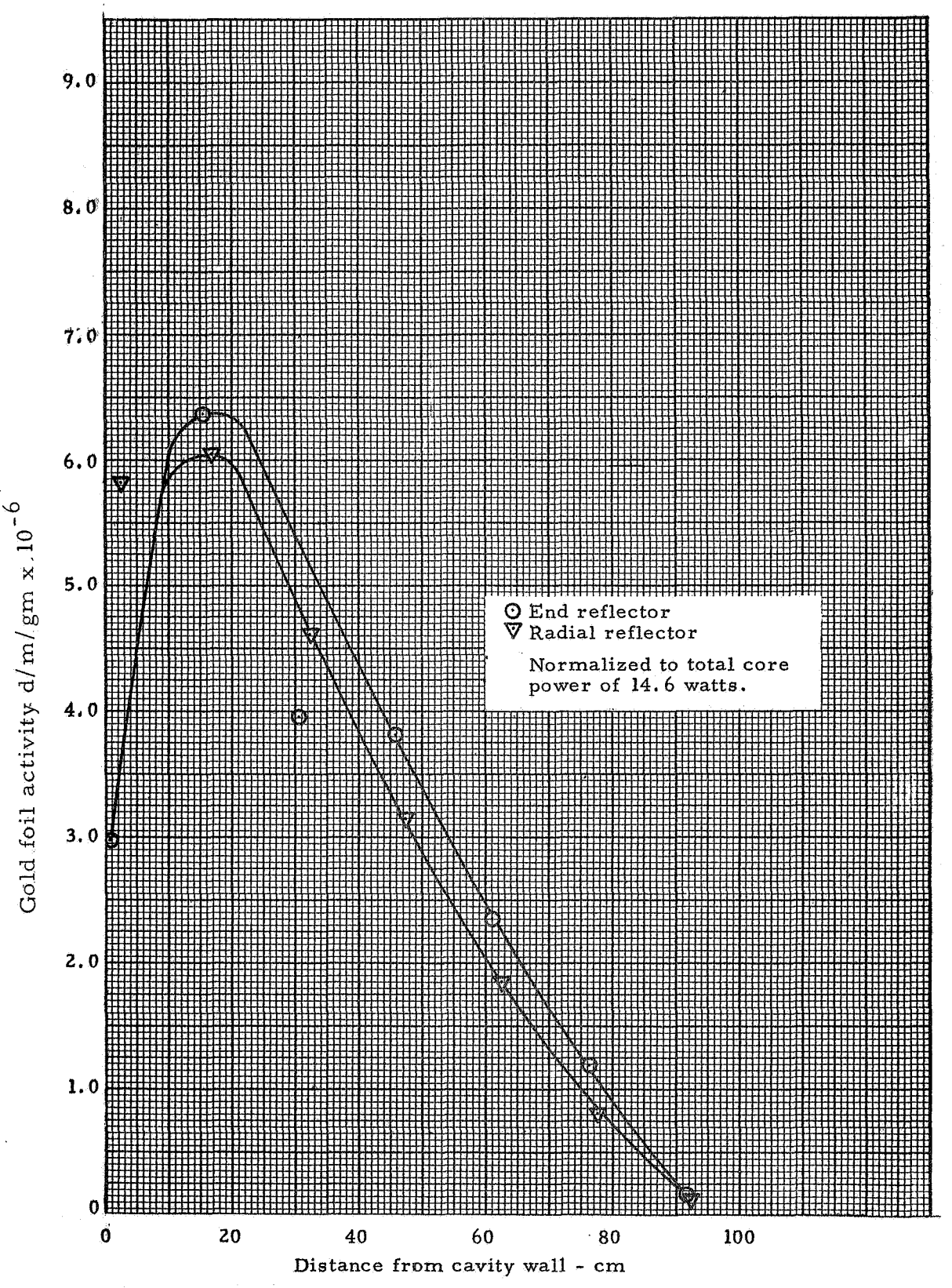


Fig. 7.18 Bare gold foil activity distribution in the reflectors Mockup No. 2, pure D_2O reflector

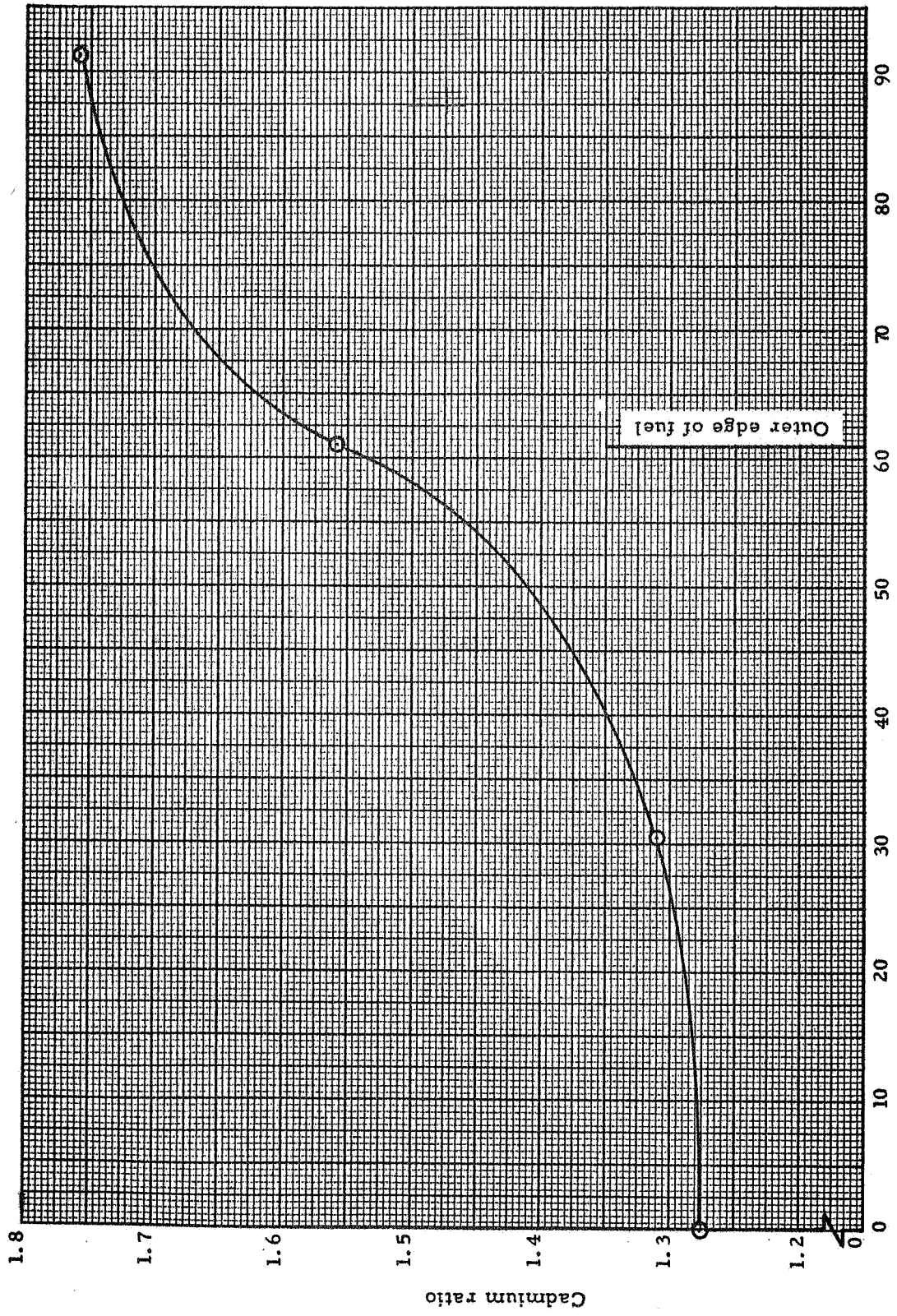


Fig. 7.19 Gold foil cadmium ratio radial profile - Mockup No. 2, pure D_2O reflector

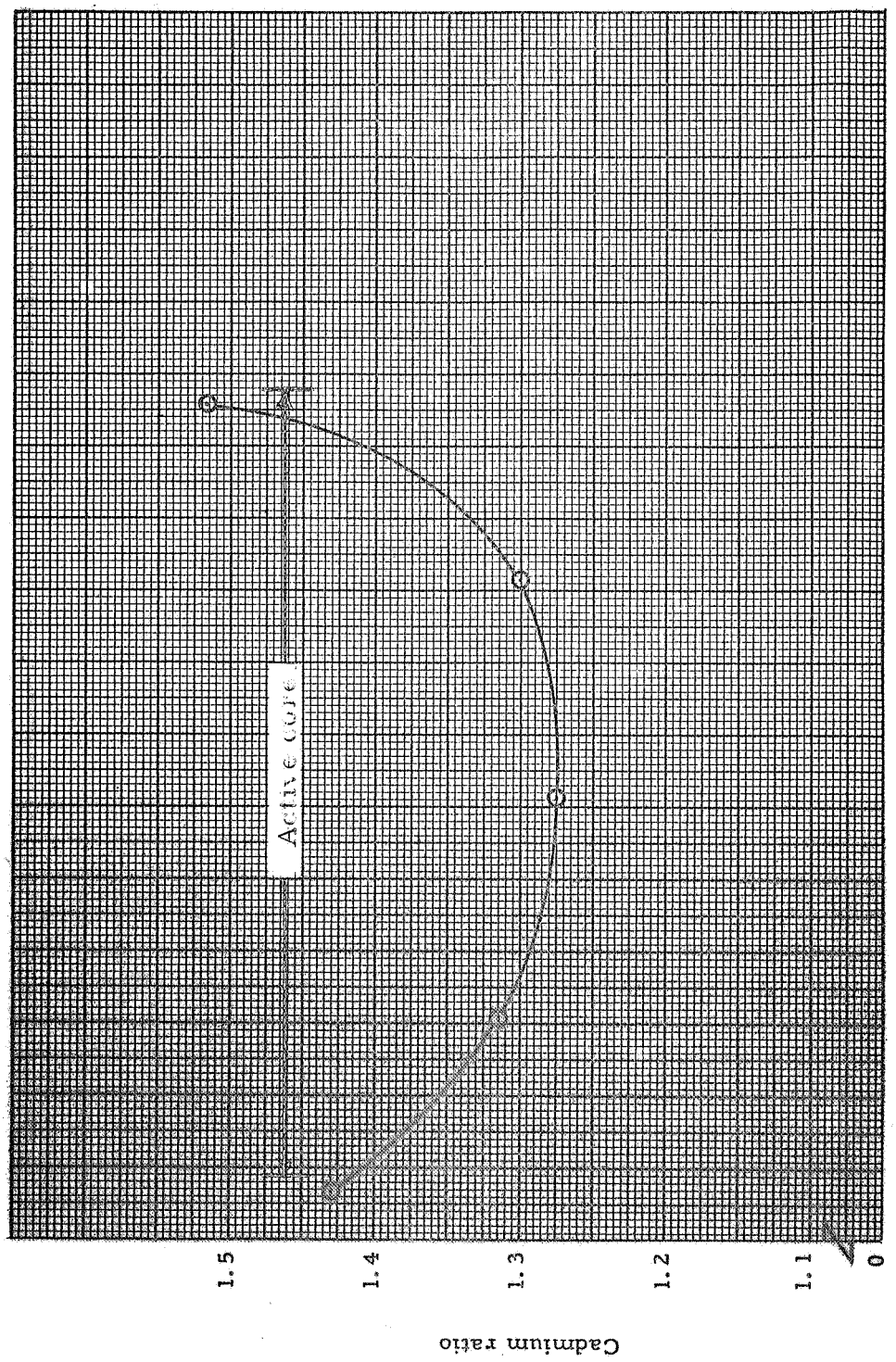


Fig. 7.20 Gold foil cadmium ratio axial profile - Mockup No. 2, pure D_2O reflector

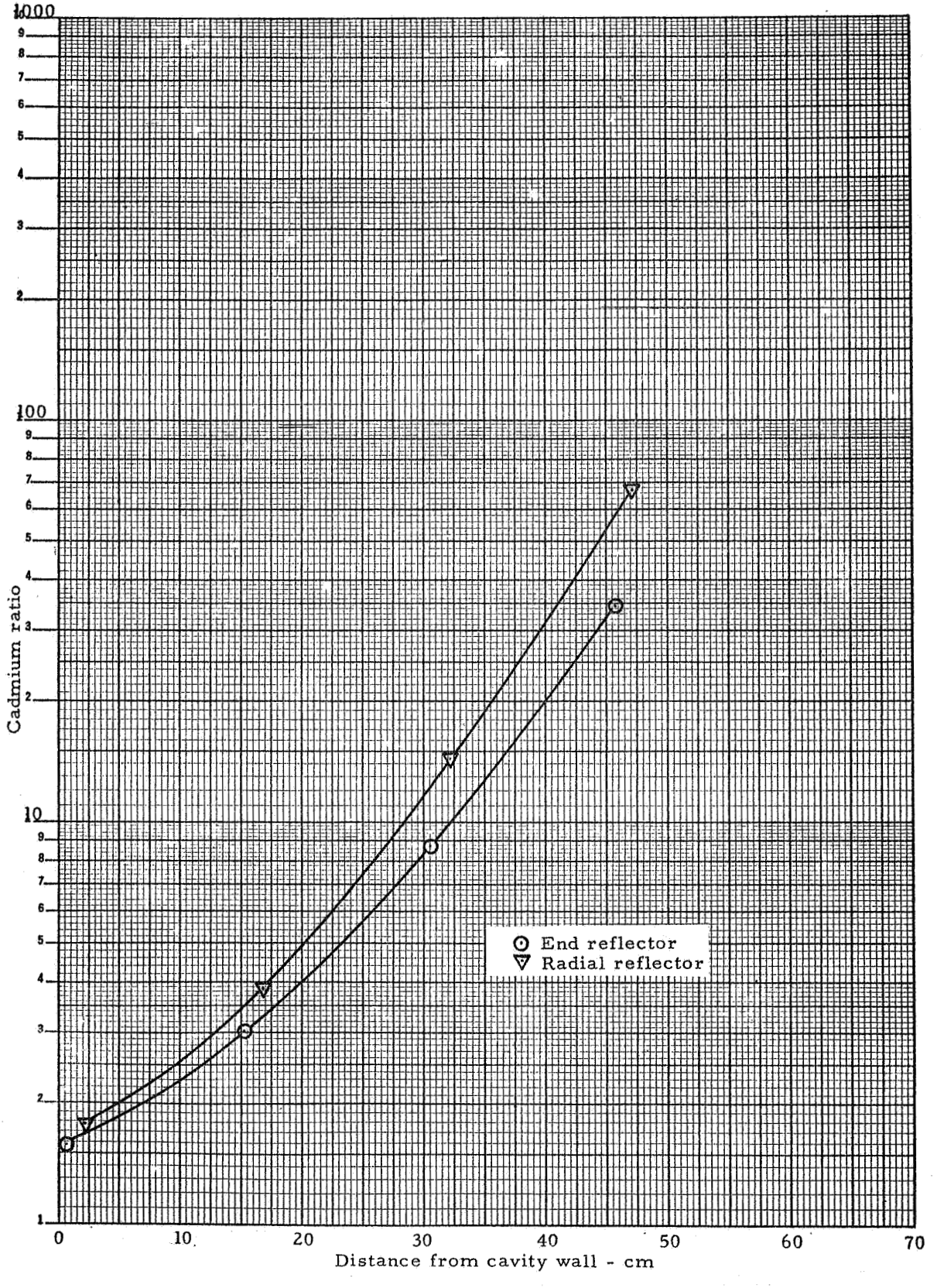


Fig. 7.21 Gold foil cadmium ratios in the radial and end reflectors Mockup No. 2, pure D_2O reflector

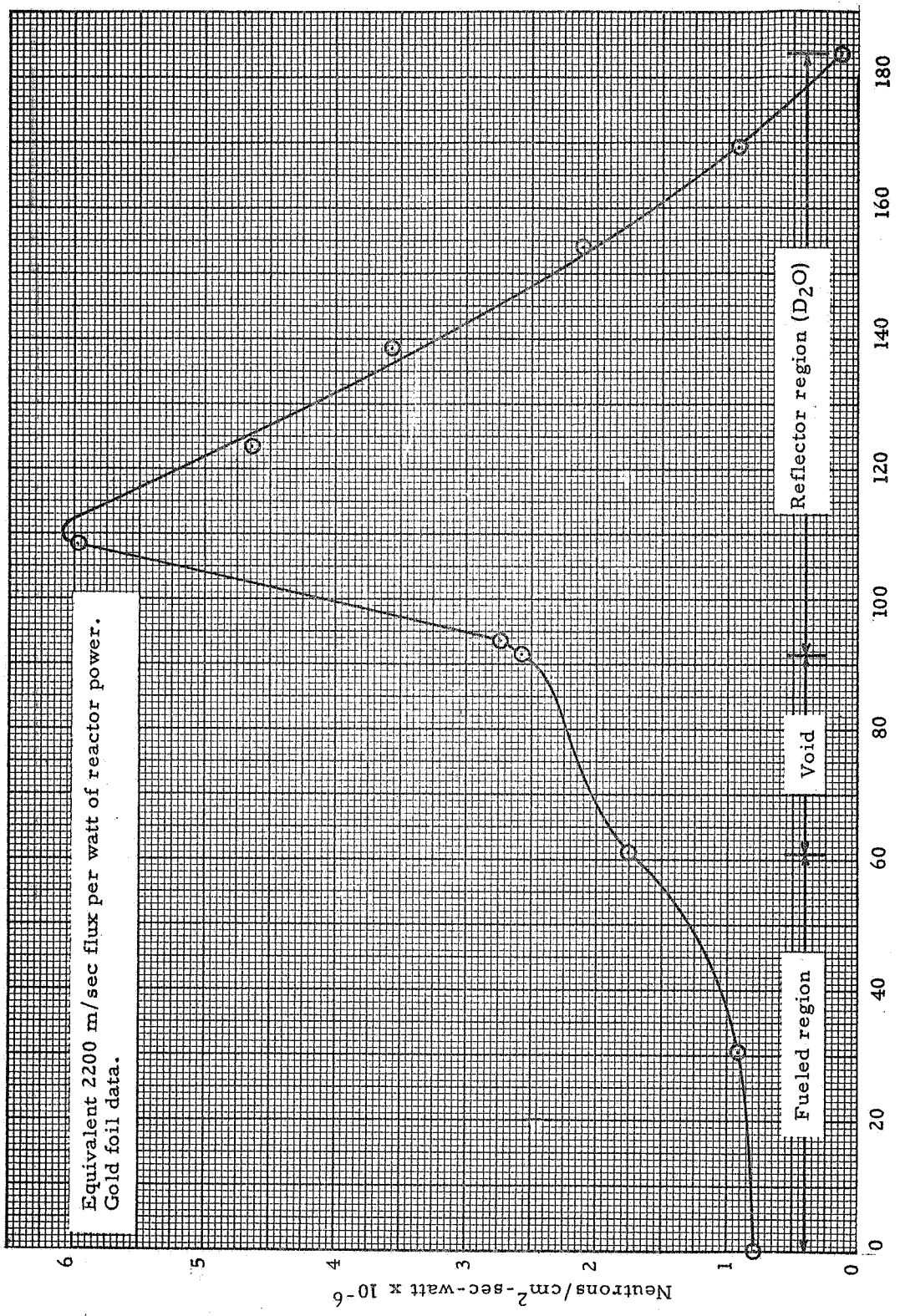


Fig. 7.22 Thermal neutron flux distribution radially through axial center of core Mockup No. 2, pure D_2O reflector

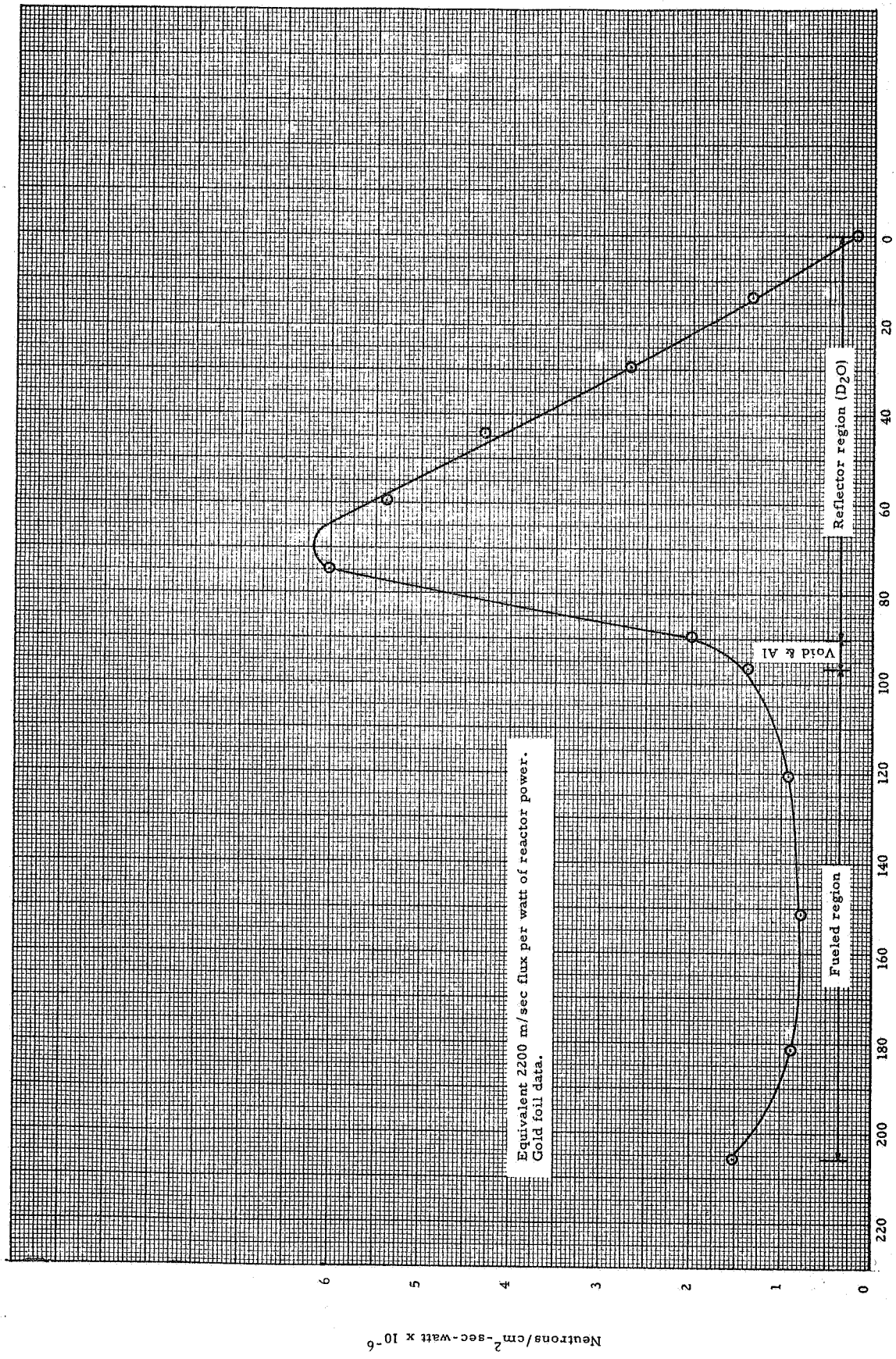


Fig. 7.23 Thermal neutron flux distribution axially through radial center of core Mockup No. 2, pure D_2O reflector

8.0 MOCKUP NO. 2 EXPERIMENT - D_2O AND Be REFLECTOR

Following the pure D_2O reflector experiment, the beryllium was again placed around the cavity at an average distance of 6.5 cm from the wet surface of the cavity wall and several types of measurements were obtained including material worths and power mapping.

8.1 Initial Loading

Prior to the addition of beryllium to the radial reflector the core contained 7930 sheets of fuel or a total fuel loading of 20.8 kg of uranium. The beryllium was added and sufficient elements removed to reduce the fuel loading to 6270 sheets of fuel (16.4 kg) and from this point the loading was incrementally increased to a critical assembly. With 50 sheets per fuel element and a total loading of 10,400 sheets (27.2 kg of uranium), the reactor was critical and k-excess was 0.563±0.012%Δk. The inverse multiplication data obtained for this fuel loading process are given in Table 8.1 and the average of the three channels is shown in Figure 8.1. The fuel element loading was increased from 40 to 50 sheets of fuel by filling in the stages which contained 2 sheets per stage (refer to Figure 7.4) and by adding a single sheet on top of each of the type 2 fuel orientation stages. The type of element in each of the 208 positions was the same as shown in Figure 7.5.

8.2 Reactivity Measurements

8.2.1 Rod Worths

Only one actuator was calibrated with this configuration and that was Actuator No. 6. Three separate measurements were made and the average rod worth was -(0.7085±0.0146)%Δk.

8.2.2 Material Worths

The worth of fuel was measured at five different radial locations within the active core region, the results of which are given in Table 8.2 and Figure 8.2. Each measurement was obtained from period differences thus eliminating any uncertainty associated with rod worths. A volume weighted average fuel worth of 0.712×10^{-3}%Δk/gm was obtained from the curve given in Figure 8.2 which is for a fuel loading of 27.2 kg of uranium. The estimated standard error for this fuel worth measurement is about 5%.

The worth of the beryllium can then be deduced by taking the average fuel worth between this assembly and the pure D_2O reflected mockup, multiplying by the total difference in fuel loading and correcting for the difference in k-excess. The calculation is as follows:

1.	k-excess difference	+0.332±0.013%Δk
2.	Be end plates and other hardware	+2.726±0.100%Δk
3.	Uranium difference -6.4kg x (0.908±0.085)%Δk/kg	-5.811±0.215%Δk
	Net	-2.752±0.237%Δk

This represents the decrease in reactivity due to placing 10.16 cm thickness of beryllium around the cavity at an average inner radius distance of 6.5 cm from the wet surface of the cavity wall in the D_2O radial reflector.

The critical mass for this reactor assembly corrected for the excess reactivity and extra aluminum in the core in the form of fuel elements and other aluminum core components is as follows:

1. k-excess (27.2 kg U) = 0.563%Δk

2. 159.94 kg Al in active core, 159.94/44.3 = 3.61 kg U

The correction for item 1 based on the above fuel worth amounts to 0.82 kg of uranium giving a total uranium correction of 4.43 kg. The corrected critical mass is, therefore, 22.8 kg. It will be noted that under item 2, above, the value of 44.3 kg of Al/kg of U was used to convert the aluminum to its equivalent in uranium. This value was obtained from an interpolation between the measured value of 51.0 kg of Al per kg of uranium reported in Section 7.2 for a fuel loading of 20.74 kg and a value measured for a configuration following this mockup experiment in which the result was 34.2 kg of aluminum per kg of uranium at a fuel loading of 37 kg of uranium. The 44.3 kg of Al/kg of U at a loading of 27.2 kg compares satisfactorily with the results of 40 kg of Al/kg of U measured on Mockup No. 1 at a loading of 28 kg.

8.3 Power Distribution

8.3.1 Bare Catcher Foils

Foil exposures were made with all but Actuator No. 6 withdrawn and Actuator No. 6 was pulled on the average, about 9 cm. The D_2O temperature was nominally 21°C.

Sufficient bare catcher foils were exposed within the cavity region to produce a radial power profile at the axial center of the core and an axial profile at the radial center of the core. These data are given in Table 8.3 and Figures 8.3 and 8.4. Table 8.3 also contains the cadmium covered catcher foil data. The radial power gives a peak power ratio at the outer edge of the fuel (on the axial midplane) with respect to the core center of 2.81, and the radial average to 61 cm (the outer edge of the fuel) was 1.592. The average axial power normalized to the core center was 1.232 with power levels of 2.14 and 2.09 with respect to the core center at the separation plane and back end of the core, respectively. All of the bare catcher foil data appear to have excellent consistency fitting a smooth curve with very little variance from the curve.

8.3.2 Cadmium Ratios

The catcher foil cadmium ratios within the cavity region are presented in Table 8.4 and Figures 8.5 and 8.6. At the core center the ratio is 6.4 and this increases to 14.7 at the outer radial edge of the fuel. The cavity wall shows a cadmium ratio of 23.3, at the axial center of the cavity. The ends of the core at the radial center of the reactor give

cadmium ratios of 12.9 and 11.9 for the separation plane and the back end of the core, respectively. The higher ratio at the separation plane is due to the 30.5 cm hole in the end reflector.

8.4 Gold Foil Data

8.4.1 Bare Gold

The gold foil data obtained from exposure of foils in the cavity and reflector regions are found in Table 8.5 and the bare foil results are shown graphically in Figures 8.7, 8.8 and 8.9. Both bare and cadmium covered foil results are given in Table 8.5. Figures 8.7 and 8.8 show the radial and axial distribution within the cavity normalized to the core center. The radial profile (Figure 8.7) shows the gold foil activity at the outer edge of the fuel (at the axial midplane) to be 1.64 times that at the core center and the volume weighted average calculated out to the edge of the fuel is 1.198. The axial distribution, given in Figure 8.8, has an average of 1.088 integrated over the active core region with respect to 1.0 at the core center. The axial profile shows the activation flux at the separation plane to be somewhat lower than at the other end of the reactor which is the opposite of that observed from the catcher foils. Both sets of foils were exposed at the same locations and on the same foil exposure run so the differences cannot be attributed to any error in foil position. No obvious reason can be given for this difference between the catcher foil and gold profiles.

The distribution of bare gold foil activity within the reflector regions, as shown in Figure 8.9 appears to be perfectly normal with respect to other results from similar configurations. The presence of beryllium in the radial reflector coupled with the required heavier fuel loading of the core caused the activation flux in the end reflector to be enhanced, thus giving a considerable difference between the two reflector regions. Based on previous cavity reactor assemblies, this is primarily due to the change in fuel loading and the close proximity of the end reflector to the active core.

8.4.2 Cadmium Ratios

The cadmium ratios for this reactor are given in Table 8.6 and Figures 8.10, 8.11 and 8.12. The corrected cadmium ratios were obtained by calculating the infinitely dilute foil activity as discussed under Section 4.4.2. At the center of the core, the cadmium ratio was 1.17 and this increased to 1.48 and 1.58 at the outer edge of the fuel and at the cavity wall, respectively. These data are along the axial center of the reactor. The ends of the active core at the radial center of the reactor show cadmium ratios of 1.39 and 1.33, with the ratio at separation plane being the highest.

The data obtained in the reflector regions give very consistent results with the radial reflector giving a softer spectrum than the end reflector as shown in Figure 8.12. This difference between the two reflector regions is normal for the amount of uranium in the reactor.

8.5 Thermal Neutron Flux Distribution

The thermal neutron flux was calculated at each foil position where both bare and cadmium covered foil data were available. Extrapolated cadmium foil activities were used to obtain the flux values beyond about 50 cm in the reflector regions. The flux values thus calculated are presented in Table 8.7 and Figures 8.13 and 8.14. These data appear to be normal in every respect and fit a smooth curve very well.

TABLE 8.1

Initial Loading of Mockup No. 2 After Inserting Beryllium in Radial Reflector

Increment	Number Fuel Sheets in Reactor	Channel 1 CPM	Channel 1 CRo/CR	Channel 2 CPM	Channel 2 CRo/CR	Channel 3 CPM	Channel 3 CRo/CR	Average CRo/CR	Rod Positions
adjusted CRo	6270	1674		1991		1420			In
adjusted CRo	6270	1926		2312		1613			Out
base loading	6270	11325	.148	11531	.173	9004	.159	.159	In
	6270	17744	.109	17546	.132	13880	.116	.116	Out
1	7915	18641	.0898	18566	.1072	14724	.0964	.0978	In
1	7915	38178	.0504	38157	.0606	29756	.0542	.0551	Out
2	8510	22664	.0739	24596	.0809	17658	.0804	.0784	In
2	8510	57635	.0334	61583	.0375	43478	.0371	.0360	Out
3	9380	30025	.0558	31648	.0629	23105	.0615	.0601	In
3	9380	122452	.0157	126807	.0182	88944	.0182	.0175	Out
4	9900	36677	.0456	38896	.0512	28363	.0501	.0490	In
4	9900	415504	.0046	414914	.0059	280352	.0058	.0054	Out
5	10400	47309	.0354	50396	.0395	37475	.0379	.0376	In
5	10400	Critical with Actuator No. 6 at 823							

TABLE 8.2

Fuel Worth Measurements Mockup No. 2 - Be in Radial Reflector

Radial Position (cm)	Reactivity Difference (%Δk) (2)	Fuel Mass (1) Difference (gm)	Fuel Worth per gram (%Δk) (2) x 10^3
11.2	0.0679	153.3	0.443
30.8	0.0759	154.6	0.491
45.9	0.1042	154.6	0.674
55.2	0.1364	154.6	0.882
59.5	0.1809	153.3	1.180

(1) Uncleaned fuel sheets assumed to weigh 2.62 gm each.
(2) Estimated standard deviation is ±2%.

TABLE 8.3

Catcher Foil Data

Mockup No. 2 - Be in Radial Reflector

Foil Number	Type	Location Radial (cm)	Location Axial (cm)	Normalized Counts	Ratio of Local to Core Center (Foil No. (X))
Run 1081					
1	Bare	0	93.3	79404	2.490
2	Bare	0	96.5	66544	2.087
3	Bare	0	105.3	48327	1.516
4	Bare	0	120.6	37019	1.161
5	Bare	0	135.8	33110	1.038
6	Bare	0	151.1	31884	1.000 (X)
7	Bare	0	166.3	33023	1.036
8	Bare	0	181.5	34679	1.088
9	Bare	0	196.8	47614	1.493
10	Bare	0	205.8	68271	2.140
11	Bare	0	209.5	76004	2.383
12	Bare	15.2	151.1	33173	1.040
13	Bare	30.5	151.1	34293	1.075
14	Bare	45.7	151.1	50361	1.579
15	Bare	61.0	151.1	89512	2.807
16	Bare	76.2	151.1	114039	3.576
17	Bare	91.4	151.1	128021	4.015
Run 1083					
1	Cd cov.	0	96.5	5602	
2	Cd cov.	0	120.6	5030	
3	Cd cov	0	151.1	4952	
4	Cd cov	0	181.5	5116	
5	Cd cov.	0	205.8	5282	
6	Cd cov.	30.5	151.1	6125	
7	Cd cov.	61.0	151.1	6076	
8	Cd cov.	91.4	151.1	5496	

TABLE 8.4

Catcher Foil Cadmium Ratios Mockup No. 2 - Be in Radial Reflector

Location		Normalized Counts		Cadmium Ratio
Radial (cm)	Axial (cm)	Bare Foil	Cd Covered Foil	
0	96.5	66544	5602	11.88
0	120.6	37019	5030	7.35
0	151.1	31884	4952	6.44
0	181.5	34679	5116	6.78
0	205.8	68271	5282	12.93
30.5	151.1	34293	6125	5.60
61.0	151.1	89512	6076	14.73
91.4	151.1	128021	5496	23.29

TABLE 8.5

Gold Foil Data

Mockup No. 2 - Be in Radial Reflector

Foil No.	Type	Location		Foil Weight (gm)	Specific Activity d/m/gm x 10^{-6}
		Radial (cm)	Axial (cm)		
Run 1081					
31	Bare	0	0	0.0420	0.230
30	Bare	0	13.9	0.0380	1.570
29	Bare	0	29.1	0.04177	3.108
28	Bare	0	44.4	0.0356	5.021
27	Bare	0	59.6	0.0361	6.958
26	Bare	0	74.9	0.0376	8.004
25	Bare	0	89.4	0.0360	3.624
1	Bare	0	93.3	0.0343	3.109
2	Bare	0	96.5	0.0335	2.947
3	Bare	0	105.3	0.0341	2.513
4	Bare	0	120.6	0.0384	2.125
5	Bare	0	135.8	0.0338	2.138
6	Bare	0	151.1	0.0376	2.045
7	Bare	0	166.3	0.035415	2.071
8	Bare	0	181.5	0.0358	2.135
9	Bare	0	196.8	0.0384	2.319
10	Bare	0	205.8	0.0417	2.717
11	Bare	0	209.5	0.0414	2.917
12	Bare	15.2	151.1	0.03657	2.120
13	Bare	30.5	151.1	0.0400	2.086
14	Bare	45.7	151.1	0.040445	2.408
15	Bare	61.0	151.1	0.0402	3.352
16	Bare	76.2	151.1	0.0399	3.811
17	Bare	91,4	151.1	0.0357	4.204
18	Bare	93.2	151.1	0.0392	4.796
19	Bare	107.7	151.1	0.0414	6.103
20	Bare	123.0	151.1	0.0411	4.800
21	Bare	138.2	151.1	0.0368	3.228
22	Bare	153.5	151.1	0.0390	2.037
23	Bare	168.7	151.1	0.0379	1.086
24	Bare	183.9	151.1	0.0367	0.306
Run 1082					
2	Cd cov.	0	59.6	0.0330	1.749
1	Cd cov.	0	89.4	0.0335	0.353
3	Cd cov.	0	96.5	0.0415	1.544
4	Cd cov.	0	120.6	0.0354	1.500
5	Cd cov.	0	151.1	0.0408	1.398

TABLE 8.5
(Continued)

Foil No.	Type	Location Radial (cm)	Location Axial (cm)	Foil Weight (gm)	Specific Activity $d/m/gm \times 10^{-6}$
Run 1082 (Cont'd)					
6	Cd cov.	0	181.5	0.0325	1.496
7	Cd cov.	0	205.8	0.0319	1.540
8	Cd cov.	30.5	151.1	0.0425	1.355
9	Cd cov.	61.0	151.1	0.0475	1.433
10	Cd cov.	91.4	151.1	0.0307	1.894
11	Cd cov.	93.2	151.1	0.0333	1.967
12	Cd cov.	123.0	151.1	0.03217	0.130
Run 1083					
1	Cd cov.	107.7	151.1	0.033845	0.710
2	Cd cov.	138.2	151.1	0.033515	0.018
3	Cd cov.	0	74.9	0.0318	1.391
4	Cd cov.	0	44.4	0.0421	0.0456

TABLE 8.6

Gold Foil Cadmium Ratios Mockup No. 2 - Be and D_2O Reflector

Location		Bare Foil Activity	Cd Foil Activity	Cadmium	Corrected Cadmium
Radial (cm)	Axial (cm)	d/m/gm x 10^{-6}	d/m/gm x 10^{-6}	Ratio	Ratio
0	44.4	5.021	0.0456	110.1	44.4
0	59.6	6.958	0.353	19.7	10.2
0	74.9	8.004	1.391	5.75	3.15
0	89.4	3.624	1.749	2.07	1.49
0	96.5	2.947	1.544	1.91	1.33
0	120.6	2.125	1.500	1.42	1.19
0	151.1	2.045	1.398	1.46	1.17
0	181.5	2.135	1.496	1.43	1.21
0	205.8	2.717	1.540	1.76	1.39
30.5	151.1	2.086	1.355	1.54	1.20
61.0	151.1	3.352	1.433	2.34	1.48
91.4	151.1	4.204	1.894	2.22	1.58
93.2	151.1	4.796	1.967	2.44	1.66
107.7	151.1	6.103	0.710	8.60	4.35
123.0	151.1	4.800	0.130	36.9	17.0
138.2	151.1	3.226	0.018	179.2	79.0

TABLE 8.7

Thermal Neutron Flux Mockup No. 2 - Be and D_2O Reflector

Location		
Radial (cm)	Axial (cm)	$n/cm^2/sec/watt \times 10^{-6}$
0	0	0.199
0	13.9	1.361
0	29.1	2.690
0	44.4	4.315
0	59.6	5.731
0	74.9	5.818
0	89.4	2.847
0	96.5	1.094
0	120.6	0.585
0	151.1	0.520
0	181.5	0.604
0	205.8	1.161
30.5	151.1	0.604
61.0	151.1	1.574
91.4	151.1	2.102
93.2	151.1	2.565
107.7	151.1	4.729
123.0	151.1	4.063
138.2	151.1	2.784
153.5	151.1	1.765
168.7	151.1	0.942
183.9	151.1	0.265

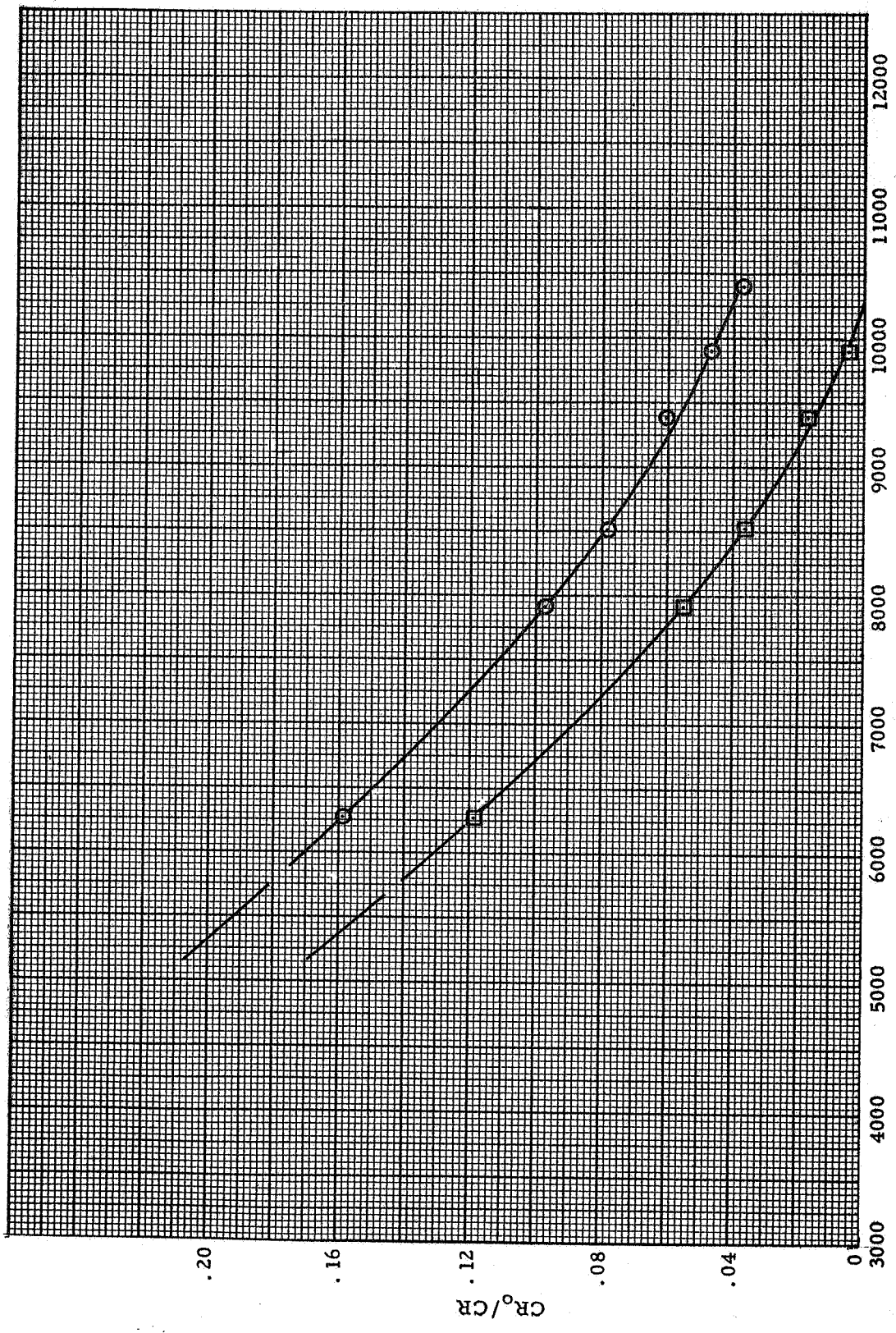


Fig. 8.1 Inverse multiplication curve - average of three channels - Mockup No. 2

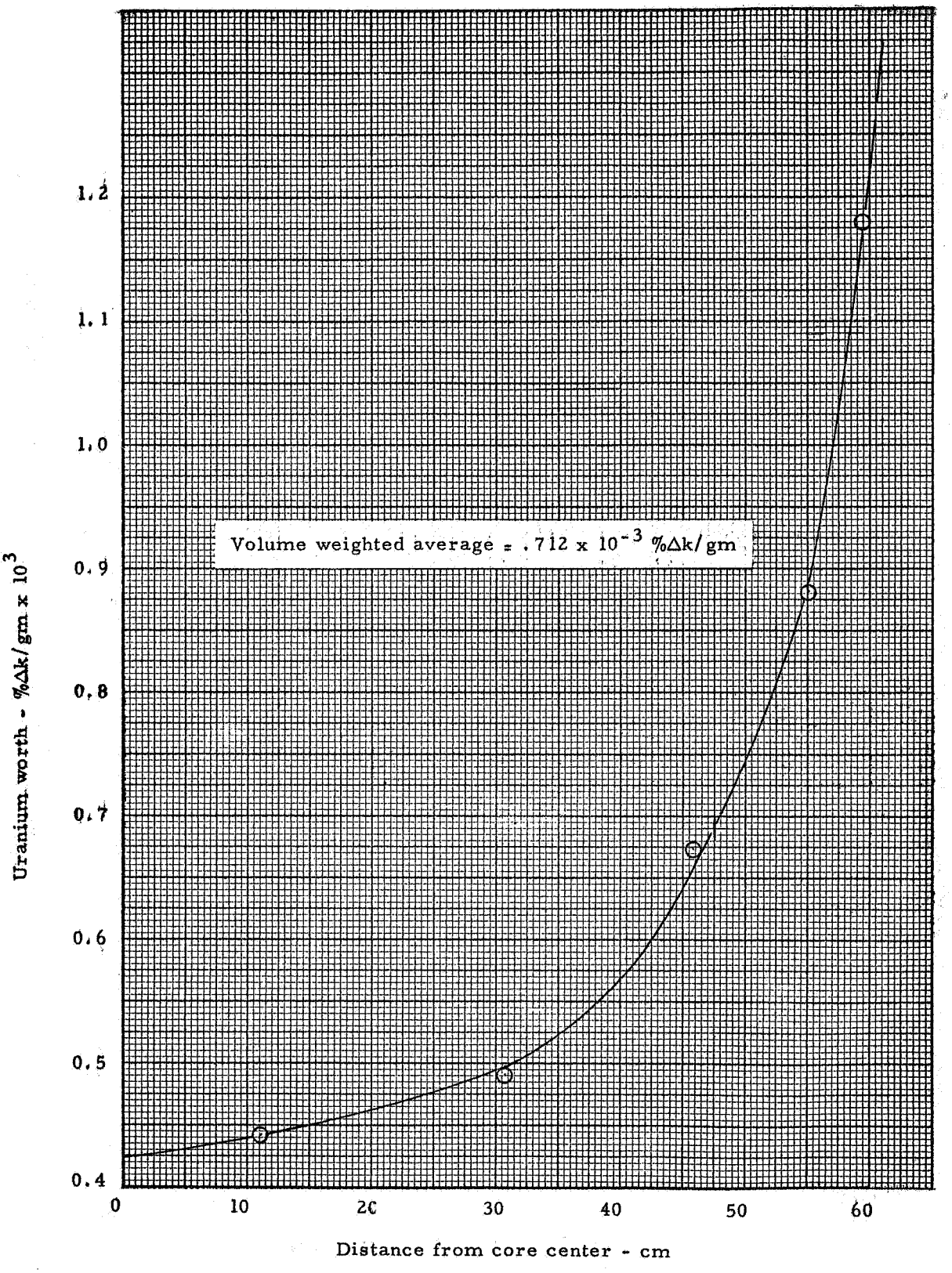


Fig. 8.2 Uranium worth within the active core - Mockup No. 2

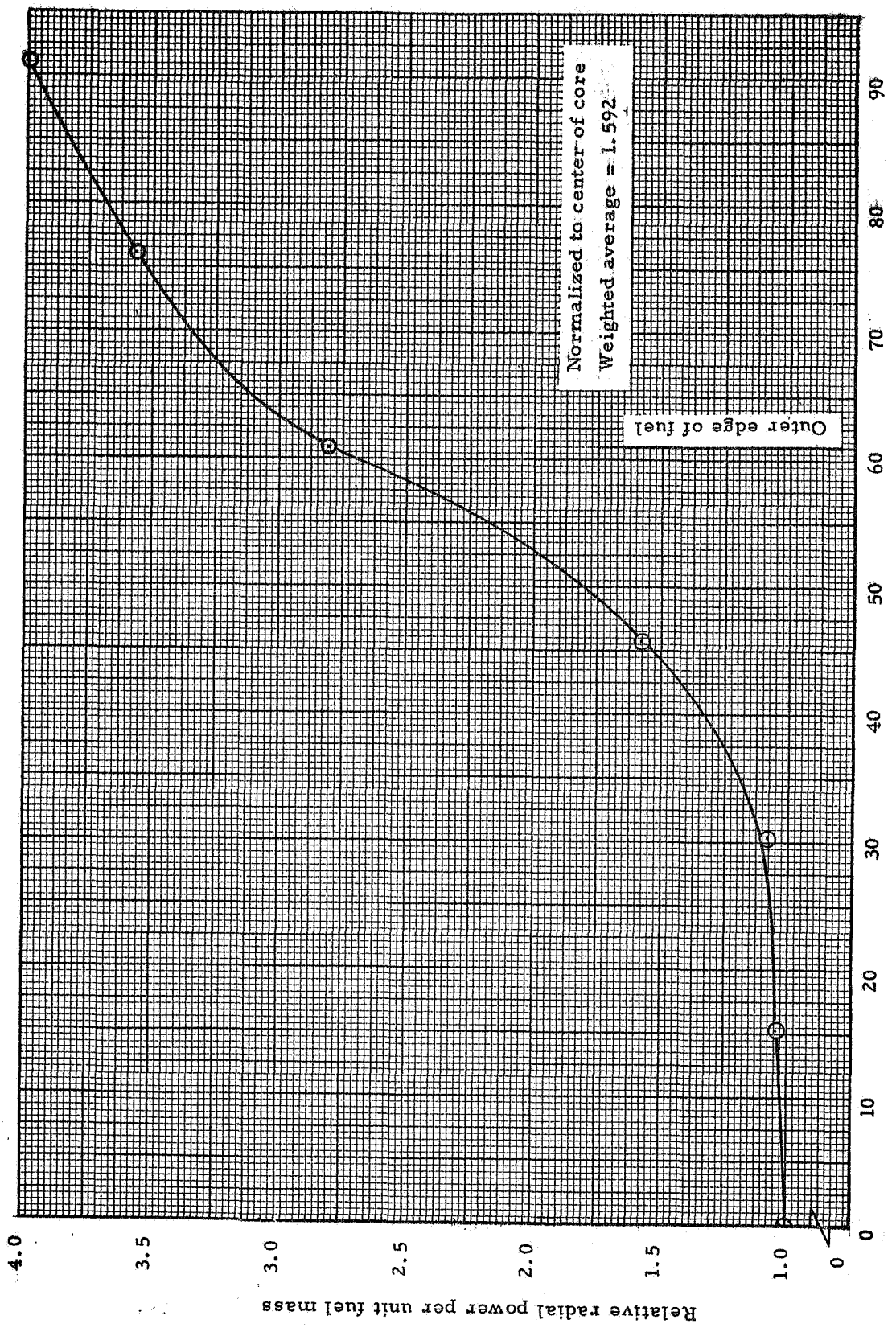


Fig. 8.3 Radial power distribution from bare catcher foils - Mockup No. 2

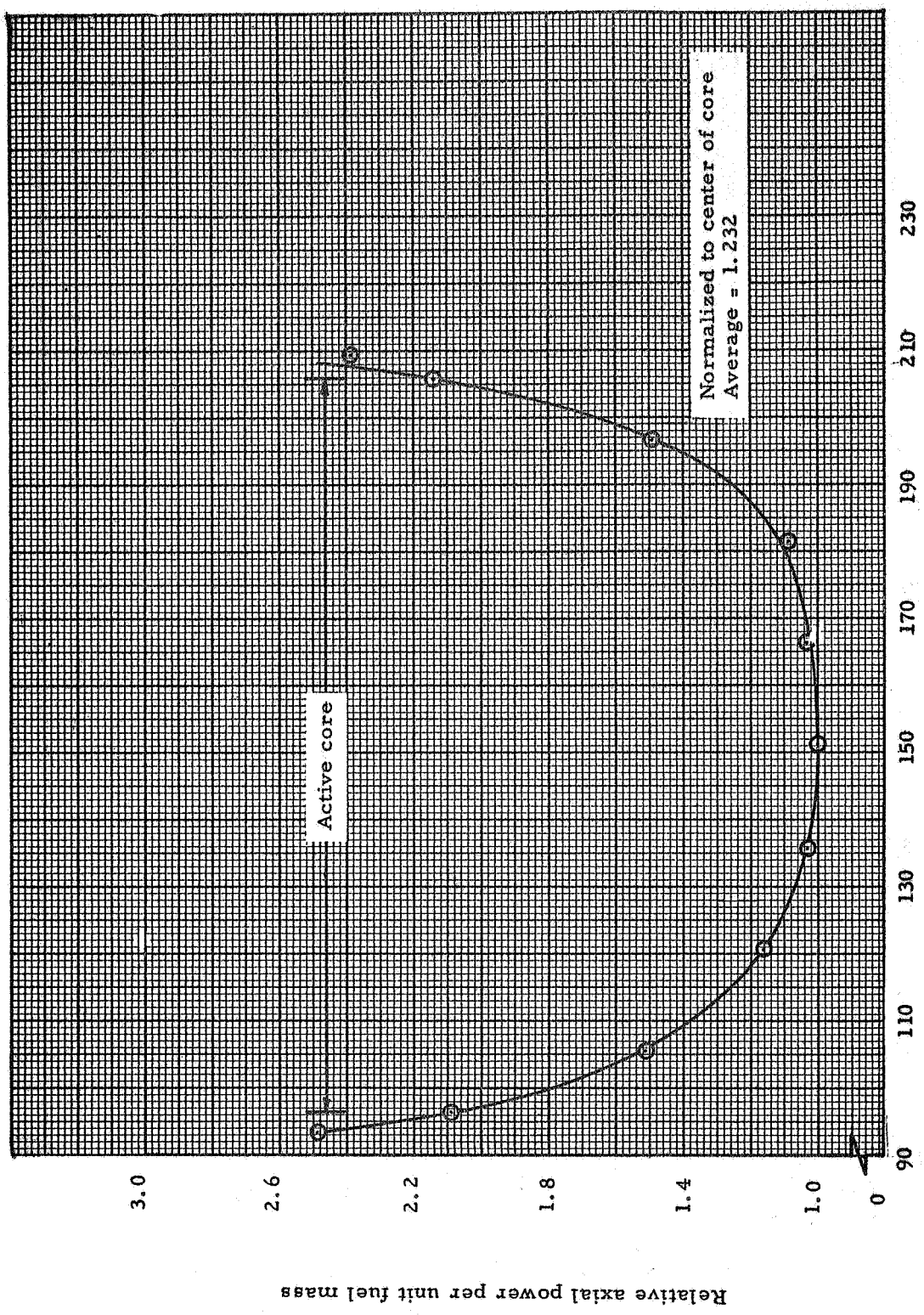


Fig. 8.4 Axial power distribution from bare catcher foils - Mockup No. 2

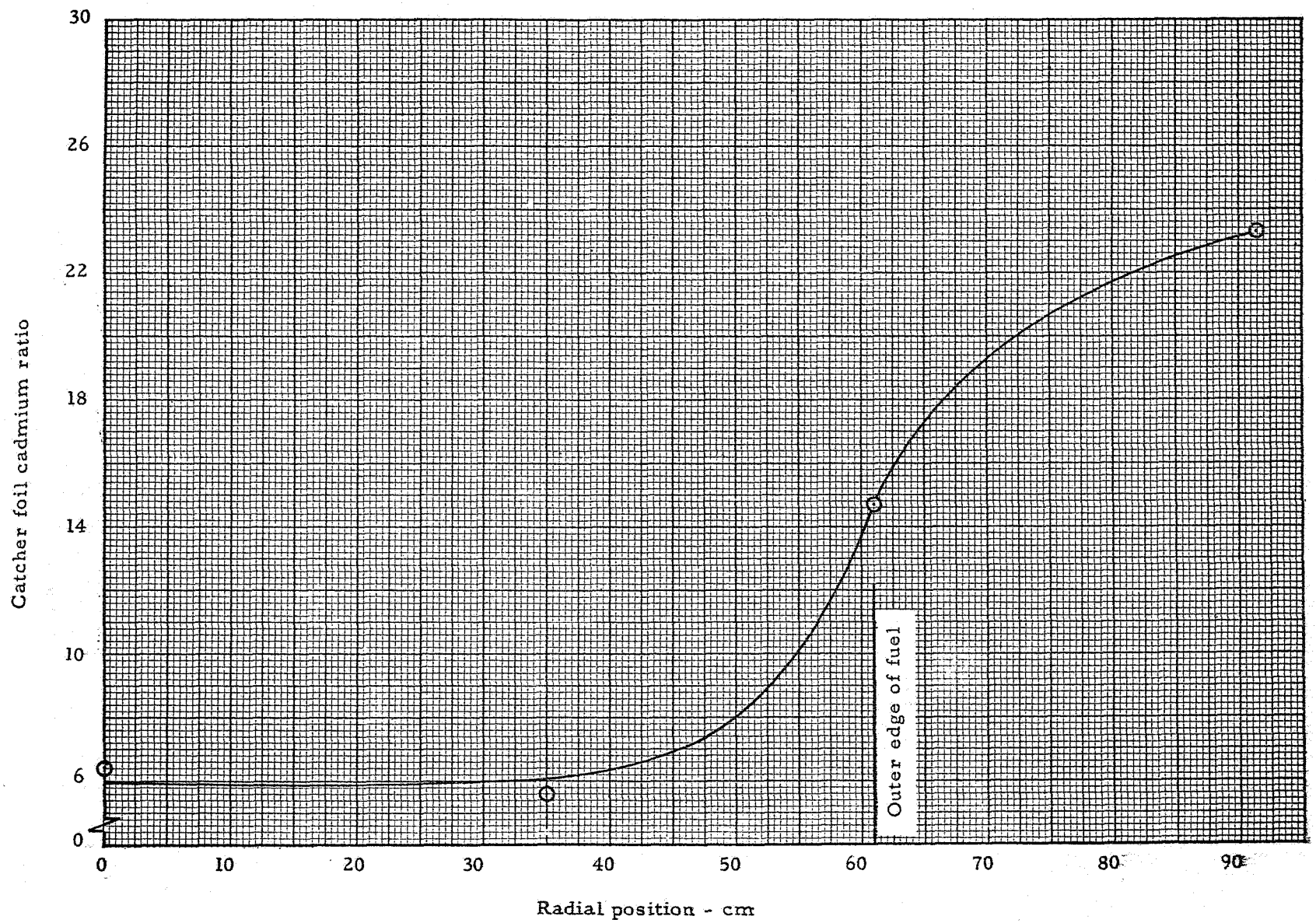


Fig. 8.5 Catcher foil cadmium ratio radial profile - Mockup No. 2, Beryllium in D_2O reflector

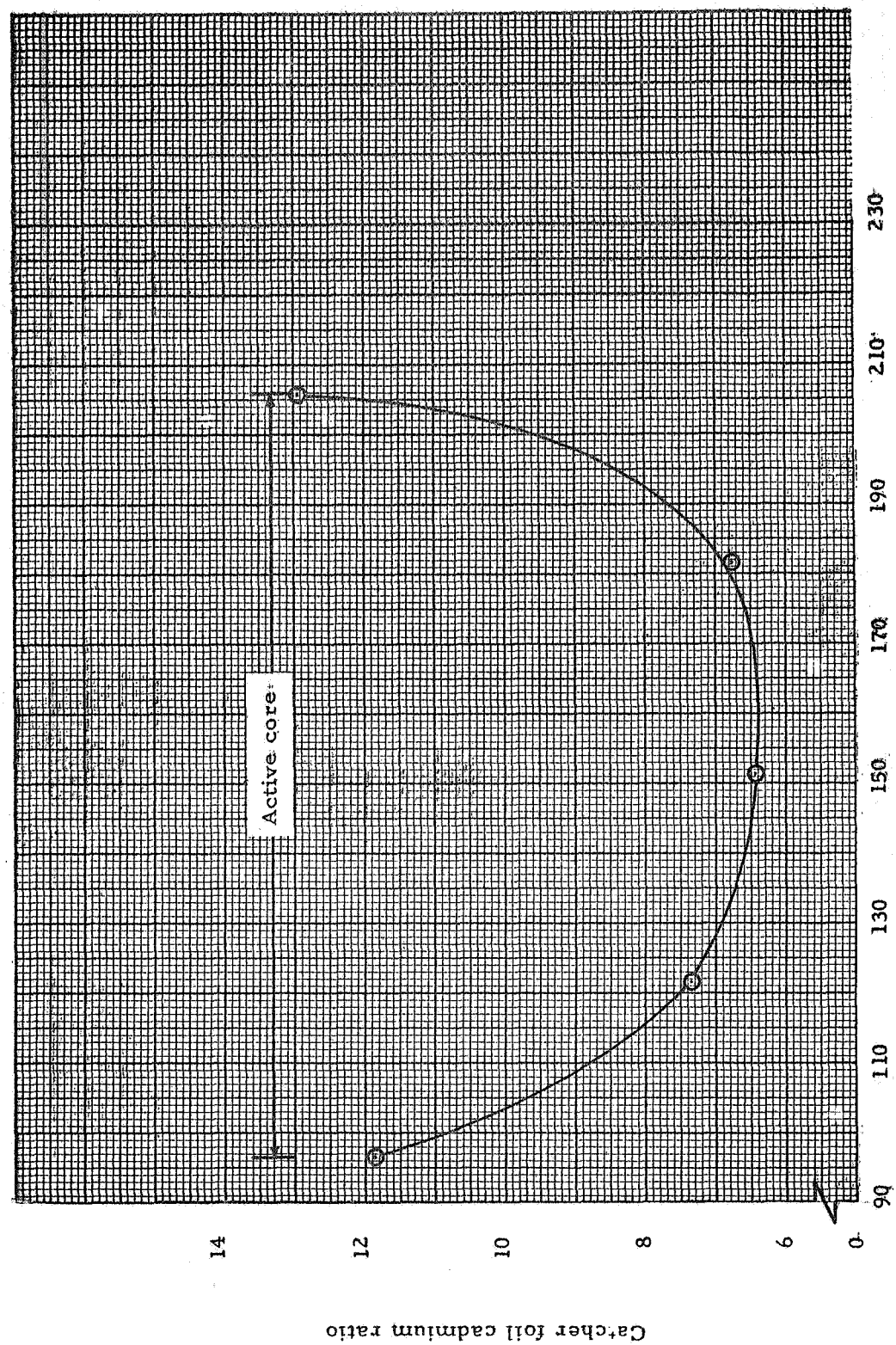


Fig. 8.6 Catcher foil cadmium ratio axial profile - Mockup No. 2, Beryllium in D_2O reflector

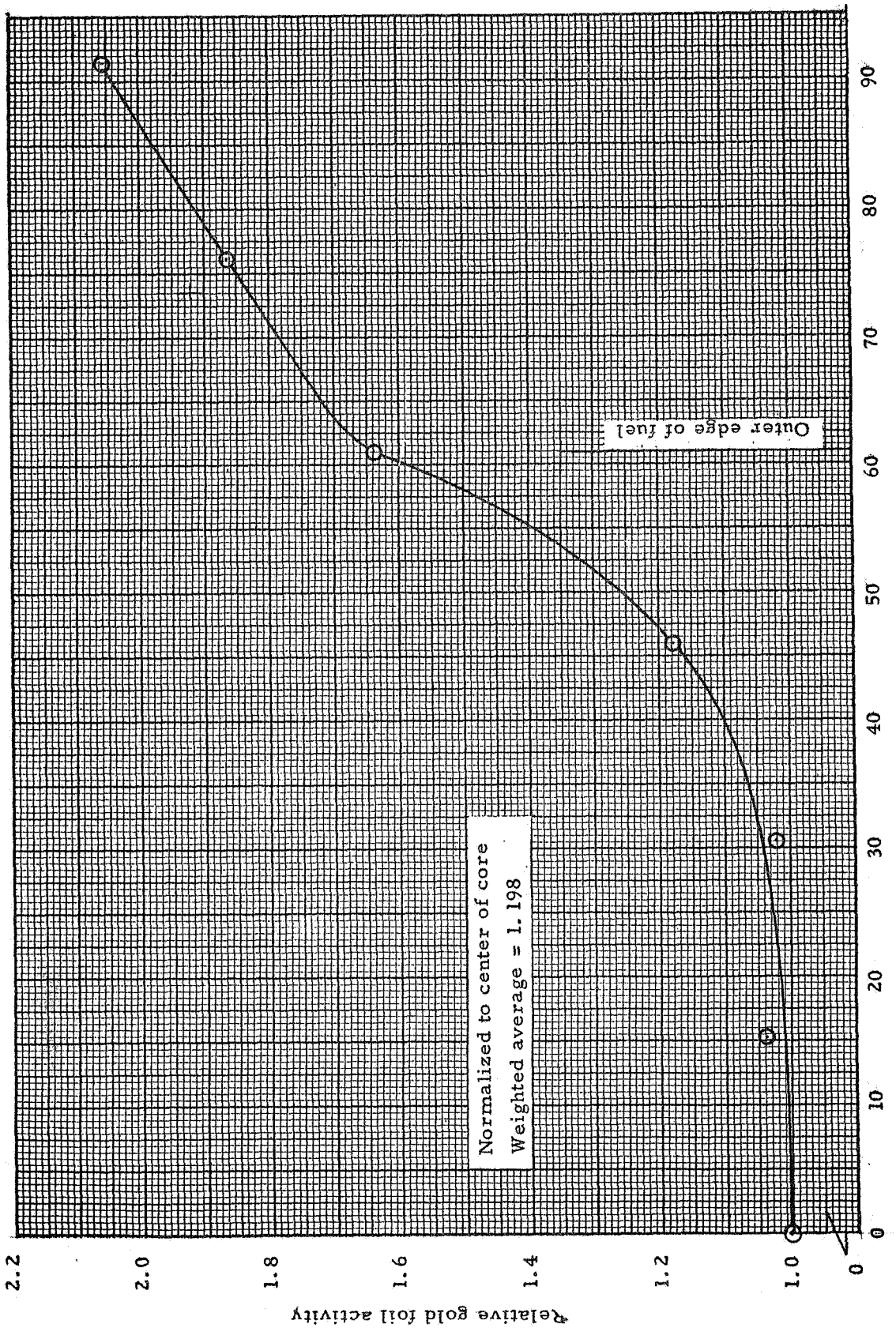


Fig. 8.7 Radial distribution of bare gold foil activity - Mockup No. 2, Beryllium in D_2O reflector

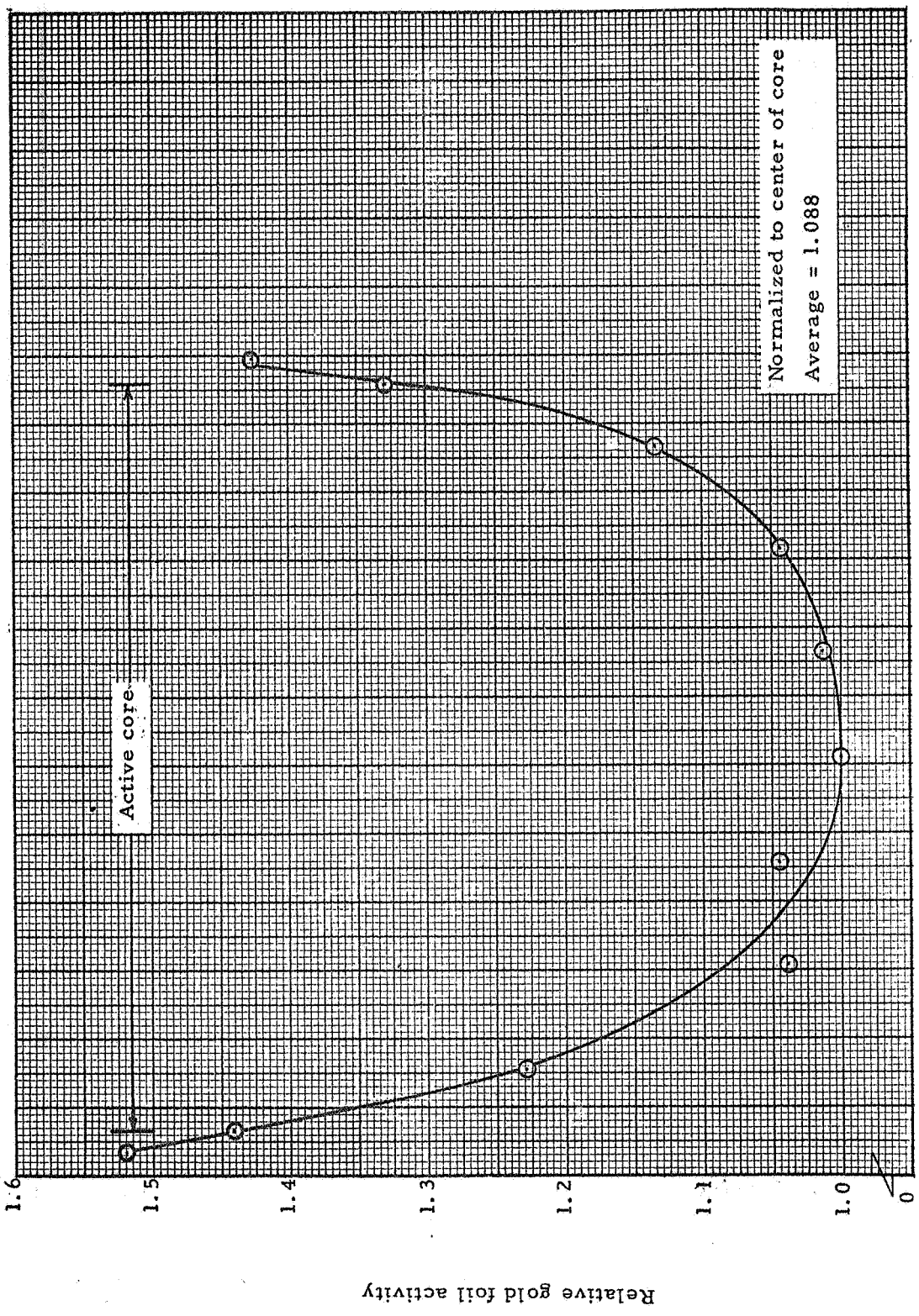


Fig. 8.8 Axial distribution of bare gold foil activity - Mockup No. 2, Beryllium in D_2O reflector

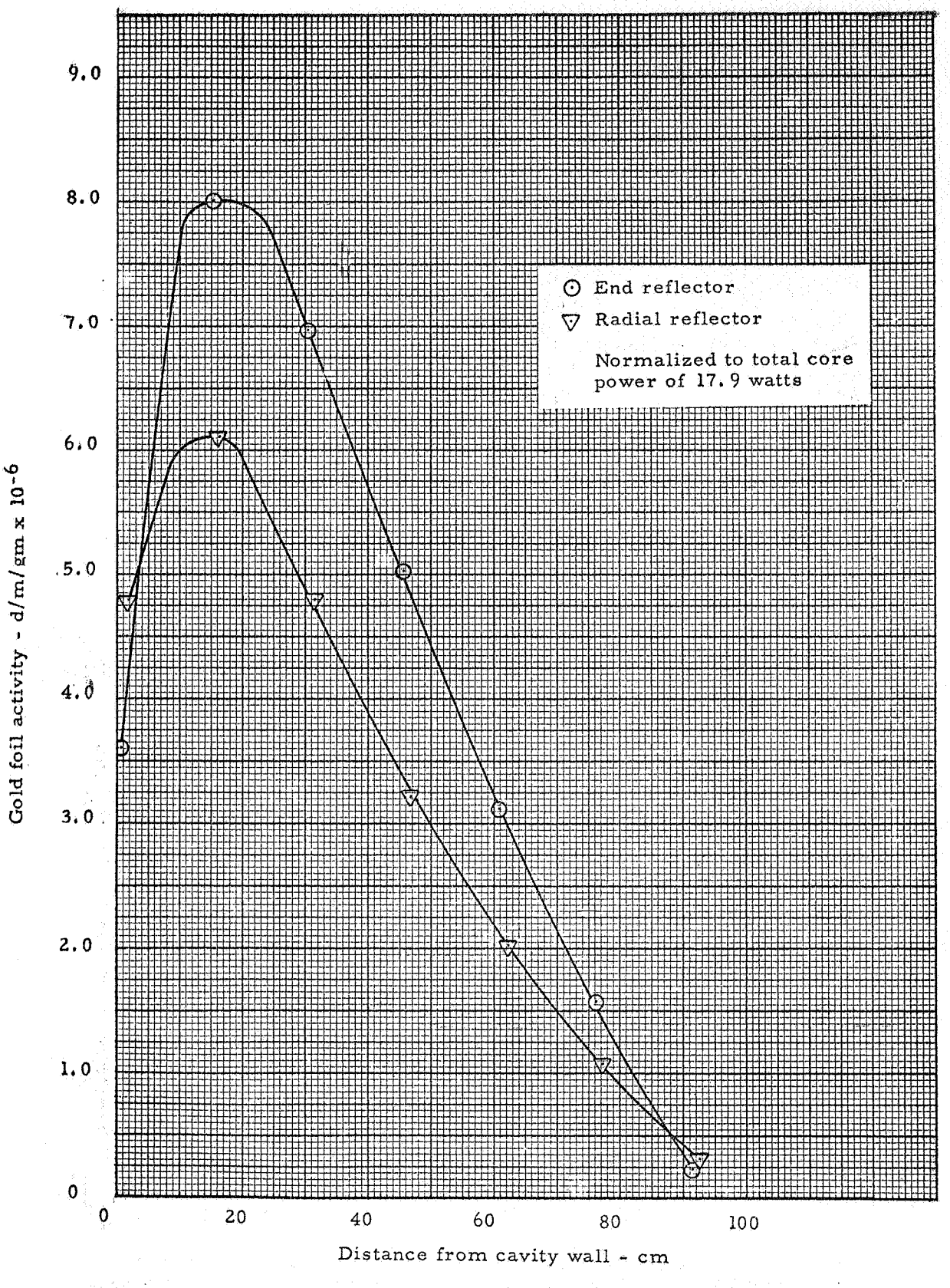


Fig. 8.9 Bare gold foil activity distribution in the reflectors Mockup No. 2, Beryllium in D_2O reflector

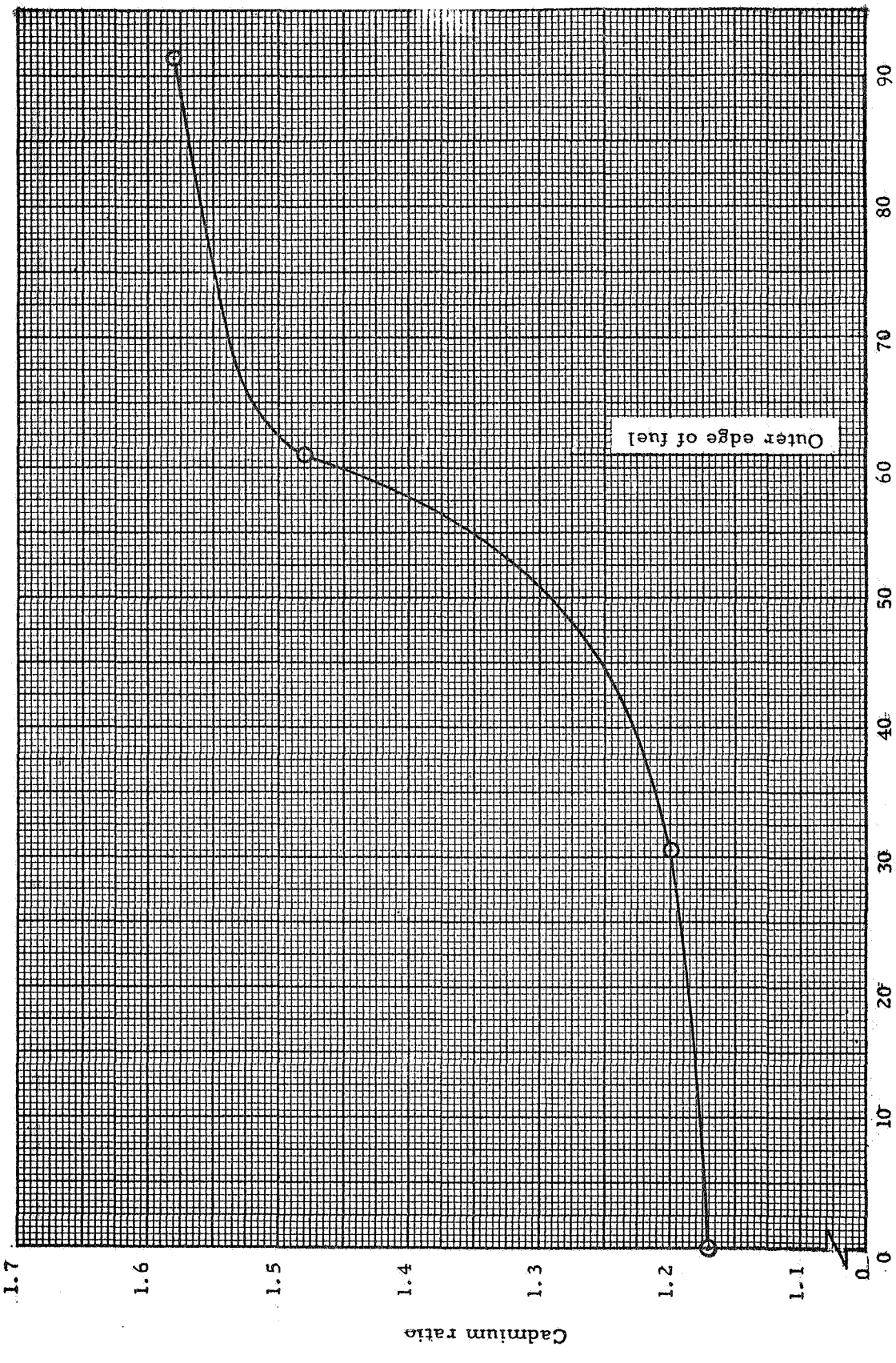


Fig. 8.10 Gold foil cadmium ratio radial profile - Mockup No. 2, Beryllium in D_2O reflector

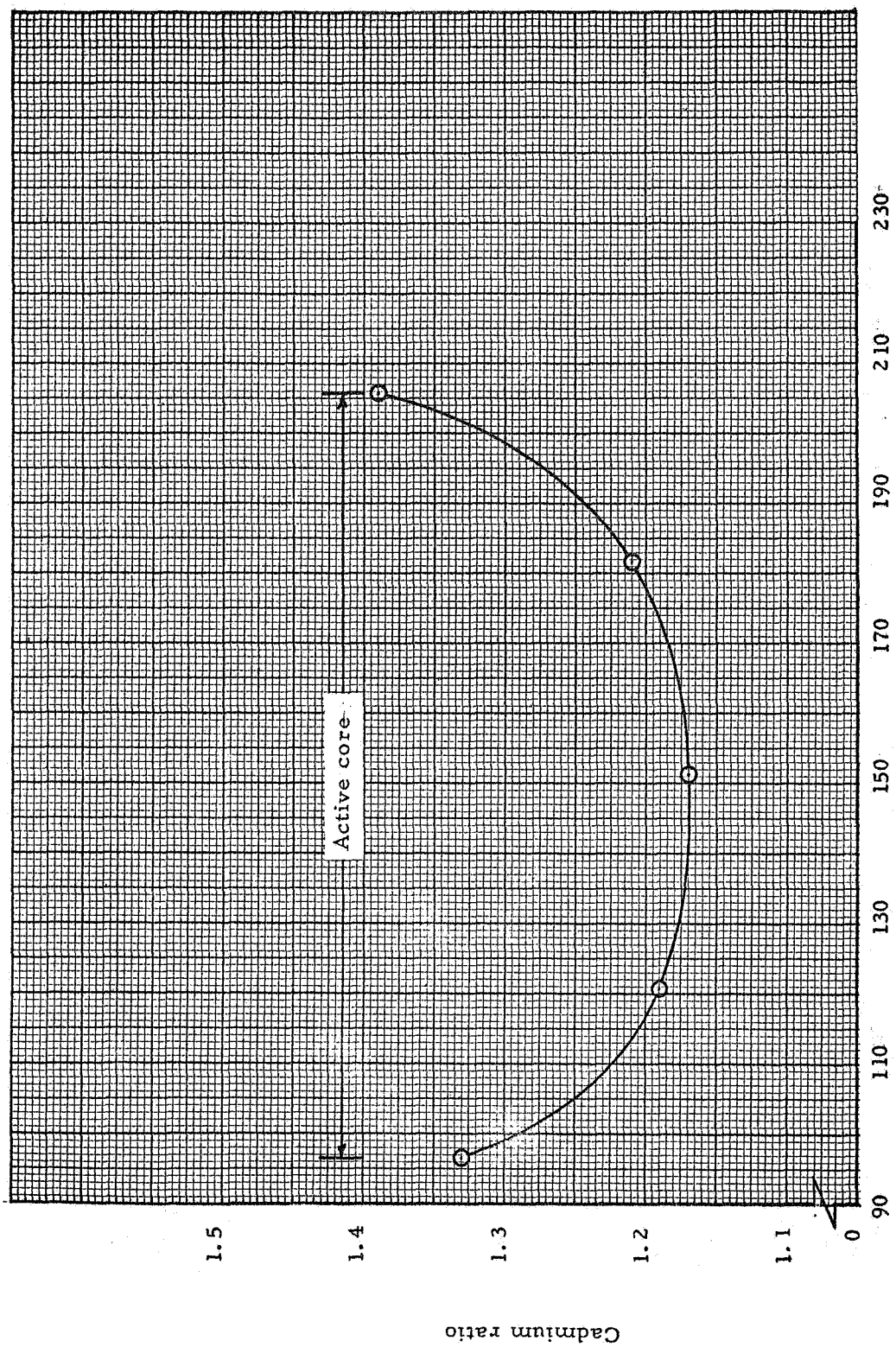


Fig. 8.11 Gold foil cadmium ratio axial profile - Mockup No. 2, Beryllium in D_2O reflector

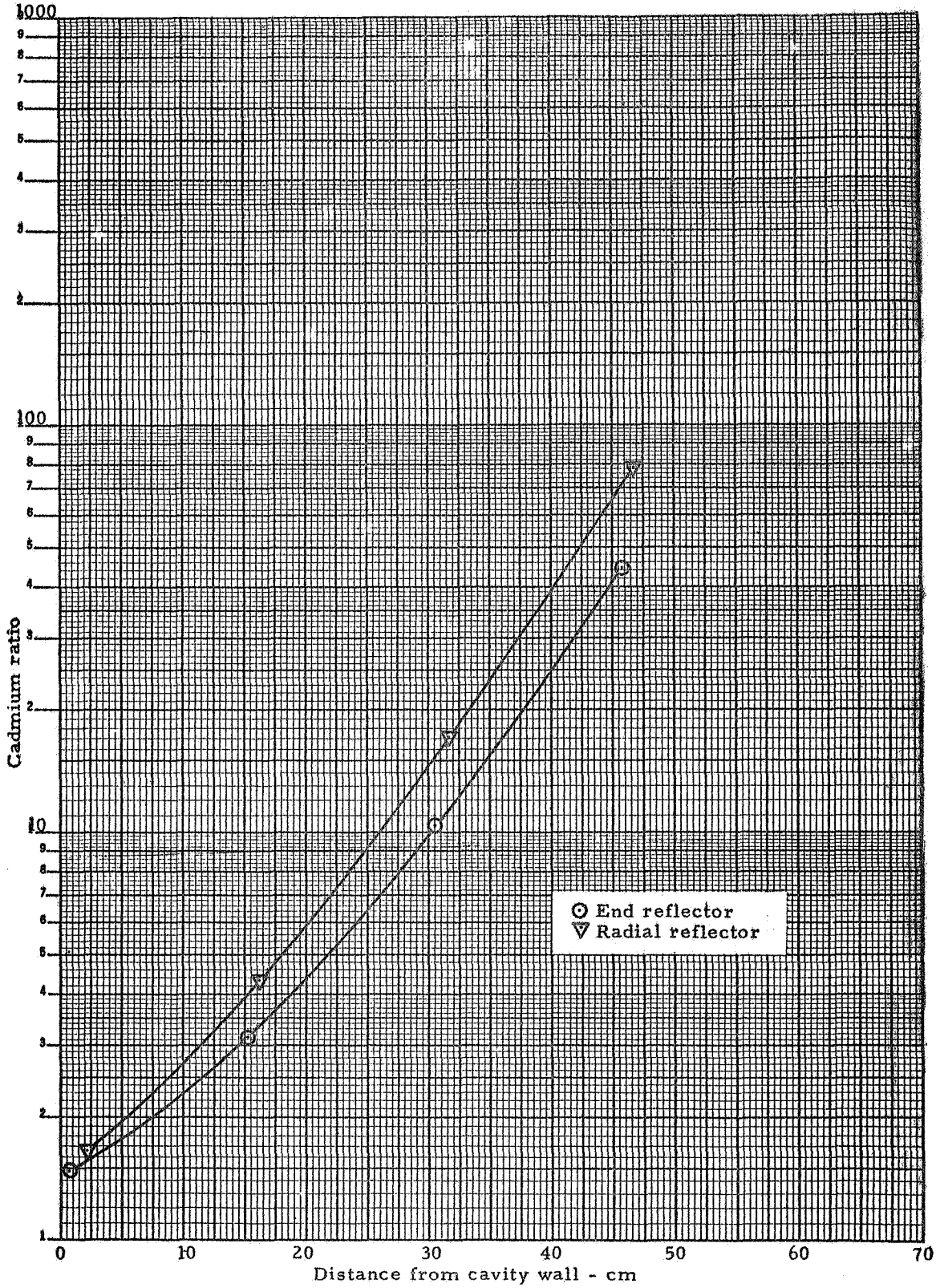


Fig. 8.12 Gold foil cadmium ratios in the radial and end reflectors Mockup No. 2, Beryllium in D_2O reflector

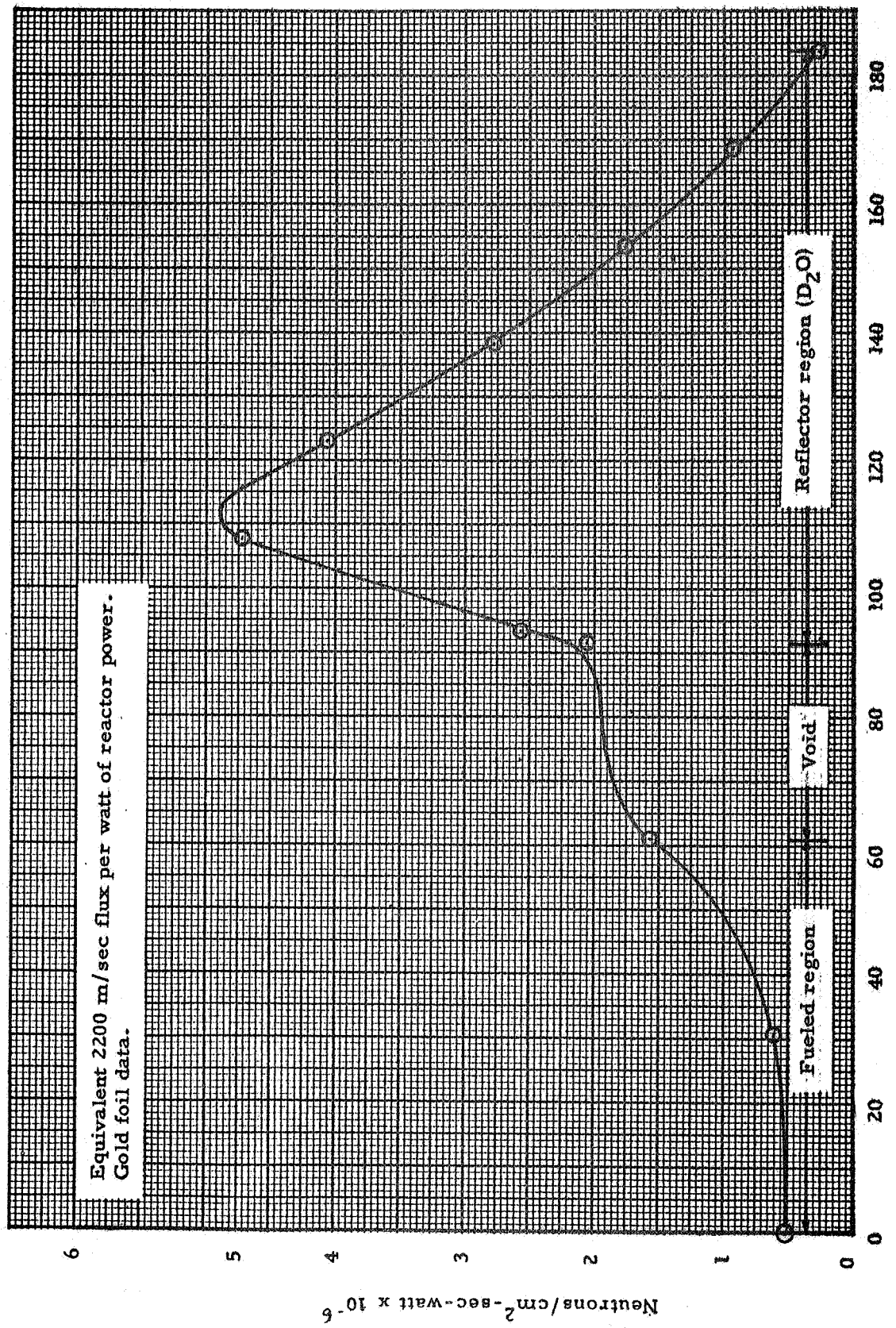


Fig. 8.13 Thermal neutron flux distribution radially through axial center of core Mockup No. 2, Beryllium in D_2O reflector

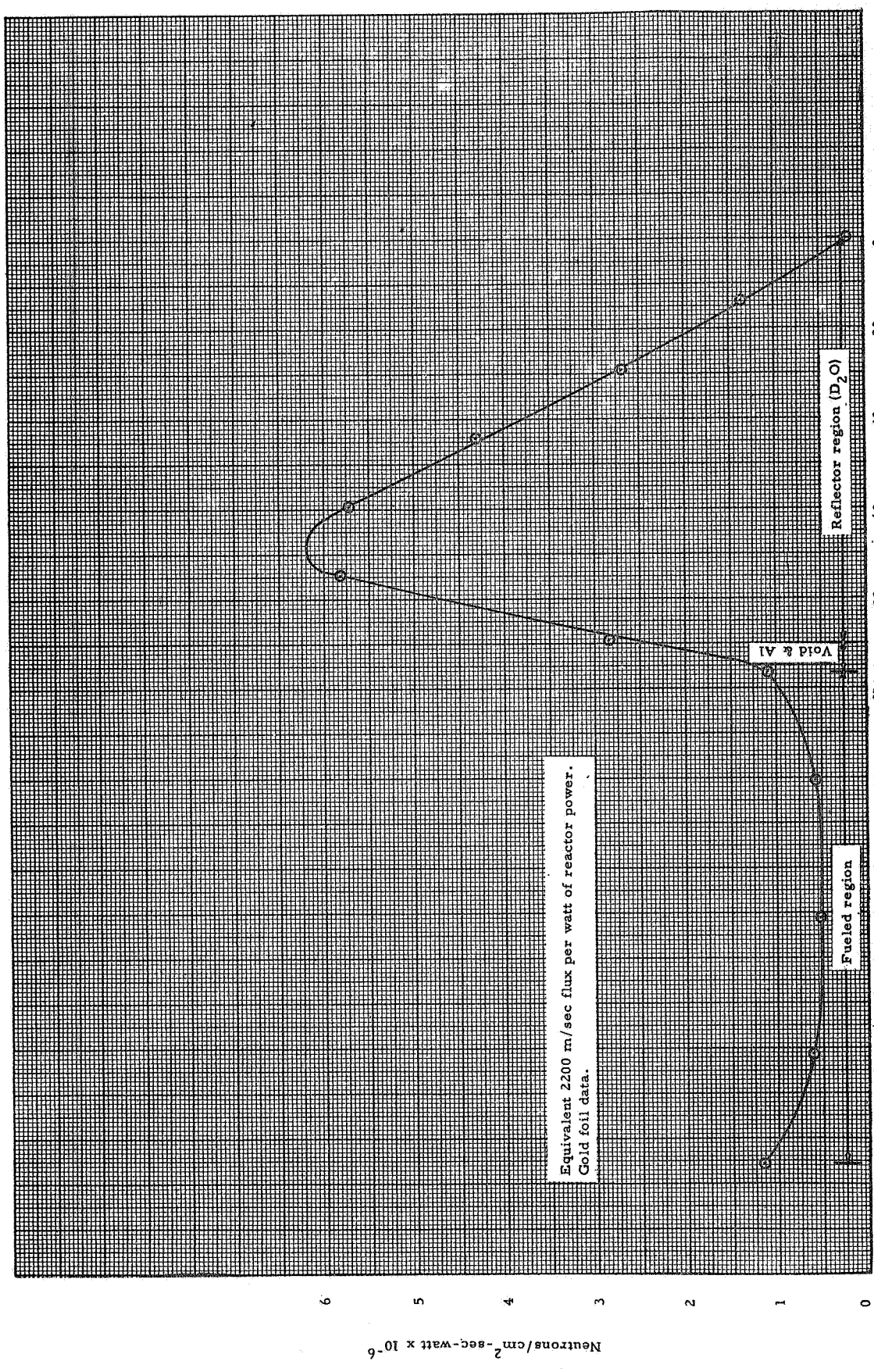


Fig. 8.14 Thermal neutron flux distribution axially through radial center of core Mockup No. 2, Beryllium in D_2O reflector

9.0 COMPARISON OF MOCKUP AND UF_6 REACTORS

9.1 Critical Mass and Reactivity Worths

9.1.1 Rod Worths

The rod worths measured for each of the three major reactors are given for comparison in Table 9.1. Actuators 1, 2, and 3 should be worth the same as they are at identical radial locations. Actuators 5, 6, and 7 are also at the same radial positions but further from the center and therefore; less effective. It will be noted that identical rods or actuators are worth the same on all three configurations within 5% of the average. Where multiple measurements were made resulting in smaller uncertainties, the comparison between the various configurations is ±3%. There is, of course, some slight difference in the rods just due to fabrication and the equivalent locations may differ slightly. Furthermore, rod worth should vary somewhat with the flux shape in the reflector, and the latter is dependent on the fuel loading. Considering all these factors, the values presented in Table 9.1 appear to be consistent within the expected variations which is virtually constant rod worth between the three configurations.

9.1.2 Material Worths

Fuel worth measurements were obtained on each of the mockup and UF_6 configurations and these are given in Table 9.2. These data are also presented graphically in Figure 9.1 along with the Al worth, and it will be noted here that the fuel worth values as determined in the mockup reactors were consistently higher than for the UF_6 reactors by a substantial margin at a given fuel loading.* The reason for this difference is the jagged outer boundary presented by the mockup reactors vs. the smooth outer boundary of the UF_6 cylinder. Computer calculations of fuel worth cannot represent the jagged outer boundary in adequate spatial detail, still leaving sufficient energy detail. Such calculations, however, do not show any significant dependence of fuel worth on the companion core materials.

There is a noticeable dependence of fuel worth on the amount and location of the surrounding "UF_6 tank" material and on the total physical size of the fueled region. The UF_6 tank and its mockup had identical masses, but the mockup material was at a slightly greater radius than the UF_6 tank and the mockup fuel volume was larger, an effect which calculations indicate should account for about a 2% increase in fuel worth. The effect of the jagged outer boundary of the fueled region on the average worth of fuel is illustrated in Figure 9.2. The rapid increase in fuel worth near the edge of the core results in very large worths for that fuel which "juts out" beyond the otherwise uniformly dense core region. Note that Figure 9.2 was obtained from data on full fuel cartridges measured in the mockup experiment, and therefore, is not precise in regard to point values of fuel worth. Calculations performed with the nuclear models presented in Section 10 all give fuel worths that agree with the gaseous

---

* Note, all gas fuel worths have been corrected for the fluorine contribution, about 2% of the total worth.

UF_6 experiment results, and not with the mockup reactor results. The dotted curve in Figure 9.2, however, shows how the UF_6 experimental result would be lower than the mockup reactor result, and in this case the difference is approximately 13%. If an additional 2% credit is considered for the actual physical size difference discovered in the calculations (discussed above and in this case may amount to a double correction), then the 15% to 20% difference between measured gas vs foil worths is resolved. This is an inherent difference caused by the construction of the mockup experiment. It is impossible to provide an experimentally feasible foil mockup which satisfies both a condition for uniform distribution of the fuel in the "fuel volume" as well as a uniform outer boundary as seen by the neutrons emerging from the reflector into the cavity. The mockup No. 1 reactor certainly presented a more uniform outer boundary, but the fuel distribution was less desirable than with the mockup No. 2. The inadequacy of the mockup No. 1 will be discussed in Section 9.2 where critical loadings are compared.

The worth of aluminum as measured within the core region is also given in Table 9.2. Figure 9.3. is a plot of the aluminum worth vs fuel loading, in terms of kg of Al per kg of fuel. The aluminum worth is also plotted vs $\%\Delta k/kg$ in Figure 9.1. The aluminum worth is quite important in extrapolating to a mockup loading without any aluminum. The uncertainty in this correction is particularly large in extrapolating to the 17 kg loading of the UF_6 all D_2O reactor, from the values shown in Figure 9.3 measured at a loading of slightly over 20 kg.

The worth of the 10.16 cm thick annulus of beryllium plus the hardware at the 6.5 cm location was measured for the UF_6 and mockup No. 2 reactors with the following results:

1.	UF_6 reactor	$-(5.83 \pm 0.24)\%\Delta k$
2.	Mockup No. 2	$-(5.48 \pm 0.22)\%\Delta k$

Previous measurements, as reported in Reference 1, gave a value of $-(5.09 \pm 0.35)\%\Delta k$ which agrees very well with the mockup reactor within the experimental error. It is possible that the beryllium worth varies slightly with the two types of reactors due to inherent differences between the gas and foil cores to the total fuel mass (which differed by nearly 20%), and/or to fluorine in the UF_6 reactor and aluminum support structure for the fuel in the mockups. The supporting hardware for the beryllium, which included the end plates and aluminum trays, was worth $-(2.73 \pm 0.10)\%\Delta k$ leaving the net Be worth to be less negative by this amount.

9.1.3 Critical Mass Comparisons

A number of corrections are needed in order to compare directly the critical masses of the gaseous experiment with those of the mockups. The major correction is for the aluminum support structure within the core of the mockup. The mockup No. 2 experiment also had an effectively larger core than the gaseous experiment, and the effective size must be established for the mockup core so that previous data on various core sizes (Reference 1, page 50) can be used to correct the critical mass.

The aluminum correction can be obtained from Figure 9.3. The aluminum worth could only be measured in the mockup reactor. Though calculations indicate that the worth is virtually independent of the differences in aluminum and fluorine in the two reactors, the extrapolation to the 17 kg uranium loading of the reactor without aluminum structure is quite uncertain.

In making the correction for aluminum in the mockup reactors two approaches can be used depending on the base condition, i.e., whether the mockup is corrected to the UF_6 reactor or visa versa. By using the curves given in Figures 9.1 and 9.3 the following corrections for aluminum are obtained.

Mockup No. 1 (Be-D_2O Reflector)

83 kg of Al worth 1.37 ± 0.14%Δk Equivalent U from mockup fuel worth curve at average core loading of 27.3 kg	2.0 kg U
Equivalent U from UF_6 fuel worth curve at average core loading of 24.5 kg	2.0 kg U

Mockup No. 2 (D_2O Reflector)

160 kg Al at 52 kg Al per kg U at average fuel loading of 19.3 kg (Mockup curve)	2.9 kg U
160 kg Al at 45 kg Al per kg U at average fuel loading of 19.1 kg (UF_6 curve)	3.6 kg U

Mockup No. 2 (Be-D_2O Reflector)

160 kg Al at 46 kg Al per kg U at average fuel loading of 25.5 kg (Mockup curve)	3.5 kg U
160 kg Al at 33 kg Al per kg U at average fuel loading of 25.0 kg (UF_6 curve)	4.9 kg U

These values show the magnitude of the aluminum correction.

The mockup No. 1 core size was nominally confined to the same cylindrical volume as the gaseous core. There was a slight difference in length, the mockup being about 0.6 cm longer than the gaseous core since fuel sheets could not be confined to a specific location with an accuracy of better than 0.6 cm. In addition, the mockup was off center by approximately 2.54 cm, so that the gap at the open end of the cavity was 3.8 cm and at the closed end 8.9 cm. This is expected to have little influence on the result, however, an effect of0.03%Δk is deduced from the data on page 33 of Reference 1.

The mockup No. 2 core, however, was definitely larger than the gaseous core. Furthermore, the outer boundary of the mockup core was quite jagged rather than truly cylindrical. Table 9.3, lists the significant dimensions of the two cores. The effect of the irregular boundary is the most difficult portion of the correction to estimate. Experiments were conducted on the variation of fuel worth as the orientation of fuel in the outer fuel cartridges. The results showed no unusual values of fuel worth,

except as the effective radius of the fuel changes; and then, the measured fuel worth followed closely the curve of Figure 9.2. Other measurements investigated the perturbations in the flux near the outer core boundary caused by the aluminum structure that supported the fuel. The effects of the structure were negligible, both on the flux and on the fuel worth, which showed no variation depending on the proximity of fuel to the aluminum.

Several schemes can be used to define the effective radius or volume of the mockup No. 2 core. One is by the mean chord length, 4 V/S (V = volume, S = surface). However, there then arises the question of how to define V and S. The "rubber band" (stretching a rubber band around the volume and thus defining a new V and S) approximation is usually recommended, but only if end effects are insignificant. In the cavity core, the end effects of the 121.9 cm long by (approximately) 121.9 cm diameter core are significant. Table 9.3 lists results of the various methods of computing mean chord lengths..

Another approach is to obtain the average apparent maximum radius as viewed from locations at the inner radius of the D_2O (cavity wall). This result gives an overall effective core diameter of 129.0 cm. Still another consideration is to evaluate the average thickness of paths through the axial center-line and perpendicular to it, as viewed from various locations along the cavity wall. This result gives an effective diameter of 127.8 cm. Both of these results are slightly larger than the results from the mean chord length analysis in Table 9.3. However, the density of fuel within the outside annulus of the larger core is less. For instance, the actual maximum fuel diameter is 130.0 cm, but in the region between 121.9 cm and 130.0 cm the fuel density is only 25% of the density of the region of the main core inside the 121.9 cm.

It has been concluded that appropriate effective dimensions for the core of mockup No. 2 are either a mean chord length of 80.3 cm, or an effective core diameter of 130.0 cm (51.2 in.) with a 25% normal fuel density in the 121.9 cm to 130.0 cm annulus. The results from Reference 1 of various core sizes have been extracted and listed below in a form suitable for comparing the sizes of the gaseous and mockup cores.

		Data from Reference 1			
Core Length (cm)	Core Radius (cm)	Mean Chord Length (4 V/S) cm	$\frac{4VN}{S}$	Critical Mass U^{235} kg	Fuel Density (N) U^{235}/cc
121.9	45.7	66.5	60.0×10^{20}	18.0	9.0×10^{19}
121.9	54.9	75.7	57.5	15.2	7.6
121.9	59.4	80.0	55.6	13.9	6.95
121.9	68.6	87.8	52.7	12.0	6.0

Using the above data, corrections have been made using both mean chord length--fuel density ratios and fuel mass vs radius ratios. These give the results listed in Table 9.3 . The chord length correction is small ($\sim 1/2\%$); the radius ratio correction is $\sim 1.6\%$. The average is about a 1% higher loading for a reactor confined to the UF_6 gas geometry compared to the loading with the fuel confined to the

volume of the mockup No. 2. Both methods of correction give nominally the same result, implying internal consistency in the correction methods, but this correction for the irregular boundary of the mockup No. 2 core has considerable experimental uncertainty. Thus, the measured mass of the UF_6 experiment with the all D_2O reflector was 17.27 kg U, and if it had been confined to a volume equivalent to the mockup No. 2, the mass would have been 17.1 kg. For the Be-D_2O reflector, the 23.55 kg measured mass would have been reduced to 23.3 kg. The resulting comparison of the mockup experiments is presented in Table 3.5 of Section 3.

9.2 Power Distribution

9.2.1 Bare Catcher Foils

The bare catcher foil data within the active core region for the two mockup and the UF_6 reactors with beryllium and D_2O in the radial reflector are shown together in Figures 9.4 and 9.5. The radial power profile shows the UF_6 reactor volume weighted average over the fueled region to be 1.523 compared to 1.563 and 1.592 for mockup No. 1 and mockup No. 2, respectively. The flatter profile for the UF_6 reactor was to be expected because of the lighter fuel loading which resulted in less neutron flux attenuation through the core. The two mockup reactors show essentially the same radial flux profile within the normal standard error for catcher foils of about 3% with the volume weighted averages agreeing to within 1% of the average.

The axial profiles given in Figure 9.5 also show good agreement. The main differences occur at the ends of the reactor where foil position errors can result in large errors in foil activity because of the steep power gradients. Mockup No. 1 fuel was not exactly centered in the core as was explained earlier in Section 9.1.3. This asymmetry had some effect on the axial power profile as will be noted in this figure. The curve averages, however, agree very well, each differing from the other by less than 1%.

The comparisons of the bare catcher foils from the pure D_2O reflected reactors are presented in Figure 9.6 and 9.7. The radial volume weighted average over the fueled region for the UF_6 reactor was 1.380 compared to 1.430 for the mockup. Here again, the flatter profile for the UF_6 reactor was expected because of the lighter fuel loading.

The axial comparison presented in Figure 9.7 shows very close agreement between the two sets of data except towards the end of the core containing the control rods where the profile for the UF_6 reactor is below that of the mockup. Because of the lighter fuel loading in the UF_6 reactor, it would normally be expected that the ends of the curve for this reactor would be below the mockup. This was observed to be true only on the end of the reactor towards the control rods. The same trend was noted for both the Be and D_2O and the pure D_2O reflected reactors as will be observed from Figures 9.5 and 9.7. The reason for this is not fully understood.

9.2.2 Cadmium Ratios

The cadmium ratios obtained from catcher foils within the cavity region with Be and D_2O in the radial reflector are shown in Figures 9.8 and 9.9. Within the active core, the UF_6 reactor has a higher cadmium ratio by 15% to 30% and thus a softer spectrum than do the mockup reactors. This is due, again, to the lighter fuel loading for the UF_6 reactor. Beyond the active core, the data shows considerable uncertainty and it was concluded that within the data uncertainty there was little or no difference in the void region between the three configurations.

The axial distribution given in Figure 9.9 shows excellent agreement between the two mockups except at the separation plane where mockup No. 1 is about 12% above mockup No. 2. This appears to be due to the differences in bare foil activity and was probably caused by slight differences in foil positions at this point or the way the active core regions were centered within the cavity. The cadmium ratios from the UF_6 reactor are higher than the mockups by 5 to 15% except at the separation plane where the UF_6 value falls between the mockups.

There were no cadmium covered catcher foils exposed on the UF_6 reactor with the pure D_2O reflector so there are no comparisons to be made with the mockup reactor for this configuration.

9.3 Gold Foil Data

9.3.1 Bare Gold

The bare gold data comparisons for the three configurations with Be and D_2O in the radial reflector are shown in Figures 9.10 and 9.11. The radial volume weighted averages over the fueled region were 1.234, 1.224, and 1.198 for the UF_6, mockup No. 1 and mockup No. 2 reactors, respectively, as given in Figure 9.10. The total spread in these averages is 3% and it will be noted that generally the data are within ±5% of the average for the three configurations, which is about twice the nominal standard deviation for gold foil measurement. Therefore, the radial distribution within the active core from the bare gold foils does not exhibit any measureable change between the mockup and UF_6 reactors.

The axial distributions of normalized gold foil activity shown in Figure 9.11 also shows fairly close agreement and the integrated averages over the active core were 1.116, 1.117 and 1.088 for the UF_6 mockup No. 1 and mockup No. 2 reactors, respectively. The main difference occurs at the separation plane where the UF_6 reactor data show a significantly higher activation flux than do the mockups. This may be due in part to the aluminum geometry in the UF_6 tank where the air ducting fastened to the tank. There was a 2.54 cm diameter hole in the tank at this point which allowed for power mapping through the core. There was no defined trend for any of the three configurations to be different from the other according to these axial profiles of bare gold data.

The bare gold foil comparison with the pure D_2O reflector for the UF_6 and mockup No. 2 reactors are presented in Figures 9.12 and 9.13. The volume weighted averages for curves drawn through the given points for each configuration out to the outer edge of the fuel were 1.169 and 1.204 for the UF_6 and mockup No. 2, respectively for a 3.0% difference with the UF_6 reactor showing the flattest distribution due to a lighter fuel loading.

The axial plot, Figure 9.13, shows the UF_6 reactor to be slightly lower than the mockup. In general, however, the difference is within ±5% of the average which is not unusual for gold foil data.

A comparison of the bare gold data within the radial reflector is given in Figure 9. 14. It will be observed that there is very close agreement between the UF_6 and mockup No. 2 reactors but mockup No. 1 is consistently low by 10 to 12% over the majority of the curve. No obvious explanation for this difference is apparent. The same is true of the end reflector data shown in Figure 9.15. In this latter case, however, there is a reason for the low values in the end reflector noted from mockup No. 1. This was due to the rods being equally inserted because of a relatively high k-excess. The rods suppressed the flux in this reflector region. The data from the UF_6 and mockup No. 2 reactors also show very close agreement as in the radial reflector.

9.3.2 Cadmium Ratios

The gold foil cadmium ratios within the cavity and reflector regions were measured with both the Be and D_2O and the pure D_2O reflectors. The data from the three configurations with the Be and D_2O reflector are presented in Figures 9.16 and 9.17. Within the core region, the UF_6 reactor shows a higher cadmium ratio by 2 to 4% which is probably real. At the outer edge of the fuel, however, there is a cross over and the mockup reactors give higher values than the UF_6 reactor. Part of this difference is undoubtedly due to statistical errors and it will be observed that the curves are within ±5% of the average, which is the expected uncertainty associated with gold cadmium ratio results. The lighter fuel loading on the UF_6 reactor would be expected to give slightly higher cadmium ratios within the active core, as was observed for the catcher foils, and this is exhibited to some extent in both the radial and axial cadmium ratios traverses given here in Figures 9.16 and 9.17. At the outer edge of the core, the UF_6 reactor point appears to be low and there is a logical explanation for this. The core boundary is a very sensitive region where the two types of fuel (gaseous and solid sheets) can give quite different results just due to the placement of the foils with respect to the fuel. On the mockup reactors, the catcher foils were placed outside of the outer fuel element and were in a plane parallel to its outer surface. In the UF_6 reactor, however, the foils were inserted into the measurement hole so that they were normal to the outer surface of the cylinder wall at the penetration point and half of the foil normally would have been within the active core and half outside the active core, Slight variations in the foil position at the outer surface of the reactor would therefore cause noticeable differences in the observed power distribution. The UF_6 reactor

was also a cylinder while the mockups were more octagonal in shape. The gold cadmium ratios in the reflectors are shown in Figure 9.18 and it will be observed that the three configurations give essentially the same values. Any major differences in the data occur at large distances from the cavity wall where the cadmium covered foil activities are very low and statistical uncertainties are larger.

9.4 Thermal Neutron Flux

Thermal neutron flux values were available on all three reactor configurations with both Be and D_2O in the radial reflector. These data are summarized in Table 9.4. The thermal flux ratio of mockup No. 2 to the UF_6 reactor in the radial reflector was 0.982 ± 0.038 and in the end reflector was 0.972 ± 0.017. The same ratio in the radial reflector for mockup No. 1 was 0.870 ± 0.022. Mockup No. 2 shows excellent agreement with the UF_6 reactor in these regions but mockup No. 1 is low. No experimental anomaly could be found to account for this difference. The difference with respect to mockup No. 1 could be partly caused by the 10% bias in fuel mass caused by the foil arrangement within the cavity. The end reflector was low in mockup No. 1 reactor because of the rod positions. The rods in the end reflector have not appreciably affected the flux in the radial reflector in past experiments but it may be that they have something to do with the lower bare gold foil activities and thus the lower thermal neutron flux in the radial reflector in mockup No. 1.

Within the active core region the thermal flux was, as expected, lower on the mockup reactors than the UF_6 reactor because of the extra aluminum and fuel in the mockups. The thermal flux are shown graphically in Figures 9.19 and 9.20.

TABLE 9.1

Comparison of Control Rod Worth

Actuators	UF_6 Reactor (%Δk)	Mockup No. 1 (%Δk)	Mockup No. 2 (%Δk)
2 (3 rods)			-0.775
3 (3 rods)	-0.861		
5 (3 rods)		-(0.630±0.002)	
6 (3 rods)	-(0.654±0.022)		-(0.708±0.015)
7 (3 rods)	-(0.675±0.020)	-(0.664±0.007)	
3 and 6 (6 rods)			-(1.572±0.016)
1 to 6 (17 rods)			-4.088
1 to 7 (20 rods)	-(4.674±0.049)	-(4.709±0.240)	

NOTE: Where error values are left off, the number is from a single measurement.

TABLE 9.2

Core Average Fuel Worths

Configuration	Total Core Loading (kg U)	Fuel Worth (%Δk/kg)
Mockup No. 1	27.8	0.644±0.055
Mockup No. 2	27.2	0.703 ± 0.034
Mockup No. 2	20.1	1.105±0.055
UF_6	23.4	0.766±0.054
UF_6	24.2	0.627±0.015
UF_6	24.9	0.598±0.007
UF_6	25.3	0.617±0.035
UF_6	26.0	0.588±0.043
UF_6	17.7	1.060±0.020

Aluminum Worth Measurement within Active Core

Configuration	Fuel Mass in Reactor (kg U)	Fuel Worth (%Δk/kg)	Al Worth (%Δk/kg)	kg Al / kg U
Mockup No. 1	27.7	0.644±0.055	0.0161±0.0011	40.0±4.4
Mockup No. 2	21.8	1.105±0.055	0.0202±0.0001	54.7±2.7
Mockup No. 2	20.8	1.105±0.055	0.0217±0.0015	50.9±4.3

NOTE: Mockup No. 1 used 6061 Al in the measurement. The other measurements were with type 1100 Al.

TABLE 9.3

Corrections to Critical Mass for Geometric Differences

UF_6 Tank Characteristics	
length	42.75 inches
diameter	48.0 inches
mean chord length	$\frac{4V}{S}$ = 30.75 in. (78.1 cm)
Mockup No. 2 Characteristics	Volume = 7.73×10^5 $in.^3$
length	43.1 inches
active fuel end area	1872 square inches
a. actual volume of fuel	8.07×10^5 $in.^3$
b. actual surface area of fuel	11920 $in.^2$
c. "rubber-band" side area, actual end area	10530 $in.^2$
d. "rubber-sleeve" area	10750 $in.^2$
e. "rubber-sleeve" volume	8.53×10^5 in^3
mean chord length $\frac{4V}{S}$ using	
a) and b)	27.1 in. (68.8 cm)
a) and c)	30.7 in. (77.0 cm)
d) and e)	31.7 in. (80.5 cm)
c) and e)	32.4 in. (82.3 cm)

Postulated UF_6 Cylindrical Tank of Modified Dimensions

50 inch dia. by 43 inch length - mean chord length = 31.6 in. (80.3 cm)

Mean Chord Length Correction

UF_6 all D_2O Reflector

chord length	78.1 cm
4VN/s	27.3×10^{20} for the 17.27 kg U loading and a k excess of 0.61%Δk

corrected to chord length of 80.3 cm gives 4VN/S = 27.0×10^{21} or 17.2 kg U

UF_6 with Be - D_2O Reflector

4VN/S = 37.2×10^{20} for 23.55 kg U and a k excess of 0.56%Δk

corrected to chord length of 80.3 cm gives 4VN/S = 36.75×10^{20} or 23.5 kg

TABLE 9.3
(Continued)

Radii Correction (ignores the 0.9 cm difference in fuel length)

Diameter increase from 121.9 to 130.0 cm *, if only 25%* of the normal fuel density appears in the extra annulus. A full density annulus would decrease core loading 6.5%. Thus loading would be expected to decrease only 1.6%

UF_6 all D_2O Reflector

Corrected mass = 16.99 kg U

UF_6 with Be-D_2O Reflector

Corrected mass = 23.17 kg U

Average Values for Size Difference Corrections

	All-D_2O		Be-D_2O	
	kg U	k-excess	kg U	k-excess
UF_6 actual	17.27	1.14%Δk	23.55	0.99%Δk
UF_6 corrected to Mockup No. 2 size	17.1±0.2	1.14%Δk	23.3±0.3	0.99%Δk
Mockup No. 2 actual	20.78	0.23%Δk	27.25	0.56%Δk
Corrected to UF_6 core size	21.0±0.3	0.23%Δk	27.5±0.4	0.56%Δk

* See text

TABLE 9.4

Comparison of Thermal Neutron Flux Mockup and UF_6 Reactors - Be and D_2O Reflector

Radial (cm)	Axial (cm)	$n/cm^2/sec^*/watt \times 10^{-6}$ Mockup No. 1	Mockup No. 2	UF_6	Mockup No. 1 / UF_6	Mockup No. 2 / UF_6
0	0	0.076	0.199	0.205	0.371	0.971
0	13.9	0.494	1.361	1.420	0.348	0.958
0	29.1	1.198	2.690	2.778	0.431	0.968
0	44.4	2.612	4.315	4.361	0.599	0.989
0	59.6	4.460	5.731	5.768	0.773	0.994
0	74.6	5.143	5.818	6.127	0.839	0.950
0	89.4	1.775	1.675	1.463	1.213	1.145
0	96.5	1.191	1.094	1.200 (1)	0.992	0.912
0	120.5	0.606	0.585	0.719	0.843	0.814
0	151.1	0.445	0.520	0.651	0.684	0.799
0	181.5	0.516	0.604	0.717	0.720	0.842
0	20.58	1.027	1.161	0.900 (1)	1.141	1.290
30.5	151.1	0.495	0.604	0.702	0.705	0.860
61.0	151.1	1.541	1.574	1.554	0.992	1.014
91.4	151.1	1.943	2.102	2.352	0.826	0.894
93.2	151.1	2.290	2.565	2.770	0.827	0.926
107.7	151.1	4.051	4.729	4.588	0.883	1.031
123.0	151,1	3.640	4.063	4.164	0.874	0.976
138.2	151.1	2.550	2.784	2.879	0.886	0.967
153.5	151.1	1.534	1.765	1.747	0.878	1.010
168.7	151.1	0.718	0.942	0.810	0.886	1.163
183.9	151.1	0.094	0.265	0.110	0.855	2.409

(1) Extrapolated from curve

Mockup No. 1/UF_6 - Radial Reflector = 0.870 ± 0.022

Mockup No. 2/UF_6 - End Reflector = 0.972±0.017
Radial Reflector = 0.982 ±0.038

* Thermal neutron flux is in equivalent 2200 m/sec flux. The usual Maxwell Boltzmann distributed flux would be 1.129 larger.

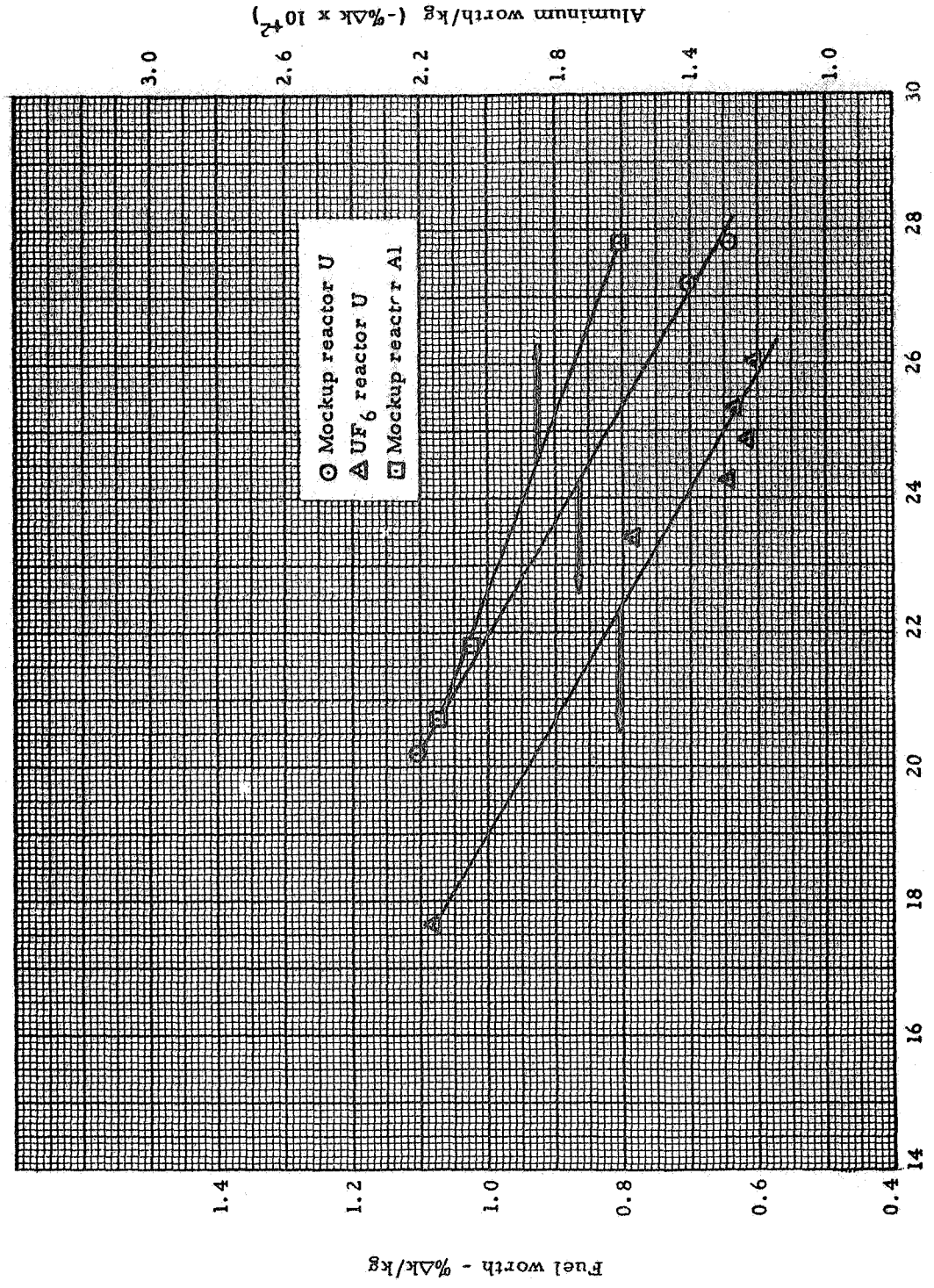


Fig. 9.1 Core loading effects on fuel and aluminum worth

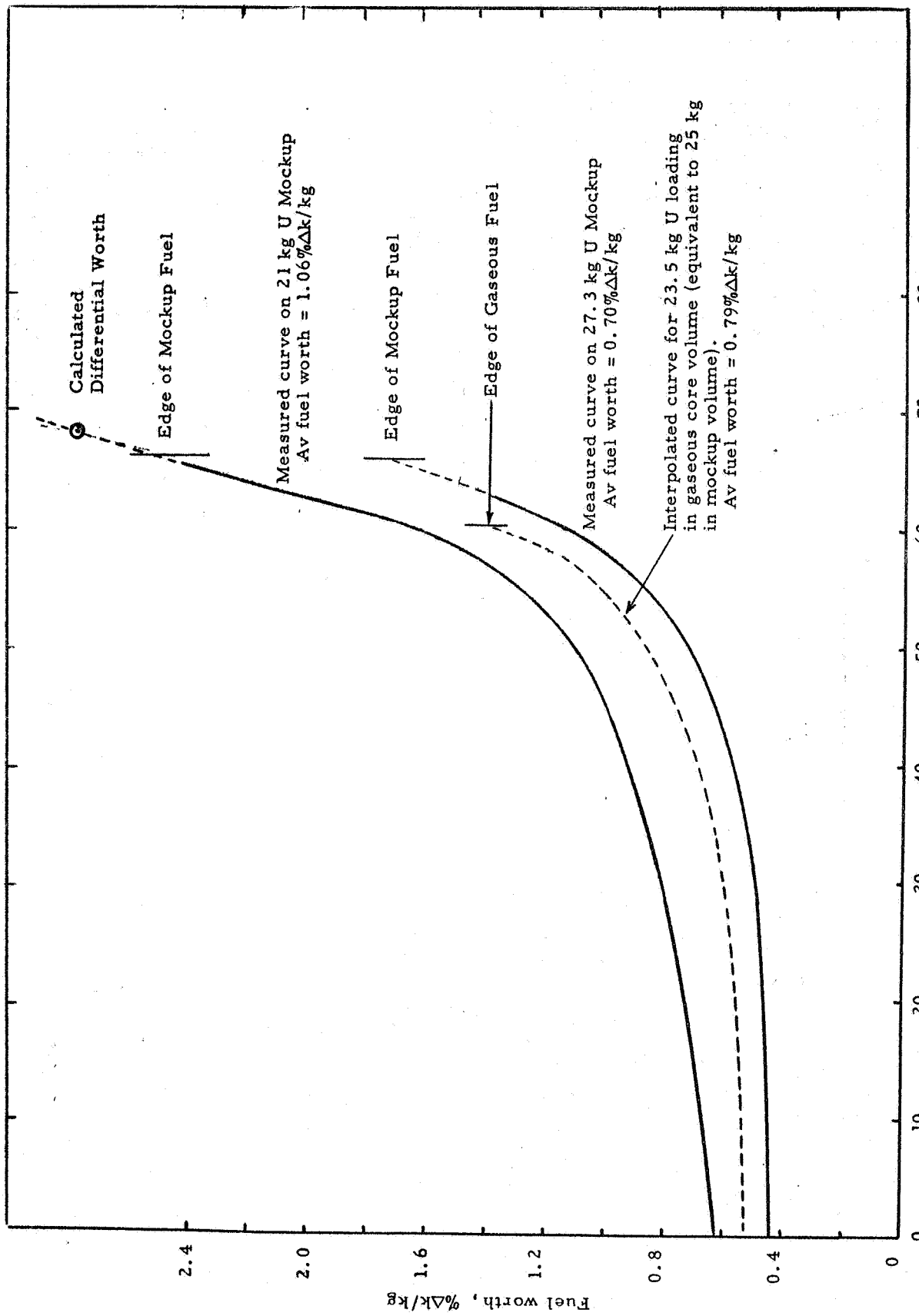


Fig. 9.2 Comparison of fuel worths on the mockup and UF_6 experiments

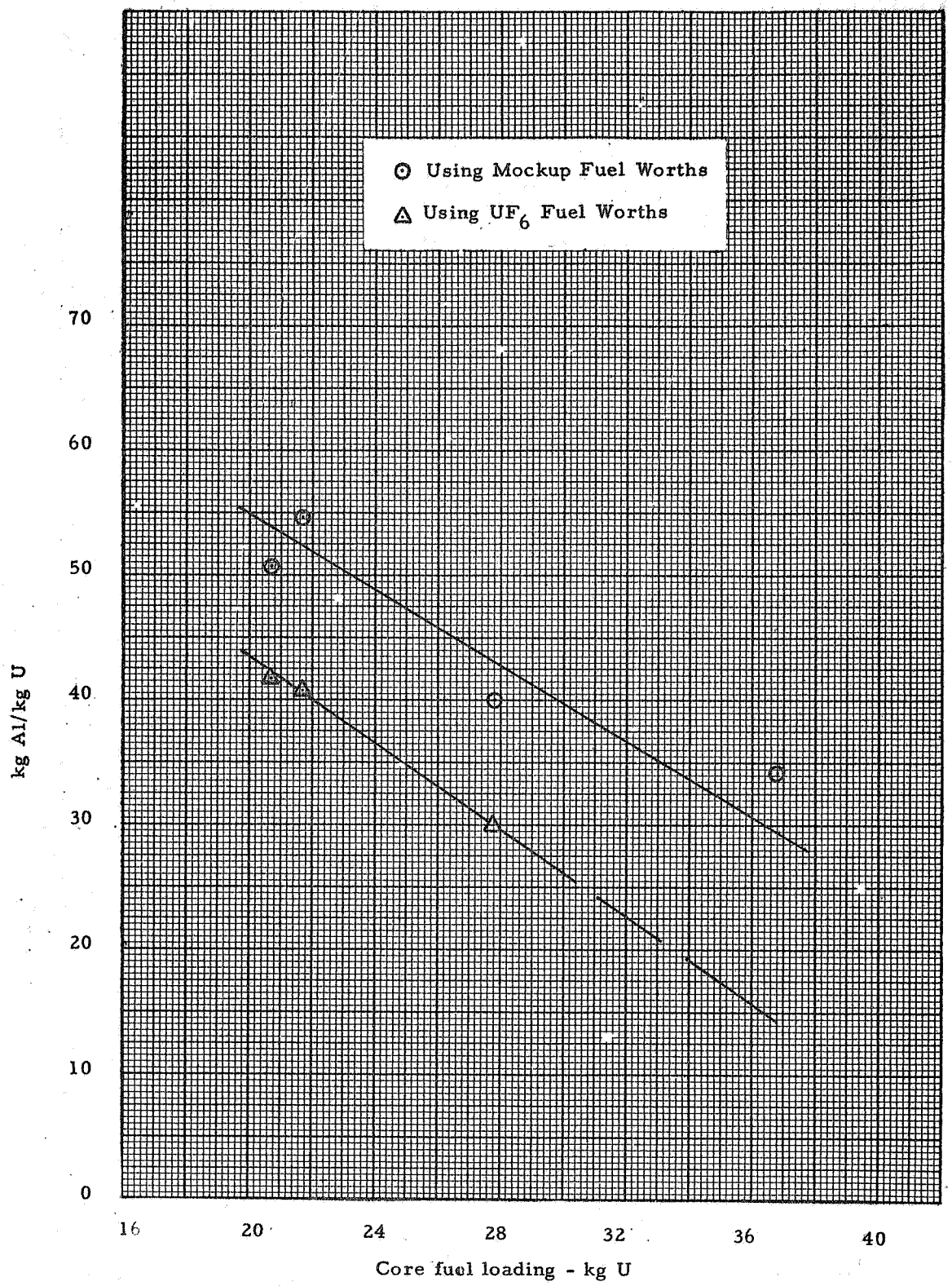


Fig. 9.3 Effect of core loading on aluminum worth with respect to uranium

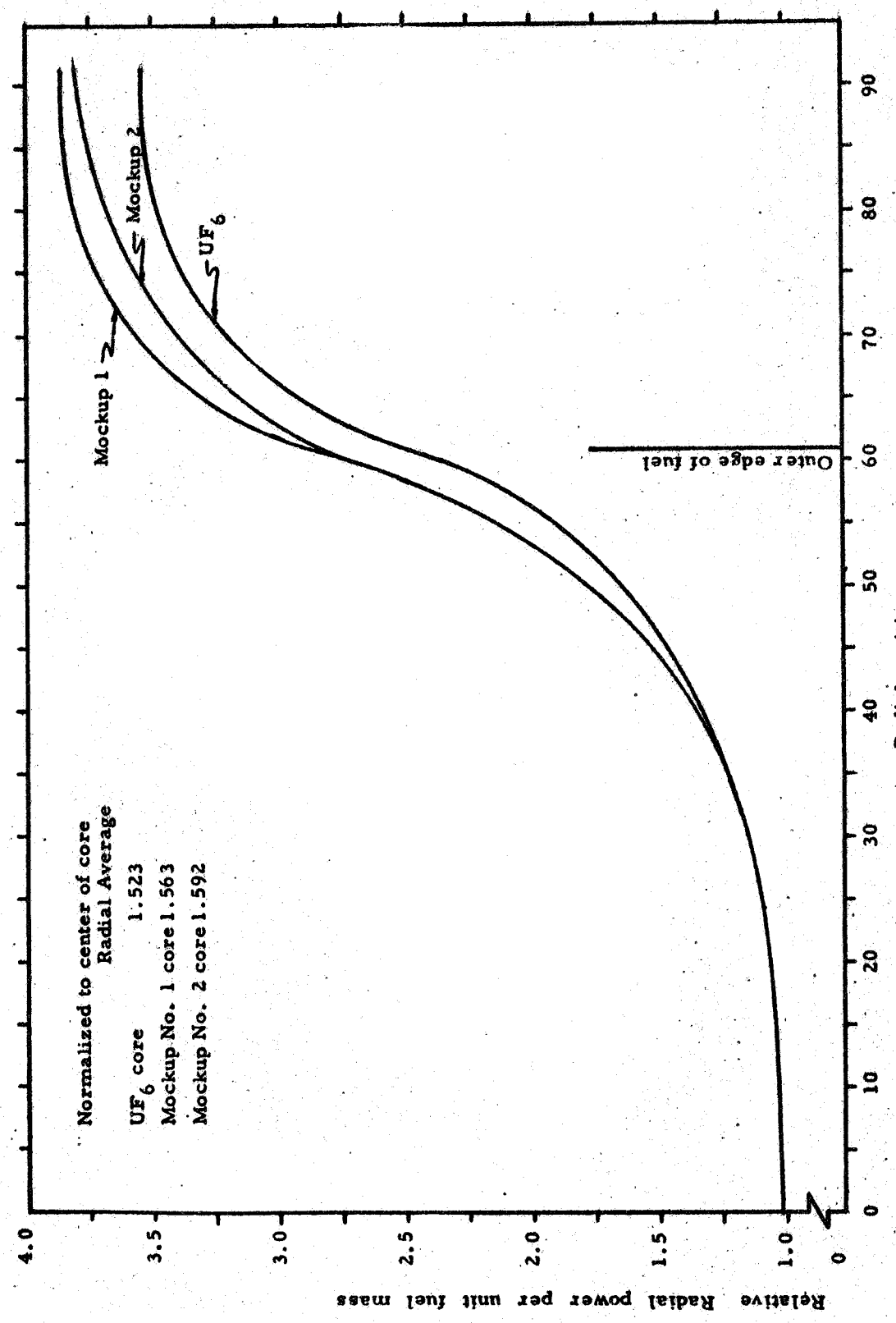


Fig. 9.4 Comparison of relative radial power distributions - beryllium in D_2O reflector

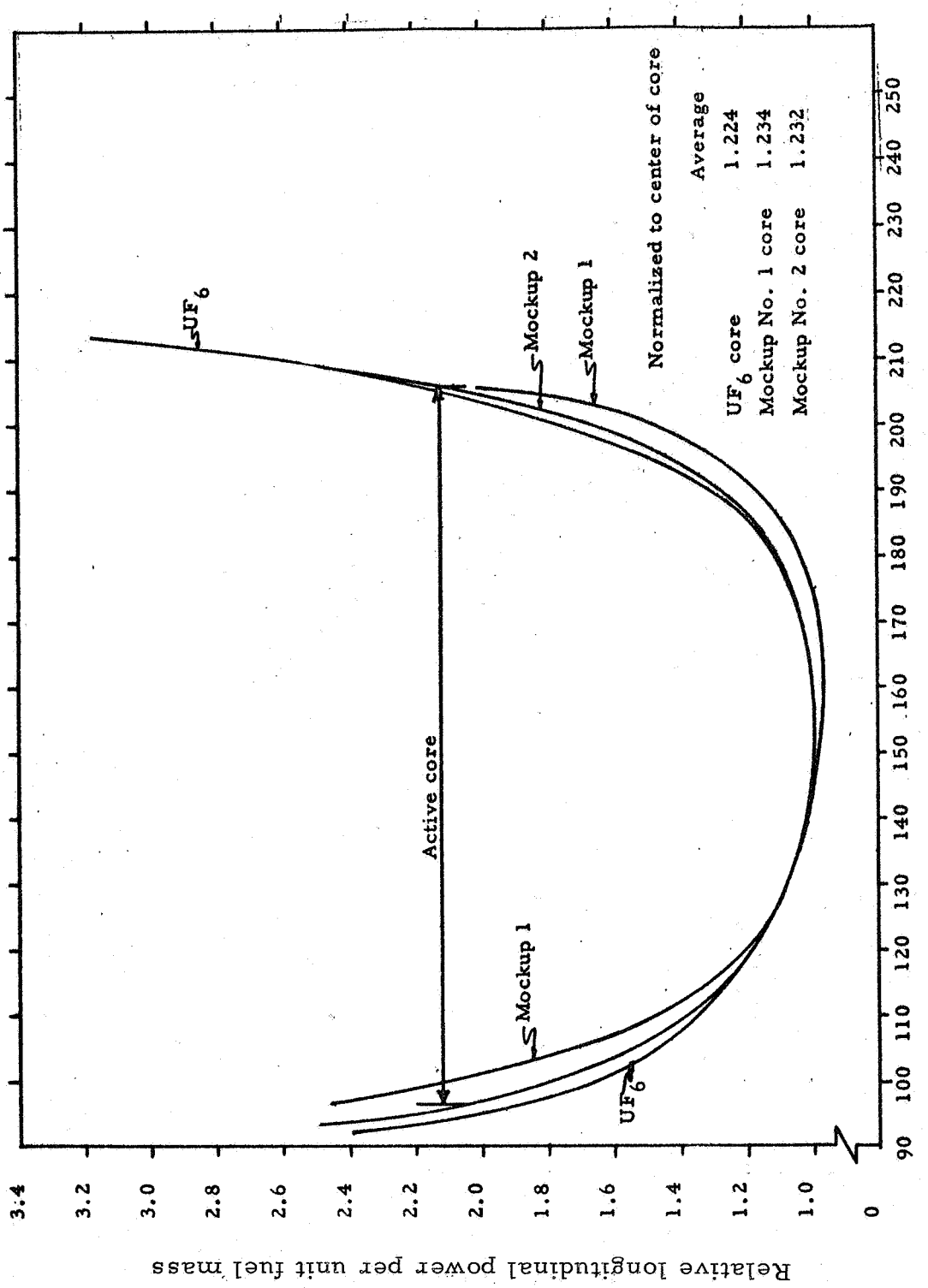


Fig. 9.5 Comparison of relative axial power distributions - beryllium in D_2O reflector

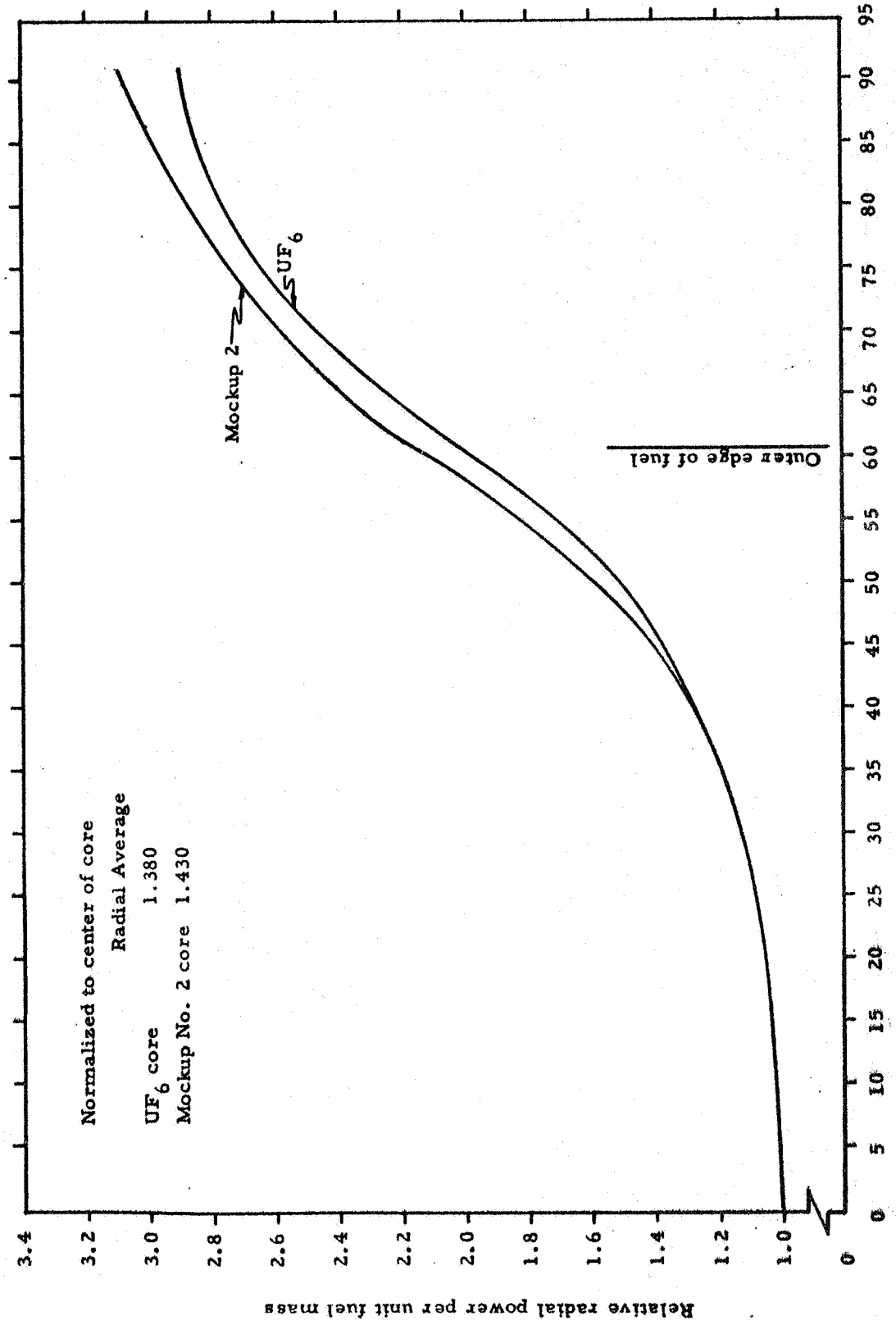


Fig. 9.6 Comparison of relative radial power distributions - pure D_2O reflector

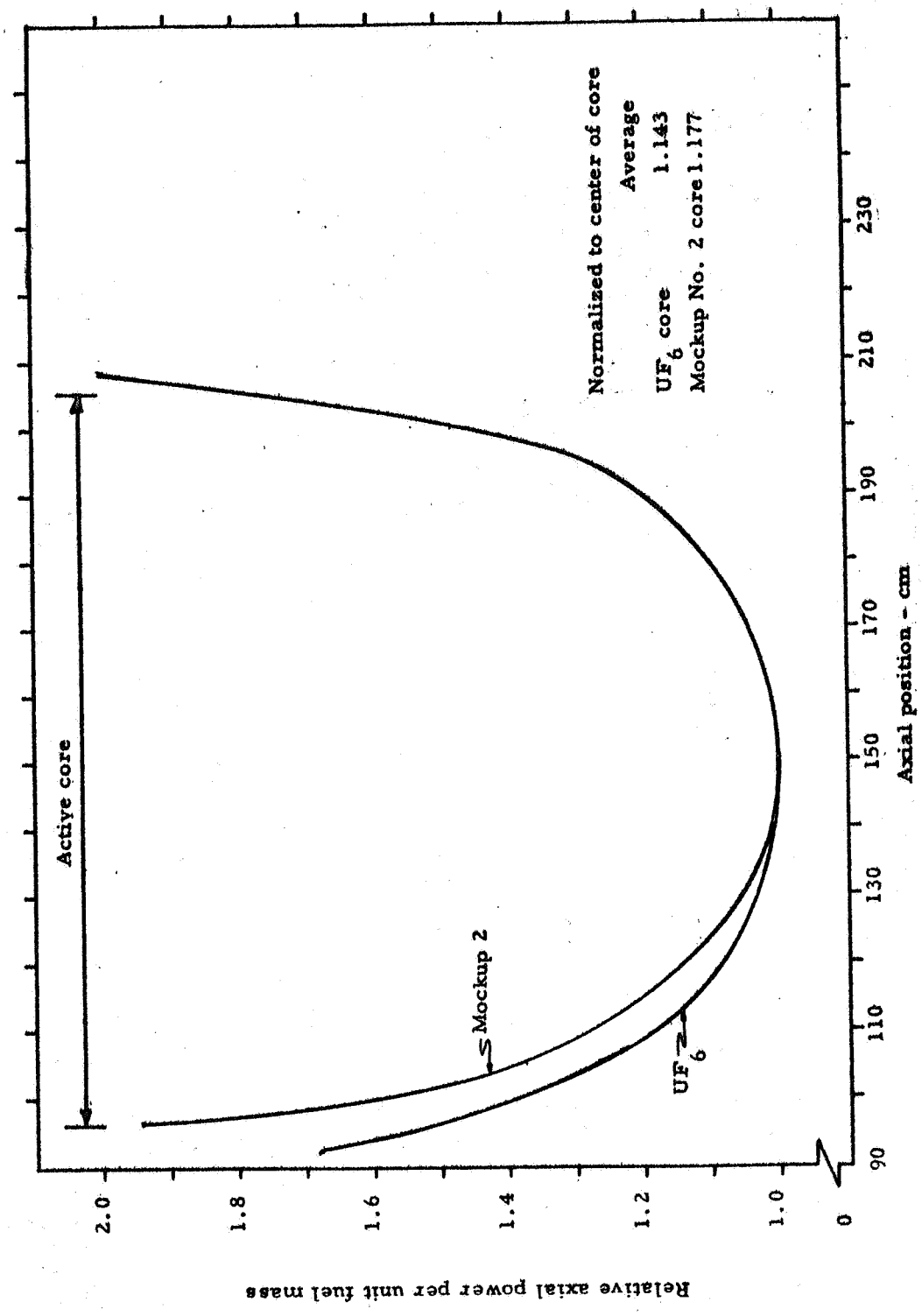


Fig. 9.7 Comparison of relative axial power distributions - pure D_2O reflector

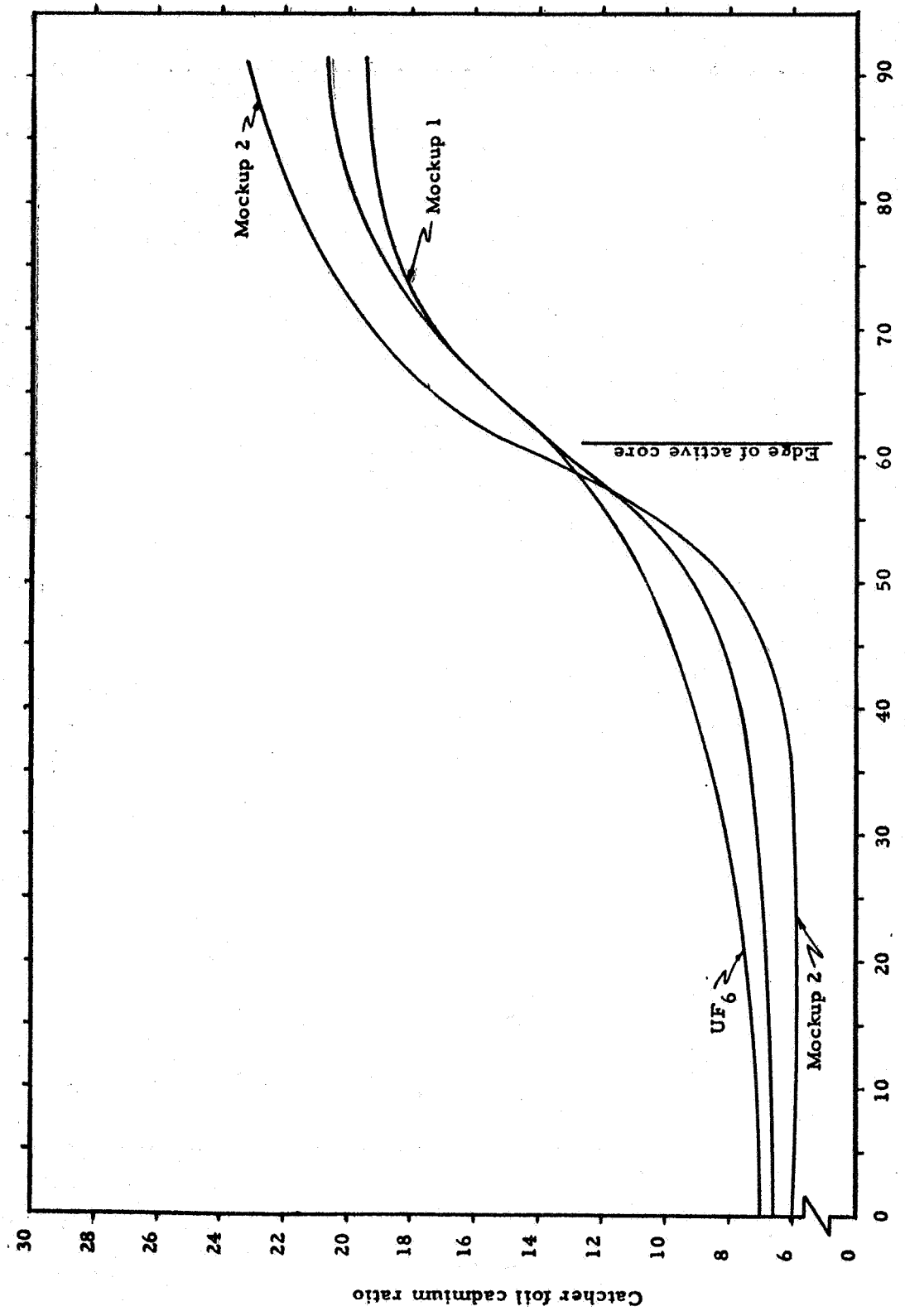


Fig. 9.8 Radial comparison of catcher foil cadmium ratios - Beryllium in D_2C reflector

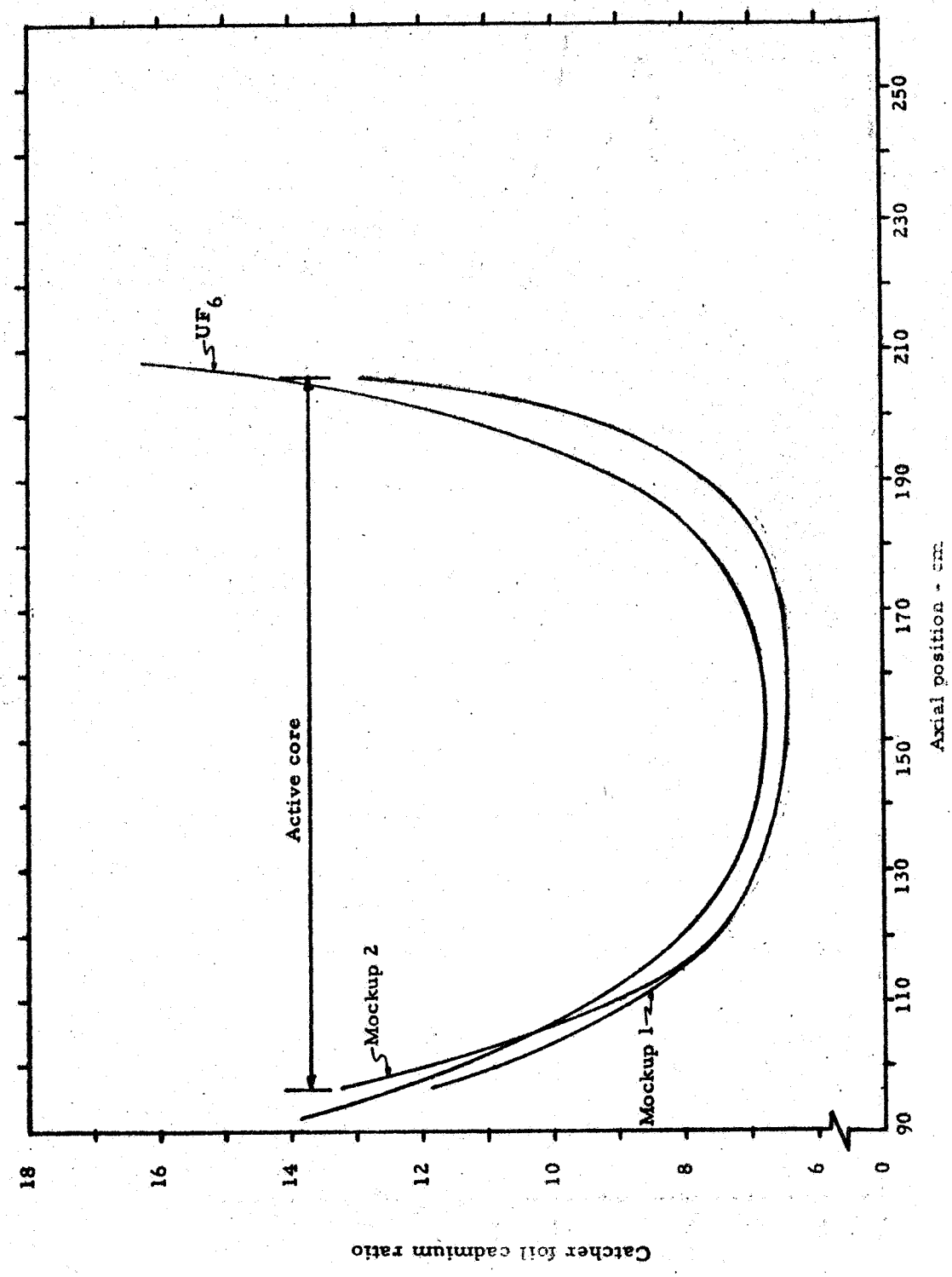


Fig. 9.9 Axial comparison of catcher foil cadmium ratios - Beryllium in D_2O reflector

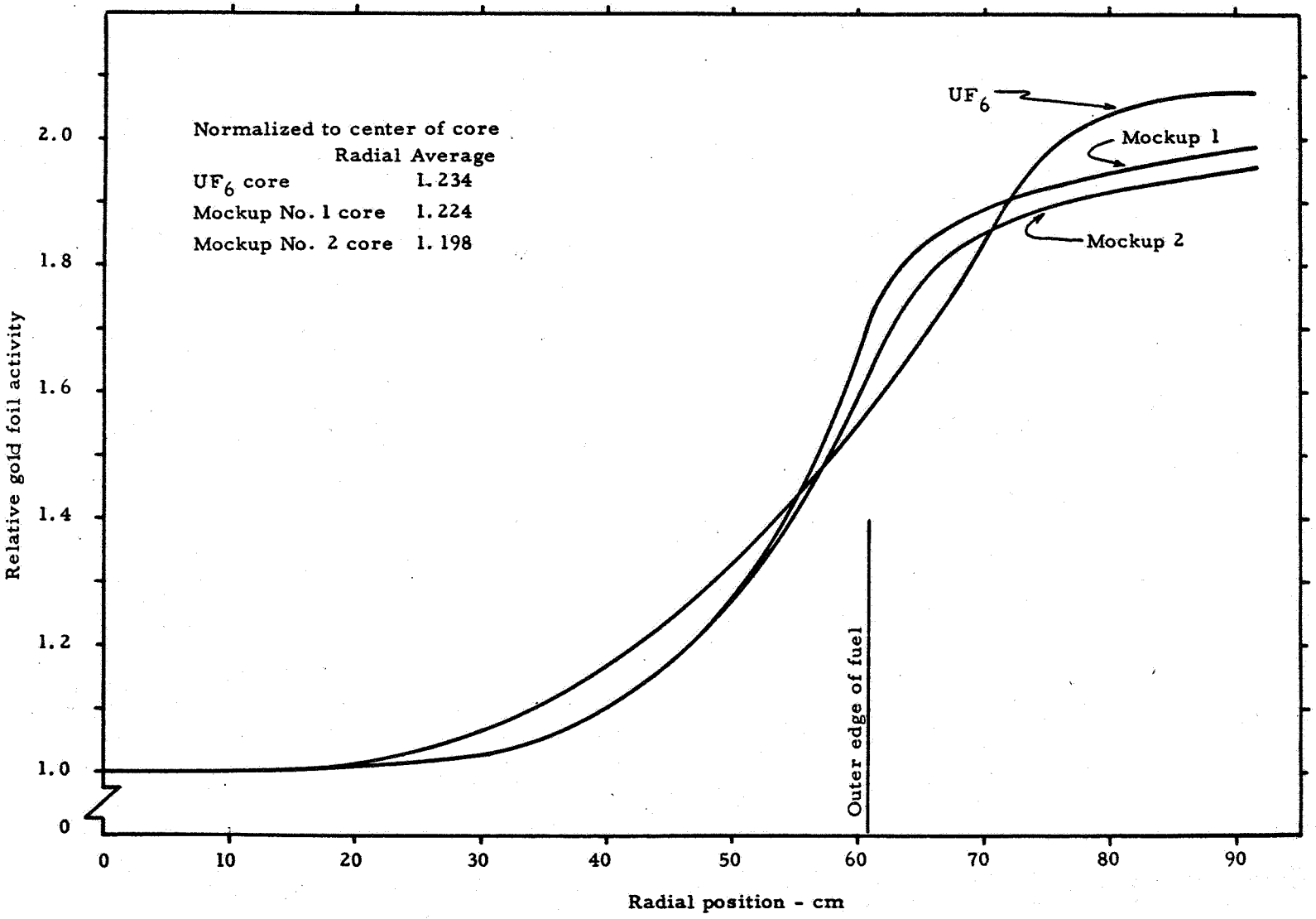


Fig. 9.10 Comparison of relative radial distribution of bare gold foil activity - Beryllium in D_2O reflector

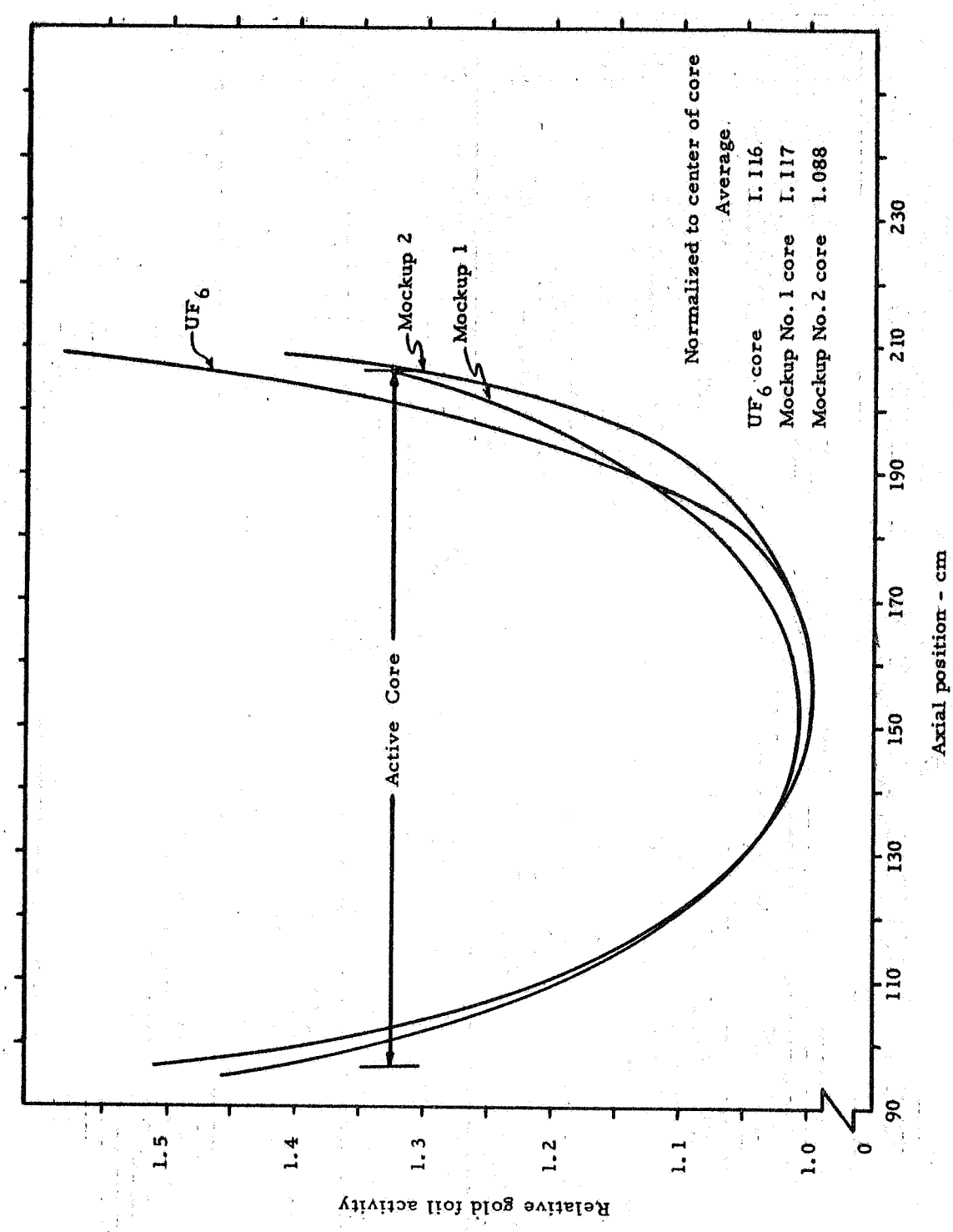


Fig. 9.11 Comparison of relative axial distribution of bare gold foil activity
Beryllium in D_2O reflector

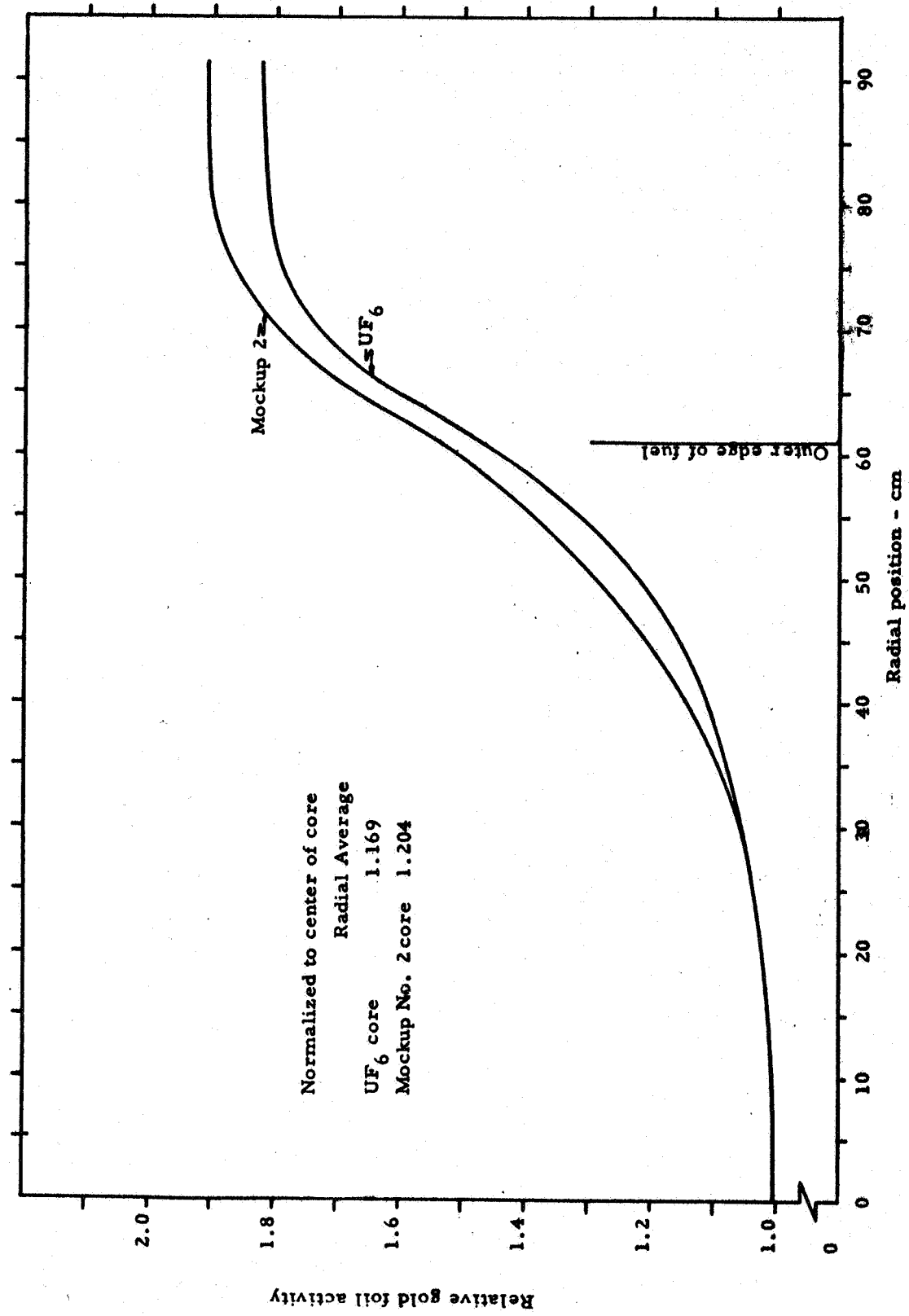


Fig. 9.12 Comparison of relative radial distribution of bare gold foil activity - Pure D_2O reflector

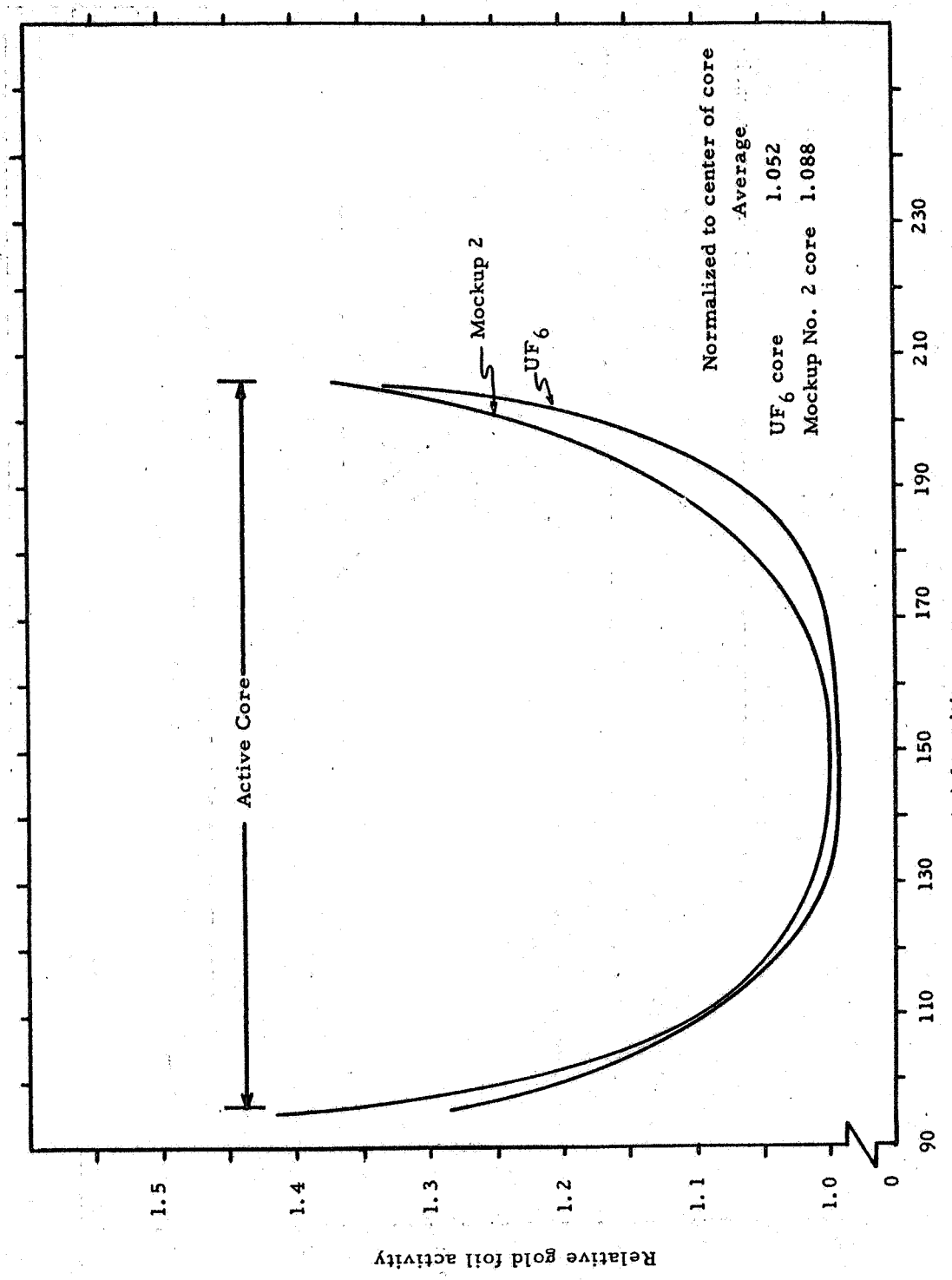


Fig. 9.13 Comparison of relative axial distribution of bare gold foil activity
Pure D_2O reflector

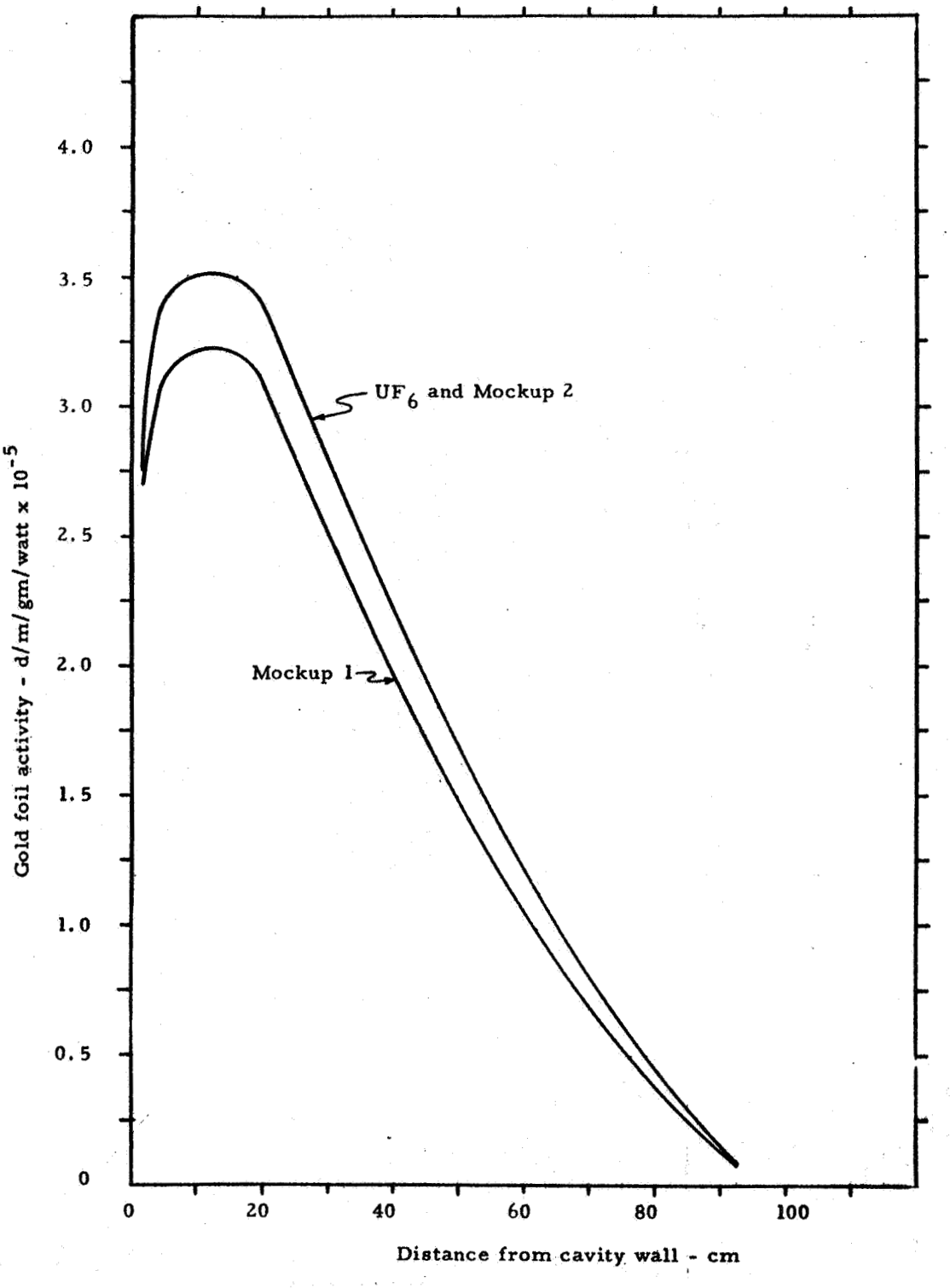


Fig. 9.14 Comparison of gold foil activity in the radial reflector Beryllium in D_2O reflector

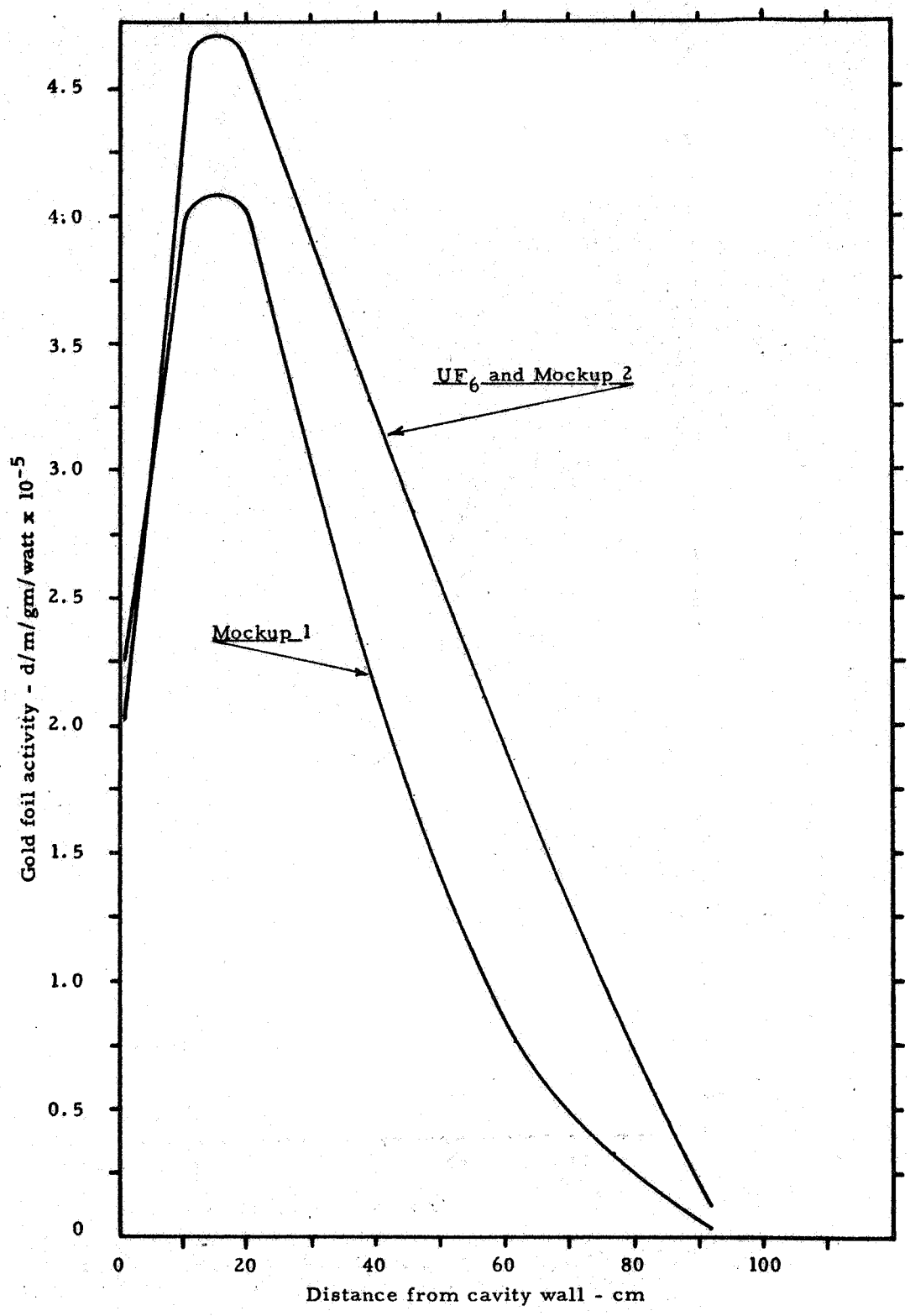


Fig. 9.15 Comparison of gold foil activity in the end reflector Beryllium in D_2O reflector

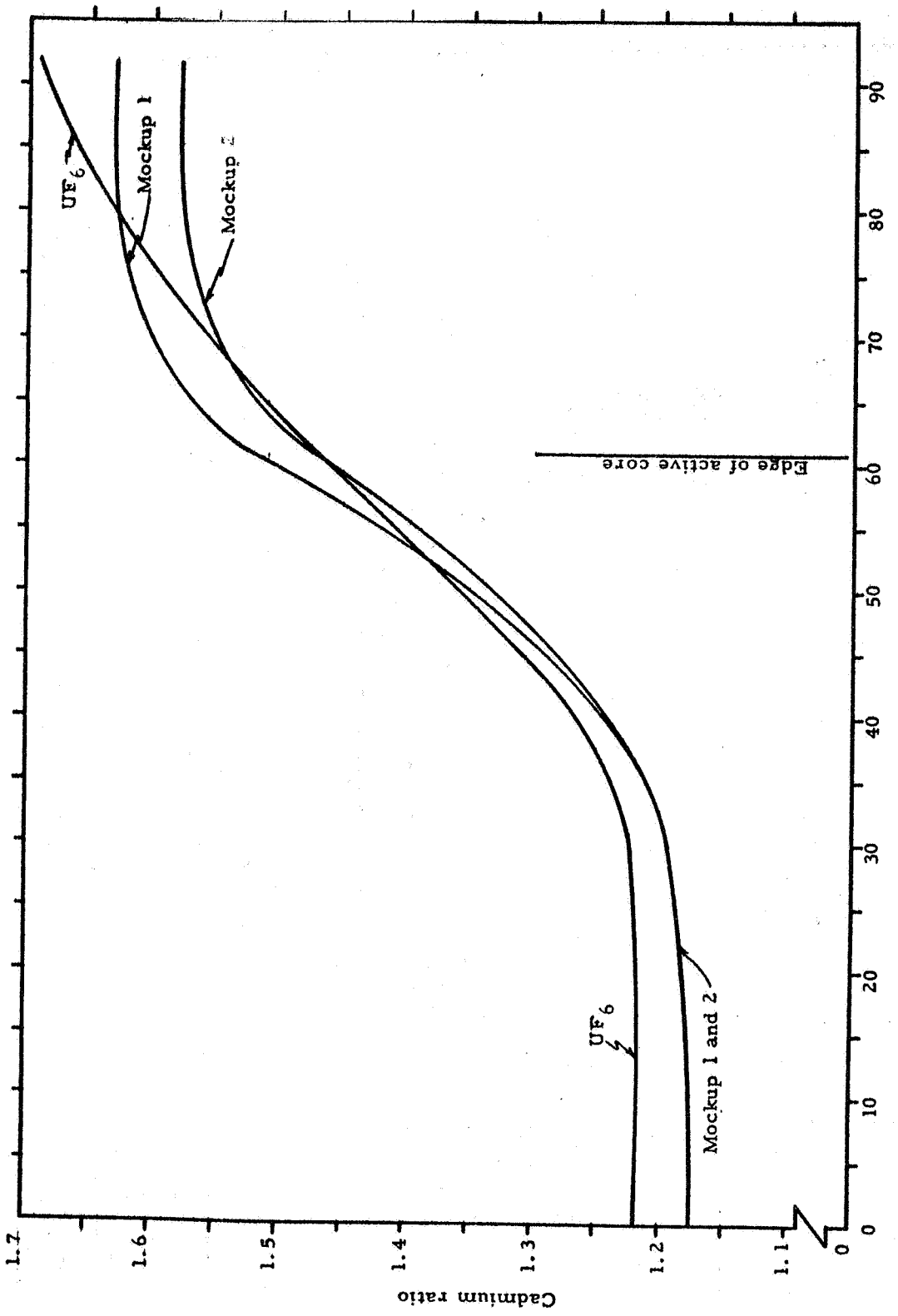


Fig. 9.16 Radial comparison of gold foil cadmium ratios - Beryllium in D_2O reflector

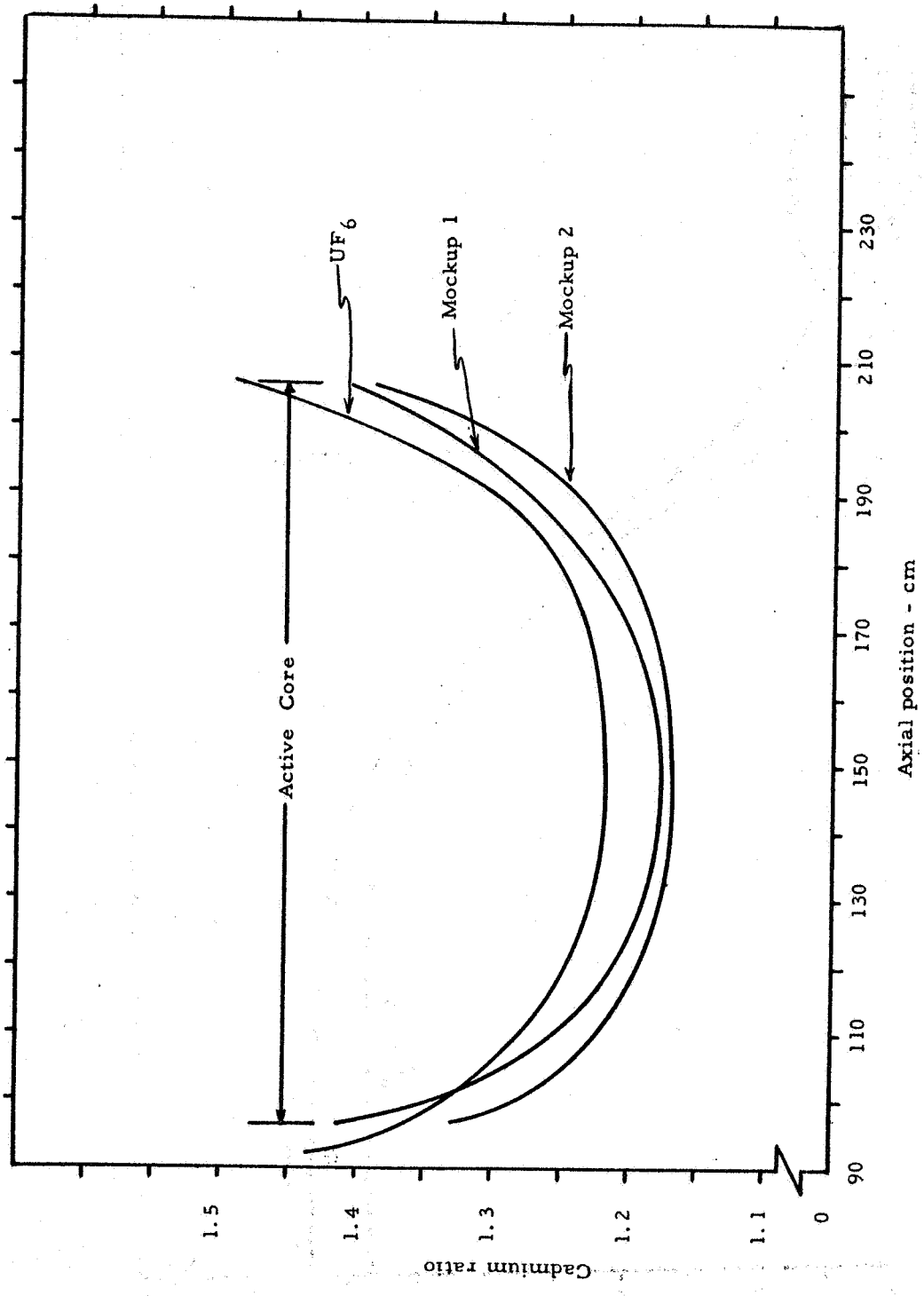


Fig. 9.17 Axial comparison of gold foil cadmium ratios - Beryllium in D_2O reflector

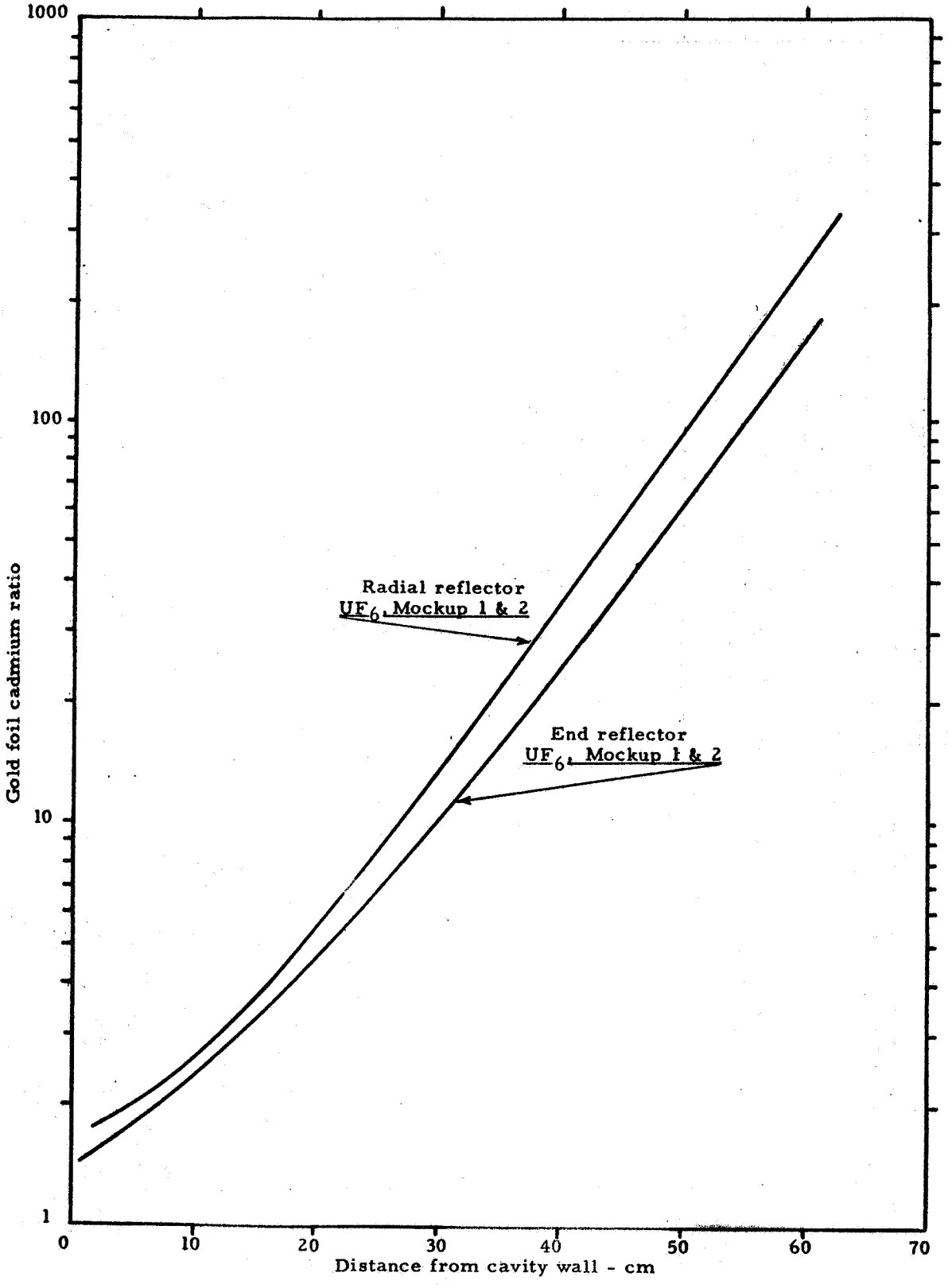


Fig. 9.18 Gold foil cadmium ratio distribution in the reflector regions Beryllium in D_2O reflector

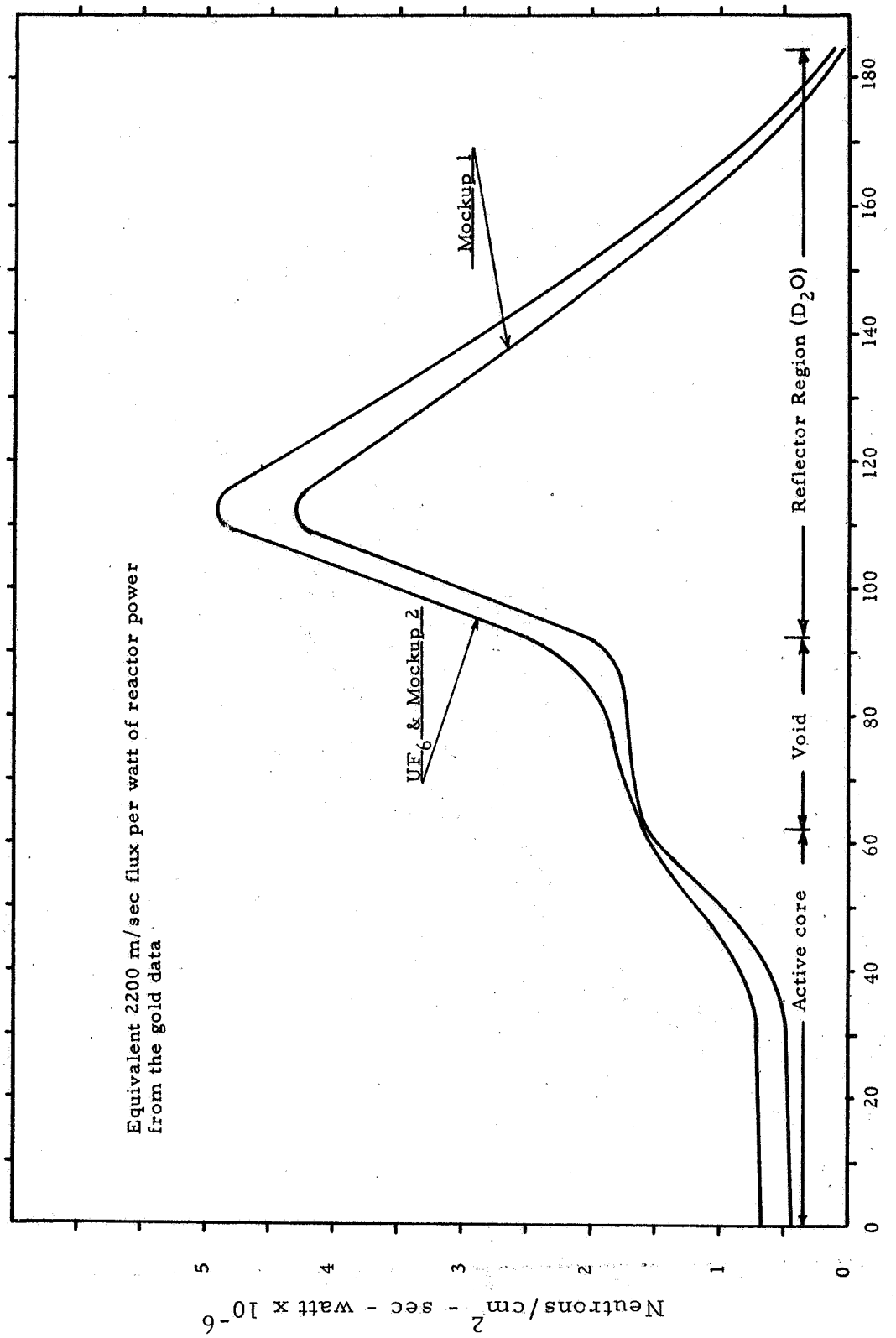


Fig. 9.19 Comparison of radial thermal neutron flux distribution - Beryllium in D_2O reflector

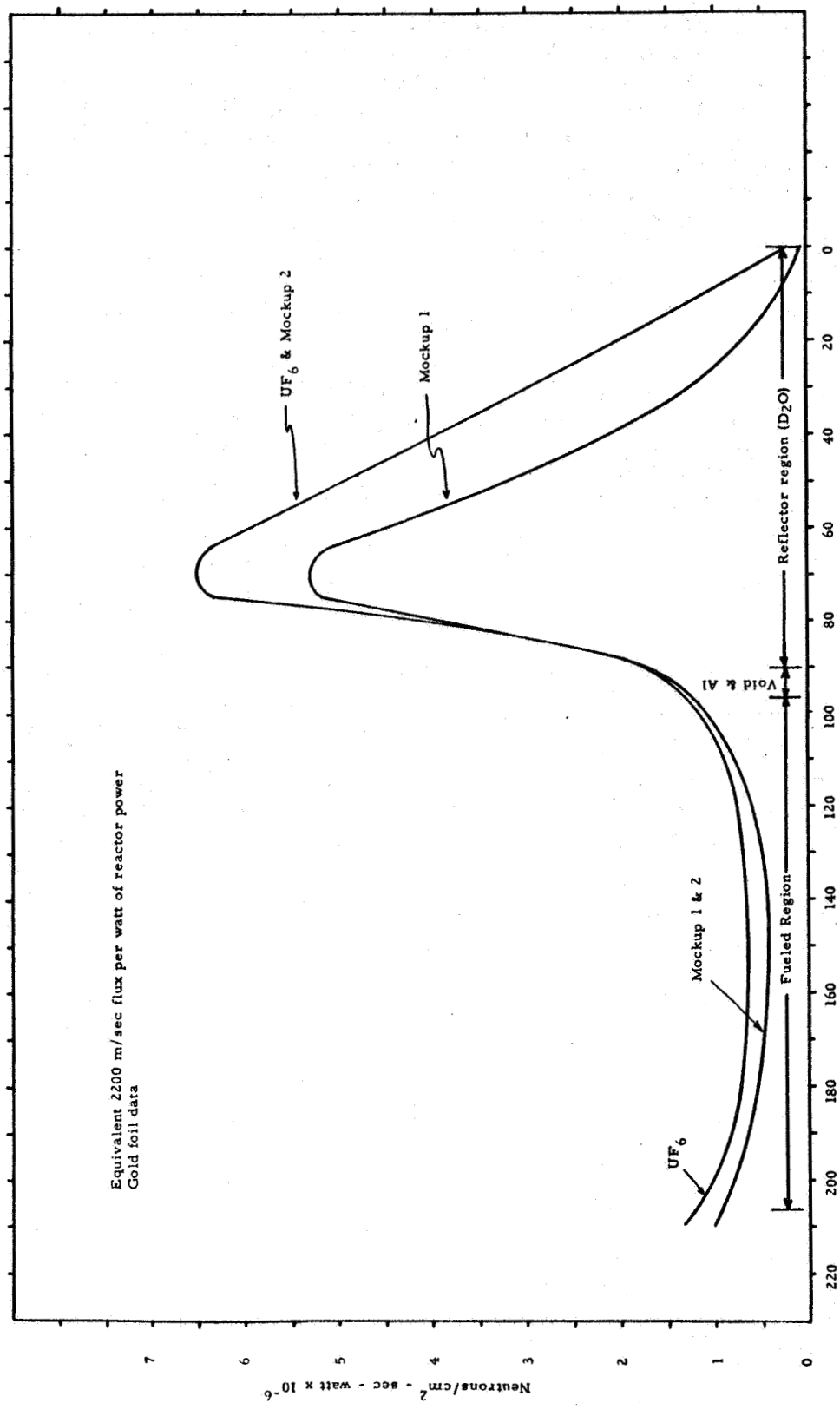


Fig. 9.20 Comparison of axial thermal neutron flux distribution - Beryllium in D_2O reflector

10.0 NUCLEAR CALCULATIONAL MODEL

The configuration of the cavity reactor critical experiment was intended to be as simple as possible to permit relatively easy correlation with reactor physics calculations. In engineering practice, however, the desired degree of simplicity could not be achieved. Since the structure was all aluminum, the departures from ideal geometry were originally considered insignificant. However, the neutronics of the cavity reactor are such that minor variations in the location of a weak absorber can have a profound influence on the reactivity of the system because of the very long thermal neutron diffusion length in the non-core regions. Because of this sensitivity, any calculational model needs to at least appropriately, if not accurately, simulate the aluminum and any other "impurities" in the system.

A two dimensional (r, z) representation is required in order to adequately represent the location and concentration of the various components of the system. Such a model is shown in Figure 10.1 and the composition of the various regions is shown in Table 10.1. However, the long convergence times required in two dimensional calculations, particularly if multithermal groups are used, dictates the desirability of performing one dimensional spherical calculations for most relative studies. Two different one-dimensional models which use volumes equivalent to those in the two dimensional model are presented in Table 10.2. In practice, these spherical models are quite adequate for calculating relative differences in reactivity between similar configurations. The spherical shape factor bias is negligibly small (0.2%Δk or less) for the first and simplest model when compared with the equivalent simplified two dimensional model. The multiplication that should be calculated for these models of the UF_6 experiment with the all D_2O reflector and Be-D_2O reflector are 1.018 and 1.014, respectively. (Note, the table gap is not included in the spherical model.)

Detailed results of calculations using these three models will be presented in a subsequent report.

TABLE 10.1

Nuclear Model Region Composition

Case 1 - All D_2O Reflector

Case 2 - Be - D_2O Reflector

CASE 1
VOLUME FRACTIONS

REGION	D_2O	Al.	
1	1.0	0	
2	.99355	.00645	
3	.9509	.0491	
4	.9752	.0248	
5	.9743	.0257	
6	.9831	.0169	
7	.9858	.0142	
8	.9884	.0116	
9	.8381	.1619	
10	.9720	.0280	
11	.9765	.0235	
12	.9808	.0192	
13	.9681	.0319	
14	.9832	.00648	.01032 VOID
15	1.0	0	
16	1.0	0	
17	0	1.0	
18	0	.6785	
19	0	.2732	.0231 CF_2
20	VOID		
21	FUEL		

CASE 2
VOLUME FRACTIONS

REGION	D_2O	Al.	SS	CF_2	Be
15	.0642	.7749	.0323	.1286	—
16	.047	—	—	—	.953
21	FUEL (1.335 × CASE 1)				

ATOM DENSITY $\times 10^{-24}$

FUEL	D_2O	Al.	Be	CF_2	SS(304)
$U^{234} = 2.1 \times 10^{-7}$	D = .06626	Al = .05813	Be = .123666	C = .0265	Fe = .06116
$U^{235} = 3.258 \times 10^{-5}$	$H = 14.6 \times 10^{-5}$	$Si = 3.5 \times 10^{-4}$		F = .0530	Ni = .00774
$U^{236} = 1.05 \times 10^{-7}$	O = .03317	$Fe = 2.0 \times 10^{-4}$			Cr = .01747
$U^{238} = 2.07 \times 10^{-6}$		$Cu = 7.6 \times 10^{-5}$			C = .000319
$F = 2.098 \times 10^{-4}$		$Mn = 4.4 \times 10^{-5}$			
		$Mg = 6.7 \times 10^{-4}$			
		$Cr = 8.0 \times 10^{-5}$			
		$Zn = 2 \times 10^{-4}$			
		$Ti = 3 \times 10^{-5}$			

TABLE 10.2

A. Spherical Calculational Model of UF_6 Experiment - One Region Core

Region	Outer Radius (cm)	Materials Mixtures	
		All D_2O Reflector	Be - D_2O Reflector
1	67.1	25.65 kg UF_6 (17.27 kg U)	34.972 kg UF_6 (23.55 kg U)
2	70.7	0.4224 VF 6061 Al	
3	91.446	Void	
4	92.715	1.0 VF 6061 Al	
5	100.278	3.063% Al, 96.808% D_2O	4.182% Al, 0.122% SS 0.485% Teflon, 95.082% D_2O
6	112.109	2.225% Al, 97.668% D_2O	3.232% Al, 41.087% Be 55.574% D_2O
7	124.726	1.198% Al, 98.716% D_2O	
8	159.324	0.943% Al, 99.015% D_2O	
9	196.018	0.714% Al, 99.248% D_2O	

NOTE: Material compositions are listed in Tables 3.2 and 10.1.

Densities are assumed to be:

Al	2.7 gm/cc
Be	1.85 gm/cc
SS	8.0 gm/cc
Teflon	2.2 gm/cc
D_2O	1.104 gm/cc with 0.22% H_2O

TABLE 10.2

(Continued)

B. Spherical Model for Four-Region Core for the UF_6 Experiments

Loading (kg U)	Region	Spherical Radius (cm)	Radial Width of Region (cm)	Volume Fractions				
				Fuel	Al (6061)			
17.27	1	60.998		1.0	--			
	2	67.848	6.85	0.29721	0.09985			
	3	74.669	6.821	0.24397	0.00724			
	4	81.454	6.785	0.20442	0.00691			
	5	91.445	9.991	--	0.05089			
				Reflector Volume Fractions				
	All D_2O Reflector			D_2O	Be	Al(6061)	Stainless Steel	CF_2 2.3 g/cc
	6	92.714				1.0		
	7	100.267	7.553	0.96808		0.03063		
	8	112.098	11.831	0.97668		0.02225		
	9	124.715	12.617	0.98716		0.01198		
	10	196.0	71.285	0.99163		0.0080		
	Be and D_2O Reflector							
	6					1.0		
	7			0.95082		0.04182	.00122	.00485
	8			0.55573	.41088	0.03232		
	9			0.98716		0.1198		
	10			0.99163		0.0080		

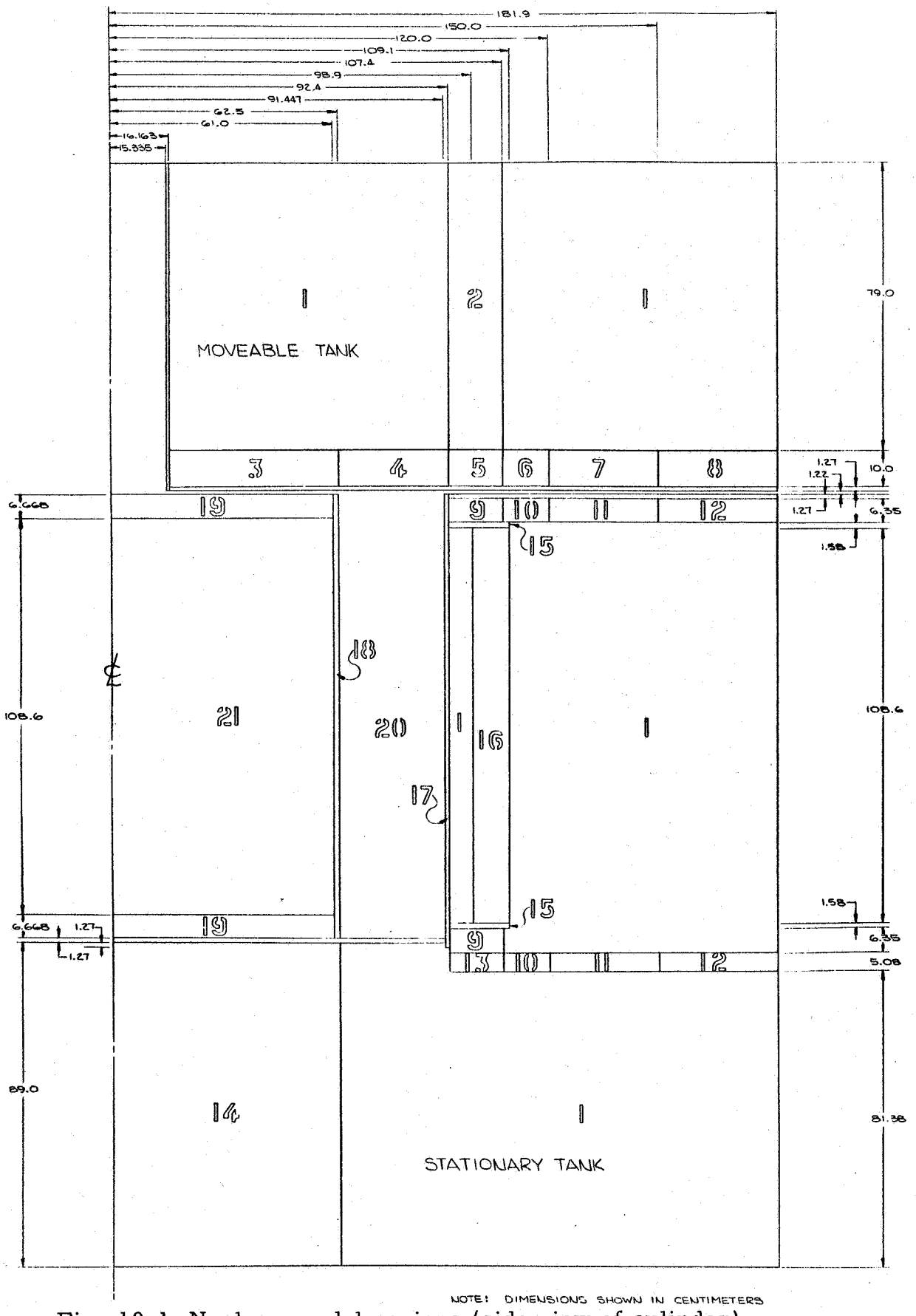


Fig. 10.1 Nuclear model regions (side view of cylinder)

REFERENCES

1. Pincock, G. D., Kunze, J. F., "Cavity Reactor Critical Experiment, Volume I," General Electric Company, NMPO-ITS, September 6, 1967, (NASA CR-72234).

2. Mills, C. B., Nuclear Science and Engineering, 13, p. 301 (August 1962).

3. Jarvis, G. A., "Cavity Reactor," Proceedings of an Advanced Nuclear Propulsion Symposium, (LA-3229-MS), p. 344.

4. Thie, J. A., "Reactor Noise," Rowman and Littlefield, (1963)

5. Seifritz, W., Stegemann, D., and Vath, W., Proceedings of Neutron Noise, Waves, and Pulse Propagation, Gainesville, Florida, (1966), Paper 3-1.

6. Velez, C., "Autocorrelation Functions of Counting Rate in Nuclear Reactor," Nuclear Science and Engineering, 6, p. 414 (1959).

INDEX

Aluminum

mass in core - 44, 46, 119, 138, 208
mass in UF_6 experiment - 44, 78
worth in core - 28, 29, 42, 43, 46, 53, 133, 214
correction for - 201, 214

Axial reference point - 61

Beryllium

location and size in reflector - 18, 23, 32
worth in reflector - 119, 174, 200

Beryllium oxide - 81

Cadmium ratios (see specific configurations) - 18, 19, 50, 219, 220, 227, 228, 229

Calculational models - 232

Catcher foils - 18, 47

Control system

critical positions - 19
rod shape curves - 20, 21, 141, 157
worth (see also specific configurations) - 45, 80, 132, 207

Core structure
Mockup No. 1 - 61-63
Mockup No. 2 - 131, 138, 152-155
UF_6 - 78, 98-100

Critical loading - 25, 33, 34, 35

bias - 26,
corrections - 33, 34
comparison - 34

Delayed neutrons
β-effective - 19
decay constants and fractions - 22

Dimensions - 17, 23, 24, 25, 30, 151

Ducting and tubing, worth of - 82

Fission power - (see power distribution)

INDEX
(Cont'd)

Fluorine worth - 52

Flux

thermal neutron - 27, 40, 211, 230, 231

Fuel

arrangement - 61, 62, 63
critical loading - 34, 209, 210
composition - 31
distribution effects in gas experiment - 120
fuel sheet mass variations - 134, 142
handling of UF_6 - 79
impurities - 29, 46, 47
reactivity coefficients - 28, 35, 41, 105, 134, 160, 186, 208, 212

Generation time (neutron lifetime) - 85

Gold foil activation - 38, 39, 221-226

Heating - cooling effects - 79, 103, 104

Heavy water purity - 18

Inverse multiplication - 51, 64, 87, 140

Kinetics

delayed neutrons - 19, 22
transfer function - 118

Mean chord length - 202

Noise measurements - 85, 118

Nuclear models - 232

Power distribution (see also specific configurations) - 27, 36, 37, 215-218

Pressure-temperature relation for UF_6 - 102

Reactivity coefficients - 52, 88, 208

Reference point (axial) - 61

References - 237

INDEX

(Cont'd)

Reflector

dimensions - 17, 23
beryllium - 18, 23, 32, 119, 174, 200
temperature effects - 29

Size differences - 201-203, 209

Stainless steel - worth of - 119

Teflon - 32, 52, 78

Temperature

core - 79, 103, 104
reflector - 29

Transfer function - 118

Uranium hexafluoride - 98, 102

temperature effect on reactivity - 79, 103, 104
transfering of - 79, 102

Volume fractions, masses, etc. - 30, 232

DISTRIBUTION

INTERNAL

Idaho

JF Kunze
JW Morfitt
RB O'Brien
GD Pincock
FL Sims

Library (2)

Evendale

WE Edwards
GF Hamby (3)
WB Henderson
MA Zipkin

Library (2)

EXTERNAL

AEC, CAO

CL Karl

AEC, ORO

WL Smalley

AEC, DTIE

NASA Scientific & Technical
Information Facility
P. O. Box 33
College Park, Maryland

NASA-Lewis Research Center

TJ Flanagan
RE Hyland (3)
JC Liwosz (2)
NT Musial
RW Patch
RG Ragsdale
FE Rom
Report Control Office (1)
Nuclear Technology Office (1)
Library (2)

Mr. D. R. Bartz
Manager, Research & Advanced
Concepts Section
Propulsion Division
Jet Propulsion Laboratory
Pasadena, California 91103

Mr. J. R. Beyster
General Atomic
P. O. Box 608
San Diego, California 92115

Dr. C. J. Bridgman
Associate Professor of Physics
Air Force Institue of Technology
Wright-Patterson Air Force Base,
Ohio 45433

Mr. J. A. Brousseau
Chief, Propulsion Systems
Technology
Mail Stop 47-18
The Boeing Company
Seattle, Washington 98124

DISTRIBUTION

(Continued)

Dr. Wayne G. Burwell
United Aircraft Corporation
Research Laboratories
400 Main Street
East Hartford, Connecticut 06108

Dr. Robert W. Bussard
Electro-Optical Systems, Inc.
300 N. Halstead Street
Pasadena, California 91107

Mr. James Carton
Advanced Concepts
REON Division
Aerojet-General Corporation
Sacramento, California 95801

Dr. C. C. Chang
Head, Space Sciences & Applied Physics
Catholic University of America
Washington, D.C. 20017

Dr. Peter Chiarulli
Head, Mechanics Department
Illinois Institute of Technology
Chicago, Illinois 60616

Dr. Joseph Clement
Nuclear Engineering Department
Georgia Institute of Technology
Atlanta, Georgia 30301

Dr. Ralph S. Cooper
Donald W. Douglas Laboratories
2955 George Washington Way
Richland, Washington 99352

Mr. J. S. Cory
Donald W. Douglas Laboratories
2955 George Washington Way
Richland, Washington 99352

Mr. Jerry P. Davis
Building 122-3
Jet Propulsion Laboratory
4800 Oak Grove Drive
Pasadena, California 91103

Dr. Robert Dillaway
Nucleonics Department
Rocketdyne
6633 Canoga Avenue
Canoga Park, California 91303

Dr. D. W. Drawbaugh
Astronuclear Laboratory
Westinghouse Electric Corporation
Pittsburgh, Pennsylvania 15236

Mr. Frederick C. Durant, III
Assistant Director, Astronautics
National Air Museum
Smithsonian Institute
Washington, D.C. 20560

Dr. Andrew Fejer
Head, Mechanical & Aerospace Engineering Department
Illinois Institute of Technology
Chicago, Illinois 60616

Dr. William M. Foley
United Aircraft Corporation
Research Laboratories
400 Main Street
East Hartford, Connecticut 06108

Dr. Robert H. Fox
Institute for Defense Analysis
400 Army-Navy Drive
Arlington, Virginia 22202

Mr. A. P. Fraas
Oak Ridge National Laboratory
P. O. Box Y
Oak Ridge, Tennessee 37831

Mr. E. A. Franco-Ferreira
Metals & Ceramics Division
Oak Ridge National Laboratory
P. O. Box X
Oak Ridge, Tennessee 37831

Mr. L. A. Gore
Space Technology Laboratories
One Space Park
Redondo Beach, California 90277

DISTRIBUTION
(Continued)

Dr. Jerry Grey
Grey-Rad Corporation
61 Adams Street
Princeton, New Jersey 08540

Professor Robert A. Gross
School of Engineering & Applied Science
Columbia University
New York, New York 10027

Dr. A. V. Brosse
Research Institute of Temple University
4150 Henry Avenue
Philadelphia, Pennsylvania 19144

Dr. George Grover
N-5
Los Alamos Scientific Laboratory
P. O. Box 1663
Los Alamos, New Mexico 87544

Dr. S. V. Gunn
Rocketdyne Division of North American Aviation
6633 Canoga Avenue
Canoga Park, California 91303

Professor Elias P. Gyftopoulos
Room 24-109
Massachusetts Institute of Technology
Cambridge, Massachusetts 02139

Dr. James W. Hadley
"R" Division Leader
Lawrence Radiation Laboratory
P. O. Box 808
Livermore California 94551

Mr. L. P. Hatch
Brookhaven National Laboratory
Upton, Long Island, New York 11101

Dr. Clifford J. Heindl
Building 180-805
Jet Propulsion Laboratory
4800 Oak Grove Drive
Pasadena, California 91103

Dr. R. J. Holl
Missiles & Space Systems Division
Douglas Aircraft Company
Santa Monica, California 90405

Mr. William J. Houghton
Department 7040, Building 2019A2
Aerojet-General Corporation
P. O. Box 1947
Sacramento, California 95809

Mr. Henry Hunter
Space Technology Laboratories
One Space Park
Redondo Beach, California 90277

Mr. Maxwell Hunter
Department 50-01, Building 102
Lockheed Missiles & Space Co.
P. O. Box 504
Sunnyvale, California 94408

Mr. J. W. Hilburn
Whiteshell Nuclear Research Establishment
Atomic Energy of Canada United
Pinawa, Manitoba, Canada

Professor Abraham Hyatt
1700 E. Imperial Highway
El Segundo, California 90246

Dr. Kurt P. Johnson
Advanced Space Technology, A2-263
Douglas Missiles & Space Systems Division
Santa Monica, California 90405

Mr. Carmen Jones
Rocketdyne Division of North American Aviation
6633 Canoga Avenue
Canoga Park, California 91303

Mr. Willis Y. Jordan, Jr.
Chief, Planetary & Nuclear Systems Group
Advanced Systems Office R-AS
Marshall Space Flight Center
Huntsville, Alabama 35812

DISTRIBUTION
(Continued)

Dr. Larry Kaufman
Director of Research
Manlabs, Inc.
21 Erie Street
Cambridge, Massachusetts 02139

Lt. Col. M. R. Keller
Aerospace Research Laboratories (ARN)
Wright-Patterson Air Force Base, Ohio
45433

Professor J. L. Kerrebrock
Room 33-115
Massachusetts Institute of Technology
Cambridge, Massachusetts 02139

Dr. John J. Keyes, Jr.
Reactor Division
Oak Ridge National Laboratory
P. O. Box Y
Oak Ridge, Tennessee 37831

Dr. D. E. Knapp
Donald W. Douglas Laboratories
2955 George Washington Way
Richland, Washington 99352

Mr. Walter F. Krieve
Building S
TRW Systems
One Space Park
Redondo Beach, California 90278

Mr. George T. Lalos
U. S. Naval Ordnance Laboratory
White Oaks, Silver Springs,
Maryland 20900

Dr. Zalman Lavan
Illinois Institute of Technology
M. A. E. Department
Technology Center
Chicago, Illinois 60616

Mr. David Mallon
Allison Division
General Motors Corporation
2355 S. Tibbs Avenue
Indianapolis, Indiana 46206

Professor Edward Mason
Room NW12
Massachusetts Institute of
Technology
Cambridge, Massachusetts 02139

Mr. George H. McLafferty
United Aircraft Corporation
Research Laboratories
400 Main Street
East Hartford, Connecticut 06108

Dr. Robert V. Meghreblian
Jet Propulsion Laboratory
4800 Oak Grove Avenue
Pasadena, California 91103

Dr. A. J. Miller
Oak Ridge National Laboratory
P. O. Box Y
Oak Ridge, Tennessee 37831

Mr. James Nance
General Atomic
P. O. Box 608
San Diego, California 92101

Professor Clyde Orr, Jr.
Chemical Engineering Department
Georgia Institute of Technology
Atlanta, Georgia 30301

Mr. Frank S. Owen
United Aircraft Corporation
Research Laboratories
400 Main Street
East Hartford, Connecticut 06108

Dr. Donald Parks
General Atomics Division
General Dynamics Corporation
P. O. Box 608
San Diego, California 92112

Mr. P. Patriarca
Oak Ridge National Laboratory
P. O. Box X
Oak Ridge, Tennessee 37831

DISTRIBUTION
(Continued)

Mr. John C. Peak
General Atomics Division
General Dynamics Corporation
P. O. Box 608
San Diego, California 92112

Professor Rafael Perez
Nuclear Engineering Department
University of Florida
Gainesville, Florida 32601

Professor H. C. Perkins
Energy, Mass & Momentum Transfer Laboratory
Aerospace & Mechanical Engineering Department
University of Arizona
Tucson, Arizona 85721

Dr. Ben Pinkel
RAND Corporation
1700 Main Street
Santa Monica, California 90406

Dr. Jacob B. Romero
Chemical Engineering Department
University of Idaho
Moscow, Idaho 83843

Dr. Richard Rosa
Avco Everett Research Laboratory
2385 Revere Beach Parkway
Everett, Massachusetts 02149

Dr. Martin Rosenzweig
Aerodynamic & Heat Transfer Dept.
Aerospace Corporation
P. O. Box 95085
Los Angeles, California 90045

Mr. Eli B. Roth
A.C. Electronics Division
7929 South Howell Avenue
Milwaukee, Wisconsin 53201

Dr. S. M. Scala
Manager, Theoretical Fluid Physics Section
General Electric Company
Space Sciences Laboratory
P. O. Box 8555
Philadelphia, Pennsylvania 19101

Mr. F. C. Schwenk
AEC/NASA Space Nuclear Propulsion Office
Division of Reactor Development
U. S. Atomic Energy Commission
Washington, D.C. 20545

Mr. W. L. Snapp
Aerojet-General Corporation
20545 Center Ridge Road
Cleveland, Ohio 44116

Mr. C. K. Soppet
Nuclear Integration Department
REON Division
Aerojet-General Corporation
Sacramento, California 95801

Mr. Robert J. Spindler
AVCO Corporation
Missile Systems Division
201 Lowell Street
Wilmington, Massachusetts 01887

Dr. John C. Stewart
University of Colorado
Joint Institute for Laboratory Astrophysics
Boulder, Colorado 80302

Mr. J. J. Stewart
Department 7040, Building 2019A2
Aerojet-General Corporation
Sacramento, California 95809

Dr. Henry Stumpf
Space Sciences Division
Jet Propulsion Laboratory
4800 Oak Grove Drive
Pasadena, California 91103

Mr. T. Szekely
Space Technology Laboratories
One Space Park
Redondo Beach, California 90277

Dr. Theodore B. Taylor
Defense Atomic Support Agency
Pentagon
Washington, D.C. 20301

DISTRIBUTION

(Continued)

Dr. T. P. Torda
Illinois Institute of Technology
M. A. E. Department, Technology Center
Chicago, Illinois 60616

Dr. Robert F. Trapp
Chief, Advanced Concepts & Flight Proj. (RBA)
Biotechnology & Human Research Division
National Aeronautics & Space Admin.
Washington, D.C. 20546

Dr. Robert Uhrig
Chairman, Department of Nuclear Eng.
University of Florida
Gainesville, Florida 32601

Dr. Hans von Ohain
Aerospace Research Laboratories (ARD-1)
Wright-Patterson Air Force Base, Ohio
45433

Dr. Herbert Weinstein
Chemical Engineering Department
Illinois Institute of Technology
Chicago, Illinois 60616

Professor E. P. Wigner
Department of Physics
Princeton University
Princeton, New Jersey 08540

Captain William Yingling
AEC/NASA Space Nuclear Propulsion Office
Division of Reactor Development
U. S. Atomic Energy Commission
Washington, D. C. 20545

Mr. Jerrold M. Yos
Avco Corporation
Research & Advanced Development Division
201 Lowell Street
Wilmington, Massachusetts 01887

Professor M. J. Zucrow
Atkins Professor of Engineering
Mechanical Engineering Department
Purdue University
Lafayette, Indiana 47907

Mr. J. Ravets
WANL
P. O. Box 10864
Pittsburgh, Pennsylvania 15236

Professor Chien Ho
Columbia University
Room 287 MUDD
New York, New York 10027